University of Lille

DOCTORAL THESIS

Defense at the University of Lille
On 31 March 2025 by

Emma Theerens

Impact of ultrafine particles exposure as environmental factors involved in Parkinson's disease:

In vivo and *in vitro* application on how ultrafine particles lead to neuronal cell death

Discipline
Neurotoxicology

Doctoral School
Graduate School of Biology and Health

Specialty
Molecular and cellular aspects of biology

Laboratoires
IMPECS
[IMPact of Chemical Environment on Human Health]

LilNCog
[Lille Neuroscience and Cognition]

Composition of the jury

Pr. Dr. Katja Kanninen A.I. Virtanen Institute for Molecular Sciences Kuopio, Finland	Rapporteur
Pr. Dr. Karen Smeets Centre for Environmental Science (CMK) Diepenbeek, Belgium	Rapporteur
Pr. Dr. Roel Schins School for Nutrition and Translational Research in Metabolism (NUTRIM) Maastricht, The Netherlands	Rapporteur
Dr. Luc Buée Lille Neuroscience and Cognition Lille, France	President of the jury
Pr. Dr. David Devos Lille Neuroscience and Cognition	Thesis Director
Dr. Lydia Nikasinovic IMPact of Chemical Environment on Human Health	Thesis Co-director

Université de Lille

THESE DE DOCTORAT

Soutenue à Université de Lille
le 31 Mars 2025 par

Emma Theerens

Impact de l'exposition aux particules ultrafines dans la maladie de Parkinson :

Application *in vivo* and *in vitro* sur les mécanismes de mort neuronale

Discipline
Neurotoxicologie

Ecole doctorale
l'Ecole Graduée Biologie Santé de Lille

Spécialité
Aspects moléculaires et cellulaires de la biologie

Laboratoires
IMPECS
[IMPact de l'Environnement Chimique sur la Santé humaine]

LilNCog
[Lille Neuroscience et Cognition]

Composition du jury

Pr. Dr. Katja Kanninen Institut A.I. Virtanen des Sciences Moléculaires Kuopio, Finlande	Rapporteur
Pr. Dr. Karen Smeets Centre des Sciences de l'Environnement (CMK) Diepenbeek, Belgique	Rapporteur
Pr. Dr. Roel Schins Ecole de Nutrition et de Recherche Translationelle en Métabolisme (NUTRIM) Maastricht, Pays-Bas	Rapporteur
Dr. Luc Buée Lille Neuroscience et Cognition Lille, France	Président du jury
Pr. Dr. David Devos Lille Neuroscience et Cognition	Directeur de thèse
Dr. Lydia Nikasinovic IMPact de l'Environnement Chimique sur la Santé humaine	Co-directeur de thèse

FUNDING ACKNOWLEDGEMENTS

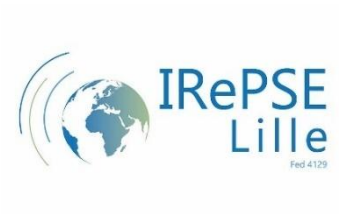

PREFACE

From a very young age, I was confronted with Parkinson's disease when my grandfather, *Opa Tino*, was diagnosed around the time I turned one. Early on, it was suspected that the cause of his condition might have been linked to a severe brain injury sustained in a car accident – what we would now describe as an environmental factor.

I think you can imagine the impression this left on a child. In April 2005, at the age of 10, I gave my first presentation about Parkinson's disease during a "News Flash" at my primary school, prompted by the passing of Pope John Paul II. Now, 20 years later, I am incredibly proud to have had the opportunity to work on this topic and bring the early impact full circle through my PhD research.

My grandfather held the unique distinction of being the longest-diagnosed Parkinson's patient under the care of Prof. Dr. Patrick Santens (University of Gent, Belgium). This path was not only his to bear; it deeply impacted our entire family, prompting us all to contribute in different ways. My mother, then the head nurse of the geriatric hospital ward, pursued further specialization as a certified Parkinson's nurse. My godmother, *Meter Mie*, started a foundation to provide financial support for the research of Prof. Dr. Santens on microbiome alterations in Parkinson's patients and the role of the gut-brain axis in disease progression. More recently, my brother-in-law, Dr. Lukas Duffner, completed his PhD at Maastricht University (the Netherlands) and now works as a Project Officer for Alzheimer Europe. While not directly linked to Parkinson's, we warmly welcomed him as another neurodegenerative disease specialist in our family.

I am immensely proud to contribute to the understanding of environmentally triggered Parkinson's disease. With this family history, I can confidently say it was written in the stars that I would one day pursue a PhD related to this topic.

As someone who shares my grandfather's traits (he also completed a PhD), I must admit that I tend to write extensively.

I hope you will enjoy reading this elaborately written PhD study.

Emma Theerens

December 2024 – Lille, France

Opa Tino
Dr. Valentin Vermeersch
(1937 – 2020)

ACKNOWLEDGEMENTS

First and foremost, I would like to express my deepest gratitude to Dr. Luc Buée, the president of my jury, for presiding over this important academic milestone. As head of the LilNCog lab, your guidance and expertise have been invaluable.

I also sincerely thank Prof. Dr. Katja Kanninen, Prof. Dr. Karen Smeets, and Prof. Dr. Roel Schins for accepting their roles as jury members. Your expertise and critical insights significantly enhance the depth of this dissertation. I hope this PhD manuscript reads like a trilling investigation into how the stealthy killer, “ultrafine particles”, targets neurons!

In 2018, I embarked on this academic adventure with a bachelor’s internship under the supervision of Prof. Dr. Guillaume Garçon. It was an incredible experience that allowed me to delve into my favorite topic, epigenetics, while also discovering a new city, immersing myself in a new culture, and improving my French language skills. Beyond the technical and scientific knowledge he imparted, his guidance inspired me to return to Lille for both Master 1 and Master 2 internships, and ultimately, to pursue a PhD. Thank you, Prof. Dr. Garçon, for encouraging me to take this journey and to have made Lille my new homeplace. Your expertise and the bond we developed paved the way for me to start this PhD and to become part of the PUF-EXPOmiR project. Although I now refer to you as my former PhD director with deepest disappointment, I want to thank you for the opportunities over the past years. I wish you all the best with your future career.

Since I worked in two laboratories (IMPECS & LilNCog-DVCD), I’m fortunate to have two directors. I hear you thinking, 'twice the work,' but I’ve also learned twice as much, met twice as many people, had twice as many opportunities,…
…, twice as much inspiration, twice as many challenges, and double the fun along the way!

For LilNCog, I would like to express my gratitude to my director, Prof. Dr. David Devos for the opportunity to work in the neuroscience field, your thoughtful critiques, and unwavering dedication. Your support has truly pushed me to my limits and paid off in terms learning about Parkinson’s disease. I hope I’ve been able to share some insights and inspiration into the toxicological aspects as well!

Dear Lydia, Dr. Nikasinovic, master of epidemiology, but as I have experienced firsthand, also a true master of being a ‘PhD Director’. Your remarkable expertise transcends boundaries, despite your background, you have guided and supervised a fundamental toxicology-based scientific project with such ease and insight. I am truly grateful that you joined as my director for the IMPECS lab portion. Your unwavering encouragement, shared perfectionism, deep commitment to scientific integrity, and inspiring life perspectives made it possible for me to ever consider giving up. Without your exceptional care; as a mentor, a colleague, and even a ‘scientific mom’, I wouldn’t be where I am

today. You taught me the art of writing an article, a skill I will carry with me throughout my career as a researcher, as I aspire to write many more. Each time I sit down to write, I will think back fondly on the invaluable moments we shared. You've had a profound impact on me, and I will never forget it!

I also would like to extend my heartfelt gratitude to our IMPECS laboratory director, Dr. Jean-Marc Lo Guidice. You are a leader who truly connects with your team, always standing behind us and providing unwavering support. We have known each other since 2018, and I can confidently say that challenging moments have only strengthened our bond. Thank you not only for your contribution to my PhD (be it scientific or financial support), but also for the personal impact you've had on me. Your efforts ensured that I was able to complete this PhD under the best possible circumstances, even amidst challenges. I sincerely hope you will continue to hold the well-deserved title of '*Meilleur Directeur Mondial*' and that your journey ahead is filled with inspiring scientific achievements, always fueled by the energy and enthusiasm of your youthful team.

When it comes to the IMPECS team, I want to acknowledge my closest colleagues from the *Pôle Recherche* lab. A heartfelt thank you to Céline Grare, Djamal Achour, Ophélie, Simonin, Sébastien Antherieu, Stephan Gabet, Ornela Adjahou, Edmone Dewaeles, as well as the previous PhDs: Jules Sotty, Yara Saleh, Romain Dusautoir, Gianni Zarcone, Florence Jacob. You crossed my path as colleagues, you stay at my path as friends. I will always cherish the memories we created together, our hilarious moments at Disneyland Paris with the nervous anticipation for the Space Mountain, preparing *our* (or was it *mine*?) secret chamber, playing *Pigeon Pigeon* or Bullshit, and so much more. These shared experiences mean so much to me, and even the humble plant flies in the lab will always remind you to me, together with the fact that I turned into Tata Emma of our IMPECS baby during this PhD journey.

Also a heartfelt thanks to my colleagues at LilNCog. Although my desk wasn't there, I began using LUHMES cells with the guidance of LUHMES-specialist Aurélie Jonneaux and the support of Flore Gouel, particularly on regulated cell death. Also special thanks to Marie-Amandine Bonte, our conversations have evolved from 'let's grab a coffee' to 'let's do a videocall', where I love the sharing moments with you, my American Postdoc Friend. Our lab is big, but of course, I would like to thank all my colleagues, from the DVCD team and beyond, especially for the BrainStorming and ACDC meetings, or our LilNCog Days. Thanks for the scientific support, and to make small talks not small in terms of value! I cannot leave LilNCog behind, if I do not take a moment to thank Madame Céline Brand. Always someone who has the right vision, dedicated to doing good. '*Le centre'*, as we say, is fortunate to have you. A true coordinator who stands for the interests of science and humanity. Your commitment has been invaluable in ensuring our projects run smoothly and efficiently at every level.

This work was not mine alone; as mentioned earlier, this PhD research is part of the PUF-EXPOmiR project. I would like to mention the two partners in crime, Emeline Barbier and Jessica Carpentier, who focused on the *in vivo* aspect of the project, working on the other organs, alongside the brain and conducting tests related to oxidative stress and neuroinflammation. From the side of LilNCog, I want to thank Charlotte Laloux (LiiFFE, PLBS platform) for the support during the behavioral testing. A special thanks also goes to Kelly Timmerman, you constructed the brain slice protocol, guided me in working with the cryostat and the immunohistochemistry protocols. Working as a team on such a large project is essential, and their contributions were invaluable.

I would like to thank our technical collaborators from the department of the *Institut Mines Télécome (IMT)* Nord Europe for their collection of UFP, as well as their work on granulometry and metal analysis. Special thanks go to Laurent Alleman, Espéranza Perdrix, and Véronique Riffault. Also thanks to Prof. Dr. Pierre Gosset and Nathalie Goetinck from the *Centre Biologie Pathologie* for their help with the Transmission Electron Microscopy. And to Prof. Dr. Mohamed Lamdani for his sharing knowledge about statistics.

By this way, I would also like to explain my special thanks to the Centre of Environmental Science (*Centrum voor Milieukunde – CMK,* University of Hasselt, Belgium), where I had the pleasure for being a guest researcher. A special thanks to Prof. Dr. Michelle Plusquin for making this opportunity possible, and Prof. Dr. Bert Brône (Biomed) for the engaging discussion on markers for synaptic impairment. But of course, I am also grateful to all my colleagues at CMK, especially Kenneth Vanbrabant and Leen Rasking, who are working on an international multiorgan project of ultrafine particle influences. You showed me the value of working on a shared model, with specialist across Europe, demonstrating that good communication can make it possible! Beyond our scientific interests, we also had plenty of enjoyable moments together, from sharing meals and celebrating the number of cohort participants with Bruno's pizza, to enjoying apero's at Fitlink. I hope more opportunities for shared experiences will come, whether they be in a professional or personal context. Thank you, Kenneth and Leen, thank you CMK!

Also a thanks to Prof. Dr. Armelle Baeza (*Unité de Biologie Fonctionnelle et Adaptive, Université Paris Cité*) and Dr. Stéphane Hunot (Laboratory Director at the Paris Brain Institute (ICM) – *Equipe 'thérapeutique expérimentale de la maladie de Parkinson'*) for their scientific advice and support during our annual meetings of the PhD following up.

I also want to give a special thanks to my previous academic life, which began in Leuven, Belgium. I am grateful to Dr. Hilde Theunckens, Dr. Vicky De Preter, and Dr. Karolien Descamps from the University College Leuven-Limburg for facilitating my journey to Lille in 2018. This continued with an Erasmus experience during my Master's, where Prof. Dr.

Joris Winderickx recognized my strong interest in returning to Lille and took on the role of co-promoter.

Thanks also to EURON, the European Graduate School of Neuroscience, which encourages neuroscience collaborations across seven universities. As the PhD representative for the University of Lille, I appreciate the support and opportunities provided by EURON. Thank you to our director, Dr. Gunter Kenis, and coordinator Damaris Kentgens-Zwaanswijk, you make borders disappear for the sake of science!

Thank you to the Doctoral Graduate School of Biology and Health (*l'Ecole Graduée Biologie Santé*) for believing in me and providing continuous support throughout this three-year journey. A special thanks to director Prof. Dr. Patrick Vermersch, and coordinator François Delcroix, whose guidance made it possible for me to complete this work and my PhD, paving the way for my future in the scientific world. I am deeply appreciative of their support. Additionally, I would like to thank Prof. Dr. Anne Tailleux for coordinating the Precision Health programme, and the financial support to go abroad to the CMK.

Of course, a special thanks goes to all my friends and family for their support, for understanding how busy I was during this journey, and for being a sympathetic ear when needed one. But above all, I want to thank my parents. Without their unwavering support, I would have never made it this far. They encouraged me to study, to work hard, and to never give up. Their guidance thought me to follow the right path and to literally push boundaries. Their perspective on life and education has shaped who I am today. I know they are proud of me, but they should also know, I am equally proud of them!

And last but not least, my two men, my home, supported me till the end! A heartfelt thank you to my loyal companion, Watson. He reminded me to take breaks, usually for treats or belly rubs. Your wagging tail has been a constant source of motivation! Thank you to my lovely partner, Florian, for being my rock throughout this rollercoaster of a PhD journey. Your unwavering support, patience (especially during the last stressed-out days), financial support when I no longer had a salary, and belief in me have meant more than I can ever put into words. Whether it was pretending to understand my research, celebrating small victories, or simply being there with hugs, you made this process infinitely more bearable. I couldn't have done it without you, well, maybe I could have, but it definitely wouldn't have been more manageable!

Luckily there was no page limit for this part… I hope you are still bright and early to read this PhD!

SUMMARY

FIGURE SUMMARY

TABLE SUMMARY

SUPPLEMENTARY DATA SUMMARY

Figures

Tables

ABBREVIATIONS

$^{\bullet}OH$	Hydroxyl radical
$^{\bullet}NO$	Nitric oxide
$^{\bullet}O_2^-$	Superoxide
4-HNE	4-hydroxynonenal
58-OA	58-related OA
AA	Anthracene
Ab	Antibody
ACB	Alveolar-capillary barrier
ACSL4	Acyl-CoA Synthetase Long Chain Family Member 4
ACSM	Aerosol chemical speciation monitor
AD	Alzheimer's Disease
ADRB2	Beta-2 adrenergic receptor
AhR	Aryl hydrocarbon receptor
AIF	Apoptosis-Inducing Factor
AINP	Alumina nanoparticles
ALOX15	Arachidonate 15-lipoxygenase
AMPK	AMP-activated protein kinase
AMS	Aerosol mass spectrometer
AN	Acenaphthene
ANL	Acenaphthylene
APAF1	Apoptotic protease activating factor 1
ARNT	Aryl hydrocarbon receptor nuclear translocator
ATF	Activating Transcription Factor
ATF6	Activating transcription factor 6
ATG	Autophagy-related gene protein
ATP	Adenosine triphosphate
BaA	Benzo[a]antracene
Baf A1	Bafilomycin A1
BAK	BCL-2 antagonist or killer
BaP	Benzo[a]pyrene
BAX	BCL-2-associated X protein
BBB	Blood-brain barrier
BbF	Benzo[b]fluoranthene
BBOA	Biomass burning OA
BCL-2	B-cell lymphoma 2
BDNF	Brain-derived neurotrophic factor
BeP	Benzo[e]pyrene
bFGF	Basic Fibroblast Growth Factor
BghiP	Benzo[g,h,i]perylene
BH3-only	B-cell lymphoma 2 (BCL-2) homology 3
BiP	Binding immunoglobulin protein
BkF	Benzo[k]fluoranthene
BSCB	Blood-spinal cord barrier

BTB	Blood-testis barrier
CAT	Catalase
CCOA	Coal combustion OA
cGPx4	Cytosolic glutathione peroxidase 4
CH	Chrysene
CHU	Centre Hospitalier Universitaire
CM-H2DCFDA	Diacetate 2',7'-dichlorodihydrofluorescein
CNS	Central nervous system
CNT	Carbon nanotubes
CO	Carbon monoxide
COA	Cooking-like OA
COX-2	Cyclooxygenase-2
CP	Ceruloplasmin
cPLA2	Cytosolic phospholipase A2
CREB	cAMP Response Element-Binding Protein
CRS	Chronic restraint stress
CSOA	Cigarette smoke OA
CYP	Cytochrome P450 enzymes
DA	Dopamine
DAMP	Danger-associated molecular patterns
DAT	Dopamine transporters
DBahA	Dibenzo[a,h]anthracene
DEP	Diesel exhaust particles
DFCH-DA	Dichloro-dihydro-fluorescein diacetate
DFO	Deferoxamine
DFP	Deferiprone
DMEM/F-12	Dulbecco's Modified Eagle Medium/Nutrient Mixture F-12
DMT1	Divalent metal transporter 1
Dp	Diameter particles
DRP1	Dynamin-related proteins
DTNB	5,5'-dithiobis(2-nitrobenzoic acid)
DTT	Dithiothreitol
eBC	equivalent black carbon
EOPS	Zone free from specific pathogenic organisms
EPA	Environmental Protection Agency
EPM	Elevated plus-maze
ER	Dndoplasmic reticulum
ERK1/2	Extracellular signal-regulated kinase 1/2
EU	European Union
EUL	Endotoxin Units
FA	Fluoranthene
FADD	FAS-associated death domain
FE	Fluorene
FELASA	Federation of European Laboratory Science Associations
Fer-1	Ferrostatin-1

FPN	Ferroportin
FTH	Ferritin heavy chain
FTL	Ferritin light chain
GAD	Glutamic Acid Decarboxylase
GAPDH	Glyceraldehyde-3-phophate dehydrogenase
GCL	Gamma-glutamylcystein ligase
GDP	Gross domestic product
GFAP	Glial fibrillary acid protein
GPx	Glutathione peroxidase
GQD	Graphene quantum dots
GR	Glutathione reductase
GSH	(Reduced) Glutathione
GSSG	Oxidized glutathione / Glutathione Disulfide
GST(-P)	Glutathione S-transferase (P subunit)
H_2O_2	Hydrogen peroxide
HAH	Halogenated Aromatic Hydrocarbons
HBEpiC	Human bronchial epithelial cells
HERC2	E3 ubiquitin protein ligase antibody
hESC	human embryonic stem cells
HMOX1	Heme oxygenase
HNE	Hydroxynonenal
HO	Heme oxygenase
HOA	hydrocarbon-like OA
HpCDD	Heptachlorodibenzo-p-dioxin
HpCDF	Heptachlorodibenzofuran
HPLC	High-performance liquid chromatography
HR	Hazard ratio with its 95% interval confidence
HRGC/HRMS	High-resolution gas chromatography/mass spectrometry
HRP	Horseradish peroxidase
HUVEC	Human umbilical vein endothelial cells
HxCDD	Hexachlorodibenzo-p-dioxin
HxCDF	Hexachlorodibenzofuran
Iba1	Ionized Calcium-Binding Adapter Molecule 1
ICAM-1	Intercellular cell adhesion molecules
ICP-MS	Inductively Coupled Plasma Mass Spectrometry
IFN-γ	Interferon γ
IKK	IκB kinase
IL	Interleukins
IMT	Institut Mines Télécome
IP	Indeno[1,2,3-c,d]pyrene
IP-10	Interferon Gamma-Induced Protein 10
iPSC	induced pluripotent stem cells
IRBE2	Iron responsive element binding protein 2
IRE1α	Inositol-requiring enzyme 1 α

KC/GRO-α	Keratinocyte Chemoattractant/human Growth-Regulated Oncogene
KEAP1	Kelch-like ECH-associated protein 1
LAL	Limulus Amebocyte Lysate
LC3	Microtubule-associated protein 1 light chain 3
LDH	Lactate dehydrogenase
LOH	Lipid alcohols
LOOH	Lipid hydroperoxides
LO-OOA	Less oxidised-oxygenated OA
LPO	Lipid peroxides
LPS	Lipopolysaccharides
LPX	Liproxstatin-1
LUHMES	Lund Human Mesencephalic (neuronal cell line)
L-VGCC	L-type voltage-gate calcium channels
MAP2	Microtubule-Associated Protein 2
MAPK	Mitogen-activated protein kinase
MBP	Myelin Basic Protein
MCP-1	Monocyte Chemoattractant Protein
MCR	*Mort cellulaire régulée*
MDA	Malondialdehyde
MFN1	Mitofusin 1
MIA	Maternal immune activation
MIF	Macrophage Migration Inhibitory Factor
MIP	Macrophage Inflammatory Protein
MOA-B	Monoamine oxidase-B
MOMP	Mitochondrial outer membrane permeabilization (
MO-OOA	More oxidised-oxygenated OA
MP	*Maladie de Parkinson*
$MPDP^+$	1-methyl-4-phenyl-1,2,3,6-tetrahydropyridinium ion
MPP+	1-Methyl-4-phenylpyridinium (a neurotoxin)
MPTP	1-methyl-4-phenyl-1,2,5,6-tetrahydropyridine
Mt	Metallothionein
mTOR	mammalian target of rapamycin
MWCNT	Multi-walled carbon nanotubes
Nap	Naphthalene
NBIA	Neurodegenerative disorders with brain iron accumulation
NC	Negative control
N-Ethylmaleimide	NEM
NeuN	Neuronal nuclear
Nfl	Neurofilament Light Chain
NF-κB	Nuclear factor-κB
N-GQD	Nitrogen-doped graphene quantum dots
NIK	NF-κB-inducing kinase
NLRP3	NOD-,LRR-and pyrin domain-containing protein 3
NMDA	N-methyl-D-aspartate

NOR	Novel Object Recognition
NOS2	Nitric oxide synthase 2
NOX1	NADPH oxidase 1
NQO-1	NAD(P)H quinone oxidoreductase
NR2B	N-methyl-D-aspartate (NMDA) receptor subunit
NRF2	Nuclear factor erythroid-2-related factor 2
NSC	Neuronal stem cells
O_2	Oxygen
OA	Organic aerosol
OCDD	Octachlorodibenzodioxin
OCDF	Octachlorodibenzofuran
Olig2	Oligodendrocyte Transcription Factor 2
$ONOO^-$	Peroxynitrite
OPA1	Optic atrophy 1 protein
OR	Odds ratio with its 95% interval confidence
PAH	Polycyclic Aromatic Hydrocarbons
PAN	Peroxyacyl nitrates
PARP-1	Poly(ADP-ribose) polymerase-1
PBDD/F	Polybrominated dibenzo-p-dioxins and furans
PC	Polycarbonate
PCB	Polychlorinated biphenyls
PCB 105	2,3,3',4,4'-pentaCB
PCB 114	2,3,4,4',5-pentaCB
PCB 118	2,3',4,4',5-pentaCB
PCB 123	2',3,4,4',5-penta
PCB 126	3,3',4,4',5-pentaCB
PCB 156	2,3,3',4,4',5-hexaCB
PCB 157	2,3,3',4,4',5'-hexa
PCB 167	2,3',4,4',5,5'-hexaCB
PCB 169	3,3',4,4',5,5'-hexaCB
PCB 189	2,3,3',4,4',5,5'-heptaCB
PCB 77	3,3',4,4'-tetraCB
PCB 81	3,4,4',5-tetraCB
PCNA	Proliferating cell nuclear antigen
PD	Parkinson's disease
PeCDD	Pentachlorodibenzo-p-dioxin
PeCDF	Pentachlorodibenzofuran
PERK	Protein kinase R (PKR)-like endoplasmic reticulum kinase
PFA	Paraformaldehyde
PH	Phenanthrene
PI3K	Phosphoinositide 3-kinase
PM	Particulate matter
pNA	p-nitroaniline
Prx	Peroxiredoxins

$Prx\text{-}S_2$	Oxidized Prx
PSD-95	Postsynaptic density protein
PtdIns3K	class III phosphatidylinositol 3-kinase
PUF	*Particules ultrafines*
PUFA	Polyunsaturated fatty acids
Pyr	Pyrene
Rapa	Rapamycin
RCD	Regulated cell death
RIPA	Radioimmunoprecipitation assay buffer
RONS	Reactive Oxygen and Nitrogen Species
ROS	Reactive oxygen species
RR	Risk ratio with its 95% interval confidence
RyR	Ryanodine receptors
SAGE	Sciences de l'Atmosphère et Génie de l'Environnement
SFOA	Solid fuel OA
SHG	Second harmonic generation
SN	Substantia Nigra
SOD	Superoxide dismutase
SOPF	Specific opportunistic and pathogen free
STS	Staurosporine
SVOC	Semivolatile organic compounds
SWCNT	Single-walled carbon nanotubes
tBID	(truncated) BH3-interacting domain death agonist
TCDD	Tetrachlorodibenzo-p-dioxin
TCDF	Tetrachlorodibenzofuran
TDPX-2	thioredoxin peroxidase 2
TEF	Toxicity Equivalency Factor
TEM	Transmission Electron Microscopy
TEQ	Toxicity Equivalent
TfR	Transferrin receptor
TGR	Thioredoxin glutathione reductase
TH	Tyrosine hydroxylase
TiO_2	Titanium dioxide
TNF-α	Tumor Necrosis Factor α
TPAF	Two-photon excited autofluorescence
TRX	Thioredoxin
$Trx\text{-}(SH)_2$	Reduced Trx
TrxR	Thioredoxin Reductase
$Trx\text{-}S_2$	Oxidized Trx
UFP	Ultrafine particles
ULK	Unc-51-like autophagy-activating kinase
UPR	Unfolded protein response
VCAM-1	Vascular cell adhesion molecules

VDAC	Voltage-dependent anion channel
VEGFA	Vascular Endothelial Growth Factor A
vGLUT	Vesicular Glutamate Transporter
VMAT2	Vesicular monoamine transporter 2
VOC	Volatile organic compounds
WB	Western blot
WHO	World Health Organization
XO	Xanthine oxidase
ZnO	Zinc oxide
ZnPP	Zinc protoporphyrin
β2AR/PI3K/Akt	β-Adrenergic Receptor-PI3K Signaling Crosstalk

ABSTRACT (ENGLISH)

Parkinson's disease (PD), the second most prevalent age-related neurodegenerative disorder, involves progressive dopaminergic neuronal loss in the Substantia Nigra *pars compacta*, driven by regulated cell death (RCD) pathways. While aging is the primary risk factor, PD's etiology is complex, with over 90% of cases being sporadic and linked to environmental factors and gene-environment interactions. Although genetic variants (e.g., *PARK2, GBA, LRRK2, SNCA*) contribute to familial PD, environmental influences such as air pollution-derived ultrafine particles (UFP) remain underexplored. Ferroptosis – an iron-dependent RCD involving lipid peroxidation – has emerged as a prevalent mechanism in PD pathology. While individual effectors, promotors, and inhibitors of ferroptosis have been studied, our lab (LilNCog) was the first to provide a comprehensive view of its role across *in vitro*, *ex vivo*, and *in vivo* PD models. The objective of this PhD research was to evaluate whether UFP exposure induces PD-related features, such as oxidative stress, neuroinflammation, and ultimately neuronal RCD; and to assess the possible contribution of UFP to PD-etiopathology using *in vitro* and *in vivo* models.

***In vivo* analysis**

Ten-week-old male BALB/c mice (n = 12/group) were intranasally exposed to UFP-doses (0, 10 or 30 µg) twice weekly for 12 weeks. An additional group was submitted to the same exposure schedule, followed by a 12 week recovery. Behavioral testing (i.e., open field, elevated plus-maze, Y-maze, spontaneous alternation, passive avoidance test) revealed no significant motor, anxiety, or cognitive impairments. However, brain metal analysis, aryl hydrocarbon receptor (AhR) and metallothionein (Mt) gene expression confirmed the UFP presence in whole brain tissue, followed by transmission electron (TEM) and femtosecond pulsed laser microscopy confirming UFP deposition particularly in the prefrontal cortex and SN. Increased glutathione oxidation, enhanced GPx activity, and upregulation of Nrf2 and Nf-κB pathways accompanied by the release of pro-inflammatory cytokines, indicated adaptative cellular defenses against oxidative stress and neuroinflammation. Interestingly, markers of RCD, including apoptosis (p-BAD/BAD, caspase-3), autophagy (ATG7, LC3b), ferroptosis (FTH1, 4-HNE), necroptosis (p-RIP3/RIP3, MLKL) and parthanatos (AIF, MIF) were suppressed in whole-brain tissue, reflecting robust adaptive resilience. No neuronal loss was detected in neurodegenerative key regions such as the SN (via TH staining) or the striatum (via NeuN staining).

However, PD is characterized at the endpoint through dopaminergic neurodegeneration, but before upstream events such as oxidative stress and neuroinflammation take place. More specific, the accumulation of UFP in the SN raises concerns about their potential

to trigger ferroptosis in dopaminergic neurons, which we answered through an *in vitro* approach.

***In vitro* analysis**

Therefore, LUnd Human MESencephalic (LUHMES) cells (CRL-2927™), differentiated into mature dopamine-like neurons, were exposed to UFP (2 and 10 µg/cm²) for 24 hours. Iron uptake (TfR), intracellular iron storage (ferritin), glutathione status (GSSH/GSH ratio, glutathione peroxidase activity: GPx, protein level cGPx4, x_c^-/SLC7A11, P53), and lipid peroxidation (4-HNE) were investigated, together with the potential inhibition by some specific ferroptotic inhibitors (liproxstatin-1: LPX, deferiprone: DFP). Additionally, selective autophagy (NCOA4), autophagic cell death (LC3b) and apoptosis (BAX, caspase-3/7, -8 and -9 activities) were studied as well to get a complete RCD overview. Comparative exposure to 5 µM 1-methyl-4-phenylpyridinium (MPP^+), a toxin widely used in PD models, was applied to assess the degree of UFP neurotoxicity in comparison to a well-characterized model of dopaminergic cell death.

This study is the first to demonstrate that acute exposure to iron-containing urban-industrial UFP leads to dopaminergic cell alterations via the P53/x_c^-/GSH/cGPx4 axis. Importantly, the ability of LPX to mitigate these ferroptotic changes supports the hypothesis that chronic exposure might lead to neurodegeneration. Moreover, both MPP^+ and UFP exposures produced similar outcomes, particularly in terms of increased oxidative stress, disruption of the GSH/GSSG balance, and GPx activation.

An article on this in vitro study is currently under evaluation by the journal *Toxicology and Applied Pharmacology*.

Given the increasing incidence of PD, particularly in highly polluted urban areas, the lack of effective therapies, and the absence of policies addressing UFP exposure, this PhD research underscores the need for greater awareness of UFP neurotoxicity.

RESUME (FRANÇAIS)

La maladie de Parkinson (MP), deuxième trouble neurodégénératif lié à l'âge en termes de prévalence, se caractérise par une perte progressive des neurones dopaminergiques de la Substantia Nigra *pars compacta*, perte médiée par des voies de mort cellulaire régulée (MCR). Bien que le vieillissement soit le principal facteur de risque, l'étiologie de la MP est complexe. Plus de 90% des cas sont sporadiques et associés à des facteurs environnementaux ainsi qu'à des interactions gène-environnement. Bien que certaines variants génétiques (par ex., *PARK2, GBA, LRRK2, SNCA*) soient liés à des formes familiales de MP, les influences environnementales, telles que les particules ultrafines (PUF) issues de la pollution atmosphérique, restent peu étudiées. La ferroptose – une MCR fer-dépendante impliquant la peroxydation lipidique – s'est imposée comme un mécanisme prévalent dans la pathologie de la MP. L'objectif principal de cette these était de déterminer les effets neurotoxiques de l'exposition aux PUF, en se concentrant sur les caractéristiques liées à la MP, telles que les modifications des fonctions motrices et cognitives, le stress oxydatif neuronal, les altérations métalliques cérébrales, la neuroinflammation et la neurodégénérescence, notamment à travers les voies de MCR.

Étude *in vivo*

Des souris mâles BALB/c âgées de 10 semaines (n = 12/groupe) ont été exposées par une instillation intranasale à différentes doses de PUF (0, 10 ou 30 µg) deux fois par semaine pendant 12 semaines. Un groupe supplémentaire a suivi le même schéma d'exposition, suivi d'une récupération de 12 semaines sans exposition aux PUF. Les tests comportementaux (actimétrie en openfield, labyrinthe en croix surélevé, Y-maze spatial, alternance spontanée en Y-maze, test d'évitement passif) n'ont révélé aucune altération significative des fonctions motrices, de l'anxiété ou des capacités cognitives. Toutefois, des analyses métalliques du cerveau, ainsi que l'expression des gènes du récepteur des hydrocarbures aromatiques (AhR) et de la métallothionéine (Mt), ont confirmé la présence de PUF dans le cerveau entier. Cette présence a été validée par microscopie électronique à transmission (TEM) et microscopie laser femtoseconde, indiquant une accumulation de PUF en particulier dans le cortex préfrontal et la Substantia Nigra (SN).

Une augmentation de l'oxydation du glutathion, une activité accrue de la GPx et une régulation positive des voies Nrf2 et NF-κB, accompagnées de la libération de cytokines pro-inflammatoires, ont montré des réponses adaptatives cellulaires contre le stress oxydatif et la neuroinflammation. Fait intéressant, les marqueurs de MCR, y compris de l'apoptose (p-BAD/BAD, caspase-3), de l'autophagie (ATG7, LC3b), de la ferroptose (FTH1, 4-HNE), de la nécroptose (p-RIP3/RIP3, MLKL) et de la parthanatose (AIF, MIF), étaient supprimés dans le tissu cérébral entier, traduisant une résilience adaptative

robuste. Aucune perte neuronale n'a été détectée dans les régions clés de neurodégénérescence telles que la SN (TH) ou le striatum (NeuN).
Une publication est en cours de rédaction pour cette partie.

Cependant, la MP se caractérise par une neurodégénérescence dopaminergique en phase terminale, précédée d'événements en amont tels que le stress oxydatif et l'inflammation. Plus spécifiquement, l'accumulation de PUF dans la SN soulève des inquiétudes quant à leur potentiel à induire une ferroptose dans les neurones dopaminergiques. L'étude *in vitro* permet de répondre à cette question.

Étude *in vitro*
Des cellules LUHMES (Lund Human Mesencephalic Cells, CRL-2927™), différenciées en neurones dopaminergiques matures, ont été exposées à des PUF (2 et 10 µg/cm²) pendant 24 heures. Ont été examinés l'absorption du fer (TfR), le stockage intracellulaire de fer (ferritine), l'état redox du glutathion (rapport GSH/GSSG, activité de la glutathion peroxydase : GPx, protein niveaux de cGPx4, x_c^-/SLC7A11, P53) et la peroxydation lipidique (4-HNE), avec une évaluation de l'inhibition potentielle par des inhibiteurs spécifiques de la ferroptose (liproxstatine-1 : LPX, déféripRone : DFP). Des études complémentaires ont porté sur l'autophagie sélective (NCOA4), la mort cellulaire autophagique (LC3b) et l'apoptose (BAX, activités des caspases-3/7, -8 et -9). Une exposition comparative à 5 µM de 1-méthyl-4-phénylpyridinium (MPP^+), une toxine largement utilisée dans les modèles de MP, a permis de comparer la neurotoxicité des PUF à celle d'un modèle bien établi de mort neuronale dopaminergique.
Cette étude est la première à démontrer qu'une exposition aiguë à des PUF urbains et industriels contenant du fer induit des altérations neuronales dopaminergiques via l'axe P53/x_c^-/GSH/cGPx4. La capacité de la LPX à atténuer ces altérations ferroptotiques renforce l'hypothèse qu'une exposition chronique pourrait conduire à une neurodégénérescence. En outre, les expositions à la fois au MPP^+ et aux PUF ont produit des résultats similaires, notamment une augmentation du stress oxydatif, une perturbation de l'équilibre GSH/GSSG et une activation de la GPx.
Un article relatif à l'étude *in vitro* est actuellement en cours d'évaluation dans la revue *Toxicology and Applied Pharmacology*.

Face à l'augmentation de l'incidence de la MP, en particulier dans les zones urbaines fortement polluées, au manque de thérapies efficaces et à l'absence de réglementation sur les PUF, les travaux de thèse soulignent l'urgence de sensibiliser davantage au potentiel neurotoxique des PUF.

CHAPTER I. INTRODUCTION

I. RESEARCH CONTEXT

I.1 Parkinson's disease

Parkinson's disease (PD), the second most prevalent age-related neurodegenerative disorder (Hirtz *et al.*, 2007), affects worldwide over 10 million people. (Ball *et al.*, 2019), with 1-2% of the population over age 50 impacted (Thomas & Beal, 2007).

The primary locus is the nigrostriatal pathway, containing Substantia Nigra *pars compacta* (SN*pc*) with neuromelanin pigmented dopaminergic neurons and axons projecting to the putamen (a section of the dorsal striatum). The classic unilateral feature is the selective and progressive cell death of dopaminergic neurons of the SN*pc*, leading to the lack of neurotransmitter dopamine (DA). Depletion of DA in the basal ganglia causes delayed and uncoordinated movement, which directly explains the motor symptoms (bradykinesia, resting tremor, rigidity, and postural instability) (Mhyre *et al.*, 2012). Besides, there are multiple and variable non-motor symptoms, such as cognitive decline, depression, anxiety, and a total dysautonomia (Fearnley & Lees, 1991). Equally important to the dopaminergic neuronal cell death is the appearance of α-synuclein aggregates, the so-called Lewy Bodies or Lewy neurites, which classifies PD as the most frequent synucleinopathy (Miller *et al.*, 2021).

Only the most dominant molecular and cellular alterations causing this neurodegenerative disease are covered in this chapter. For instance, an increase in free toxic radicals might contribute to mitochondrial dysfunction. When the detoxification of reactive intermediates fails, oxidative stress occurs, which contributes to the formation of protein and cellular damage (Chang & Chen, 2020). Excessive autoxidation causes lipid peroxidation, another hallmark of PD (Liu *et al.*, 2008). This chain reaction by which membrane phospholipids (e.g., polyunsaturated fatty acids (PUFA)) are oxidatively degraded into lipid hydroperoxides (LOOH) and generates numerous toxic by-products, results in membrane damage. According to a post-mortem PD brain analysis, lipid peroxidation adducts (e.g., hydroxynonenal (HNE)) are localized in Lewy bodies (Castellani *et al.*, 2002). To indicate the importance of this feature, another study suggests that lipid peroxide by-products (e.g., malondialdehyde (MDA)) may serve as a plasma staging disease biomarker of PD (de Farias *et al.*, 2016). Moreover, the fact that iron ions promote PUFA breakdown into HNE is another remarkable feature (Guéraud *et al.*, 2010) especially, as there is a strong correlation between iron accumulation and neurodegenerative diseases, as demonstrated in 1924 (Lhermitte *et al.*, 1924). The increase of iron content in the SN*pc* is confirmed by several post-mortem and MRI

studies (Dexter, Wells, *et al.*, 1989; Jellinger *et al.*, 1990; Sofic *et al.*, 1991; Sofic *et al.*, 1988). Disrupted iron brain metabolism leads to the formation of oxygen free-radical species such as superoxide anions ($O_2^{\bullet -}$) and hydroxyl radicals ($^{\bullet}OH$), which can exacerbate in cell damage and produce neuroinflammation, also one of the key hallmarks of PD (Dashtipour *et al.*, 2015).

I.2 Ultrafine particles and their brain translocation

Since the early 20th century, rapid industrialization and urbanization have significantly intensified environmental pollution (Wu *et al.*, 2016). Air pollution has become a growing concern worldwide, particularly in developing nations (Cohen *et al.*, 2017). According to the World Health Organization's (WHO) global environmental pollution database, all of the top 20 most polluted cities are located in developing countries. Moreover, nearly 98% of cities in these regions with populations exceeding 100 000 do not meet the WHO air quality standards (X. Zhang *et al.*, 2018). People in metropolitan areas are affected by acute, subchronic, or chronic exposures to air pollution, via diesel, industrial, or refinery exhaust emissions.

The heterogeneous composition of air pollutants includes ozone (O_3), nitrogen dioxide (NO_2) and sulphur dioxide (SO_2), as well as particulate matter (PM), an airborne component that contributes to a variety of diseases. Due to the diversity of its characteristics, including size, sources, and composition, PM has a wide range of effects. The general subdivision is based on grain size. This is an appropriate classification as the health problems are directly linked to the aerodynamic diameter of particles. The transportation in the atmosphere and/or inhaling ability is size-dependent. Therefore, the Environmental Protection Agency (EPA) provides a two-part classification: inhalable particles or PM_{10} with an aerodynamic diameter less than 10 µm, and fine inhalable particulates with an aerodynamic diameter of maximum 2.5 µm, commonly known as $PM_{2.5}$ (United.States.Environmental.Protection.Agency, 2022). Some articles or researches prefer the three-part classification, next to PM_{10} and $PM_{2.5}$; $PM_{0.1}$ is also distinguished. Those ultrafine particles (UFP) with a maximum aerodynamic diameter of 0.1 µm, are included to the classification as they have specific health effects on various organs, including the brain, due to their escape from phagocytosis by alveolar macrophages and their easily passage into the bloodstream crossing the alveolar-capillary barrier (ACB) by the biological gas exchange process (Fig.1) (Mühlfeld *et al.*, 2008; Oberdörster & Utell, 2002; Schraufnagel, 2020). Repeated exposure to UFP can cause cellular mitochondrial alterations in body tissue (Sotty *et al.*, 2020), followed by peripheral inflammation (Kumar *et al.*, 2013).

As above-mentioned, the brain is not spared; intravenous-administered UFP penetrates the blood-brain barrier (BBB), a protective barrier made up of endothelial cells

that restricts the entry of unnecessary substances into the central nervous system (CNS) (Kreuter, 2001). This penetration indicates that these particles do reach the brain. Recent research has shown that the penetration of nanoparticles is an exacerbating effect. Specifically, it has been clarified that reactive oxygen species (ROS) produced by diesel exhaust particles (DEP) and urban particles can disrupt the BBB (Oppenheim *et al.*, 2013). Exposure to these pollutants leads to endothelial cell damage in the brain's blood vessels, evidenced by increased expression of intercellular (ICAM-1) and vascular (VCAM-1) cell adhesion molecules activated through the ERK/AKT/nuclear factor-κB (NF-κB) pathway (Rui *et al.*, 2016). Additionally, *in vitro* studies using rat brain capillaries show that PM, including UFP, triggers the production of proinflammatory cytokines and ROS, while reducing the expression of key tight junction proteins suggesting that these particles might compromise the integrity of the BBB (Hartz *et al.*, 2008; Kim *et al.*, 2022). On the other side, a small but considerable portion of inhaled UFP (estimated between 2 and 16%) can penetrate directly the olfactory mucosa and translocate via the olfactory epithelium and olfactory bulb until the olfactory cortex (Ajmani *et al.*, 2016), where it can be transported by neurons, via transsynaptic transport, to other brain regions (Oberdörster *et al.*, 2004; Oberdörster & Utell, 2002). Interestingly, nasal and olfactory barriers in persons living in high-polluted areas can be broken down, allowing UFP to enter the brain more easily through the olfactory bulb (Calderón-Garcidueñas *et al.*, 2010). Additionally, various types of exogenous nanoparticles, such as ZnO, Fe_3O_4, TiO_2, and carbon black particles, have also been detected in human cerebrospinal fluid and therefore been investigated in *in vitro* BBB models (Guo *et al.*, 2021; Qi *et al.*, 2022).

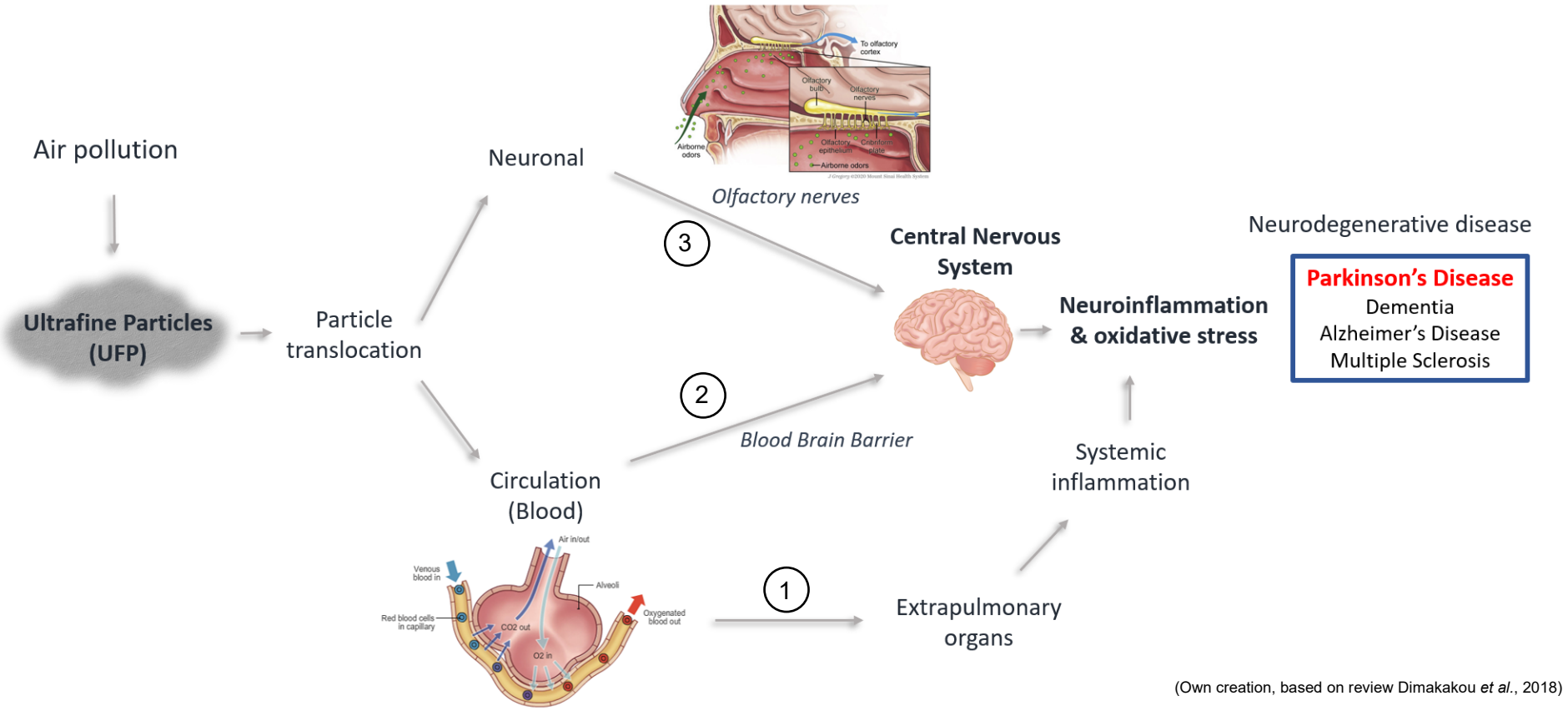

(Own creation, based on review Dimakakou *et al.*, 2018)

Figure 1: Ultrafine particles brain translocation.

[1] Ultrafine particles (UFP) as a part of air pollution can enter the circulation and effects extrapulmonary organs, leading to a systemic inflammation that induces oxidative stress and neuroinflammation in the central nervous system (CNS). [2] When in circulation, UFP can damage the blood-brain barrier (BBB) or can pass directly through their small size to reach the CNS. [3] Additionally, the CNS can be reached by the neuronal particle translocation as it can be up taken by olfactory nerves which are not protected by the BBB (Dimakakou *et al.*, 2018).

Abbreviations: BBB: blood-brain barrier; CNS: central nervous system; UFP: ultrafine particles

UFP are considered highly neurotoxic compared to larger particles. Their effects include (1) causing overall inflammation of the body, which can indirectly stimulate neuroinflammation, and (2) directly inducing neuroinflammation and oxidative stress by translocating to the CNS. This translocation can occur either indirectly through the circulation by crossing the BBB and blood-spinal cord barrier (BSCB), or directly via the olfactory bulb (Dimakakou *et al.*, 2018). (Fig.1)

Until recently, UFP was not studied so much, as it was thought that those particles are short-lived and disappeared through heterogeneous and homogeneous aggregation within seconds or minutes. This hypothesis led to the exclusion of UFP as regulated pollutants in the Clean Air Act (CAA), which imposes restrictions on six primary air pollutants (i.e., CO, Pb, NO_2, O_3, SO_2 and $PM_{2.5}$ / PM_{10}). This is contradictory as UFP account for the majority of vehicle emission and is constantly generated in large quantities to which individuals are exposed, making the toxicity of UFP extra relevant to study (Oberdörster & Utell, 2002). Fig. 2 illustrates that, while UFP contribute minimally to the overall mass of PM, they constitute a significant proportion in terms of particle number. Consequently, UFP tend to arrange themselves through nucleation processes (Bagley *et al.*, 2002).

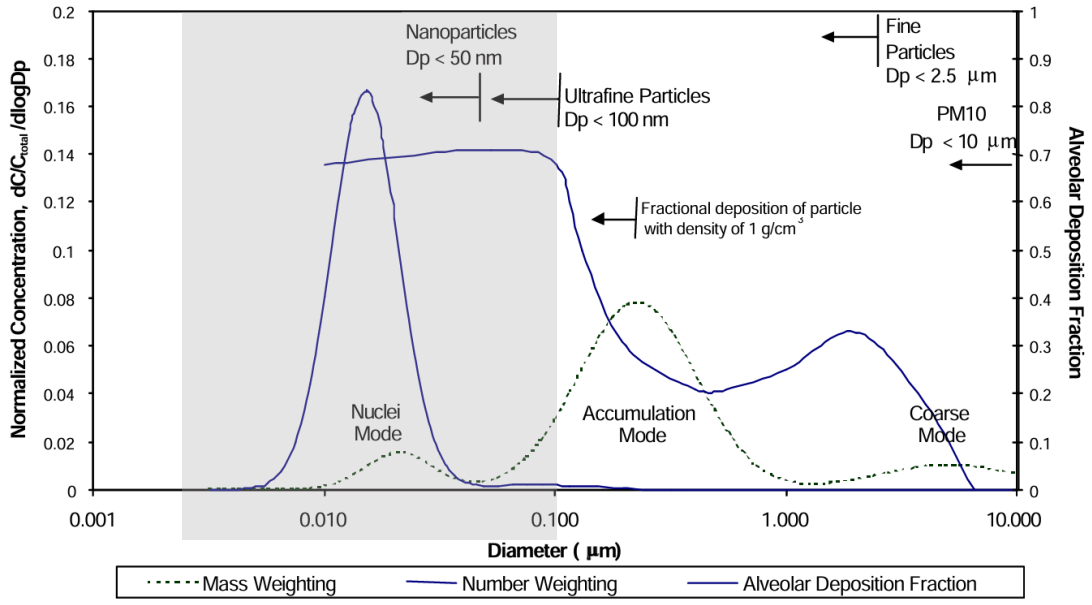

Figure 2: Relationships between the aerosol particle number and mass-weighted size distributions, alongside the alveolar deposition curve.

The grey square highlights the ultrafine particles (UFP), which, despite having a low mass contribution, are present in high numbers. Additionally, the alveolar deposition is notably high, indicating that UFP can easily penetrate deep into the lungs, with minimal retention in the upper airways, bronchial tubes, and bronchioles (Bagley *et al.*, 2002).

Abbreviations: Dp: Diameter particles; UFP: Ultrafine particles.

In addition to the fact that UFP can account for a significant portion of air pollution, size also affects their translocation, as shown Fig. 2, where the Alveolar Deposition Fraction is particularly high for UFP. Regarding toxicity, mice intranasally exposed to 14 nm carbon black particles for four weeks exhibited increased mRNA levels of inflammatory markers such as interleukin (IL)-1β, Tumor Necrosis Factor α (TNF-α), CCL2, CCL3, and CXCL9 in their olfactory bulbs, compared to those exposed to larger particles (Long *et al.*, 2013; Yamamoto *et al.*, 2006). Probably, two mechanisms govern the size-selective transport of UFP in the olfactory bulb: one at the level of olfactory receptors in the epithelium, and the other during axonal transport to the olfactory bulb (Ajmani *et al.*, 2016).

I.3 Ultrafine particules source and composition

The considerable heterogeneity and variability in the composition of PM make it challenging to fully characterize its physical, chemical, and biological properties. This complexity is due to the diverse sources of emissions, whether natural or human-made, as well as the influence of weather conditions on the transport, dispersion, and transformation of these particles, which can vary across time and location.

Anthropogenic (human-made) sources include (1) combustion engines (diesel and petrol), (2) solid-fuel combustion (coal, heavy oil, or biomass) for energy production in households and industry, (3) industrial activities (construction and mining), and (4) road traffic-related erosion and wear of brakes and tires. Natural source of primary PM involve soil and dust re-suspension, particularly in arid regions or during events like the long-range transport of Sahara dust from North Africa to Europe. In contrast, secondary particles formed in the atmosphere through chemical or physical reactions involving primary particles and atmospheric components (NH_3, SO_2, NOx, or organic compounds), or through the atmospheric transformation of gaseous pollutants. For instance, nitrogen oxides, mainly emitted by traffic and some industrial processes, and sulfur dioxide, released during the combustion of sulfur-containing fuels, undergo such transformations in the atmosphere (Ryou *et al.*, 2018; Saleh *et al.*, 2023; Thangavel *et al.*, 2022).

The physical and chemical properties of particulates, along with their toxicokinetics — that is, how they are distributed and persist in the body — are directly influenced by their composition. The presence of highly harmful compounds determines their oxidative, allergenic, and carcinogenic potential, highlighting the importance of analyzing their makeup to assess their toxicity. Complete combustion would turn all carbon of the fuel into carbon dioxide and water. But PM are produced during the incomplete combustion of fossil fuels, biomass, and biofuels. Combustion-derived PM typically has a

carbonaceous core known as ‘black carbon’. The carbon core is often coated with several layers of various substances, including inorganic compounds (such as sulfates, nitrates, ammonia, sodium chloride), toxic metals, semivolatile organic compounds (SVOC) and mineral dust. Additionally, biological components such as sea salt, allergens (pollen) and microbial compounds (spores) are also present in PM. Moreover, UFP have a high surface area relative to their mass, this means that UFP have a larger area available for adsorptions of gases and other compounds, making them more reactive compared to larger particles (Ariya & Amyot, 2004; Kristensen *et al.*, 2023; Ryou *et al.*, 2018; G. Zhang *et al.*, 2020).

Particles can either be directly emitted into the air as “primary PM” or formed through chemical reactions between primary particles and atmospheric components. Reactions between gaseous precursors (SO_2, NO_x, NH_3 and non-methane VOC) in the atmosphere can also result in the formation of “secondary PM”. As a result, aerosols can shift between size ranges. The atmospheric surface area distribution related to mass transfer and particle removal was first described by Whitby (1976), and illustrated in Fig. 3. The smallest size range, the Aitken nuclei range, includes UFP from 0.001 to 0.08 μm. This range encompasses primary aerosols from combustion sources like diesel engines, as well as secondary aerosols formed through the coagulation of primary particles into chain-like agglomerates. The next range, the accumulation mode, spans 0.08 to 1.0 μm. It contains particles emitted within this size range and those that grow through coagulation and condensation from the nuclei range. Finally, the coarse aerosol range convers particles from 1.0 to approximately 40 μm. These aerosols typically result from mechanical processes such as grinding, mechanical fracture, and material handling or natural sources, such as volcanic eruptions. Under most conditions, there is minimal transfer between the nuclei and accumulation modes to the coarse particle mode (Whitby *et al.*, 1976).

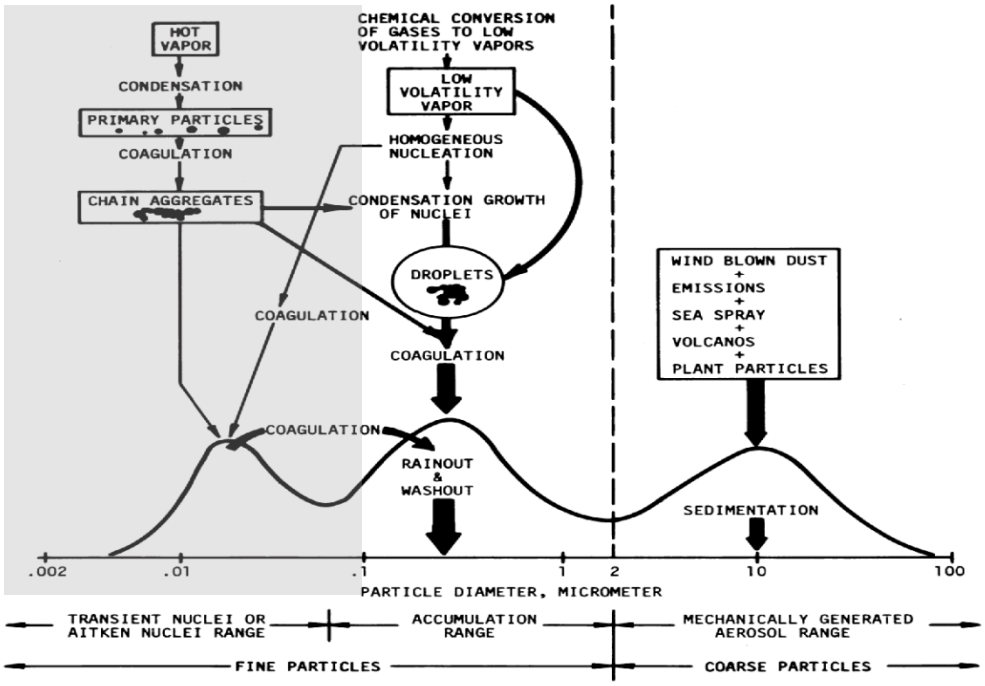

Figure 3: Atmosphere dynamics of particulate matter in the formation of secondary particles.

Secondary aerosols are produced through the reaction of primary particles and gases, a process that involves three key steps: [1] Nucleation mode: High-temperature emissions and vapor conditions from gas emissions lead to the nucleation of ultrafine particles (UFP), forming initial nuclei, also known as Aitken nuclei. [2] Condensation: As the atmosphere cools, fine particles, typically less than 2 µm in diameter, condense into liquid droplets. [3] Agglomeration: Weather conditions, such as turbulence, can cause aerosols to agglomerate. As particles grow in size due to agglomeration, larger, coarse particles may eventually sediment out of the air (Whitby *et al.*, 1976).

Abbreviations: UFP: Ultrafine particles

Before digging deeper onto the possible implication of UFP as contributor to PD, an overview of the main characteristics of UFP is showed in Fig. 4.

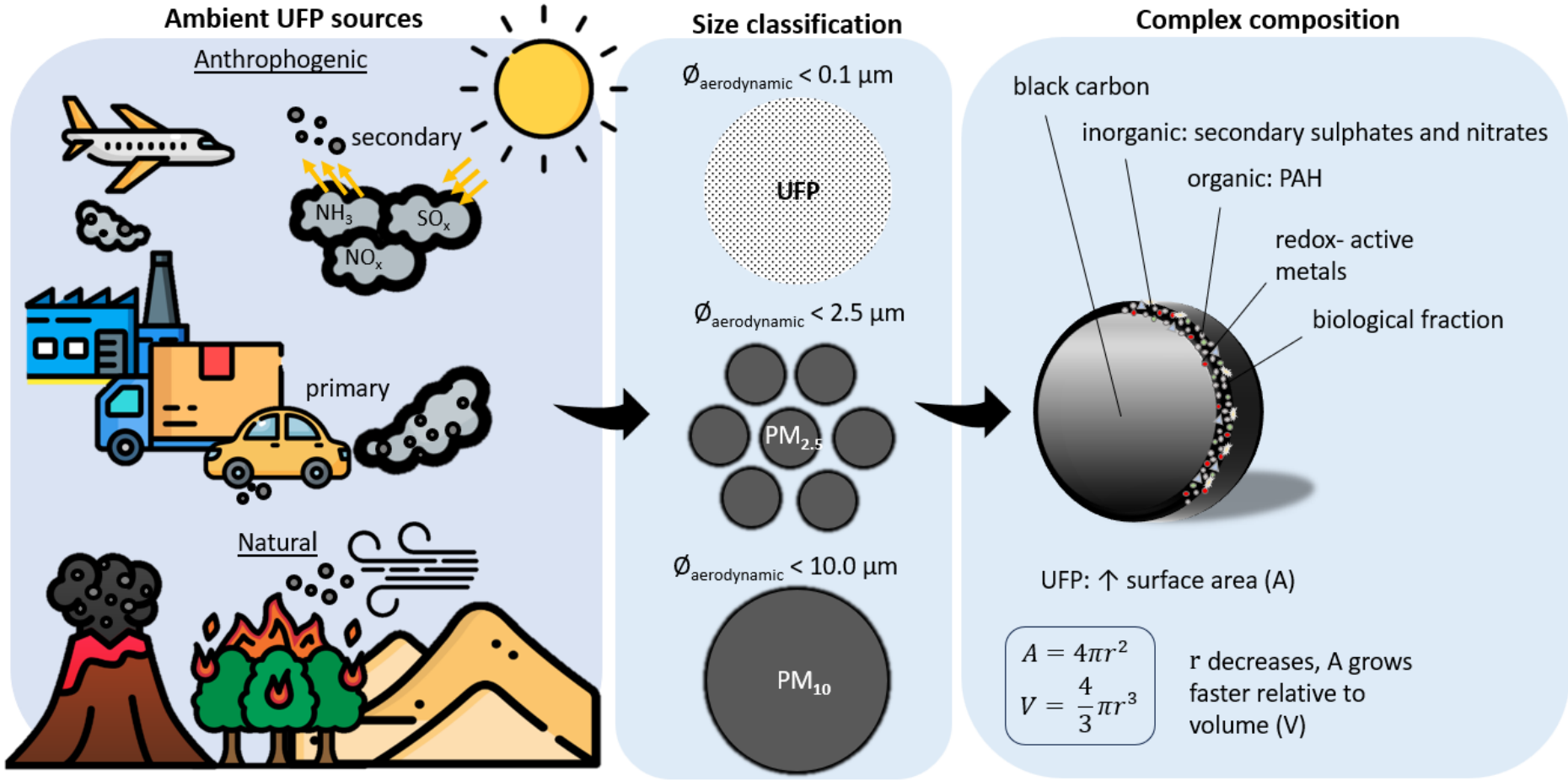

Figure 4: Ambient ultrafine particle sources, Size classification, and Complex composition of UFP. (Own creation)

[1] Sources of ultrafine particles (UFP): UFP originate from various sources, classified as anthropogenic or natural. Anthropogenic sources include agricultural operations, industrial processes, combustion of wood and fossil fuels, construction and demolition activities, and road dust resuspension. Natural sources encompass volcanic eruptions, wildfires, and dusty roads. Primary particulate matter (PM) are directly emitted from sources and can react with atmospheric compounds. Additionally through complex reactions between gaseous precursors (e.g., SO_2, NO_x, NH_3 and non-methane volatile organic compounds (VOC)) secondary pollutants may occur, such as secondary PM or tropospheric ozone (O_3), peroxyacyl nitrates (PAN), photochemical oxidants, formed in the presence of sunlight. [2] Size classification: PM is typically classified by size into three groups: coarse particles (PM_{10}), fine particles ($PM_{2.5}$), and UFP ($PM_{0.1}$) each time the number is indicating the maximum size in micrometer, meaning that UFP have an maximum aerodynamic diameter of 0.1 µm (100 nm). [3] Complex composition: UFP consist of a black carbon core surrounded by inorganic and organic compounds, biological materials, and redox-active metals. Smaller particles, such as UFP, have a larger relative surface area, allowing more toxic compounds to attach, increasing their potential toxicity.

Abbreviations: PAN: Peroxyacyl nitrates; PM: Particulate matter; UFP: Ultrafine particles; VOC: Volatile organic compounds

I.4 Environmental etiology of Parkinson's disease

Although aging remains the main risk factor for developing neurodegenerative diseases, they are multifaceted heterogeneous disorders from which the clinical and pathological aspect is very complex, with a mostly unknown etiology. Knowing that PD is associated to gene variants (*PARK2, GBA, LRRK2, SNCA*), it is also known that more than 90% of the PD cases are sporadic, highlighting to the importance of the environment or gene-environment interactions (Jin *et al.*, 2014). Some pesticides (paraquat, rotenone) (Tanner *et al.*, 2011)), metals (manganese (Martins *et al.*, 2019)) or solvents (trichloroethylene (Liu *et al.*, 2018)) are environmental elements thought to be connected to PD, making studies between environment and PD very attractive. To give a complete overview of previous studies, this chapter covers following paragraphs: 1.4.1 The MPTP/MPP^+ model, pharmacological tool for parkinsonism; 1.4.2 Epidemiological evidence of particulate matter as a contributor to Parkinson's disease; 1.4.3 Particulate matter exposure resulting in cognitive decline and dementia in elderly people; 1.4.4 Possible underlying mechanisms of ultrafine particles as risk factor of Parkinson's disease.

I.4.1 The MPTP/MPP^+ model, pharmacological tool for parkinsonism

The first evidence that environment can trigger PD was demonstrated by (Davis *et al.*, 1979). IV injections with meperidine analogues ensured the development of parkinsonism in a 23-year-old man. This paved the way to further investigation with other drug IV injections. Langston and Ballard (Langston *et al.*, 1983) identified a potent dopamine neuron toxicant, namely 1-methyl-4-phenyl-1,2,5,6-tetrahydropyridine (MPTP) which can pass through the BBB, where it converts by monoamine oxidase-B (MOA-B) of glial cells (astrocytes) into dihydropyridinium ion ($MPDP^+$) (Reviewed in (Przedborski *et al.*, 2001). After auto-oxidation, the component is structurally changed again into toxic 1-methyl-4-phenylpyridinium (MPP^+). Due to its polarity, dopamine transporters (DAT) can selectively uptake MPP^+ into the dopaminergic neurons (Dauer & Przedborski, 2003). Whereafter, it inhibits the mitochondrial complex I, resulting in reduction of adenosine triphosphate (ATP). In addition, the accumulation of MPP^+ in DA neurons results in mitochondrial ROS production (Muralikrishnan & Mohanakumar, 1998). Furthermore, MPP^+ stimulates the release of DA (Obata & Chiueh, 1992), followed by DA auto-oxidation, resulting in formation of cytotoxic quinones and extremely reactive oxygen radicals, which can further progress in various types of ROS (Umek *et al.*, 2018).

Evidently, being exposed to MPTP is clearly a rare phenomenon. It is not an often-reported toxin, the risk of people acquiring PD by this toxin is quite low. On the other

hand, as it fuels a PD-phenotype, it has become an excellent tool for modeling PD *in vitro* and *in vivo* (Dauer & Przedborski, 2003; Fox & Brotchie, 2010; Przedborski *et al.*, 2001).

I.4.2 Epidemiological evidence of particulate matter as a contributor to Parkinson's disease

Since it is unquestionably that urban air pollution is a toxicological risk and a public health concern, it attracts significant attention. The majority of the health conditions being researched are related to lung and allergic diseases, but a variety of other health issues, such as cardiovascular effects or even premature mortality, are also prominent research topics. Moreover, new data has recently emerged pointing to a negative correlation between air pollution and CNS diseases (stroke, dementia, Alzheimer's Disease (AD), multiple sclerosis) has recently emerged (Block & Calderón-Garcidueñas, 2009; Noorimotlagh *et al.*, 2021; Peters *et al.*, 2019). A few epidemiological studies have specifically investigated the potential association between $PM_{2.5}$ and the risk or incidence of PD, as shown in Table 1.

Most studies have been conducted on populations whose data come from large national health insurance databases. A few case-control studies are also available. Pollution data on $PM_{2.5}$, in turn, are derived from modeling based on data from air quality monitoring networks. Most studies highlight significant associations between the incidence, hospitalization (worsening), or symptomatology of PD and long-term exposure to $PM_{2.5}$, with association indicators ranging from 1.09 to 1.42.

The first study investigated the prevalence of PD among Agricultural Health Study participants in two communities, North Carolina and Iowa . Moreover, in two studies the rate of hospitalization for PD was investigated in 50 Northeastern American cities.

Globally, a very high association reports a fourfold increased risk of PD when $PM_{2.5}$ concentrations exceed twice the WHO air quality standards. In addition, several studies report a dose-response relationship, which supports the hypothesis of a causal link. In conclusion, recent epidemiological data support a significant relationship between long-term and short-term exposure to $PM_{2.5}$. Given that UFP are included in the measurements of $PM_{2.5}$, it is reasonable to hypothesize that UFP, whose toxic potential is considerably higher compared to that of $PM_{2.5}$, are likely responsible for the observed associations.

Table 1. Epidemiological studies on $PM_{2.5}$ exposure and Parkinson's disease outcomes (published between 2014 and 2024).

Reference	Population (country)	Design	Association
(Zanobetti *et al.*, 2014)	Adults (USA) (n= 6,982,678 overall deaths and 40,496) hospitalizations for PD	Case-crossover study	Risk of PD hospitalization: increase of 3.23%, [1.08, 5.43] for a short term 10 µg/m^3 increase in the 2 days average
(Kioumourtzoglou *et al.*, 2016)	Adults (USA) (n= 9.8 millions of subjects followed up)	Population-based cohort	Risk of first PD admissions: HR = 1.08 [1.04, 1.12] per 1-µg/m^3 increase in annual $PM_{2.5}$ concentrations
(Liu *et al.*, 2016)	Adults (USA) Cases PD n= 1,556 Controls n= 3,313	Nested case-control study	Risk of PD among never smoker females: OR of $PM_{2.5}$ Q5 vs. Q1 = 1.79 [1.01, 3.17]
(Shin *et al.*, 2018)	Adults (Canada) (n= 22,000,000)	Population-based cohort	Each interquartile increment (3.8 µg/m^3) of $PM_{2.5}$ was associated with a 4% increase in incident PD OR = 1,04 [1.01-1.08]
(Wang *et al.*, 2020)	Adults (China) (n= 10,077,029)	Meta-analysis (3 cohorts and 3 case/control studies)	With every 10 µg/m^3 increment, the risk of RR = 1.03 [0.98, 1.07], 1.21 [0.95, 1.54], and 1.01 [0.97, 1.05] for the total PM, $PM_{2.5}$, and PM_{10}, respectively
(Rhew *et al.*, 2021)	Adults (USA) (High exposed n= 1,665,073 person-years Low-exposed n= 357,574 person-years)	Population-based exposed ($PM_{2.5}$ ≥ 10 µg/m^3) and low-exposed ($PM_{2.5}$ ≤ 7.61 µg/m^3)	Disease-specific mortality: OR = 1.10 [0.95–1.27] Hospital admissions: OR = 1.33 [1.24–1.44] and specifically OR = 1.31 [1.21–1.42] for white population and OR = 1.2 [0.91–1.61] for African-American
(Jo *et al.*, 2021)	Adults (Korea) (n= 78,830)	Population-based cohort	No significant association with $PM_{2.5}$
(Nunez *et al.*, 2021)	Adults with PD (USA) (n= 8,100 annual admissions)	Population-based data base for hospital admission and hospitalization	Risk of PD aggravation: RR =1.09 [1.04, 1.14] for a $PM_{2.5}$ increase from 8.1 to 10.4 µg/m^3
(Luo *et al.*, 2023)	Adults with COPD (Taiwan) Cases n= 137 Controls n= 548	Case-control study	Risk of PD: OR = 4.091 [1.180 -14.188] for subjects exposed to 2.0 times the WHO level ([concentration≥ 2]× 25 µg/m^3 × number of exposure months)
(Krzyzanowski *et al.*, 2024)	Adults (USA) Cases PD n= 346 Controls n= 4813	Case-control study	- Risk of PD: OR = 1.23 [1.11-1.35] for the top quintile of $PM_{2.5}$ exposure compared with the bottom quintile - Risk of Akinetic rigid presentation OR per each 1-µg/m^3 increase in $PM_{2.5}$, OR = 1.36 [1.02-1.80] - Risk of dyskinesia among PD subjects only: HR per 1-µg/m^3 increase in $PM_{2.5}$, HR = 1.42 [1.17-1.73]
(Cao *et al.*, 2024)	Women (n=47 108) (USA)	Population-based cohort	No association with $PM_{2.5}$
(Chen *et al.*, 2024)	Adults (n= 454,583) (Taiwan)	Population-based cohort	HR = 1.22 [1.20-1.23] per interquartile range increase in $PM_{2.5}$ exposure (10.17 µg/m^3)

Abbreviations: OR = odds ratio with its 95% interval confidence; RR = risk ratio with its 95% interval confidence; HR = hazard ratio with its 95% interval confidence

I.4.3 Particulate matter exposure resulting in cognitive decline and dementia in elderly people

Long-term exposure to ambient air pollution has been associated to cardiovascular and cerebrovascular diseases, for example it is described in the literature that air pollution is linked to carotid intima media thickness (Cathryn Tonne 2012; Künzli *et al.*, 2005; Wilker *et al.*, 2013) and arterial stiffness (Chang-fu Wu 2010). It is known that those vascular and inflammatory alterations may have a negative influence on the brain and cognitive functions. However, the impact of air pollution on dementia and cognitive decline in elderly is not fully understood.

Older women who have been long-termed exposed to $PM_{2.5}$ and PM_{10} at levels that are frequently encountered by many people in the United States had worse cognitive decline (Weuve *et al.*, 2012). Those levels of PM can be due to vehicle emission, as a cohort study indicated that living near a major traffic road is associated with an increased incidence of dementia (H. Chen, J. C. Kwong, R. Copes, K. Tu, *et al.*, 2017). From an epidemiological study on both, cognitive status and molecular toxicity hallmarks, it is known that elderly living in rural areas had a cognitive status (by Mini-Mental State Examination (MMSE) test) in a negative correlation with plasma total antioxidant status (TAS) and lipid peroxides (LPO), and a positive association with superoxide dismutase (SOD) activity. Thus, PM have a detrimental impact on elderly people's cognition by increasing oxidative stress. Older individuals in urban regions exhibited higher levels of oxidative stress, leading to a nearly five-fold higher risk of cognitive impairment compared to those living in rural areas (Sánchez-Rodríguez *et al.*, 2006). For example, the impact of air pollution on linguistic competence became more pronounced with age, especially in men and individuals with lower education levels who have learning and memory impairments (X. Zhang *et al.*, 2018). A more global study, using a neuropsychological test battery CERAD-Plus (including the MMSE test), as well as the Stroop score and Sniffing score, suggest that chronic exposure to traffic-related PM may be involved in the development of mild cognitive impairment (Ranft *et al.*, 2009). When cognitive impairment interferes with daily activity and our capacity to compete them, it may become severe and progress into dementia. For example, $PM_{2.5}$ is associated with lower verbal learning scores (Gatto *et al.*, 2014) and dementia incidence (hazard ratio HR = 1.04) (H. Chen, J. C. Kwong, R. Copes, P. Hystad, *et al.*, 2017). Thereby, traffic air pollution is associated with the risk on vascular dementia (Oudin *et al.*, 2016). Furthermore, only the fine particle fraction $PM_{2.5}$ is associated with cognitive decline, and not the PM_{10} coarse particles (Ailshire & Crimmins, 2014). Also, the Heinz Nixdorf Recall Study revealed substantial correlations between $PM_{2.5}$ and mild cognitive impairment, but not with PM_{10}, $PM_{10-2.5}$, NO_x, and NO_2 (Tzivian *et al.*, 2016). However, the association

between fine particles and cognitive impairment is somewhat inconsistent. A cross-sectional analysis found no association of cognitive impairment with increased exposure to $PM_{2.5}$ (Loop *et al.*, 2013).

It is important to consider that individuals with dementia or other cognitive decline disorders, such as neurodegenerative diseases, often experience anxiety as a symptom. To manage this, they are frequently prescribed antidepressant medications. Also, PM can induce anxiety and despair behaviors contributing to depressive-like responses. For example, a previous cohort study of nurses in the US found a positive association between long-term exposure to $PM_{2.5}$ and phobic anxiety (Power *et al.*, 2015). In India, cooking with biomass has been associated with an increased risk of depression among women (Banerjee *et al.*, 2012). Similarly, in the US, depression has been linked to exposure to both ozone and $PM_{2.5}$ in a cohort of women (Marianthi-Anna *et al.*, 2017). To support human observations, animal experiments demonstrating the effects of air pollution on neurological and behavioral consequences are limited. A long-term exposure of $PM_{2.5}$ to male mice led to depressive-like behaviors and impaired spatial learning and memory, together with an increased cytokine gene-expression level (i.e., TNF-α, IL-1β) and oxidative stress marker heme oxygenase (HO)-1, as well as reduced hippocampal dendritic spin density (Fonken *et al.*, 2011).

I.4.4 Possible underlying mechanisms of ultrafine particles as risk factor of Parkinson's disease

A literature review published in 2013 identified the five main mechanisms explaining the links between exposure to PM and PD (Antony *et al.*, 2013). This chapter provides a more detailed discussion of these mechanisms.

Neuronal oxidative stress

Oxygen is vital for energy production (ATP) in many organisms, particularly through oxidative phosphorylation in the electron transport chain within the inner mitochondrial membrane. This process generates ROS, which play crucial roles in physiological functions such as defense against infections, cell signaling, and division (Zhou *et al.*, 2014). Also in the brain are ROS not solely detrimental. For instance, $NO^{\bullet}$ regulates essential physiological processes, such as long term potentiation – important for learning and memory (Izumi *et al.*, 1992; Schuman & Madison, 1991), axon growth (Rabinovich *et al.*, 2016), and pruning (Wang *et al.*, 1995).

However, ROS are highly reactive molecules containing unpaired electrons (e.g., $O_2^{\bullet -}$, $RO_2^{\bullet}$, $^{\bullet}OH$) that can interact with cellular components, causing irreversible damage to lipids, proteins, and nucleic acids. This damage can disrupt membrane integrity, impair

protein functions, and induce gene mutations, potentially leading to cell death (Yang & Lian, 2020).

The brain is particularly vulnerable to oxidative damage due to its unique characteristics: high energy demands, elevated oxygen consumption, abundant iron and PUFA, limited antioxidative defenses, and the susceptibility of neurotransmitters to oxidation. Combined with a delicate blood supply, these factors render brain an easy target for oxidative stress, as observed in neurodegenerative disease, like PD (Cobley *et al.*, 2018; Dias *et al.*, 2013). These inherent vulnerabilities make the brain also susceptible to external sources of oxidative stress. Among these, PM, or more specific Polycyclic Aromatic Hydrocarbons (PAH) and Halogenated Aromatic Hydrocarbons (HAH), can translocate cellular membranes due to their highly lipophilic nature. In the cytoplasm, the aryl hydrocarbon receptor (AhR) is bound to molecular complexes (Hsp90, XAP2 and p23). When PAH/HAH or PM, acting as AhR ligands, reach cells, they cause the aryl hydrocarbon receptor nuclear translocator (ARNT) to heterodimerize with AhR and translocate to the nucleus (Swanson *et al.*, 1995). AhR/ARNT then bind to consensus xenobiotic responsive elements (XRE, 5′-GCGTG-3′) located upstream of target genes (e.g., Cytochrome P450 (CYP) enzymes) (Hankinson, 1995). CYP1A1 and CYP1B1 are the two predominant enzymes that are involved in the process of metabolic activation (Shimada & Fujii-Kuriyama, 2004; Shimada *et al.*, 1989).

CYP1A1 is the most studied CYP enzyme and its expression levels have served as a biomarker for environmental and occupational exposure to PAH and organochlorines (Mescher & Haarmann-Stemmann, 2018). Therefore, it is reasonable to consider CYP1A1 as the candidate model enzyme to carry out metabolism and toxicity research on PAH. The catalytic cycle of the CYP-mediated PAH metabolism involves several key stages: binding, electron transfer, formation of an iron-oxygen intermediate, oxidation, and product release. This process generates epoxides, which are reactive genotoxins that can damage DNA, while also producing elevated levels of ROS (Chen *et al.*, 2021). Therefore, it can be said that some CYP subfamily enzymes, such as CYP1A1 and CYP1B1, are responsible for the bioactivation of the majority of xenobiotics (Ioannides & Lewis, 2004).

To maintain a state of redox homeostasis and prevent oxidative lesions, cells control the concentration of ROS (Milkovic *et al.*, 2014; Mirończuk-Chodakowska *et al.*, 2018), notably through antioxidant defense systems:

(1) Enzymatic (e.g., SOD, catalase (CAT), glutathione peroxidase (GPx), thioredoxin (TRX)) regulated by the Nuclear factor erythroid-2-related factor 2 (NRF2) signaling pathway,

(2) Non-enzymatic antioxidants (e.g., glutathione (GSH), vitamins A, C, and E, coenzyme Q10 (ubiquinol)).

(1) Enzymatic defense system:

Once ROS is established, it activates various signaling pathways, including NF-κB (of significance in inflammation and immunity) (Cf. Neuroinflammation, p. 25) (Lingappan, 2018; Morgan & Liu, 2011), phosphoinositide 3-kinase (PI3K)/AKT (Kitagishi & Matsuda, 2013), mitogen-activated protein kinase (MAPK) (Zhang *et al.*, 2016), but of course, as mentioned above also the NRF2 signaling pathway, which serves as a master regulator of ROS levels. NRF2 is encoded by the *NFE2L2* gene and, in the absence of oxidants, is sequestered in the cytoplasm, bound to the cytoskeleton by Kelch-like ECH-associated protein 1 (KEAP1) and degraded by the proteasome. Under basal and unstressed conditions, NRF2 has a short half-life of ~20 min depending on the cell type (Kobayashi *et al.*, 2004). In contrast, ROS modify certain cysteine residues on KEAP1, disrupting its role in NRF2 degradation. This allows to translocate to the nucleus. Then, it forms a heterodimer with small proteins such as Maf, Jun, Fos, or the Activating Transcription Factor (ATF), enabling it to interact with the antioxidant response element (ARE) and induce the expression of genes encoding detoxification enzymes that have antioxidant, detoxifying, and cytoprotective activity (Bayo Jimenez *et al.*, 2022; Kensler *et al.*, 2007).

Although NRF2 is the key transcriptional regulator of antioxidants and inflammatory responses, controlling the expression of over 250 genes, the link between its protective actions, downstream pathways, and environmental factors in the development of chronic diseases remains poorly understood (Bayo Jimenez *et al.*, 2022). The adverse health effects of air pollution depend on the nature and reactivity of their individual components, but a common mechanism among them is the induction of oxidative stress. For instance, exposure to DEP and quinones has been associated with the upregulation of NRF2 and phase II detoxifying enzymes, including HO-1 and -2, thioredoxin peroxidase 2 (TDPX-2), glutathione S-transferase P subunit (GST-P), NAD(P)H dehydrogenase, and proliferating cell nuclear antigen (PCNA) (Koike *et al.*, 2002). In $NRF2^{-/-}$ KO mice, DEP exposure resulted in higher levels of DNA adduct formation and damage (Aoki *et al.*, 2001). Similarly, $NRF2^{-/-}$ KO mice exposed to benzo[a]pyrene (component of our UFP Cf. Supplemental Data Table S1 (UFP Lille) and Table S2 (UFP Dunkirk), p. 236, 237)) exhibited increased DNA adduct formation, depletion of GST and NAD(P)H quinone oxidoreductase (NQO-1), and subsequent tumor growth (Ramos-Gomez *et al.*, 2003; Ramos-Gomez *et al.*, 2001). Compounds such as sulforaphane, found in broccoli and Brussels sprouts, and curcumin, have shown potential as NRF2 inducers, offering protection against the harmful effects of benzo[a]pyrene and DEP (Fahey *et al.*, 2002; Heber *et al.*, 2014). NRF2 deficiency also exacerbates $PM_{2.5}$-induced injury in the olfactory bulb, reducing protective phase II detoxification enzymes such as HO-1 and NQO-1, while increasing mitochondrial ROS production and NF-κB phosphorylation.

This is accompanied by microglia activation, the release of pro-inflammatory mediators (e.g., TNFα and IL-1β), and subsequent neuronal damage (X. Chen *et al.*, 2018).

In another study, rats exposed to concentrated $PM_{2.5}$ exhibited depressive-like behaviors alongside toxic element deposition (Li, Be, Al, Cr, Co, Ni, Se, Cd, Ba, Ti and Pb) in the prefrontal cortex. This exposure significantly reduced GSH levels and GSH/GSSG ratio and increased NRF2 expression 1.84-fold compared to controls, leading to elevated NQO-1 (4.10-fold) and γ-GCS (2.40-fold) (Chu *et al.*, 2019).

Controlled by NRF2, three key antioxidant enzymes – Peroxiredoxins (Prx) (from the thioredoxin system), GPx, and CAT – catalyze the breakdown of H_2O_2 into water (Lu & Holmgren, 2014). However, brain mitochondria exhibit minimal CAT expression, with an estimated concentration of 1.2 μM – approximately 50 times lower than in the liver (Patra *et al.*, 2001). In contrast, brain concentrations of Prx3, Prx5, and GPx1 are approximately 60 μM, 20 μM, and 2 μM, respectively (Cox *et al.*, 2009; Starkov *et al.*, 2014). These observations justify the focusing on the GPx and Trx systems in this study, as both play vital roles in the CNS, protecting neuronal cells (Ren *et al.*, 2017).

The Trx defense system:

Mammalian cells contain three Trx isoforms: Trx1 in the cytosol, Trx2 localized in mitochondria, and a testis-specific thioredoxin glutathione reductase (TGR) (Lu & Holmgren, 2009). These isoforms operate through a disulfide-dithiol exchange mechanism, reducing disulfide bonds in oxidized proteins. Reduced Trx (Trx-$(SH)_2$) donates electrons to these proteins, converting disulfides into thiol groups, thus regulating protein function and protecting cells from oxidative damage. This reduction is facilitated by Thioredoxin Reductase (TrxR), which uses NADPH to regenerate reduced Trx from its oxidized form (Trx-S_2), ensuring the system remains active. Additionally, the Trx system collaborates with Prx, reducing their oxidized forms (Prx-S_2) to enable detoxification of H_2O_2 and other peroxides. This interplay between Trx and Prx is essential for managing oxidative stress, particularly in mitochondria, where ROS are abundant. A visual overview is provided in Fig. 5, and this mechanism is well described in the review by (Pannala & Dash, 2015).

The GPx system:

GPx enzymes are selenocysteine-containing proteins that require selenium as a cofactor. They use reduced glutathione (GSH) as an electron donor to reduce harmful peroxides into water or corresponding alcohols, thereby mitigating oxidative stress (Flohe *et al.*, 1973; Rotruck *et al.*, 1973). There are eight known isoforms, with GPx1 being the most abundant and widely studied. GPx1 is present in both neurons and glial cells (Power & Blumbergs, 2009; Trépanier *et al.*, 1996) and primarily detoxifies H_2O_2

and organic hydroperoxides. In brain tissue, however, GPx1 is expressed at lower levels in dopaminergic neurons of the SN*pc*, compared to regions such as the ventral tegmental area (VTA) (Trépanier *et al.*, 1996), making it less prominent in the context of PD. In contrast, GPx4, also known as phospholipid hydroperoxide GPx, plays a critical role in protecting cell membranes by reducing lipid peroxides (Maiorino *et al.*, 1990; Zhang *et al.*, 1989). (Cf. Similarities between ferroptotic mechanisms during Parkinson's disease and ultrafine particle toxicity, p. 28 for the context of GPx4 in PD)

Under physiological conditions, a high ratio of GSH/GSSG maintains a reducing environment in the cell, essential for proper cellular function and antioxidant defense. This is supported by glutathione reductase (GR), which regenerates GSH from GSSG using NADPH as the reducing agent. The interplay between GPx and GR ensures the continuous cycle of peroxide reduction and GSH regeneration, as depicted in Fig. 5. However, during oxidative stress, GPx activity increases, disrupting the GSH/GSSG ratio, leading to a significant decrease in GSH levels and an increase in GSSG. The GPx activity together with the GSH ratio is a well-established indicator of oxidative stress, as recently also reviewed by (Pei *et al.*, 2023).

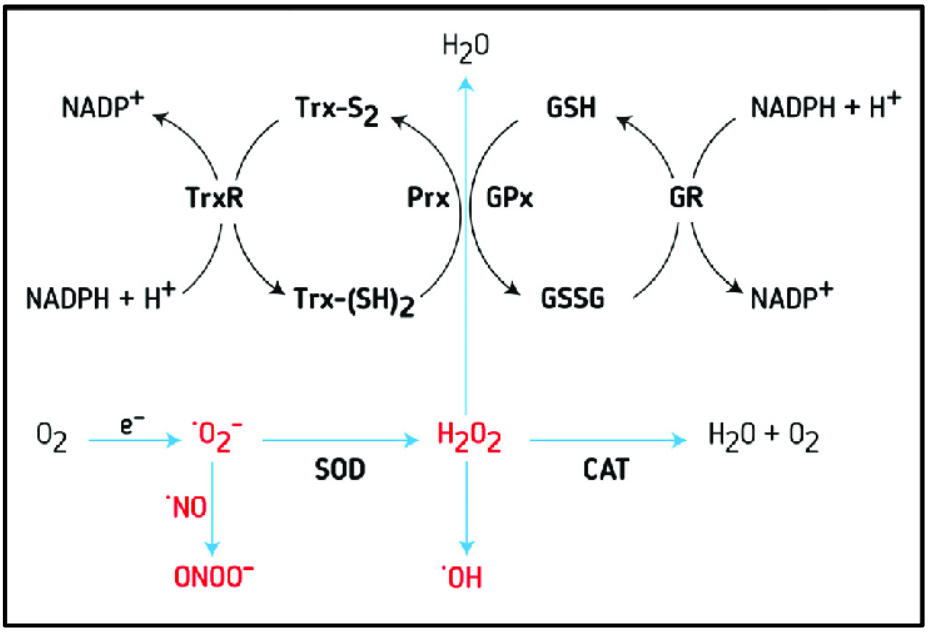

Figure 5: Enzymatic defense systems.

Oxidative stress arises from the accumulation of Reactive Oxygen Species (ROS), which are generated when molecular oxygen (O_2) gains an electron, forming superoxide ($^{\bullet}O_2^-$), a reactive free radical. Superoxide can react with nitric oxide ($^{\bullet}NO$) to produce peroxynitrite ($ONOO^-$), a highly reactive compound that contributes to cellular damage. Alternatively, superoxide is catalyzed by superoxide dismutase (SOD) to form hydrogen peroxide (H_2O_2), which itself can degrade into the highly reactive hydroxyl radical ($^{\bullet}OH$) in the presence of transition metals. To prevent the harmful effects of ROS, cells employ enzymatic defense systems to neutralize H_2O_2 before it generates more damaging radicals. Three key enzymes catalyze the conversion of H_2O_2 into water: catalase (CAT): A heme-containing enzyme; Peroxiredoxins (Prx): Thiol-based enzymes that reduce H_2O_2 by transferring electrons from their cysteine residues; Glutathione peroxidases (GPx): Selenium-dependent enzymes that use reduced glutathione (GSH) to detoxify H_2O_2 and lipid peroxides. Both Prx and GPx operate in tightly regulated loops to maintain cellular redox balance. Prx relies on the thioredoxin (Trx) system, where thioredoxin reductase (TrxR) regenerates reduced Trx using NADPH. Similarly, GPx is supported by the glutathione reductase (GR) system, which recycles oxidized glutathione (GSSG) back to GSH using NADPH. These interconnected systems ensure the continuous neutralization of ROS, safeguarding cellular integrity (Jovanović *et al.*, 2022).

Abbreviations: CAT: Catalase; GPx: Glutathione peroxidases; GR: Glutathione reductase; GSH: (reduced) glutathione; GSSG: Oxidized glutathione; H_2O_2: Hydrogen peroxide; O_2: Oxygen; $ONOO^-$: Peroxynitrite; $^{\bullet}OH$: Hydroxyl radical; Prx: Peroxiredoxins; ROS: Reactive Oxygen Species; SOD: Superoxide dismutase; Trx: Thioredoxin; TrxR: Thioredoxin reductase.

(2) Non-enzymatic defense system:

"An imbalance between pro-oxidative and antioxidant mechanisms, resulting in the accumulation of reactive oxygen and nitrogen species (RONS), serving as an initial factor for various diseases", is how oxidative stress can be defined (Bhat *et al.*, 2015). Non-enzymatic antioxidant molecules, which directly scavenge RONS, play a vital role in mitigating oxidative stress and protecting cellular integrity. Among the many non-enzymatic antioxidants, as described above, GSH holds particular importance due to its

abundance, reactivity, and multifaceted role in cellular defense. GSH is the most prevalent low-molecular-weight thiol in the cytoplasm, where it functions as a crucial thiol buffer. Its high concentration and reactive thiol (-SH) group, derived from the cysteine amino acid in its tripeptide structure (glutamate-cysteine-glycine), enable it to directly neutralize a variety of ROS and RNS, converting them into less harmful substances. This makes GSH indispensable in maintaining cellular redox balance, particularly in compartments such as the cytosol, mitochondria, and even the nucleus, where oxidative stress can disrupt critical processes.

The synthesis of GSH is a dynamic and highly regulated process, with cysteine availability being the rate-limiting factor. *De novo* synthesis involves the enzymatic coupling of glutamate, cysteine, and glycine, as shown in Fig. 6. Continuous production is essential, as GSH is rapidly consumed during oxidative stress. Studies using radioisotopes have demonstrated that cysteine availability directly dictates the cellular capacity to replenish GSH pools (Lyons *et al.*, 2001).

Given its central role in redox regulation and antioxidant defense, this PhD focused on the investigation of GSH in both, acellular tests, evaluating the oxidative potential of UFP, and cellular tests (*in vivo* and *in vitro*) were conducted to assess GSH's role in countering oxidative stress. Especially, knowing that GSH is decreased during PD, however, it is unclear of the GSH deficiency is an etiological factor or a disease consequence (Bjørklund *et al.*, 2021).

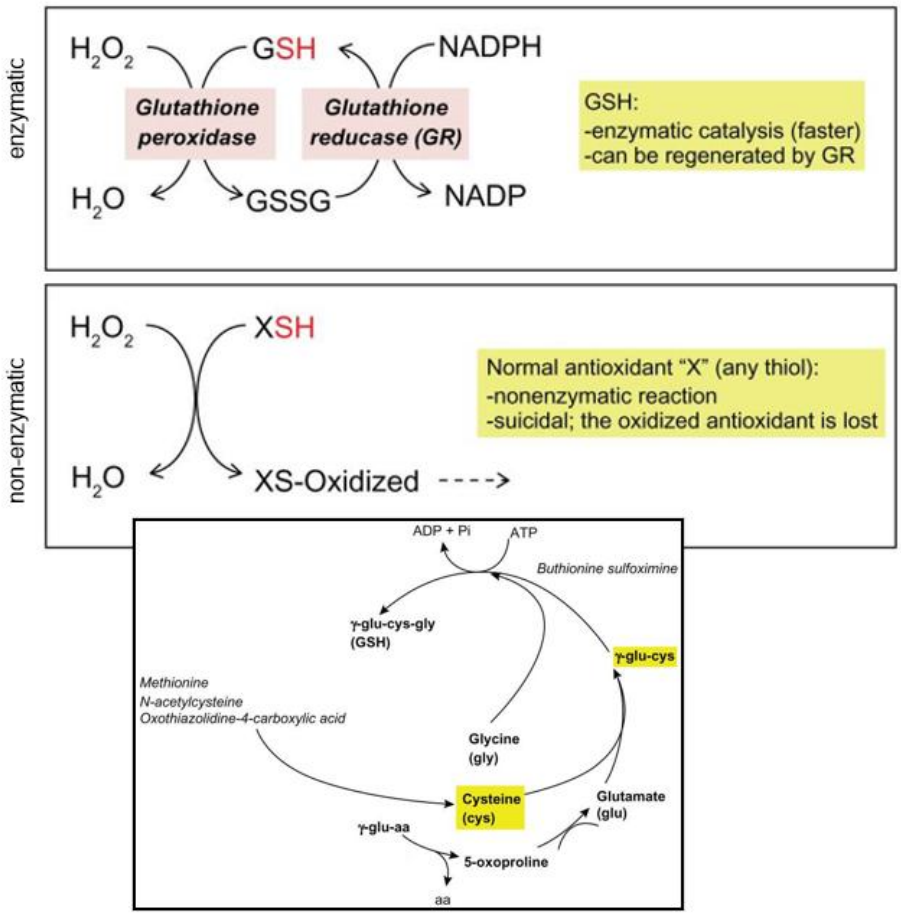

Figure 6: Enzymatic and non-enzymatic roles of glutathione in antioxidant defense, along with its tripeptide *de novo* synthesis.

The first panel illustrates the enzymatic role of glutathione (GSH) in detoxifying peroxides H_2O_2 through glutathione peroxidase (GPx), coupled with its regeneration via glutathione reductase (GR) in a NADPH-dependent cycle. The second panel highlights the non-enzymatic antioxidant function of GSH, where its thiol group directly scavenges reactive oxygen and nitrogen species (RONS) resulting in its oxidation and necessitating constant regeneration to maintain redox balance. GSH is a tripeptide composed of glutamate, cysteine, and glycine, synthesized *de novo* to maintain its concentration. Starting from cysteine and glutamate there are two enzymatic steps: the first catalyzed by glutamate-cysteine ligase (GCL) and the second by glutathione synthetase (GS) (figures adapted from (Ghezzi, 2011).

Abbreviations: GCL: Glutamate-cysteine ligase; GPx: Glutathione peroxidases; GR: Glutathione reductase; GS: Glutathione synthetase; GSH: (reduced) Glutathione; GSSG: Oxidized glutathione; H_2O_2: Hydrogen peroxide; O_2: Oxygen; $ONOO^-$: Peroxynitrite; $^{\bullet}OH$: Hydroxyl radical; Prx: Peroxiredoxins; ROS: Reactive Oxygen Species; SOD: Superoxide dismutase; Trx: Thioredoxin; TrxR: Thioredoxin reductase.

An overview of all oxidative stress related mechanisms started from UFP inhalation can be found inf Fig. 7.

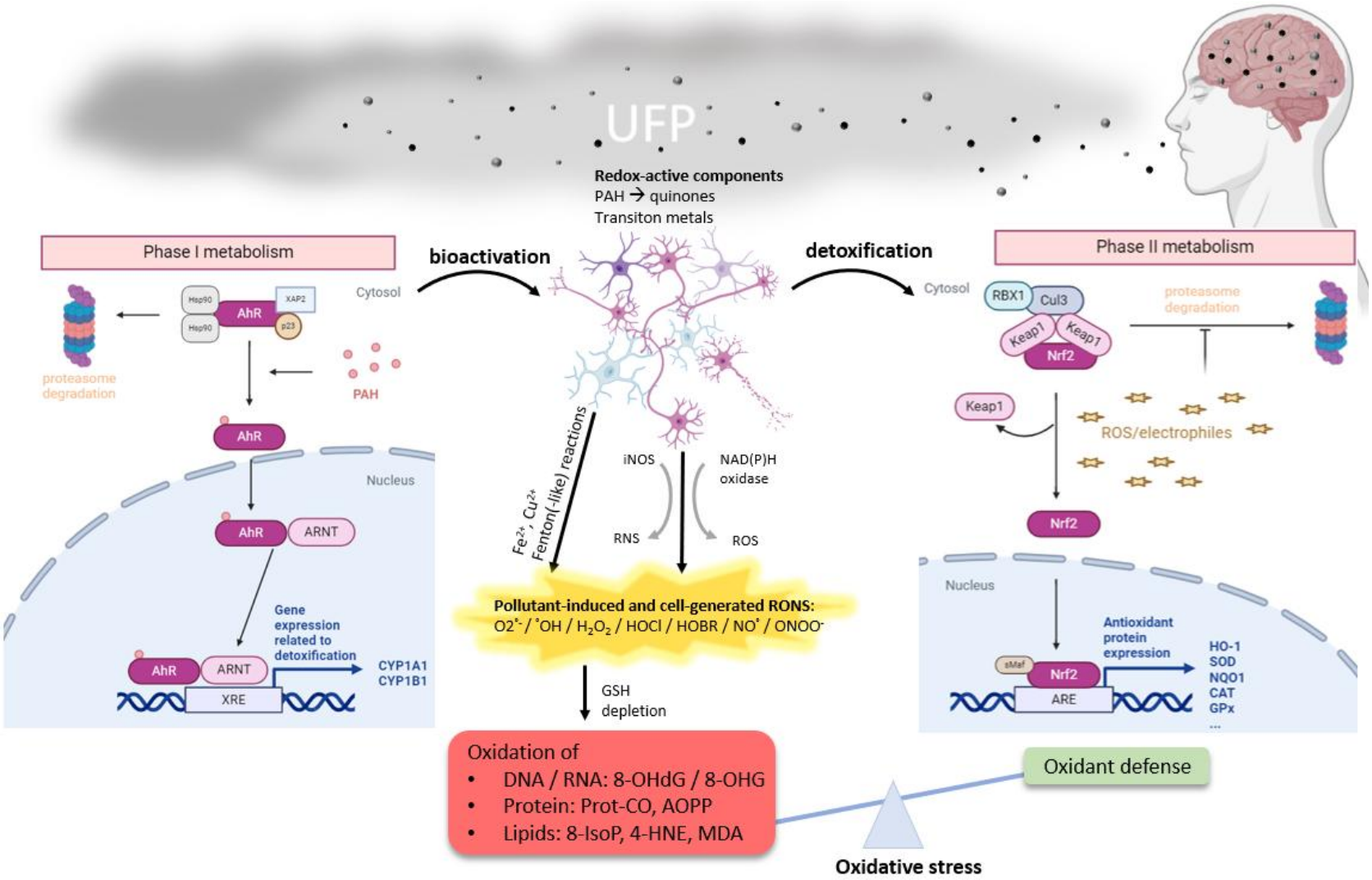

(Own creation)

Figure 7: Ultrafine particle-induced Phase I (AhR) and phase II (NRF2) metabolism in cellular defense against oxidative stress.

Inhalation of UFP can trigger oxidative stress in brain tissue. Among the most redox-active compounds in ultrafine particles (UFP) are Polycyclic Aromatic Hydrocarbons (PAH), which upon transformation into quinones, activate the aryl hydrocarbon receptor (AhR). AhR, as a transcription factor, upregulates the expression of detoxification enzymes such as Cytochrome P450 enzymes (CYP)1A1 and CYP1B1. These enzymes facilitate the bioactivation of compounds by adding reactive groups, which can increase Reactive Oxygen and Nitrogen Species (RONS) production. The accumulation of RONS can lead to the oxidation of DNA/RNA, proteins, and lipids, potentially causing cellular damage if not neutralized by antioxidants like glutathione (GSH). As compensation, detoxification mechanisms such as the phase II Nuclear factor erythroid-2-related factor 2 (NRF2) pathway will be activated, leading to transcription of detoxification enzymes and antioxidant enzymes. When the balance between enzymatic oxidative defense and antioxidant capacity is disrupted, resulting in excessive RONS, cells enter an oxidative stress state.

Abbreviations: AhR: Aryl hydrocarbon receptor; CYP: Cytochrome P450 enzymes; GSH: Glutathione; NRF2: Nuclear factor erythroid-2-related factor 2; PAH: Polycyclic Aromatic Hydrocarbons; RONS: Reactive Oxygen and Nitrogen Species; UFP: Ultrafine particles.

Brain metal overload

Intracellular metal concentrations are deregulated in the SN*pc* of PD patients. Several studies on dopaminergic neurons are showing an increase of iron (American neurological, 2013; Ayton & Lei, 2014; Dexter *et al.*, 1987; Dexter, Wells, *et al.*, 1989; Riederer *et al.*, 1989; Sofic *et al.*, 1988; Visanji *et al.*, 2013) and decreased copper levels (American neurological, 2013; Dexter *et al.*, 1987; Dexter, Wells, *et al.*, 1989; Loeffler *et al.*, 1996; Uitti *et al.*, 1989), while findings about zinc are controversial (Davies *et al.*, 2014; Dexter, Carter, *et al.*, 1989; Hirsch *et al.*, 1991; Uitti *et al.*, 1989).

The presence of (heavy) metals must be taken into consideration in studies on PM or UFP. Indeed, as indicated in Fig. 8, the cellular toxicity can start through three different ways; (1) by their small size they are easily up taken into cells by endocytosis and/or passive diffusion, whereafter they translocate into different subcellular compartments, (2) they attack the lipid bilayer of the plasma membrane leading directly to lipid peroxidation, (3) PM contains metals in the exchangeable fraction from which ions can be released and translocated, for example active by receptor-mediated endocytosis transporters (Fe^{3+} by transferrin (Tf)), leading to direct lysosome dysfunction or mitochondrial damage by Fenton-(like) reactions.

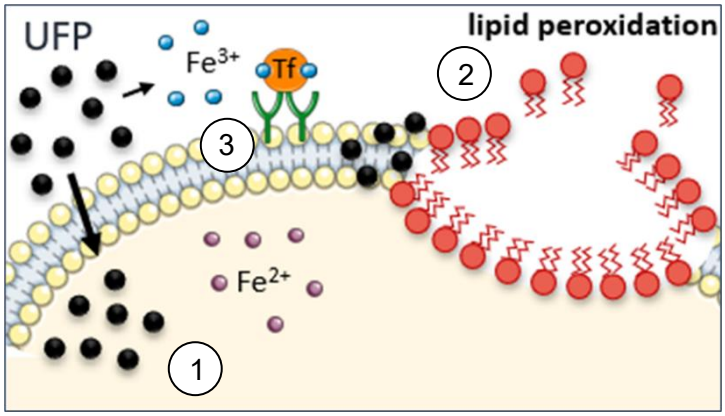

(Own creation)

Figure 8: Suggested mechanisms how ultrafine particles led to cellular toxicity.

[1] Ultrafine particles (UFP) are taken intracellular by endocytosis, [2] it attacks directly the plasma lipids leading to lipid peroxidation, or [3] soluble metals of the exchangeable fraction of UFP are intracellular translocated by transmembrane receptors.

Abbreviations: UFP: Ultrafine particles.

As the third way is a direct attack of metals, it is advised to do a metal composition analysis before starting a particle toxicological raid. Environmental toxicological epidemiological data, on the other hand, do not support a metal composition analysis and should thus be interpreted with caution. However, those studies are quite intriguing since they are based on everyday life and the contaminated air that we all breath. According to such a study, inhabitants of Mexico City had higher metal levels (such as

Fe) in their olfactory bulbs than residents of the control city (Calderón-Garcidueñas *et al.*, 2013). Also, rodent *in vivo* studies described the metal deposition (Fe, Cu, Zn) in olfactory bulbs after intranasal exposure of nanoparticles (Y.-Y. Kao *et al.*, 2012; Liu *et al.*, 2009; Wang *et al.*, 2007).

As particles can undergo translocation from their initial exposure side through the olfactory bulb and the frontal cortex to other regions of the brain, an elevated metal level should be found as well. Thought, this depends on the metal itself as not all heavy metals are able to undergo such transport. For instance, it has been discovered that cadmium (Cd), which is linked to olfactory impairment (Gobba, 2006), does not undergo additional retrograde transport beyond the olfactory bulb (Nordic Pharmacological, 1996; Tjälve & Henriksson). Moreover, metal translocation to other brain regions is also size depending. For instance, Manganese (Mn) particles of 1.3 µm undergo translocation, but particles of 18 µm did not (Fechter *et al.*, 2002).

Although some metals (Aluminum) are not transition metals to accelerate redox reactions, it can cause neurotoxicity by producing ROS (Shah *et al.*, 2015), or even more, learning and memory impairment can be induced by nano-aluminum related to mitophagy (Huang *et al.*, 2021).

Olfactory dysfunction

Olfactory bulbs are unique, as the BBB does not shield them, and receive direct input from the olfactory epithelium in the nasal cavity and are therefore very sensitive for environmental toxins (Hanson & Frey, 2008; Oberdörster *et al.*, 2004).

Considering that (1) over 95% of all PD patients experience olfactory loss (hyposmia) in early onset of their pathology, (2) metal deposition (Fe and Ca) is discovered in post-mortem PD olfactory bulbs, and (3) the olfactory bulb may be one of the first regions for α-synuclein aggregation; it makes olfactory dysfunction an interesting feature of PD (Gardner *et al.*, 2017). Furthermore, as previously stated, UFP can enter the cerebrum via the olfactory bulb. Regardless of the negative effects of UFP, olfactory impairment may occur.

Therefore, Calderon-Garciduenas focused on olfactory bulbs as important region during neurotoxicity in post-mortem studies. In 2014, they found that olfactory bulb of high-polluted residents of Mexico City contained cyclooxygenase-2 (COX-2) and β-amyloid, but none of countryside-living inhabitants did (Calderón-Garcidueñas *et al.*). They also discovered PM in the glomerular olfactory bulb region or the olfactory nerve in children and young adults living in highly polluted areas (Calderón-Garcidueñas, Solt, *et al.*, 2008).

There is also a direct link between metal toxicity and olfactory dysfunction. Hyposmia was found by testing olfactory function in neurodegenerative disorders with brain iron

accumulation (NBIA) patients. This suggest that dysregulated iron metabolism, by iron or ferritin deposition, is toxic to the olfactory system (Dziewulska *et al.*, 2013).

Alfa synuclein

Abnormal accumulation of filamentous α-synuclein, referred to as Lewy bodies or Lewy neurites, is a typical hallmark of PD. *In vitro* studies revealed that elevated levels of iron, copper (Uversky *et al.*, 2001), and zinc (Golts *et al.*, 2002; Kim *et al.*, 2000) can cause α-synuclein aggregation. This suggests that brain protein deposition may also be caused by air pollution. As previously mentioned, Calderon-Garciduenas reported in 2004 that β-amyloid deposition was found in the olfactory bulbs of residents of Mexico City. However, in 2008, they conducted an extensive follow-up autopsy and revealed that, in addition to β-amyloid, α-synuclein deposition was observed, as well as more significant levels of inflammatory markers COX-2, IL-1β and CD14 in the same olfactory brain tissue (Calderón-Garcidueñas *et al.*, 2010).

In addition to aggregate detection, it is also important to know how UFP can lead to α-synuclein deposition. Considering that oxidative stress and neuroinflammation can result in accumulation of oxidized cytoskeletal and mitochondrial respiratory chain proteins, these unfolded or misfolded proteins may lead to endoplasmic reticulum (ER) stress. Under physiological conditions ER stress commits the unfolded protein response (UPR), largely through protein kinase R (PKR)-like endoplasmic reticulum kinase (PERK), endoribonuclease inositol-requiring enzyme 1 α (IRE1α), and Activating transcription factor 6 (ATF6) proteins that becomes dissociated from Binding immunoglobulin Protein (BiP) at the ER membrane and reduces unfolded protein load to maintain cell viability and function (Hetz, 2012). Therefore, an increased level of chaperone protein BiP in the lumen of the ER is connect to a higher raid of proteins with incorrect tertiary and quaternary structures. It is interesting that postmortem studies of PD-patients and experimental PD models (MPTP/MPP^+ models) revealed that the upregulation of BiP is linked to an increased α-synuclein expression and therefore implicated in the pathogenesis of PD (reviewed by (Enogieru *et al.*, 2019). In a study where rats were exposed to UFP there was a higher transcript level of BiP found in the hippocampus. This gives the first suggestion that UFP exposure may be linked to ER stress and UPR. Moreover, rats exposed to coarse particles, of which UFP is part, had an increased expression of BiP chaperone protein in the corpus striatum, one of the brain region associated with PD (Guerra *et al.*, 2013).

Neuroinflammation

Neuroinflammation refers to the immune response within the brain and spinal cord, typically triggered by infection, injury, or chronic exposure to environmental toxins. It

primarily involves the activation of resident immune cells, such as microglia and astrocytes. Under normal conditions, microglia maintain a resting state, continuously surveilling the CNS environment. However, upon encountering harmful stimuli, they become overactivated, changing their morphology (amoeboid state evident by markers like Iba1) and releasing pro-inflammatory cytokines (TNFα, IL-1β, IL-6), chemokines (CCL2, CXCL10), and, occasionally, neurotrophic factors like brain-derived neurotrophic factor (BDNF). Astrocytes, critical for supporting CNS homeostasis and regulating the BBB, also become reactive during neuroinflammation, releasing pro-inflammatory mediators and altering BBB integrity.

While these immune responses are essential for initial defense and repair, chronic activation of microglia and astrocytes can lead to persistent neurodegeneration, and is therefore a hallmark of PD (Ramesh *et al.*, 2013). Chronic exposure to PM has also been shown to exacerbate neuroinflammation, evidenced by increased glial fibrillary acid protein (GFAP) levels, a marker of gliosis (Chu *et al.*, 2019; Finch *et al.*, 2002), and decreased BDNF in the prefrontal cortex (Chu *et al.*, 2019). Additionally, nanometer-sized DEP exposure also induces oxidative stress and activates microglial NADPH oxidase, resulting in ROS production and dopaminergic cell death (Block *et al.*, 2004). This suggest that microglia-induced neuroinflammation is critical in UFP-related neuronal damage, evolving in synaptic function impairment and worsened cognition (Gui *et al.*, 2023; Ku *et al.*, 2017).

At molecular level, NF-κB is a master transcription factor central to the neuroinflammatory response. It regulates the expression of almost 500 genes, including those encoding pro-inflammatory cytokines (IL-1, IL-6, IL-8, TNF), enzymes (COX-2, LOX, iNOS), chemokines, adhesion molecules, cell cycle regulatory molecules, and angiogenic factors (Ahn & Aggarwal, 2005; Duh *et al.*, 1989; Gupta *et al.*, 2010; Kaltschmidt *et al.*, 1993). In the CNS, NF-κB plays roles in neurogenesis (Rolls *et al.*, 2007) and synaptic plasticity related to learning and memory (Ahn *et al.*, 2008; Levenson *et al.*, 2004; O'Riordan *et al.*, 2006). Its activation is closely tied to chronic neuroinflammation in neurodegenerative diseases, a published paper of this year suggests even that NF-κB inhibition may be the key to treating of PD (Song *et al.*, 2024).

As shown in Fig. 9, the NF-κB signaling system operates through two main pathways: the canonical pathway and the non-canonical pathway, each playing distinct roles in cellular responses to various stimuli. The canonical pathway is primarily activated by pro-inflammatory cytokines (TNF-α, IL-1β), microbial components (e.g., LPS), and cellular stress, and probably the main route for PM-induced activation of NF-κB. It involves the IκB kinase (IKK) complex (IKKα, IKKβ, and IKKγ) and NF-κB dimers composed of RelA (p65) and p50, which are initially inhibited by IκB proteins. Upon stimulation, the IKK complex phosphorylates IκB, marking it for degradation. This releases the NF-κB dimers,

which translocate to the nucleus to activate the corresponding genes. The non-canonical pathway is activated by specific developmental and immune signals, such as lymphotoxin β, BAFF, CD40 ligand, and RANKL. This pathway relies on the activation of NF-κB-inducing kinase (NIK), which in turn activates IKKα. IKKα phosphorylates p100, leading to its partial degradation into p52. The resulting RelB/p52 dimers migrate to the nucleus to regulate the expression of genes involved in adaptive immunity, lymphoid organ development, and chronic immune responses (The NF-κB signaling pathway in neurological inflammation was reviewed by (Shih *et al.*, 2015).

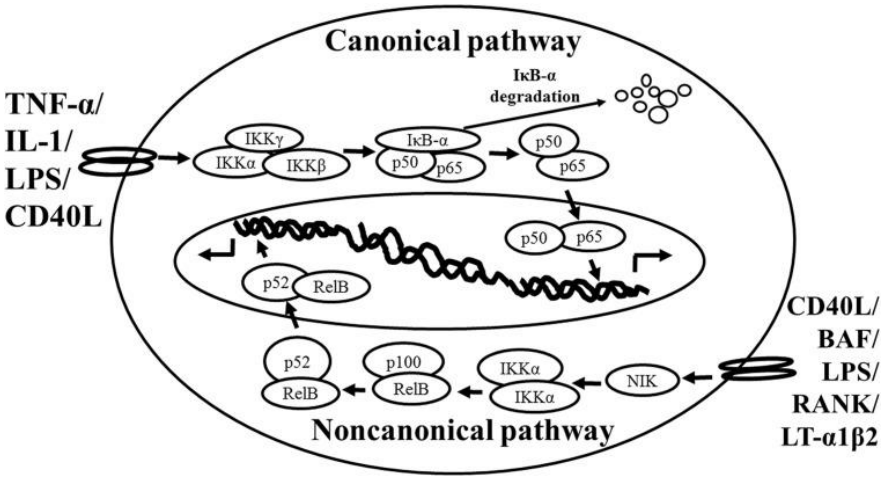

Figure 9: Schematic representation of the canonical and non-canonical NF-κB activation pathways.

The canonical pathway (top) is triggered by diverse stimuli such as Tumour Necrosis Factor alpha (TNF-α), IL-1, LPS, and Toll-like receptor ligands (e.g., CD40L). It relies on the IκB kinase (IKK) complex (IKKα, IKKβ, and NF-κB essential modulator (NEMO)), which phosphorylates IκBα, leading to its degradation and the release of NF-κB dimers (p50-p65) to activate target genes.
The non-canonical pathway (bottom) is activated by specific signals like BAFF, LTα1β2, RANK, and CD40L. It depends on NF-κB-inducing kinase (NIK), which recruits IKKα to phosphorylate p100. This generates the active p52/RelB complex, enabling nuclear translocation and target gene expression (Shih *et al.*, 2015).

Abbreviations: IKK: IκB kinase; IL: interleukin; LPS: Lipopolysaccharides; NIK: NF-κB-inducing kinase; TNF-α: Tumour Necrosis Factor alpha

NF-κB has also been identified as a critical signal transducer influencing cellular permeability, endocytosis, and intracellular trafficking at the level of the BBB (Stone *et al.*, 2011), highlighting its involvement in neuronal toxicity induced by PM. Recent studies have explored the link between PM and neuroinflammation. For instance, research on canines from highly polluted Mexico City revealed increased brain inflammation compared to those from less polluted location (Tlaxcala, Mexico). Brain tissues from Mexico City dogs heightened activation of NF-κB, increased iNOS synthesis, and reactive astrocytes presence (Calderón-Garcidueñas *et al.*, 2002). Similarly, exposure to concentrated PM in mice led to elevated NF-κB levels, alongside increased pro-

inflammatory cytokines IL-1 and TNF-α (Campbell *et al.*, 2005). This trend was also observed in children from polluted regions, where higher levels of IL-1β and COX-2 were detected in the frontal cortex (Calderón-Garcidueñas, Mora-Tiscareño, *et al.*, 2008).

One of the most concerning components of UFP is their metal content. Metals such as Co, Mn, and Cu are known to elicit distinct inflammatory responses. For example, elevated Co levels were linked to reduced COX-2 expression, whereas Mn and Cu correlated with increased COX-2 expression, demonstrating the complex interplay between PM composition and inflammatory pathways (Calderón-Garcidueñas *et al.*, 2013). Mice exposed to 14 nm carbon black particles for four weeks displayed significant upregulation of inflammation-related genes, including IL-1β, TNF-α, CCL2, CCL3, and CXCL9, in the olfactory bulb, though no significant changes were noted in the hippocampus (Yamamoto *et al.*, 2006). Regarding PD, UFP exposure in rats was associated with increased levels of antioxidant markers HO-1 and SOD-2, Nf-kB activation, and elevated transcript levels of IL-1β and TNF-α in the striatum, as well as NRF2-activation (Guerra *et al.*, 2013). Similarly, exposure to $PM_{2.5}$ led to significantly increases of IL-1β, IL-6, IL-8, IL-17, and caspase-1 in rat prefrontal cortex (Chu *et al.*, 2019).

Neuroinflammation and neuronal death (e.g., ferroptosis): "Chicken or the egg"-story, which comes first?

A key question remains whether PM exposure directly induces neuronal death or whether neuroinflammation is the primary driver. Evidence suggests that ferroptosis can trigger the release of danger-associated molecular patterns (DAMP), which recruit inflammatory cells and exacerbate inflammation-related damage (Jiang *et al.*, 2021; Sun *et al.*, 2020). Furthermore, studies support the role of ferroptosis in driving inflammation (N. Liu *et al.*, 2022; Wu *et al.*, 2020), suggesting a bidirectional relationship between PM-induced neuroinflammation and neuronal damage.

I.5 Similarities between ferroptotic mechanisms during Parkinson's disease and ultrafine particle toxicity

Specific stressful cellular and molecular alterations as described above (oxidative stress, neuroinflammation, iron accumulation, etc.) in the SN*pc* may lead to multiple regulated cell death (RCD), including the most prevalent RCD of PD, namely ferroptosis, but also apoptosis, and autophagy.

I.5.1 Ferroptosis and its potential implication in PD

Ferroptosis, identified in 2012 as an iron-dependent, oxidative-regulated form of necroptosis, is characterized by the accumulation of iron and subsequent the buildup of toxic lipid peroxides (Dixon *et al.*, 2012). Our lab (LilNCog – *Université de Lille*) was the first to demonstrate ferroptosis in *in vitro*, *ex vivo*, and *in vivo* models of PD (Do Van *et al.*, 2016). The primary interest in this pathway arose from the shared features between the molecular pathophysiology of PD and the ferroptosis pathway, such as iron accumulation and elevated lipid peroxidation. As shown in Fig. 10, the ferroproteins involved in the elevated import of Fe^{3+} via Tf and/or Fe^{2+} via the divalent metal transporter 1 (DMT1) result in an imbalanced intracellular iron level during ferroptosis. Furthermore, Fe^{2+} is oxidized by ferroxidases (ceruloplasmin (CP)) before being exported by ferroportin (FPN). During ferroptosis, however, this iron export is disrupted, leading to an enhanced Labile Iron Pool that catalyzes Fenton reactions, generating $^{\bullet}OH$ and lipid peroxidation. Indeed, ferritin concentration is inversely related to iron levels, and when ferritin degrades, labile iron content increases, exacerbating cellular damage, this process is also known as ferritinophagy. Iron metabolism – encompassing import (DMT1, TfR), storage (ferritin), and export (FPN1) – plays a critical role in susceptibility to ferroptosis, making these factors potential biomarkers for the condition. Mutations in genes responsible for iron homeostasis have been linked to an increased risk of PD, with studies showing that variants in CP-encoding genes are also associated with PD (Borie *et al.*, 2002; Hochstrasser *et al.*, 2004). These findings highlight the importance of iron accumulation in PD and its connection to ferroptosis. Iron buildup in glial cells and dopaminergic neurons of the SN*pc* correlates with disease severity (Davies *et al.*, 2015; Dexter, Wells, *et al.*, 1989; Hirsch *et al.*, 1991; Pyatigorskaya *et al.*, 2015).

As explained before, the emergence of oxidative stress, another major contributor to PD, is linked to the antioxidant GSH (Dringen *et al.*, 2000; Gandhi & Abramov, 2012). Under physiological conditions, the selenoprotein GPx4 reduces LOOH to non-toxic lipid alcohols (LOH) using GSH as a co-substrate. In PD patients, the high ROS levels and free radicals in the SN are associated with reduced GSH levels, resulting in insufficient antioxidant protection (Pearce *et al.*, 1997; Sian *et al.*, 1994; Sofic *et al.*, 1992). Recently, it is discovered that hypermethylation of the gene encoding the cysteine-glutamate antiporter xCT unit (SLC7A11) may contribute to decreased intracellular GSH levels in PD (Costanza L. Vallerga *et al.*, 2020).

GPx4 is the only enzyme in its hydroxy peroxide family capable of addressing cellular membrane lipid peroxidation. When GPx4 is compromised – either by gene knockdown or lack of its co-substrate, GSH – oxidative stress targets membrane lipids, initiating lipid peroxidation. From a previous study it is known that GPx4 is crucial to maintain neuronal survival, with KO of GPx4 in hippocampal and motor neurons leading to

neurodegeneration (Friedmann Angeli *et al.*, 2014). In GPx4 KO mice, paralysis occurs, but supplementation with vitamin E – another ferroptosis inhibitor – delays the onset of paralysis and death (Chen *et al.*, 2015). In forebrain-specific GPx4 KO mice, cognitive impairments (as spatial learning and memory function by Morris Water Maze task) were observed, accompanied by hippocampal neurodegeneration, which was exacerbated by a vitamin E-deficient diet (Hambright *et al.*, 2017).

The sensitivity to lipid peroxidation – and thus to ferroptosis – varies depending on the phospholipid composition of the membrane. One key group of phospholipids involved in lipid peroxidation is PUFA-containing phospholipids. Among the various classes of PUFA, the polyunsaturated ώ-6 acyl group, which includes arachidonic acid, is particularly prone to lipid peroxidation. When these PUFA undergo lipid peroxidation, they produce toxic α,β-unsaturated aldehydes, such as 4-HNE, which can damage other cellular components, including proteins, lipids, and DNA. These aldehydes can also cause structural modifications to α-synuclein, promoting oligomerization (Broersen *et al.*, 2006; De Franceschi *et al.*, 2009; Lücke *et al.*, 2006; Sharon *et al.*, 2001).

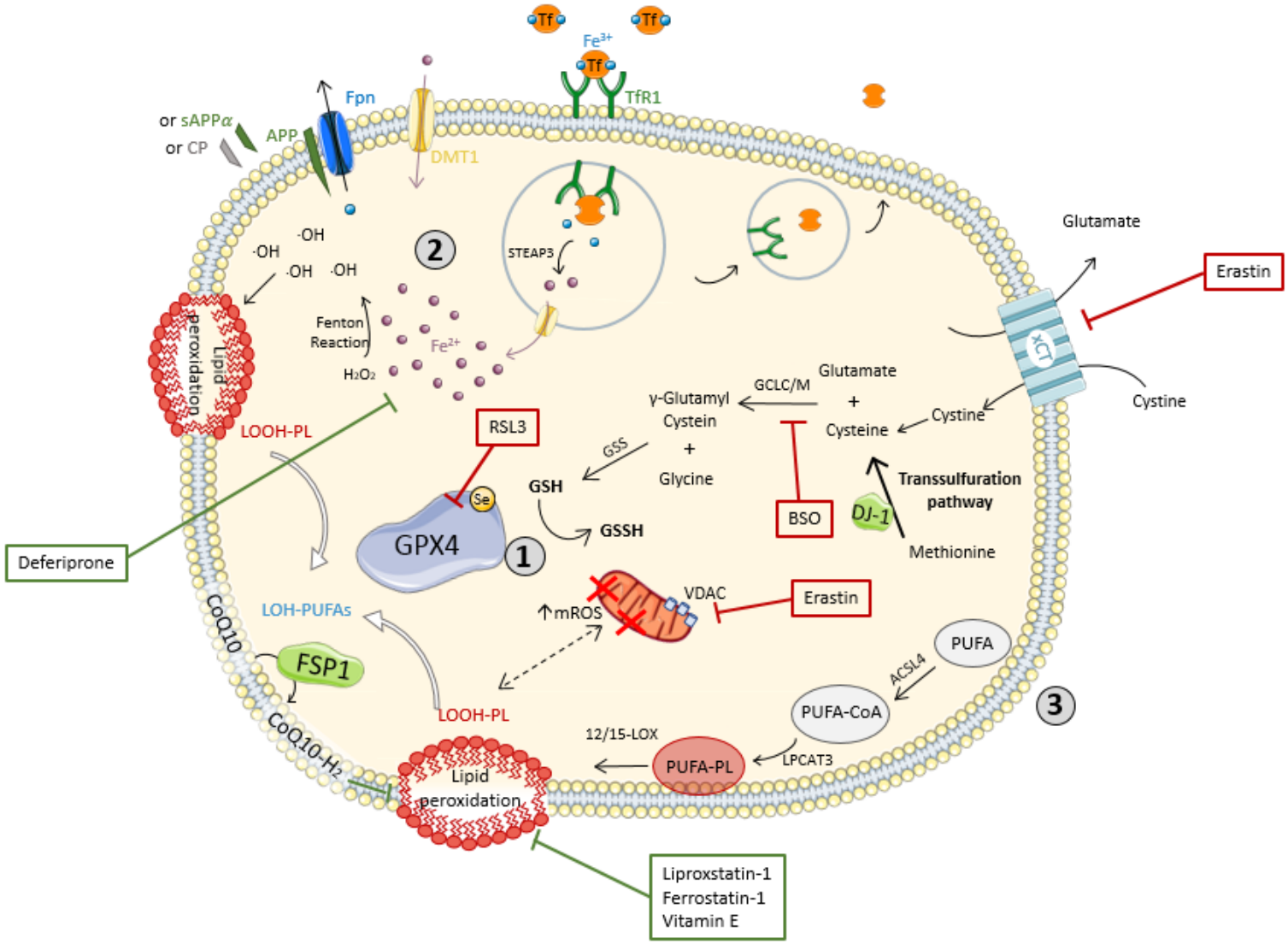

Figure 10: Overview of the main pathways involved in ferroptosis.

[1] Glutathione peroxidase 4 (GPx4) needs two glutathione residues (GSH) to convert lipid hydroperoxides (LOOH) into their non-toxic alcoholic form LOH. If there is a depletion of GSH, this reaction cannot succeed, leading to lipid peroxidation. [2] Due to the imbalance of intracellular iron level, the Labile Iron Pool catalyze hydrogen peroxide by a Fenton reaction into hydroxyl radicals (•OH), stimulating as well lipid peroxidation. [3] Lipid peroxidation can also be induced by polyunsaturated fatty acids (PUFA) that are incorporated in the plasma membrane where after an oxidation reaction by lipoxygenases leads to lipid peroxidation (Mahoney-Sánchez *et al.*, 2021).

Abbreviations: GPx4: Glutathione peroxidase 4; GSH: glutathione; LOH: lipid alcohols; LOOH: lipid hydroperoxides; •OH: hydroxyl radicals; PUFA: polyunsaturated fatty acids.

Taken together, this evidence confirms that ferroptosis plays a significant role in the physiopathology of PD, opening avenues for alternative neuroprotective treatments through the use of anti-ferroptotic molecules. In 2016, our lab demonstrated that dopaminergic neuron perished after intoxication to several neurotoxic chemicals (DA, rotenone, glutamate, etc.). However, this neuronal death could be mitigated by particular ferroptosis inhibitors, such as Ferrostatin-1 (Fer-1) and Deferiprone (DFP). Notably, the iron-chelator Fer-1 completely reversed MPP^+ toxicity, and cell viability significantly increased (two-fold) following DFP treatment (Do Van , 2016).

Ferroptosis has sparked a lot of attention in the recent years, and scientific understanding of the underlying mechanisms has expanded substantially. In conclusion, ferroptosis is intricately linked to PD in a variety of ways, including iron accumulation, oxidative stress and lipid peroxidation. Ongoing research into ferroptosis in PD holds great promise for the development of novel therapeutic strategies.

I.5.2 Questioning whether ferroptosis occur after particulate matter exposure, resulting in the induction of neurotoxicity

Some researchers have found that PM can induce typical oxidative stress damage by disrupting redox-sensitive systems or generating excessive ROS (Gu *et al.*, 2022; Guascito *et al.*, 2023; Wang *et al.*, 2019). The brain, due to its high concentration PUFA, is particularly vulnerable to redox imbalance, making it highly susceptible to damage from PM exposure (Migliore *et al.*, 2015; Qin *et al.*, 2023). Ferroptosis, as recent discovered RCD, has not been extensively studied in the context of PM exposure. However, it represents an intriguing area of research, as iron is abundant in environments with high levels of UFP. In addition, increased ROS production and lipid peroxidation – both linked to PM exposure – are central to ferroptosis. Before this PhD study, there was no published evidence on the role of ferroptosis following specific urban UFP exposures in brain tissue. This chapter, therefore, highlights the hypothesis that $PM_{2.5}$ – which contains > 90% UFP – may contribute to ferroptosis.

When human endothelial cells were exposed with $PM_{2.5}$, the particles were uptaken through endocytosis or bound to the cellular membrane, leading to observable morphological changes, such as swollen cytoplasm, vacuolar alterations and even plasma membrane rupture. FerroOrange microscopy assays revealed elevated intracellular iron levels, alongside reduced GSH, GPx activity, and NADPH levels, suggesting that $PM_{2.5}$ significantly disrupts cellular antioxidant capacity. In conjunction with the positive outcome of C11-$BODIPY^{581/591}$, lipid peroxidation was observed. Additionally, increased expression of oxidative stress-related genes (i.e., SLC7A11, NADPH oxidase 1 (NOX1), and NAD(P)H dehydrogenase quinone 1 (NQO1)) and aberrant iron-related protein expression (i.e., TFRC, FTL, and FTH1) provide evidence

of ferroptosis involvement, by which the total picture is illustrated in Fig. 11 (Wang & Tang, 2019).

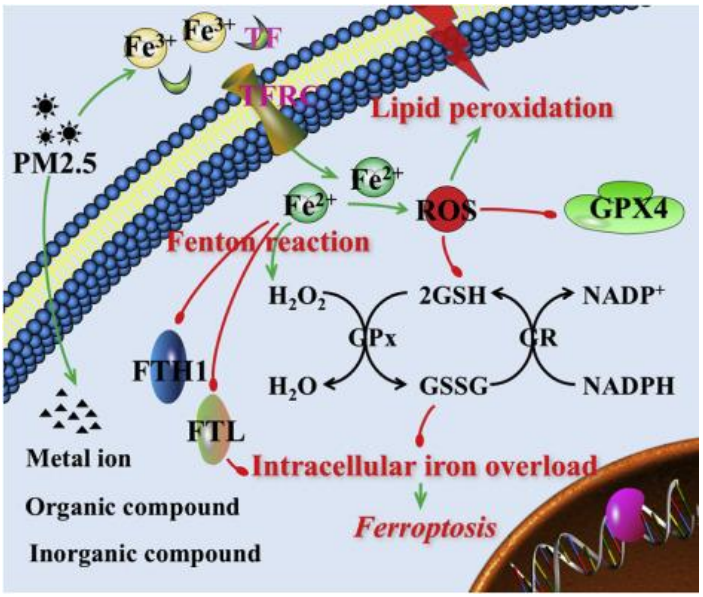

Figure 11: Schematic overview of the mechanisms underlying $PM_{2.5}$-induced endothelial cell ferroptosis.

$PM_{2.5}$ not only facilitates the uptake of organic or inorganic compounds, but also leads to an increase in cellular metal ions, particularly iron. This iron accumulation is regulated through the differential expression of iron-related genes (e.g., transferrin receptor (TfR), ferritin light chain (FTL) and ferritin heavy chain 1 (FTH1)), resulting in intracellular iron overload. The excess iron triggers increased ROS production, which in turn reduces GSH levels and induces lipid peroxidation (Wang & Tang, 2019).

Abbreviations: FTH1: ferritin heavy chain 1;FTL: ferritin light chain; TfR: transferrin receptor.

$PM_{2.5}$ exposure caused cell death in neuronal cell lines (Neuro-2a (N2A) and SH-SY5Y), which was prevented by co-treatment with Fer-1. This study by Xiong and colleagues provides the first evidence that neuronal death induced by PM exposure occurs through ferroptosis. Post-$PM_{2.5}$ exposure downregulated GPx4 and ferritin heavy chain (FTH) expression, while TfR and ferritin light chain (FTL) were upregulated, and these changes were reversed by Fer-1 treatment. $PM_{2.5}$ also caused oxidative damage, disrupting oxidant enzyme systems, which led to decreased levels of SOD and GSH, increased ROS and MDA. Bioinformatic analysis suggested that cAMP Response Element-Binding Protein (CREB) may regulate GPx4 transcription, and its reduced expression could be linked to $PM_{2.5}$-induced inhibition of the ERK/CREB pathway, thereby promoting ferroptosis (Xiong *et al.*, 2022). Notably, ferroptosis also increases the expression of COX-2 (PTGS2), a key enzyme in prostaglandin biosynthesis and inflammatory mediator production, which was similarly upregulated following $PM_{2.5}$ exposure (Wang & Tang, 2019).

Interestingly, a recent study, published this year, investigated neuroinflammation and ferroptosis after $PM_{2.5}$ exposure *in vivo* and *in vitro*. Mice exposed oropharyngeally for 28 days exhibited impaired learning in the Y-maze, elevated IL-1β and IL-6 levels, microglial activation, and hippocampal cell death. Using BV2 microglial cells, researchers identified oxidative stress and iron metabolism dysregulation, evidenced by FerroOrange, GSH depletion, elevated $NADP^+$/NADPH ratios, ROS overproduction, and lipid peroxidation. Microarray analysis revealed *Heme oxygenase* (*Hmox1*) as the most

upregulated gene, promoting iron overload by heme catabolism. Elevated FTH1, FTL1, and FPN levels indicated cellular responses to iron accumulation. Inhibiting *Hmox1* with zinc protoporphyrin (ZnPP) reduced iron overload, lipid peroxidation, and cell death, while hemin exacerbated them. Additionally, inhibiting NRF2 reduced *Hmox1* expression and iron accumulation, highlighting the NRF2-HMOX1 axis as central to $PM_{2.5}$-induced ferroptosis (Wei *et al.*, 2024).

This raises an important question: which source drives the iron overload for ferroptotic induction following PM exposure?

Potential sources include the iron originated from the UFP itself, but also mitochondrial iron released after ROS-induced damage, or iron liberated from heme by antioxidants such as HMOX.

A previous PhD study from our lab using LUHMES dopaminergic neurons showed that iron alone (Fe^{3+}, up to 100 µM, 24 hours) did not induce toxicity, suggesting protective mechanisms like ferritin storage or antioxidant pathways to exogeneous iron (Bouchaoui *et al.*, 2023). This hypothesis that the iron fraction of UFP is insufficient on its own to induce neurotoxicity.

Moreover, recent research has demonstrated that various ion-leaking nanoparticles, not limited to those containing iron, can induce ferroptosis. For instance, a study by (C. Zhang *et al.*, 2020) investigated the effects of 21 distinct nanomaterials, ranging in size from 5 to 200 nm, on human umbilical vein endothelial cells (HUVEC). As summarized in Table 2, HUVEC were exposed to these nanomaterials (10 µg/mL) for 24 hours, with erastin serving as a positive control for ferroptosis. All tested nanomaterials upregulated the transcription of *Acyl-CoA Synthetase Long Chain Family Member 4 (ACSL4)*, an enzyme that incorporates PUFA (e.g. arachidonic acid) into the lipid membranes, making them more susceptible to lipid peroxidation. Furthermore, 19 nanomaterials increased *Prostaglandin-Endoperoxide Synthase 2 (PGTS2)* expression or reduced *GPx4* mRNA levels. Interestingly, significant divalent iron staining was observed in only four nanomaterials (i.e., carbon nanotubes, α-Fe_2O_3, Co_3O_4, WO_3). Surprisingly, some of these materials lacked inherent iron content, suggesting that the iron originated intercellularly.

Given that mitochondria contain 20 - 50 % of a cell's total iron content, mitochondrial damage can release labile iron, effecting heme- and iron-sulfur-cluster biosynthesis, and alter iron metabolism genes involved in uptake, storage and export (Jhurry *et al.*, 2012; Rauen *et al.*, 2007). This interdependence between ROS formation (oxidative stress) and iron homeostasis explains how "iron free" nanoparticles can elevate intracellular free iron and trigger ferroptosis.

Table 2: Characteristics of nanomaterials, exposed to HUVEC for a global ferroptosis investigation.

The first column of the table lists the nanomaterials, followed by their primary particle size, the producer, and the presence or absence of positive staining for divalent iron, determined using Lillie staining. Total RNA was extracted for mRNA analysis via qRT-PCR to assess the expression of three ferroptotic specific markers: *Prostaglandin-Endoperoxide Synthase 2* (*PTGS2)*, *Acyl-CoA Synthetase Long Chain Family Member 4 (ACSL4)*, and *Glutathione peroxidase 4 (GPx4)*. Each exposure was conducted in three independent experiments. Statistical significance is denoted as follows: * $p < 0.05$, ** $p < 0.01$, *** $p < 0.001$, and ns (not significant) (C. Zhang *et al.*, 2020).

Nanomaterial	Primary particle size	Producer	Significant Lillie divalent iron staining	Upregulation of mRNA expression PGTS2	Upregulation of mRNA expression ACSL4	Downregulation of mRNA expression GPx4
Fullerene-C60		Aladdin		**	***	***
Carbon black		Macklin		ns	**	***
Carbon nanotube	diameter 20-40 nm, length 5-15 µm	Shenzhen Nanotech Port Co	✓	**	***	***
Graphene oxide	size 0.5-3 µm, thickness 0.55-1.2 nm	Aladdin		*	***	**
Al_2O_3	30 nm	Macklin		**	***	***
SiO_2	5-15 nm	sigma		***	***	*
α-Fe_2O_3	30 nm	Aladdin	✓	***	***	**
γ-Fe_2O_3	20 nm	Macklin		***	***	**
Fe_3O_4	20 nm	Meryer		***	***	**
TiO_2	25 nm	Macklin		***	***	**
Co_3O_4	30 nm	Macklin	✓	***	***	**
NiO	30 nm	Aladdin		***	***	***
CuO	100-200 nm	Macklin		ns	***	**
Y_2O_3	40 nm	Aladdin		***	**	***
ZrO_2	50 nm	Macklin		***	**	*
Ag	60-120 nm	Macklin		***	***	**
SnO_2	50-70 nm	Macklin		***	***	ns
La_2O_3	50 nm	Macklin		***	**	**
CeO_2	20-50 nm	Aladdin		**	***	ns
WO_3	<100 nm	Macklin	✓	***	***	**
Au	5-10 nm	Laboratory synthesis		***	**	*

Abbreviations: ACSL4: Acyl-CoA Synthetase Long Chain Family Member 4; GPx4: Glutathione peroxidase 4; PTGS2: Prostaglandin-Endoperoxide Synthase 2.

Metals

Detachable heavy metals are a significant component of UFP. These metals are among the most widespread pollutants, with elevated concentrations found in water, soil, and air pollution (Jan *et al.*, 2015). Even biologically essential elements can induce neurotoxicity when present at supraphysiological concentrations. Interestingly, metals can also trigger ferroptosis through the upregulation of intracellular iron overload. Since our UFP contain a mixture of metals (Cf. Supplemental Data Table S3 (UFP Lille) and Table S4 (UFP Dunkirk), p. 239, 240), the following section discusses the mono- and co-exposure to (multiple) metals and their potential to induce neuronal ferroptosis.

 # Aluminum

A recent study explored the combined effects of two neurodegenerative risk factors – Al exposure and chronic stress – on neuronal ferroptosis, which is associated with cognitive decline. For that study, six-week old male Wistar rats were exposed to alumina nanoparticles (AlNP) (50 mg/kg) and/or chronic restraint stress (CRS). The combined exposure exacerbated ferroptotic effects in the hippocampus, such as increased DMT1, decreased FPN1 and ferritin levels, and aggravated glutamate and GSH depletion. Additionally, there was a reduction in GPx activity and GPx4 immunofluorescence, along with high levels of LPO. There was a learning and memory dysfunction through the Interferon γ (IFN-γ)/ASK1/JNK signaling pathway. It is not surprising that ferroptosis in the hippocampus may contribute to neurodegenerative diseases like AD or contribute to depressive features (Zhang *et al.*, 2021).

 # Copper

Different metals induce decreases in GSH levels through distinct mechanisms. Notably, Cu is more effective than iron in reducing GSH levels, likely due to its inhibitory effect on gamma-glutamylcystein ligase (GCL), the enzyme responsible for GSH synthesis. While the precise mechanism remains unclear, copper's inhibition of GCL is consistent with its known ability to inhibit other ATP-dependent enzymes (Boulard *et al.*, 1972; Chen *et al.*, 2005). In contrast, iron affects GSH synthesis indirectly, possibly by increasing ROS levels, as it does not directly influence the x_c^- system or GCL activity (Maher, 2018).

 # Zinc

Zinc oxide (ZnO) nanoparticles are widely valued in industry for their exceptional optoelectronic, piezoelectric, ferromagnetic, and optical characteristics. These nanoparticles have been applied in various fields, including antimicrobial agent in skin treatments, in sunscreens for UV light absorption, as biosensors, and as food additives

(J. Wang *et al.*, 2011). Although the specific toxic effects of ZnO nanoparticles, with diameters ranging from 10 to 200 nm, reduced the viability of neuronal stem cells (NSC) in a dose-dependent manner (Deng *et al.*, 2009). Kao *et al.,* (2012) confirmed using confocal microscopy that ZnO nanoparticles are captured in membrane-bound vesicles, where they induce mitochondrial dysfunction and cell death in PC12 neuronal cells (Y. Y. Kao *et al.*, 2012).

HUVEC endothelial cells exposed to ZnO nanoparticles led to lactate dehydrogenase (LDH)-detected cell death, GSH and GPx depletion, and a dose-dependent increase in ROS levels (measured by dichloro-dihydro-fluorescein diacetate (DFCH-DA)). Additionally, MDA levels were significantly elevated, while mRNA expression of GPx4 decreased, and markers of ferroptosis, including ACSL4, arachidonate 15-lipoxygenase (ALOX15), and PTGS2, were upregulated. Co-treatment with the potent iron chelator deferoxamine (DFO) in combination with ZnO prevented cell death, attenuated LDH release, and reduced ROS levels. Further investigation of iron homeostasis revealed upregulation of TfR and DMT1 mRNA, but paradoxically, FPN1 the iron efflux pump, was also elevated. Lillie ferrous iron staining assays indicated disruption of cellular iron homeostasis, supporting the role of iron dysregulation in ZnO nanoparticle-induced toxicity. Ferroptosis is also characterized by changes in mitochondrial morphology, including a reduction or disappearance of mitochondrial cristae, increased mitochondrial density, and rupture of the mitochondrial membrane; ZnO exposure induced similar mitochondrial alterations. ZnO exposure also downregulated *mitofusin 1* (*MFN1*) and *optic atrophy 1 protein* (*OPA1)*, and upregulated *dynamin-related proteins* (*DRP1)*, genes involved in mitochondrial fusion and fission. Additionally, ZnO increased the expression of voltage-dependent anion channel (VDAC) 2 and 3, which mediate mitochondrial iron uptake. These findings indicate that ZnO nanopoarticles induce ferroptosis through a mitochondrial-driven cell death pathway. Moreover, ZnO increased the mRNA and protein expression of p53. Activated p53 binds to the x_c^- transporter subunit, and negatively regulates SLC7A11 (xCT) and reducing cystine import, which in turn decreases GSH levels. To further assess the role of Zn^{2+} in ferroptosis, parallel experiments were conducted by directly exposing cells to $ZnCl_2$ (providing an equivalent amount of Zn^{2+}). Comparable results were obtained, suggesting that dissolved Zn^{2+} plays a dominant role in ZnO nanoparticle-induced ferroptosis. The whole study overview can be found in Fig. 12 (C. Zhang *et al.*, 2020).

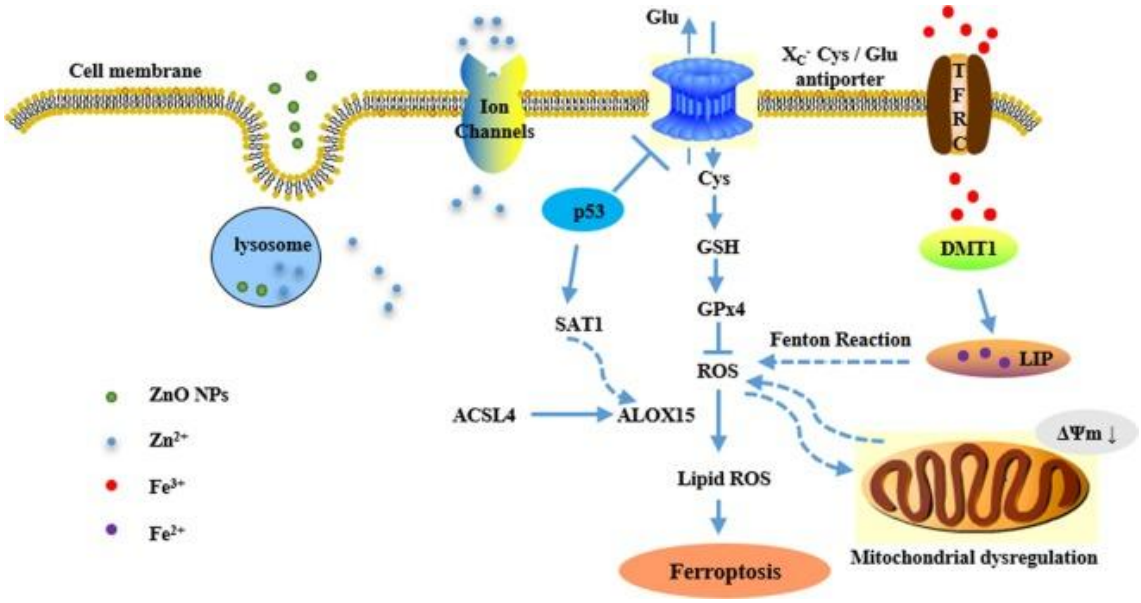

Figure 12: Schedule of ZnO nanoparticle, Zn^{2+}, Fe^{3+}, and Fe^{2+}-induced ferroptosis.

Zinc oxide nanoparticles (ZnO NPs) can cells via endocytosis and accumulate in lysosomal compartments, where they dissolve and release zinc ions (Zn^{2+}) into the cytoplasm. Both ZnO NPs and Zn^{2+} can activate p53, which suppresses the transcription of SLC7A11, leading to glutathione (GSH) depletion. Activated p53 also upregulates the SAT1 gene. Additionally, ZnO NPs and Zn^{2+} impair cellular organelles, including mitochondria, and disrupt iron metabolism. This disruption, combined with the over-accumulation of lipid ROS, culminates in ferroptosis (C. Zhang *et al.*, 2020).

Abbreviations: GSH: Glutathione ; ZnO NPs: Zinc oxide nanoparticles.

Arsenic

Arsenite (AsO_3^{3-}) is a well-recognized toxic metalloid commonly presents in the natural environment. Chronic exposure to arsenite is not only linked to cancer, cardiovascular disorders, diabetes or skin lesions but also to neurodegenerative diseases, including AD and PD (Naujokas *et al.*, 2013). Until recently, arsenite exposure was primarily known to trigger neuronal cell death via apoptosis (Yen *et al.*, 2012), autophagy (Lau *et al.*, 2013) or necrosis (Selvaraj *et al.*, 2013). A more recent study investigated arsinate's potential as an inducer of ferroptosis both *in vivo* and *in vitro*. Therefore, seven-week-old male C57BL/6J mice were treated with environmental relevant doses of arsenite (0.5, 5 and 50 mg/L) via drinking water for six months, after which the cerebral cortex was analyzed. In parallel, PC-12 cells were exposed to various concentrations for 24 hours. The results showed that arsenite induces neuronal cell death (as indicated by Neuronal-Nuclei (NeuN), Microtubule-associated protein (MAP2) markers), promotes the generation of ROS and lipid peroxidation products (MDA), increases cytoplasmic and mitochondrial Fe^{2+} levels, and alters the expression of iron responsive element binding protein 2 (IRBE2). Additionally, arsenite exposure led to

depletion of GSH, a decrease in SOD activity and ATP levels, downregulation of SLC7A11 and GPx4, activation of the MAPK pathway (pJNK1/2 and pERK1/2), and upregulation of mitochondrial VDAC expression and ER stress. These effects are all associated with ferroptosis (Tang *et al.*, 2018).

 # Metal mixture

Precise mechanisms by which metal mixtures contribute to neurotoxicity remains less clear. Interactions among metals can potentially elicit synergistic, additive, or antagonistic effects on various biological processes (Cai *et al.*, 2023).

Evidence suggests that a mixture of biologically essential nutrients, such as Fe, Zn, and Cu, can induce ferroptosis. In detail, co-exposure to Fe, Zn, and Cu in HT22 murine hippocampal neuronal cells leads to ferroptosis through several mechanisms. The exposure resulted in intracellular iron overload, increased lipid peroxidation, and significant mitochondrial abnormalities. Key biomarkers of ferroptosis were observed, including GSH depletion, decreased GPx4 levels, and increased ACSL4 expression. Metabolomic analysis revealed alterations in glycerophospholipid and arachidonic acid metabolism, with elevated levels of cytosolic phospholipase A2 (cPLA2) and arachidonic acid. Inhibition of cPLA2 attenuated ferroptosis, highlighting the crucial role of arachidonic acid metabolism in this process, as shown in Fig. 13. These findings underscore the neurotoxic potential of metal mixtures and their contribution to ferroptosis in neuronal cells (Shi *et al.*, 2023).

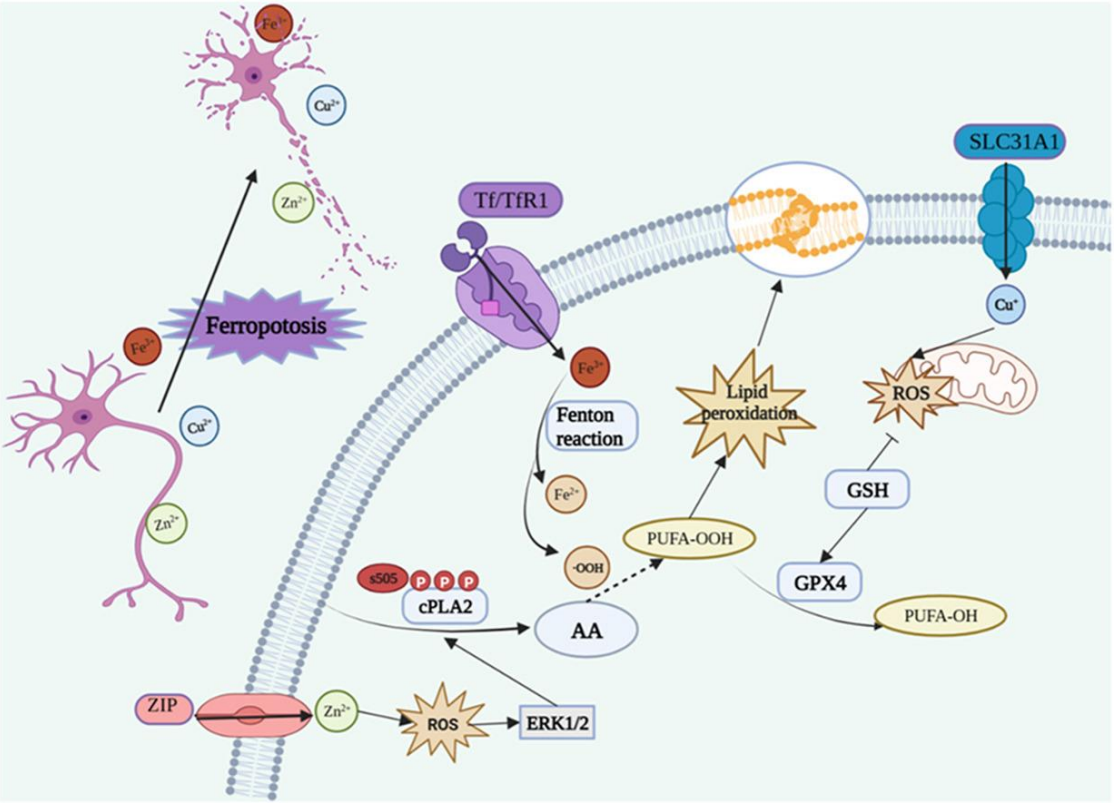

Figure 13: Co-exposure to Fe, Zn, and Cu in hippocampal neurons leads to ferroptosis via the ERK/cPLA2/AA pathway.

After co-exposure to Fe, Zn, and Cu, the phosphorylated state of ERK1/2 increased in HT22 cells, regulating the phosphorylation and activation of cytosolic phospholipase A2 (cPLA2) and its metabolite, arachidonic acid. Arachidonic acid, a polyunsaturated fatty acid (PUFA), is particularly susceptible to peroxidation. Iron overload was also observed, marked by upregulation of transferrin receptor (TfR1), ferroportin (FPN1), ferritin light chain (FTL), and ferritin heavy chain (FTH1), along with glutathione (GSH) and glutathione peroxidase 4 (GPx4) depletion and mitochondria abnormalities, including smaller mitochondria, contracted membrane, and altered cristae. Taken together, these results suggest that co-exposure to Fe, Zn, and Cu leads to neuronal ferroptosis (Shi *et al.*, 2023).

Abbreviations: cPLA2: cytosolic phospholipase A2; FPN1: Ferroportin; FTH1: Ferritin heavy chain; FTL: Ferritin light chain; GPx4: Glutathione peroxidase 4; GSH: Glutathione; PUFA: Polyunsaturated fatty acid; TfR1: Transferrin receptor.

Additionally, a study found that exposure to a combination of non-essential metals, including As, Cd, and Pb, impaired dopaminergic neurotransmission, suggesting that the metal fraction of UFP may play a role in the etiology of PD. The research demonstrated that this metal mixture impaired motor coordination and reduced DA levels in the striatum of mice, mirroring the dopamine depletion observed in PD. Furthermore, key proteins involved in dopamine regulation, such as tyrosine hydroxylase (TH), DAT, and vesicular monoamine transporter 2 (VMAT2), were significantly reduced. These findings suggest that environmental exposure to these metals may contribute to dopaminergic dysfunction (Kim *et al.*, 2021), the only question is if it is through ferroptosis.

Carbon fraction

When decomposing UFP, a significant carbon fraction is present, both in the core (black carbon) and the outside (e.g., PAH), making it important to consider whether the carbon fraction itself might contribute to ferroptosis.

 # Carbon based graphene quantum dots

Both *in vivo* and *in vitro* studies have demonstrated that nitrogen-doped graphene quantum dots (N-GQD) induce ferroptosis and inflammation in the hippocampus of intranasally exposed mice and in microglial BV2 cells. To confirm ferroptosis, mice and microglial cells were pre-treated with Fer-1, which reversed cell death. Key ferroptotic markers, including Fe^{2+} accumulation (measured using the FerroOrange probe), ROS (assessed by DCFH-DA assay), and lipid peroxidation (C11-$BODIPY^{581/591}$ dye and increased 4-HNE protein expression), were observed in N-GQD-exposed mice. Other markers, such as a reduced GSH/GSSG, increased $NADP^+$/NADPH ratio and MDA content, decreased GPx4 and SLC7A11, and elevated ACSL4 protein expression, were also found. These effects were alleviated by Fer-1. Additionally, Fer-1 inhibited microglial activation (Iba1) and secretion of inflammatory cytokines (IL-1β and TNF-α), highlighted a link between ferroptosis and neuroinflammation. The study also found that N-GQD induced cytosolic calcium overload (measured using the Fluo4 probe) by activating L-type voltage-gate calcium channels (L-VGCC) in the plasma membrane and ryanodine receptors (RyR) in the ER membrane, which triggered ferroptosis in microglia. Inhibition of these channels alleviated the intracellular ferrous iron accumulation and ER stress response, indicated by GRP78, CHOP, and ATF4 proteins (Wu *et al.*, 2022). These results are not surprising, as three decades ago, the ancestor RCD of ferroptosis, namely oxytosis was known to be a calcium-influx-dependent neuronal cell death (Lewerenz *et al.*, 2018). An overview of those mechanisms is shown in Fig. 14.

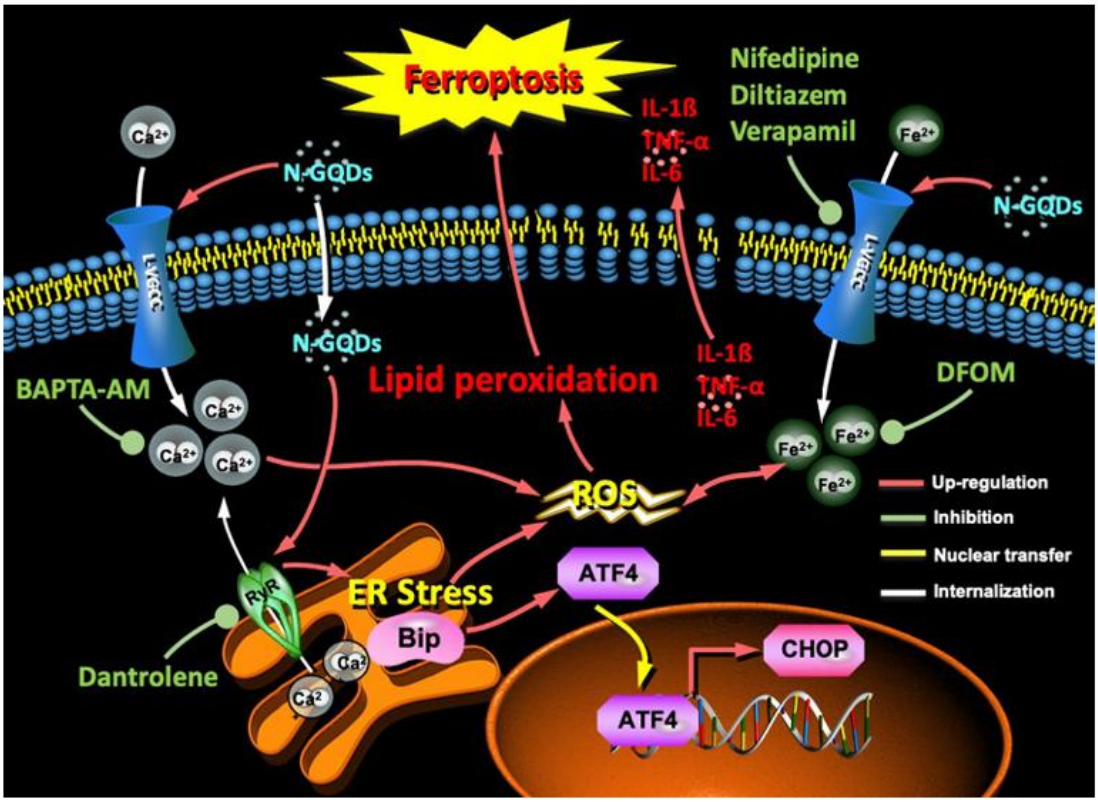

Figure 14: Schematic overview of nitrogen-doped graphene quantum dots-induced ferroptosis and inflammation in BV2 cells.

Nitrogen-doped graphene quantum dots (N-GQDs) triggered ferroptosis via iron accumulation, lipid peroxidation, glutathione (GSH) depletion, reduced glutathione peroxidase 4 (GPx4) and SLC7A11, and increased Acyl-CoA Synthetase Long Chain Family Member 4 (ACSL4) expression, all reversible by Ferrostatin-1 (Fer-1). Additionally, N-GQDs caused calcium overload by activating L-type voltage-gate calcium channels (L-VGCCs) and ryanodine receptors (RyR) channels, disrupting calcium homeostasis and inducing ER stress markers, including BiP, ATF4, and CHOP, which amplified ferroptosis (Wu *et al.*, 2022).

Abbreviations: ACSL4: Acyl-CoA Synthetase Long Chain Family Member 4; Fer-1: Ferrostatin-1; GPx4: Glutathione peroxidase 4; GSH: Glutathione; L-VGCCs: L-type voltage-gate calcium channels; N-GQDs: Nitrogen-doped graphene quantum dots; RyR: Ryanodine receptors.

 # Carbon Nanotubes

Carbon nanotubes (CNT), derived from graphene – a single-atom-thick carbon sheet – are engineered nanoparticles with unique cylindrical structures. They are categorized as in two main types: single-walled carbon nanotubes (SWCNT) or multi-walled carbon nanotubes (MWCNT), offering exceptional strength, flexibility, and conductivity. These properties make CNT highly valuable in industries ranging from electronics to medicines (De Volder *et al.*, 2013), but raise concerns about their potential toxicity, especially as global production and environmental exposure increase (Nowack *et al.*, 2013). Notably, CNT can enter the brain, posing risks to the CNS. Studies on SWCNT have demonstrated oxidative stress-related toxicity in PC12 neuronal cells, including cell viability loss, mitochondrial dysfunction, increased ROS, lipid peroxidation, and

decreased antioxidant enzyme activities (SOD, GPx, and CAT) (Wang *et al.*, 2012; Jingyun Wang *et al.*, 2011). These effects, mitigated by vitamin E (Wang *et al.*, 2012), resemble ferroptotic hallmarks, although ferroptosis was not identified at that time (Dixon *et al.*, 2012). Additionally, iron-containing MWCNT (Fe-MWCNT) exacerbate these effects, disrupting the cytoskeletal integrity, impairing neurite outgrowth, and altering the dopaminergic phenotype in PC12 cells (Meng *et al.*, 2013). A 2024 study revealed that MWCNT-induced ferroptosis is amplified by autophagy, which suppresses PGC-1α-dependent mitochondrial biogenesis in BEAS-2B lung epithelial cells (Zhu *et al.*, 2024), highlighting the importance of further exploring the ferroptosis-inducing potential of CNT.

I.6 Regulated cell death umbrella after ultrafine particle exposure

Both PD and nanoparticle exposure are closely linked to ferroptosis, underscoring the need for more research on ferroptosis in dopaminergic neurons after UFP exposure. But UFP can also trigger other RCD forms, and ferroptosis may cross-talk with distinct types of RCD, such as apoptosis and autophagy. Under certain conditions, these RCD forms can transform into one another, highlighting the importance of studying a broader landscape of RCD mechanisms following UFP exposure.

I.6.1 Autophagy and its potential implication in PD

Mechanism of autophagy

Autophagic cell death is a regulated process of self-degradation that cells use to respond to stressors such as inflammation, hypoxia, ER stress, among other pathological conditions (Ravanan *et al.*, 2017). Controlled by mammalian target of rapamycin (mTOR) and AMP-activated protein kinase (AMPK), autophagy begins with the formation of unc-51-like autophagy-activating kinase (ULK) and the class III phosphatidylinositol 3-kinase (PtdIns3K) complexes, shown in Fig. 15. This initiate autophagosome formation, a double-membraned vesicle that sequesters damaged cellular components for degradation. Maturation requires the activation of several autophagy-related proteins, the Microtubule-associated protein 1 light chain 3 (LC3) exist in the cytosol as a full-length protein (LC3b) and is cleaved by autophagy-related gene protein 4 (ATG4) to generate LC3b-I, which is conjugated to ATG3 to form LC3b-II, facilitating autophagosome expansion by ATG-5, -12, and -16 complexes. The autophagosome ultimately fuses with lysosomes for degradation and recycling of cellular components (Mathiassen *et al.*, 2017).

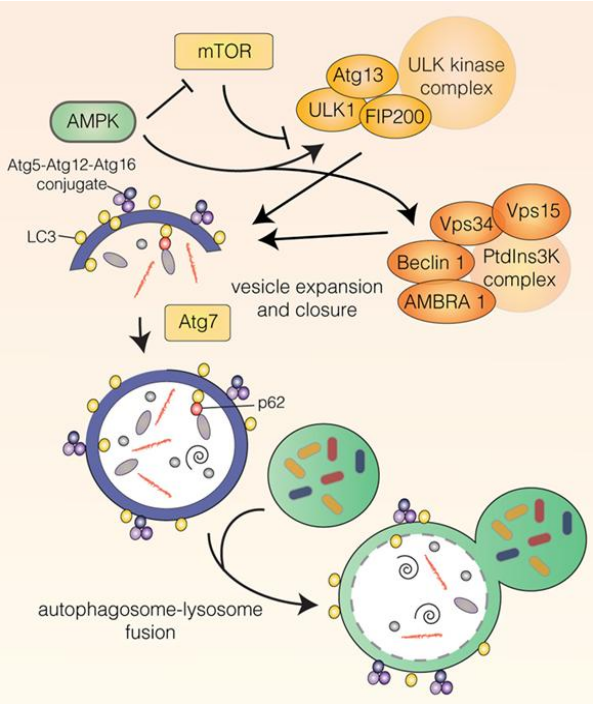

Figure 15: Autophagy.

AMP-activated protein kinase (AMPK) suppresses mammalian target of rapamycin (mTOR), this action will activate the unc-51-like autophagy-activating kinase (ULK) and the class III phosphatidylinositol 3-kinase (PtdIns3K) complex. From then on, the autophagosome will be made by making use of several autophagy-related gene (Atg) proteins and Microtubule-associated protein 1 light chain (LC3). Cell organelles and/or other harmful products are encapsulated in vesicles to provide a delineated degradation of cytoplasmic contents, allowing it to break down after fusion with the lysosome (Mathiassen *et al.*, 2017).

Abbreviations: AMPK: AMP-activated protein kinase; Atg: Autophagy-related gene; LC3: Microtubule-associated protein 1 light chain 3; mTOR: mammalian Target of rapamycin; ULK: Unc-51-like autophagy-activating kinase

Beclin-1 is another key biomarker of autophagy, serving as a core component of the class III PtdIns3K complex (Vergne & Deretic, 2010) and also p62 (SQSTM1) is widely studied in autophagy assays (Komatsu *et al.*, 2007).

Examples of autophagy in the context of Parkinson's disease

The precise role of autophagy in the context of PD remains elusive. The first morphological evidence of autophagy in dopaminergic neurons of PD patients was reported in 1997 (Anglade *et al.*, 1997). Later studies by Dehay and colleagues (2012) revealed increased LC3-II levels in Lewy Bodies within the SN*pc*, indicating elevated autophagosome formation. This increase coincided with reduced lysosomal markers, suggesting lysosomal depletion potentially driven by excessive autophagosome formation. Additionally, p62 and other autophagy-related proteins including ULK1, ULK2, Beclin-1, VPS34, and AMBRA1, have also been detected in Lewy bodies (Miki *et al.*, 2016; Zatloukal *et al.*, 2002). Mutations in genes associated with familial PD, such as *DJ-1* and *ATP13A2*, have been shown to impair lysosomal function and disrupt autophagy in *in vitro* studies (Dehay *et al.*, 2012; Gusdon *et al.*, 2011; Krebiehl *et al.*, 2010). Contradictory, it is also shown that α-synuclein overexpression can inhibit early autophagosome formation, contributing to further abnormal protein aggregation (Winslow & Rubinsztein, 2011).

Questioning if ultrafine particles can induce autophagy

$PM_{2.5}$ exposure has been shown to induce autophagy across various systems and organs, particularly affecting the respiratory system. In lung cancer cells, $PM_{2.5}$ exposure triggers autophagy through ROS production (Deng *et al.*, 2017; Deng *et al.*, 2013). $PM_{2.5}$-induced autophagy involves oxidative stress and inflammatory signaling pathways, with notable mechanisms such as nitric oxide synthase 2 (NOS2) signaling and activation of the ATR-CHEK1/CHK1 axis that subsequently activate p53-dependent autophagy and Vascular Endothelial Growth Factor A (VEGFA) production in BEAS-2B epithelial cells (Xu *et al.*, 2016; X.-M. Zhu *et al.*, 2018). In A549 human lung epithelial cells, AMPK is required during $PM_{2.5}$-induced autophagy (Wang *et al.*, 2015). Additionally, $PM_{2.5}$ exposure induces developmental toxicity in zebrafish embryos via ER stress and activation of the IRE1-XBP1 and ATF6 autophagy pathways, leading to increased mortality and malformations (Y. Zhang *et al.*, 2018). In mice, $PM_{2.5}$ triggers hepatic autophagy trough the MyD88-mediated inflammatory pathway, indicating a link to metabolic liver disorders (Qiu *et al.*, 2017). In the circulatory system, $PM_{2.5}$ activates autophagy in aortic endothelial cells via the NF-κB pathway in mice (Xia *et al.*, 2017) and human corneal epithelial cells (Fu *et al.*, 2017). Interestingly, urban China collected $PM_{2.5}$ disrupts the blood-testis barrier (BTB) integrity by down-regulating tight junction proteins (ZO-1 and occludin) and gap junction proteins (connexin43) through autophagy, as evidenced by higher levels of LC3-II and p62, along with increased levels of Gpx and SOD. Vitamins E and C could alleviate the $PM_{2.5}$-induced oxidative stress, reverse the autophagy defect, and restore the BTB integrity (Wei *et al.*, 2018).

However, there are fewer established links between PM exposure and neuronal autophagy. The fact that $PM_{2.5}$ can disrupt tight junctions and impair consequently barriers raises the question of whether UFP could induce similar effects through autophagy. In human glioblastoma LN-229 cells exposed to $PM_{2.5}$ in combination with autophagy inhibitors bafilomycin A1 (Baf A1) and Beclin 1 siRNA, forced apoptosis occurred (Yuan *et al.*, 2022). In a juvenile rat model, led PM exposure to microglia activation and induced NOD-,LRR-and pyrin domain-containing protein 3 (NLRP3)-mediated neuroinflammation, consequently reducing neuronal ROS and apoptosis (Gui *et al.*, 2024). This highlighting the potential protective role of autophagy in the CNS, and moreover, its role as an antecedent to apoptosis in the context of PM exposure.

I.6.2 Apoptosis and its potential implication in PD

Mechanism of apoptosis

Apoptosis, also known as programmed cell death, is the prototypical form of RCD. As depicted in Fig. 16, the apoptotic pathway can be initiated trough two primary mechanisms:

- Intrinsic pathway: The pathway is activated by intracellular stimuli, such as DNA damage, ischemia, or oxidative stress. These stimuli trigger endogenous cell stress signals that induce the activation of B-cell lymphoma 2 (BCL-2) homology 3 (BH3-only) proteins. These BH3-only proteins facilitate the recruitment of pro-apoptotic proteins, BCL-2-associated X protein (BAX) and BCL-2 antagonist or killer (BAK). Upon oligomerization, BAX and BAK form pores in the outer mitochondrial membrane, resulting in mitochondrial outer membrane permeabilization (MOMP). This process allows the release of pro-apoptotic factors, including cytochrome C, in the cytosol. Cytochrome C then associates with apoptotic protease activating factor 1 (APAF1) to form the apoptosome, which initiates the caspase cascade. Initiator caspase-9 activates downstream effector caspases (e.g., caspases-2, -3, -6, -7, -8 and -10), leading to the proteolytic activation of cellular substrates that drive cell death.
- Extrinsic pathway: This pathway is initiated when death receptors (e.g., CD95) are activated by their corresponding ligands (e.g., Fas ligand). The binding of these ligands to the receptors recruits the adaptor protein FAS-associated death domain (FADD), which facilitates the recruitment of initiator caspase-8. When both FADD and caspase-8 are bound to the death receptor complex, they lead to the cleavage and activation of effector caspases, specifically caspase-3 and -7, which are central to executing the apoptotic process. Additionally, caspase-8 can cleave and activate the BH3-interacting domain death agonist (BID). The truncated form of BID (tBID) enhances the formation of the BAX-BAK complex, linking the extrinsic and intrinsic apoptotic pathways (Kim *et al.*, 2015).

Figure 16: Apoptosis mechanism: [1] intrinsic and [2] extrinsic pathways.

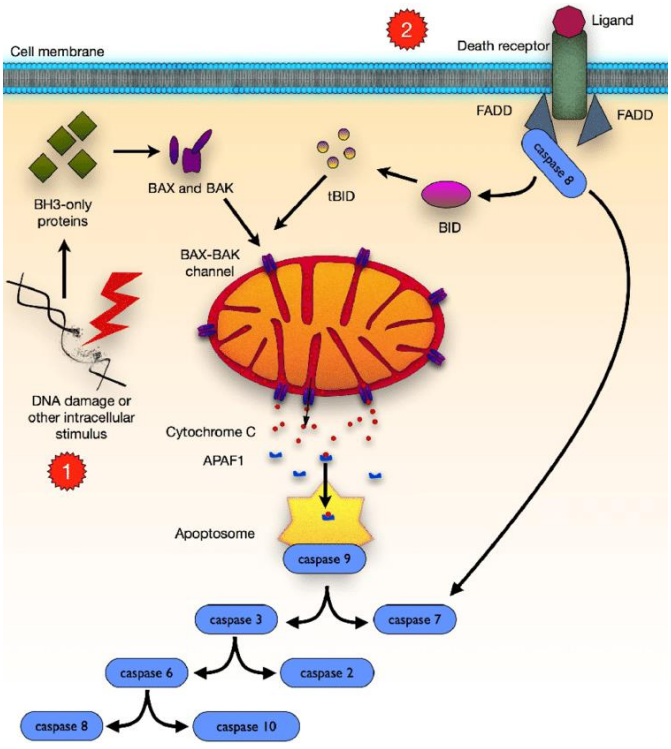

[1] DNA damage activates BCL-2 homology 3 (BH3-only) proteins, leading to the recruitment of BCL-2-associated X protein (BAX) and BCL-2 antagonist or killer (BAK). These proteins oligomerize to form channels in the mitochondrial membrane, resulting in release of cytochrome C. The formation of the apoptosome stimulates the caspase cascade. [2] Ligand binds to a death receptor, which recruits caspase-8. This initiator caspase can directly activate the caspase cascade or it stimulate the BH3-interacting domain death agonist (tBID), facilitating the formation of the BAX-BAK heterodimer (Glowacki *et al.*, 2013).

Abbreviations: BAK: BCL-2 antagonist or killer; BAX: BCL-2-associated X protein; BH3-only: B-cell lymphoma 2 (BCL-2) homology 3; tBID: (truncated) BH3-interacting domain death agonist

The involvement of apoptosis in Parkinson's disease

Numerous studies suggest that both intrinsic and extrinsic apoptosis contribute to the pathogenesis of PD. Post-mortem analysis have shown that dopaminergic neurons of the SN of PD patients exhibit increased expression of various apoptotic markers, including caspase-3 (Hartmann *et al.*, 2000; Tatton, 2000), caspase-9, and caspase-8 (Viswanath *et al.*, 2001), as well as BAX (Tatton, 2000) and the MOMP regulator glyceraldehyde-3-phophate dehydrogenase (GAPDH) (Tarze *et al.*, 2007).

Targeting apoptosis presents a potential strategy for preventing neuronal death in PD. However, evidence suggests that this approach may be insufficient. Firstly, some studies have failed to identify apoptosis as a dominant form or RCD in PD (Banati *et al.*, 1998; Kösel *et al.*, 1997), indicating that apoptosis might not be the primary RCD mechanism involved in PD pathology. Secondly, apoptosis may play a protective role by eliminating damaged or potentially harmful mutant cells, thereby preventing their survival and accumulation (Dyke *et al.*, 1997).

Questioning if ultrafine particles can induce apoptosis

$PM_{2.5}$-induced apoptosis affects various body systems, primarily through inflammation-related signaling pathways. In the circulatory system, $PM_{2.5}$ triggers apoptosis in cardiomyocytes, contributing to cardiac dysfunction through mechanisms such as Beta-2 adrenergic receptor (ADRB2) hypermethylation and activation of the β-Adrenergic Receptor-PI3K Signaling Crosstalk (β2AR/PI3K/Akt) pathway (Yang *et al.*, 2019). Mitochondrial damage, lipid accumulation, and apoptosis in macrophage foam cells also accelerate the progression of atherosclerotic plaques following PM exposure (J. Liu *et al.*, 2019). Additionally, $PM_{2.5}$ exposure induces cardiomyocyte apoptosis via the JNK/P53 pathway (Wang *et al.*, 2019) and activated the inflammatory COX-2/PGES axis in vascular endothelial cells, promoting apoptosis and inflammatory responses (Yin *et al.*, 2017). In HUVEC endothelial cells, $PM_{2.5}$ induces apoptosis through the p53-BAX-Caspase pathway in a dose-dependent manner, posing significant risks to the cardiovascular system (Wang *et al.*, 2017). In the reproductive system, $PM_{2.5}$ promotes apoptosis in human embryonic stem cells (hESC) by inhibiting the ROS-mediated NRF2 pathway (Jin *et al.*, 2019), and induces embryotoxicity through the ROS-JNK/ERK apoptosis pathway (Yuan *et al.*, 2016). In a study examining the exacerbation role of $PM_{2.5}$ on lungs of 9-week-old male C75BL/6J mice, $PM_{2.5}$ exposure exacerbated tissue damage, inflammation, and apoptosis in cigarette-inflamed lungs but had no significant impact on normal lungs. These findings were confirmed by *in vitro* studies where $PM_{2.5}$ aggravated caspase-dependent apoptosis in cigarette-inflamed human bronchial epithelial cells (HBEpiC), which could be inhibited by caspase-3 inhibitor Z-VAD-FMK (Zhou *et al.*, 2019). $PM_{2.5}$ also exacerbates apoptosis in bronchial epithelial cells through

miR-194-3p downregulation, DAPK1 targeting, and ROS-mediated mitochondrial disruption (Jin *et al.*, 2018; Li *et al.*, 2018; Zhou *et al.*, 2018). Furthermore, the MAPK/NF-κB/STAT1 and TNF-α pathways also contribute to apoptosis in lung epithelial cells (A549 and L132) (Dagher *et al.*, 2006; Dou *et al.*, 2018). Interestingly, $PM_{2.5}$ even induces mitochondrial-dependent apoptosis in keratinocytes, leading to skin irritation (Hu *et al.*, 2017).

More related to this PhD project, in a study on cortical *in vitro* cultured mouse neurons exposed to varying concentrations of $PM_{2.5}$ (12.5, 25, 50, 100, and 200 µg/mL) showed that $PM_{2.5}$ exposure altered the expression of key apoptosis-related proteins, including BAX, Bcl-2, and activated Caspase-3, leading to neuronal apoptosis. $PM_{2.5}$ exposure also reduced the levels of postsynaptic density protein (PSD-95) and N-methyl-D-aspartate (NMDA) receptor subunit (NR2B), both critical for synaptic structure and function. These effects varied by season, with winter $PM_{2.5}$ causing the most pronounced changes. This damage was associated with decreased phosphorylation of extracellular signal-regulated kinase 1/2 (p-ERK1/2) and p-CREB. A correlation was established between the chemical composition of $PM_{2.5}$ and its biological effects, confirming winter $PM_{2.5}$ had the greatest impact on neuronal apoptosis and synaptic injury (M. Chen *et al.*, 2017).

II. PROBLEM STATEMENT: WILL THE ABSENCE OF ULTRAFINE PARTICLE POLICY CONTRIBUTE TO THE RISING PREVALENCE OF PARKINSON'S DISEASE?

As previously discussed, factors such as aerodynamic diameter and composition play a critical role in determining the (neuro)toxicity of UFP. But of course, according to the fundamental toxicological principle "*the dose makes the poison*" [Paracelsus (1493 - 1541)], toxicity is also directly influenced by concentration.

This raises the first question:

II.1 Where do we find larger amounts of ultrafine particles?

A study analyzing PM_1 particle amount and composition across 22 sampling stations in Europe (2013-2019) revealed the total PM_1 mass, comprising organic aerosol (OA), equivalent black carbon (eBC), nitrate (NO_3), sulfate (SO_4), ammonium (NH_4), and chloride (Chl), was significantly higher in urban areas (12.2 ± 9.3 µg/m³ – brown spots) compared to rural areas (6.2 ± 3.3 – green spot), as shown in Fig. 17. Although the main components were similar, chemical composition varied between locations. The most abundant OA components were hydrocarbon-like OA (HOA) and biomass burning OA (BBOA), both associated with traffic emissions and solid fuel combustion. For example, in Lille, Dublin, and Helsinki, OA contributed for 35%, 46%, and 53% of the total PM1 mass, respectively. Within these, BBOA accounted for 5% (Lille), 3% (Dublin), and 0% (Helsinki), while HOA represented 4% (Lille), 9% (Dublin), and 5% (Helsinki) of the total OA. These findings underscores the variability in UFP sources and concentrations across different urban environments (Chen *et al.*, 2022).

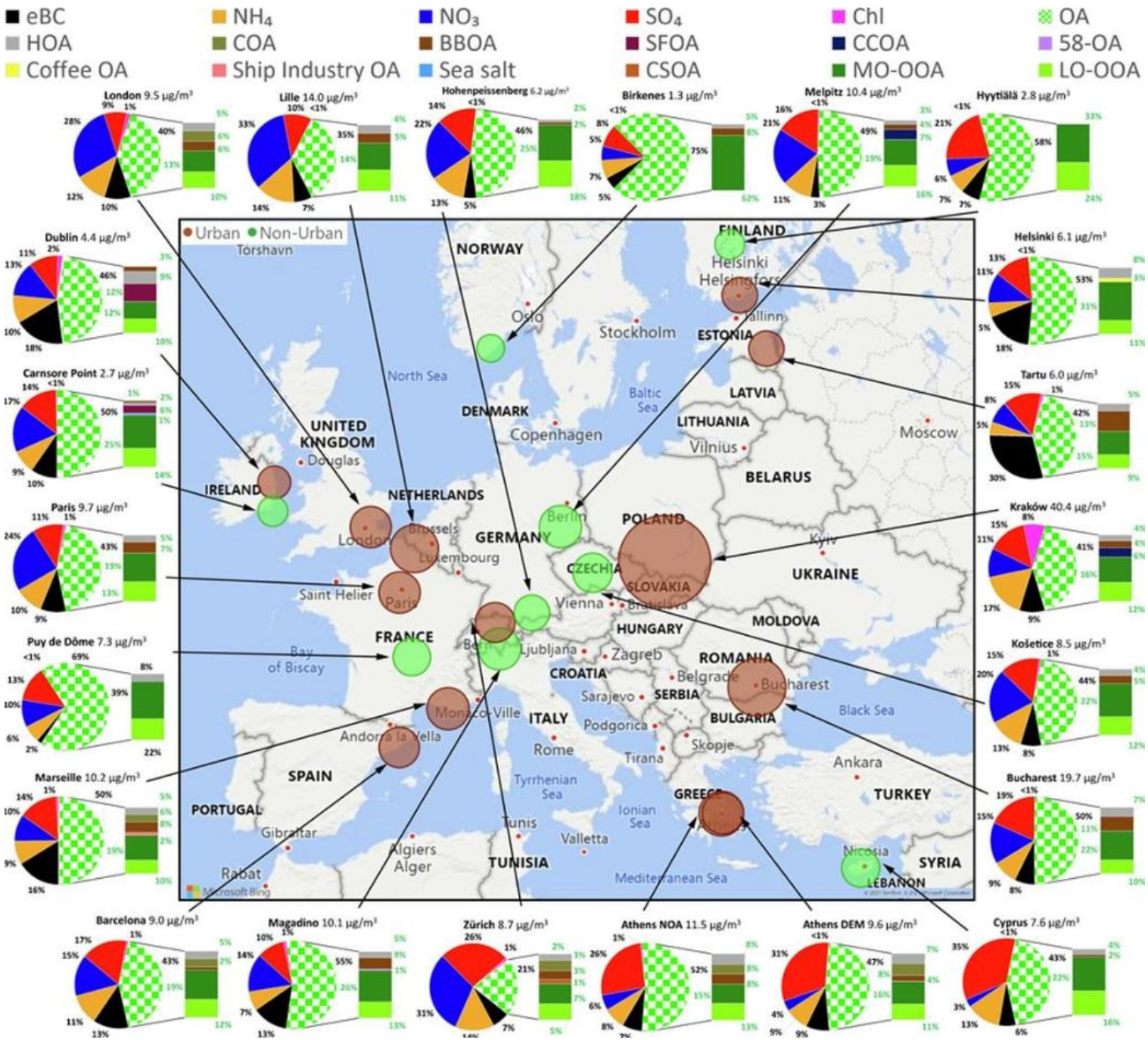

Figure 17: Geographical overview of PM_1 monitoring in Europe (2013-2019).

This map highlights 22 air quality monitoring sites, including 9 non-urban (indicated in green) and 13 urban (indicated in brown) locations, assessed using 21 aerosol chemical speciation monitors (ACSM) and 1 aerosol mass spectrometer (AMS). The PM_1 mass concentration (µg/m^3) represents the sum of organic aerosol (OA), equivalent black carbon (eBC), NO_3, SO_4, NH_4, and Chl. The composition of OA is also decomposed and indicated in the stacked bar chart (Chen *et al.*, 2022).

Abbreviations: ACSM: Aerosol chemical speciation monitor; AMS: Aerosol mass spectrometer; BBOA: Biomass burning OA; CCOA: Coal combustion OA; COA: Cooking-like OA; CSOA: Cigarette smoke OA; eBC: Equivalent black carbon; HOA: Hydrocarbon-like OA; LO-OOA: Less oxidized-oxygenated OA; MO-OOA: More oxidized-oxygenated OA; OA: Organic aerosol; SFOA: Solid fuel OA; 58-OA: 58-related OA.

It is concerning that Lille exhibits a higher concentration of PM_1 particles (14.0 µg/m^3) compared to other major European cities such as London (9.5 µg/m^3), Athens (11.5 µg/m^3), Barcelona (9.0 µg/m^3), and even Paris (9.7 µg/cm^3) (Chen *et al.*, 2022).

A review compared UFP concentration levels from various studies based on monitoring or recovery methodologies categorized results into eight measurement areas: tunnel, on road, road side, street canyon, urban, urban background, rural, and clean background. Fig. 18 represents the mean and median particle concentrations across these environments. The results indicate higher standard deviations in roadside and street canyon measurements, likely due to variations in study methodologies, including different distances from the road. Notably, as highlighted earlier (Cf. I.4.3 PM exposure resulting in cognitive decline and dementia in elderly people, p. 13), living near major roads has been associated with an increased risk of dementia. For example, roadside measurements revealed a mean particle concentration of approximately 48,180 particles/cm^3, compared to rural air, which averaged around 2,610 particles/cm^3 (Morawska *et al.*, 2008). The significantly higher UFP concentrations in roadside and urban areas suggest that individuals in these environments are more exposed, potentially contributing to neurodegenerative conditions such as PD. Therefore, to closely mimic-real life exposure, it is essential to investigate particles collected from roadside and urban sources.

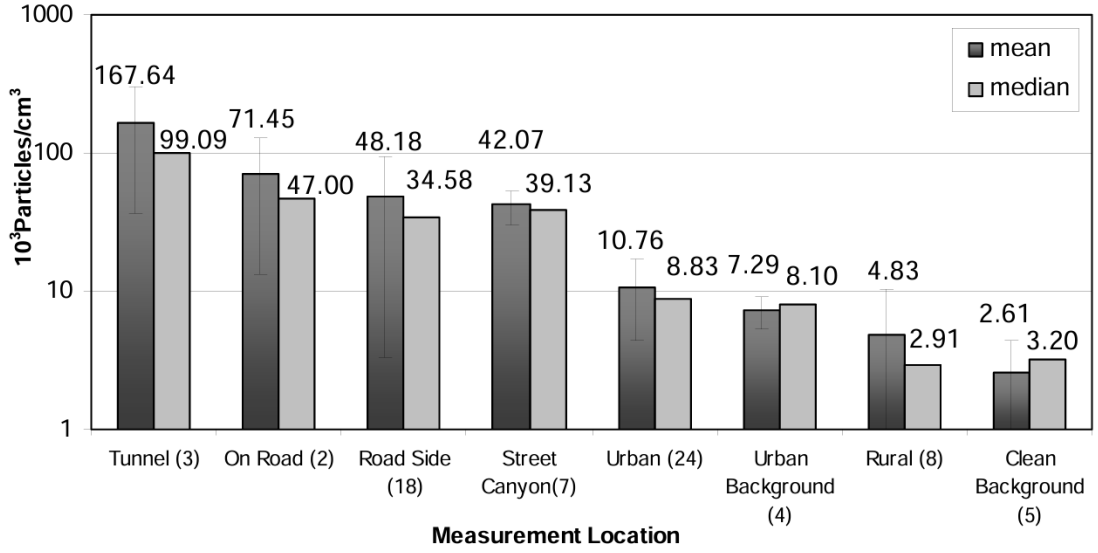

Figure 18: Mean and median particle number concentrations (10^3 particles/cm^3) from 71 studies.

This figure presents ultrafine particle (UFP) concentrations in various environments, highlighting site-dependent differences in human. Measurement locations include tunnels, on road, road side, street canyons, urban, urban background, rural, and clean background. The numbers in brackets indicate the number of measurement sites for each environment, while the values above the bars represent the mean or median concentrations (10^3 particles/cm^3) (Morawska *et al.*, 2008).

Abbreviations: UFP: ultrafine particles.

Both the study of Chen (2022) and the review of Morawska (2008) confirm that UFP concentrations are highest in urban areas, particularly near major roads or within tunnels. These findings result in a new important question:

II.2 Why have ultrafine particle concentrations been rising?

The global mean concentration of UFP is approximately 10,760 particles/cm^3, with roadside areas approximately 18-fold of rural areas (Morawska *et al.*, 2008). High humidity especially in winter season, poor air circulation, an increased number of diesel vehicles, and acceleration after traffic stops are all factors that contribute to elevated UFP concentrations (Li *et al.*, 2016). Advancements in fuel and engine technology, along with the use of catalytic converters, have successfully reduced the mass of UFP and carbon monoxide (CO) from automotive exhaust, but unfortunately, this increased the number and toxicity of UFP (Frank *et al.*, 2013; Park *et al.*, 2008). While most studies to date have concentrated on $PM_{2.5}$, which originates from both natural and anthropogenic sources, the rise in environmental nanoparticles over the past few decades is predominantly attributed to human activities, as listed in Table 3.

Table 3: Overview of anthropogenic processes that originate nanoparticles and/or ultrafine particles.

Industrialization and increased mobility are rapidly introducing more nanoparticles and UFP into the environment. This table provides a summary of key processes, domains, and their contribution to pollution.
Summarized from (Charitidis *et al.*, 2014; Donaldson *et al.*, 2005; Jan *et al.*, 2022; Lopez *et al.*, 2023; Malik *et al.*, 2023; Marcos, 2019; Mohajerani *et al.*, 2019).

Process	Domain?	How?
1) Industrialization and manufacturing processes	Nanotechnology and nanomaterials	With the rapid development of nanotechnology, industries are producing an increasing number of nanomaterials. These materials, which have unique properties at the nanoscale, are used in electronics, cosmetics, pharmaceuticals, and construction materials. As these materials are manufactured, their us and eventually discarded, can be released into the water, soil, and also air.
	Metal processing and combustion	Many industrial activities, such as metal smelting, welding, and combustion processes (e.g., coal burning), generate fine particles, including UFP and nanoparticles, as byproducts. These processes release metal-based nanoparticles/UFP into the atmosphere, which can travel long distances and contribute to air pollution.
2) Increased traffic and vehicle emissions	Combustion engines	Modern vehicles, especially those with internal combustion engines, emit nanoparticles as part of exhaust fumes. As engines burn fuel, incomplete combustion produces fine particulate matter, including UFP. Diesel engines, in particular, are major sources of ultrafine particles and nanoparticles in urban areas. Investigation in this toxicity is mostly based on DEP exposure.
	Tire and brake wear	In addition to exhaust emissions, nanoparticles are also produced from the wear and tear of tires and brakes. As vehicles travel, friction from brakes and tires generates tiny particles that include metals and rubber, adding to the environmental nanoparticle load. Brake particles have an average diameter between 1-10 µm, while tire particles are bigger, around 10-18 µm.
3) Urbanization and construction	Construction dust	In highly urbanized areas, construction activities contribute to nanoparticle pollution. The use of cement, metal cutting, grinding, and other processes releases a significant amount of PM, including nanoparticles.
	Road dust	Urban roads accumulate nanoparticles from various sources, such as vehicle emissions, industrial activities, and construction. Traffic can resuspend these particles into the air, increasing the exposure risk to the urban population.
4) Fossil fuel combustion	Power plants and energy production	Fossil fuel combustion in power plants, refineries, and industrial facilities generates a wide range of particulate matter, including UFP. Especially, the burning of coal, oil, and natural gas contribute to air pollution. These particles often contain heavy metals, carbon compounds, and other toxic substances.
5) Environmental degradation of materials	Plastic degradation	Plastics, which are widespread in the environment, can break down over time into smaller particles, including nanoparticles (differently than UFP). This process occurs due to exposure to sunlight (photodegradation), mechanical forces (wave action in oceans), and other environmental factors. Microplastics and nanoparticles are increasingly found in marine and freshwater ecosystems, contributing to pollution.
	Corrosion of metals	Metals exposed to environmental conditions, such as moisture and chemicals, can corrode and release nanoparticles into the air, water, and soil. This is common in industrial areas or regions near highways where metal structures are subject to degradation.

Increased exposure to nanoparticle and UFP poses significant risks to human health and our ecosystem. Investigating the effects of UFP, rather than $PM_{2.5}$ or PM_{10}, is crucial not only due to biological hazards but also because they are more prevalent in the environment. UFP have no boundaries and are found globally, with nearly the entire population (99%) exposed to polluted air, according the WHO data (*Billions of people still breathe unhealthy air: new WHO data*, 2022). This exposure is also recognized by UNICEF as contributing to 8.1 million deaths in 2021 (*Air pollution accounted for 8.1 million deaths globally in 2021, becoming the second leading risk factor for death, including for children under five years*, 2024). Consequently, effective policies must be implemented at both national and international levels to address this issue comprehensively. Currently, restrictions are only in place for PM_{10} and $PM_{2.5}$, indicating a need for a more coordinated, global approach. The global organizations with their corresponding PM_{10} and $PM_{2.5}$ threshold values can be found in Table. 4.

Table 4: Listing global organizations with their PM_{10} and $PM_{2.5}$ threshold values, based on annual and 24-hour exposure limits (µg/cm³).

Organization	PM_{10} [a]	$PM_{2.5}$ [a]
WHO[b]	- Max. annual mean concentration: 15 µg/m³ - Max. 24-hour mean concentration: 45 µg/m³	- Annual mean concentration: max. 5 µg/m³ - 24-hour mean concentration: max. 15 µg/m³
These are stringent targets intended to push countries toward better air quality, though many regions around the world struggle to meet them.		
European Union (EU)[c]	- Annual limit concentration: 40 µg/m³ - Daily limit (not exceeded on > 35 days/year): 50 µg/m³	- Annual limit concentration: 25 µg/m³
The EU Ambient Air Quality Directive sets legally binding, which are enforceable, meaning member states must take action to ensure air quality remains within these thresholds, or face penalties. The EU's limits are less stringent than WHO recommendations, largely due to practical considerations around economic activities in Europe.		
United States EPA Standards[d]	- 24-hour standard: 150 µg/m³ (no more than one exceedance per year on average over three years)	- Annual standard: 9 µg/m³ - 24-hour standard: 35 µg/m³
These standards are reviewed periodically, and states are required to develop implementation plans to ensure compliance. Areas that fail to meet these standards (known as nonattainment areas) must implement measures to reduce pollution levels.		
China[e]	Class 1 - Annual limit concentration: 40 µg/m³ - Daily limit: 50 µg/m³ Class 2 - Annual limit concentration: 70 µg/m³ - Daily limit: 150 µg/m³	Class 1 - Annual limit: 15 µg/m³ - 24-hour limit: 35 µg/m³ Class 2 - Annual limit: 15 µg/m³ - 24-hour limit: 35 µg/m³
The Current National Air Quality Standards from China (2016) are less stringent than WHO recommendations but represent progress for the country's heavily industrialized regions. Class 1 applies to special regions, such as national parks, while Class 2 covers all other areas.		
India[f]	- Annual mean standard: 60 µg/m³ - 24-hour mean standard: 100 µg/m³	- Annual mean standard: 40 µg/m³ - 24-hour mean standard: 60 µg/m³

[a]: concentrations are mostly expressed as micrograms per cubic meter.

[b]: https://www.eea.europa.eu/publications/status-of-air-quality-in-Europe-2022/europes-air-quality-status-2022/world-health-organization-who-air

[c]: https://environment.ec.europa.eu/topics/air/air-quality/eu-air-quality-standards_en

[d]: https://www.epa.gov/pm-pollution/timeline-particulate-matter-pm-national-ambient-air-quality-standards-naaqs

[e]: https://www.transportpolicy.net/standard/china-air-quality-standards/

[f]: http://www.arthapedia.in/index.php/Ambient_Air_Quality_Standards_in_India

Abbreviations: EPA: Environmental Protection Agency; EU: European Union; PM_{10}: particulate matter smaller than 10 µm in diameter; $PM_{2.5}$: particulate matter smaller than 2.5 µm in diameter; WHO: World health organization

Currently, UFP lacks widely adapted regulatory standards, despite growing evidence of their health risks. While there are no formal, internationally accepted exposure limits for UFP, the issue is increasingly being recognized, with the hope that UFP will be incorporated into air quality standards in the near future. This may involve more stringent vehicle emission regulations and tighter urban and industrial controls.

Looking at $PM_{2.5}$ exposure trends over recent years, there is a cause for cautious optimism. Globally, with the exceptions of Nigeria, Japan, Democratic Republic of the Congo, and Bangladesh, $PM_{2.5}$ levels have shown a slight declined from 2010 to 2020, shown on Fig. 19. The most significant improvements have occurred in Southeast Asia, East Asia, and Oceania, largely driven by better air quality in China. However, reductions in $PM_{2.5}$ exposure have only been realized recently in South Asia, whereas levels remain consistently high across Africa and the Middle East. Despite progress, there is no region that fall below the WHO guideline of a maximum average annual of 5 $\mu g/m^3$ (Cf. Table 4, p. 55).

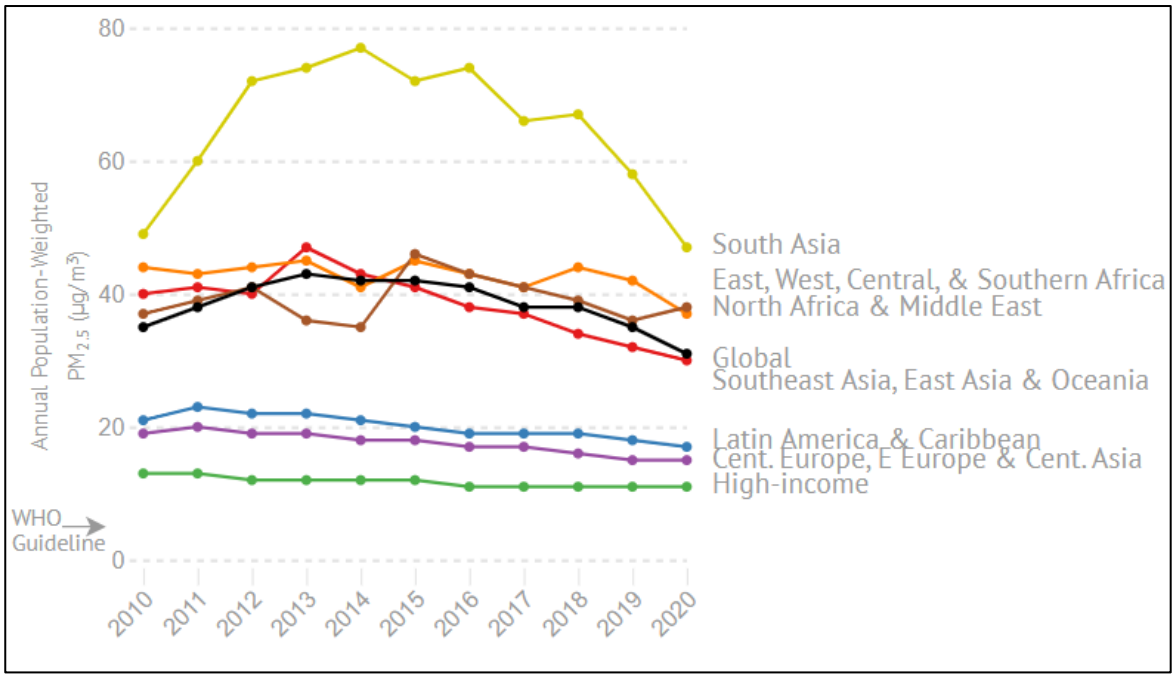

Figure 19: Average annual trends in $PM_{2.5}$ exposure ($\mu g/m^3$) between 2010 and 2020.

$PM_{2.5}$ exposure in represented geographical and socio-economic regions, including South Asia; East, West, Central & Southern Africa; North Africa & Middle East; Southeast Asia, East Asia & Oceania; Latin America & Caribbean; Cent. Europe, E. Europe & Cent. Asia; Global, and High income.

Globally the annual $PM_{2.5}$ is decreasing, with the lowest values in High-income regions. The highest concentrations can still be found in South Asia, however, as the graph shows, $PM_{2.5}$ concentrations are drastically reducing. This can be attributed to the Current National Air Quality Standards from China, induced in 2016 (*Fine particulate matter (PM2.5) is the pollutant that causes the largest health impact globally, contributing to millions of deaths each year.*, 2024).

Although there has been a slight overall reduction in $PM_{2.5}$ exposure, the global health effects of $PM_{2.5}$ are worsening, as shown in Fig. 20, with particularly sharp rises in Asia. In 2021, worldwide, 4.1 million deaths were associated to $PM_{2.5}$ pollution. This underscores the need to maintain focus on $PM_{2.5}$, a silent culprit whose long-term impact on public health continues to grow.

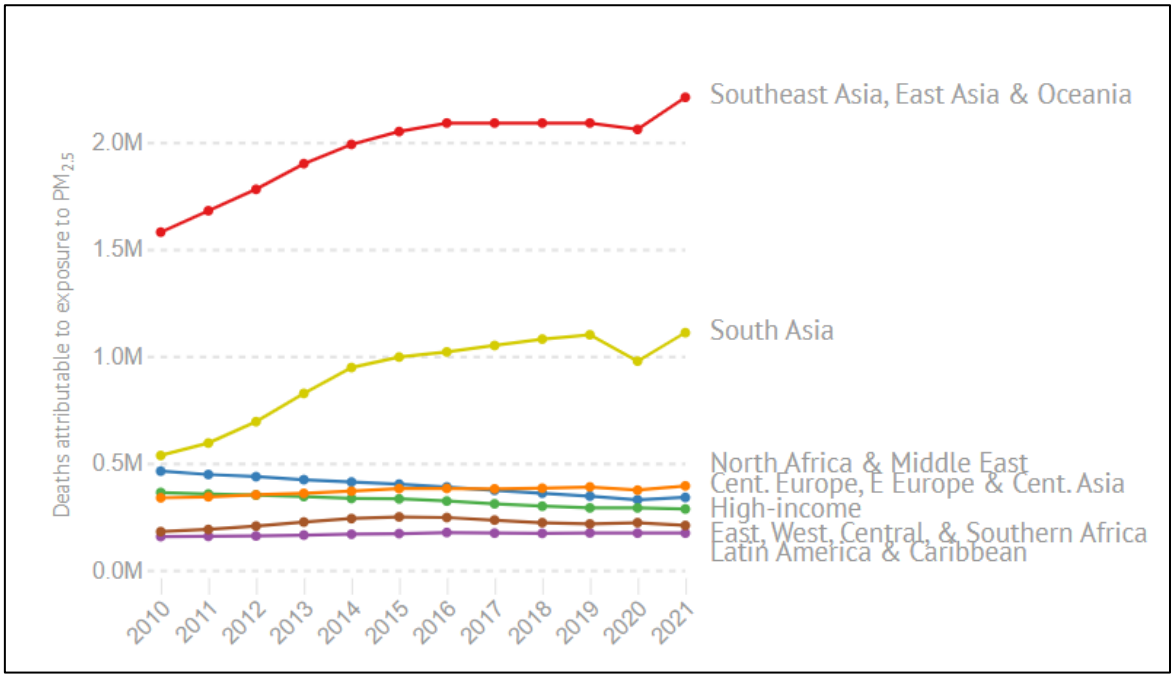

Figure 20: Annual deaths attributed to $PM_{2.5}$ exposure between 2010-2021.

The number of deaths (in millions, M) attributed to $PM_{2.5}$ exposure is shown across various regions: South Asia; East, West, Central & Southern Africa; North Africa & Middle East; Southeast Asia, East Asia & Oceania; Latin America & Caribbean; Cent. Europe, E. Europe & Cent. Asia; and High income regions.

Data represent annual deaths from 2020 to 2021, highlighting an overall increase in Asia and Oceania, with an exponential rise observed between 2020 and 2021 (*Fine particulate matter (PM2.5) is the pollutant that causes the largest health impact globally, contributing to millions of deaths each year.*, 2024).

II.3 Could particulate matter exposure be linked to Parkinson's disease prevalence?

Despite a decline in $PM_{2.5}$ levels, deaths attributed to $PM_{2.5}$ exposure increased by approximately 23% between 2010 and 2021 (*Fine particulate matter (PM2.5) is the pollutant that causes the largest health impact globally, contributing to millions of deaths each year.*, 2024). This paradox underscores the significant health burden posed by air pollution.

Two key factors likely contributing to this trend are:

1) **Population growth:** Regions with higher pollution levels often experience rapid population increases,
2) **Aging population:** The global population is aging, with older individuals being more vulnerable to air pollution-related diseases.

Given that elderly populations are particularly susceptible to air pollution exposure, the link between air pollution toxicity and age-related diseases warrants urgent investigation. This force the question whether UFP may contribute to PD development. Notably, as illustrated in Fig. 21, the prevalence of PD has been increasing over the years.

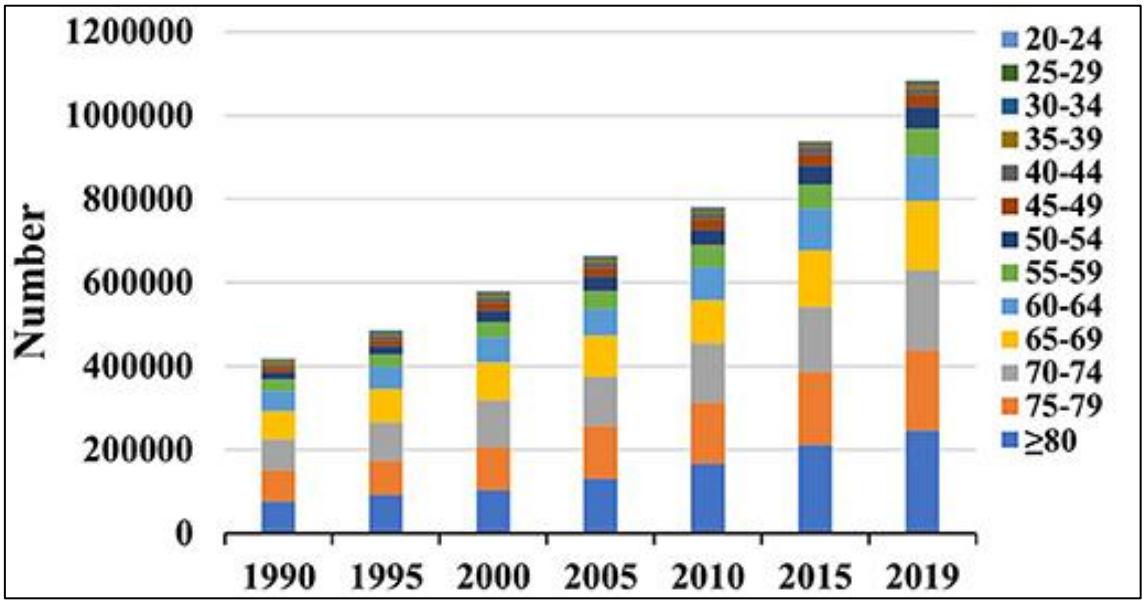

Figure 21: Global annual new incidences and age group distribution of Parkinson's disease from 1990 to 2019.

The stacked bar graph illustrates a consistent increase in PD incidence over time, with an estimated annual percentage change (EAPC) of 0.53 (95% CI: 0.44–0.62) The global prevalent of PD rose by 155.50% from 1990 to reach 8.51 million cases (95% UI: 7,29-9.84 million) in 2019. Age-related trends highlight that the highest number of years lived with disability (YLD) occurred in individuals over 80 years old (303,810 cases). A significant rise was also observed in patients aged 45 years and older, reflecting a growing burden of PD among middle-aged and elderly populations (Ou *et al.*, 2021).

Abbreviations: EAPC: Estimated annual percentage change; YLD: Years lived with disability.

The Global Burden of Disease study highlights neurological dysfunctions as the leading cause of disability worldwide, with PD emerging as the fastest-growing neurological disorder. Between 1990 and 2015, the prevalence of PD doubled, and projections indicate it could surpass 12 million cases by 2040. Historically, PD was

considered a rare disease. However, despite being non-infectious, it exhibits several traits characteristics of a pandemic (E. Ray Dorsey *et al.*, 2018; Morens *et al.*, 2009).

Firstly, it affects extensive geographic areas, with rising prevalence observed across all major regions globally (E. Ray Dorsey & Collaborators, 2018). Secondly, its dynamics are influenced by demographic and environmental shifts, such as aging populations and increasing industrialization. Shown in Fig. 22, research suggests that the burden of PD will progressively shift from Western countries to Eastern regions, particularly China (Dorsey *et al.*, 2007).

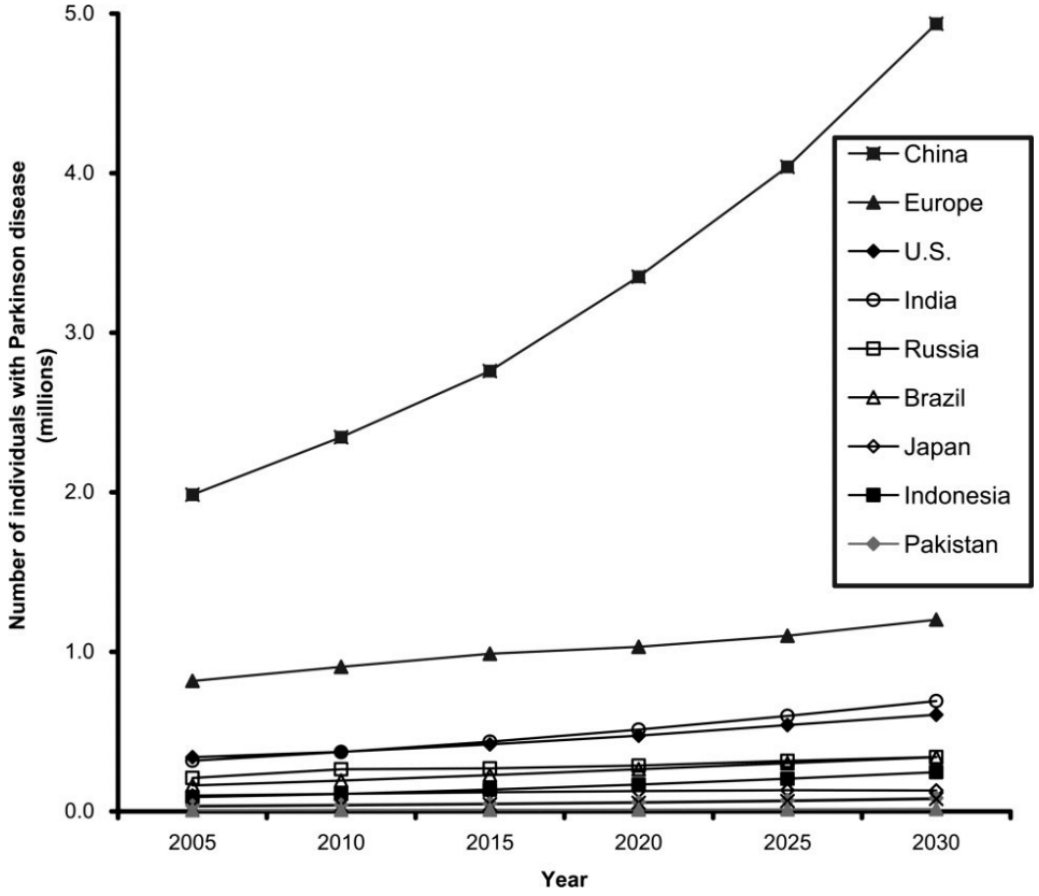

Figure 22: Projected Parkinson's disease cases among individuals aged 50 and older by country/region (2005-2030).

The number of PD cases is projected to rise globally, with a particularly exponential increase in China. The values for representative data of Western Europe are from the five most populous countries: Germany, France, the United Kingdom, Italy, and Spain (Dorsey *et al.*, 2007).

Thirdly, the rapid and widespread increase in PD prevalence is a global phenomenon affecting populations universally. This surge is driven by a complex interplay of social, political, and economic factors, including changes in lifestyle habitats and environmental

exposures. As indicated in Fig. 23, aging alone does not account for the sharp rise in PD cases; additional contributors, such as increased longevity, reduced smoking habitat, and elevated industrial by-products in our environment, are also projected to play a significant role in the disease's prevalence.

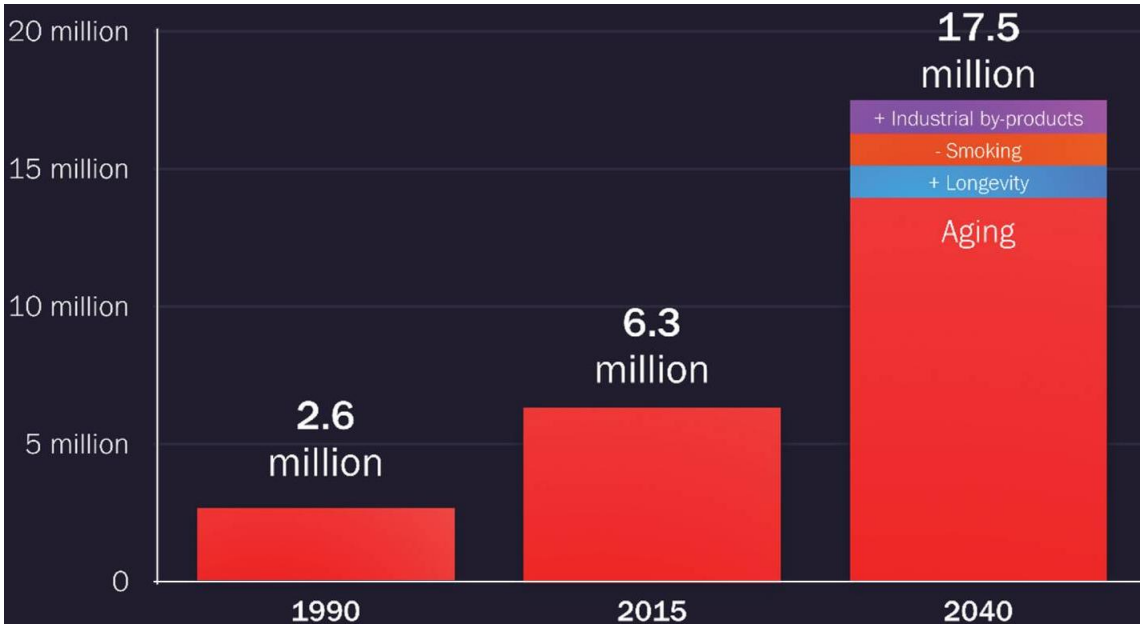

Figure 23: Predicted increase in Parkinson's disease prevalence is influenced by environmental changes.

While increased life expectancy contributes to the rising prevalence of PD, this factor alone does not fully explain the rapid growth of this age-related condition. Environmental changes are increasingly recognized as key contributors, categorized into three primary factors: increased longevity, reduced smoking rates, and higher exposure to industrial by-products (*Evidence of Impending Parkinson's Disease Pandemic Identified*, 2019).

Looking more in detail to those environmental influences, longevity reflects the growing prevalence influenced by both its incidence and the increasing survival rate of patients. As life expectancy improves globally, the overall diseases burden rises. For instance, in France, life expectancy for 65-year-old PD patients is projected to increase by three years between 2010 and 2030 (Wanneveich *et al.*, 2018), largely due to advancements in interdisciplinary care involving researchers, clinicians, pharmacists, nurses, social workers, dieticians, etc. This leading to support networks for both patients and their families. Maybe surprisingly, but smoking has been shown to reduce the risk of developing PD by approximately 40% (Scheperjans *et al.*, 2015). While declining smoking rates represent a public health achievement, they may paradoxically contribute to a higher PD incidence. A 2018 study estimated that reduced smoking rates in the US could lead to a 10% increase in PD cases (Rossi *et al.*, 2018). Similarly, rising PD

incidence between 1976 and 2005, particularly among men over 70, has been linked to declining smoking rates in previous decades (Savica *et al.*, 2016).

Various pollutants from the Industrial Revolution (1760-1840), including pesticides, solvents, and heavy metals, have been linked to PD (Goldman, 2014). Rapid industrialization, particularly in countries like China, has coincided with a sharp rise in PD rates. For example, between 1990 and 2016, China experienced the largest increase in adjusted PD prevalence rates, with more than a two-fold increase during this period (E. Ray Dorsey & Collaborators, 2018). Countries with increasing gross domestic product (GDP), including China, also show higher PD prevalence rates. Coal combustion is the dominant energy course in China, accounting for more than 70% of the total energy demands (Chen *et al.*, 2014). In northern China, the widespread use of coal for residential heating and cooking has been a primary source of $PM_{2.5}$ pollution in winter (Shen *et al.*, 2010). A study of 74 major cities found that daily average $PM_{2.5}$ concentrations exceeded the Chinese standard of 75 $\mu g/m^3$ (about twice the US EPA standard of 35 $\mu g/m^3$) for 69% of days in January, with a record-breaking daily concentration of 772 $\mu g/m^3$. Another example, despite bans in over 70 countries, the use of toxic pesticides like paraquat has increased in the US, a trend that remains unexplained in the EU (Donley, 2019).

Those are just two examples among many that illustrate how the Industrial Revolution has changed our view of productivity, where economic progress often comes at the cost of personal and environmental health. This highlights the lack of an unified consensus on balancing economic industrialization and agriculture with effective environmental protection. The need for studies like this PhD research is crucial to investigate toxin exposure and its impact on public health. Especially as it is estimated that by 2030, there will be around 260,000 PD patients in France, representing a 65% increase compared to 2010. Under these assumptions, approximately 1 in 124 individuals aged over 45 years will be diagnosed with PD, largely linked to the environmental factors (Wanneveich *et al.*, 2018).

III. CONTEXT OF THE PHD PROJECT

To address this problem statement, this PhD project was established as part of the PUF-EXPOmiR project, which investigated the toxicity of urban UFP and their potential harmful effects on various organs, including the lungs, heart, brain, liver, and kidneys. The primary objective was to enhance understanding of toxicokinetics (distribution and persistence in organs) and toxicodynamics (mechanisms such as oxidative stress, inflammation, and regulated cell death (e.g. ferroptosis)).

Funding and Context

The PUF-EXPOmir project was coordinated by Prof. Guillaume Garçon and funded (200,000 €) in 2018 by ANSES under the *Programme National de Recherche Environnement-Santé-Travail (PNR EST)*. The funding proposal highlighted several critical considerations, including: **i) The urgence of a French UFP toxicological study:** The need for a multiorgan toxicological study to highlight (inter)national prevention, particularly after a significant $PM_{2.5}$ pollution episode in 2017 across several French regions, including Hauts-de-France. This event featured exceptionally high $PM_{2.5}$ concentration (> 50 µg/m³, with peaks exceeding 100 µg/m³ for several hours) and a prolonged duration (> 1 month). **ii) The multidisciplinary scope:** The project involves involvement of two PhD candidates, Emeline B. and myself (Emma T.). The total funding allocation for this PhD project was 140,866 € for experiments by IMPECS (shared with Emeline B.) and 23,910 € for LilNCog-DVCD (for my own project) (Cf. Total overview of the finances can be found in Supplemental Data Fig. S1, p. 238).

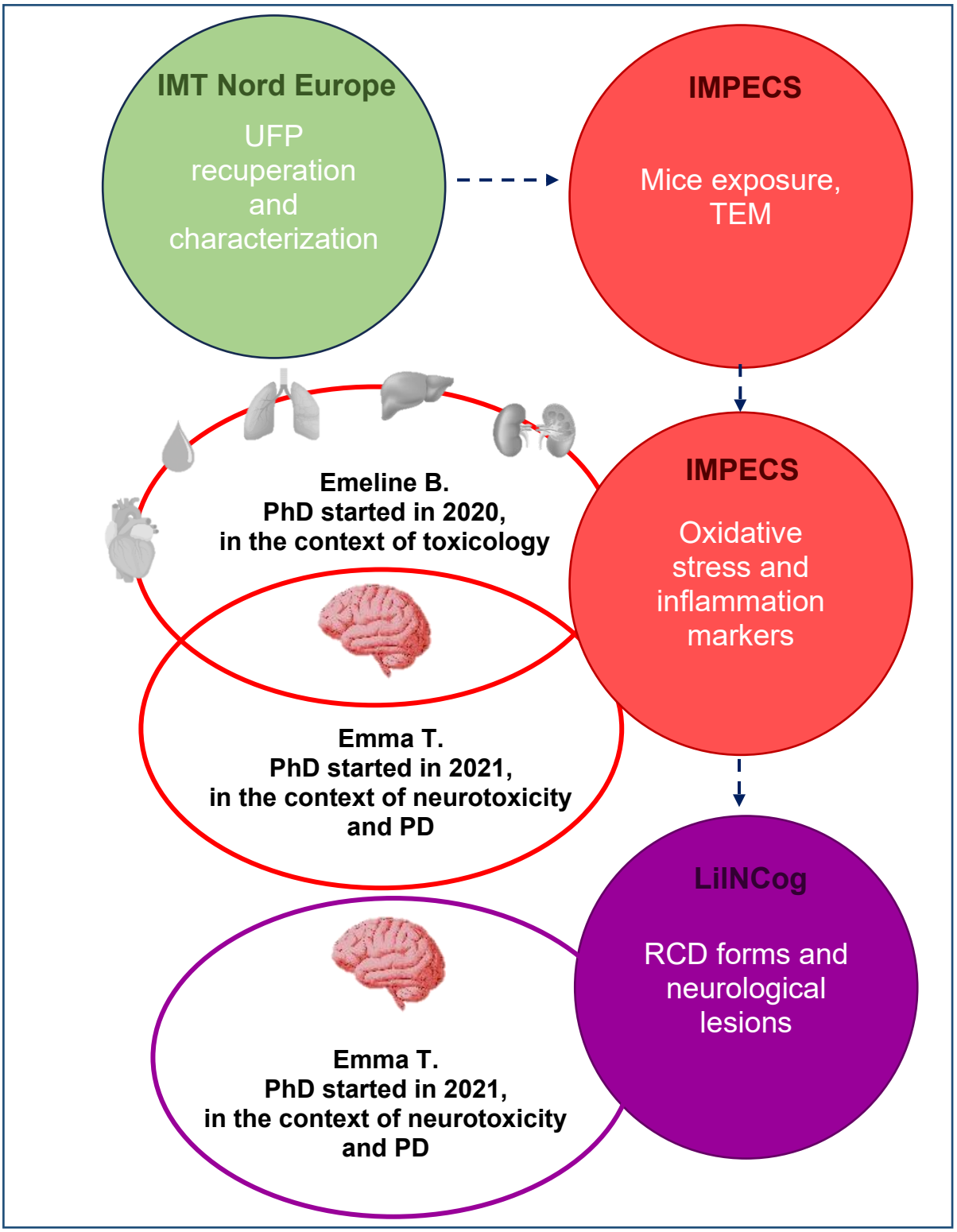

Figure 24: Overview of the *in vivo* part of the PhD, illustrating the role of each laboratory involved.

The figure highlights also the contributions of the two PhD students. My PhD focused on the brain in the context of neurotoxicity and Parkinson's disease, specifically investigating oxidative stress and neuroinflammation markers (laboratory IMPECS) and regulated cell death and neurological lesions (laboratory LilNCog). (Own creation, adapted from project proposal ANSES, 2018)

Project chronology and Collaboration among colleagues

When I began my PhD in 2021, some experiments had already been conducted (starting from May 2019). Effective time management, functional collaboration, and clear communication were essential to successfully conduct both ***in vivo*** and ***in vitro*** studies in parallel.

UFP collection (6 months)

UFP collection was guided by Espéranza Perdrix, Laurent Alleman (CERI EE IMT Nord Europe) and executed by IMPECS colleagues: Sébastien Antherieu, Djamal Achour, Céline Grare, Guillaume Garçon, and laboratory director Jean-Marc Lo Guidice.

UFP characterization

- Granulometry performed by Espéranza Perdrix, Laurent Alleman (CERI EE IMT Nord Europe),
- Physico-chemical characterization performed by Espéranza Perdrix, Véronique Riffault, Laurent Alleman (CERI EE IMT Nord Europe),
- Biological characterization (endotoxins quantification) performed by Emeline Barbier and Jessica Carpentier (IMPECS).

Mice exposure (3 months)

Intranasal exposure twice/week was conducted by Emeline Barbier and Jessica Carpentier (IMPECS).

Brain recuperation

Sacrificing mice and organ collection (e.g., brain) was coordinated by IMPECS with contributions from Sébastien Antherieu, Djamal Achour, Céline Grare, Gianni Zarcone, Emeline Barbier, Jessica Carpentier and Guillaume Garçon.

Behavioral tests

Open field, Elevated plus maze, Y maze, Spontaneous alternation, Passive avoidance test are performed by Emeline Barbier and Jessica Carpentier (IMPECS), coordinated by Charlotte Laloux (LilNCog), and afterwards interpretated during several meetings where I was involved (IMPECS/LilNCog).

Indirect UFP detection

- Metal analyzes in whole brain tissue by ICP-MS performed by Espéranza Perdrix, Véronique Riffault, Laurent Alleman (CERI EE IMT Nord Europe),
- RT-qPCR gene expression of PAH and metal metabolism enzymes in whole brain tissue, experiments by Emeline Barbier and Jessica Carpentier (IMPECS).

Dunkirk UFP oxidative potential

Optimalization of the protocol and DTT test of Dunkirk recuperated UFP, experiments performed by Ophélie Simonin (IMPECS) and myself (IMPECS/LilNCog).

Continue sustaining and proliferation of the LUHMES cell line

Direct UFP detection

- Sample preparation of TEM was performed by Jessica Carpentier and Céline Grare, whereafter Emeline Barbier (IMPECS) with guidance of Pr. Pierre Gosset and Nathalie Goetinck (CHU Lille, CBP lab) took the TEM pictures,
- Label-free detection of carbon particles by femtosecond pulsed laser microscopy performed in CMK (UHasselt) by Kenneth Vanbrabant and myself (IMPECS/LilNCog).

Cytotoxicity

6 independent fluorimetric tests

- Cell metabolism (Resa)
- Cell viability (G6PD)

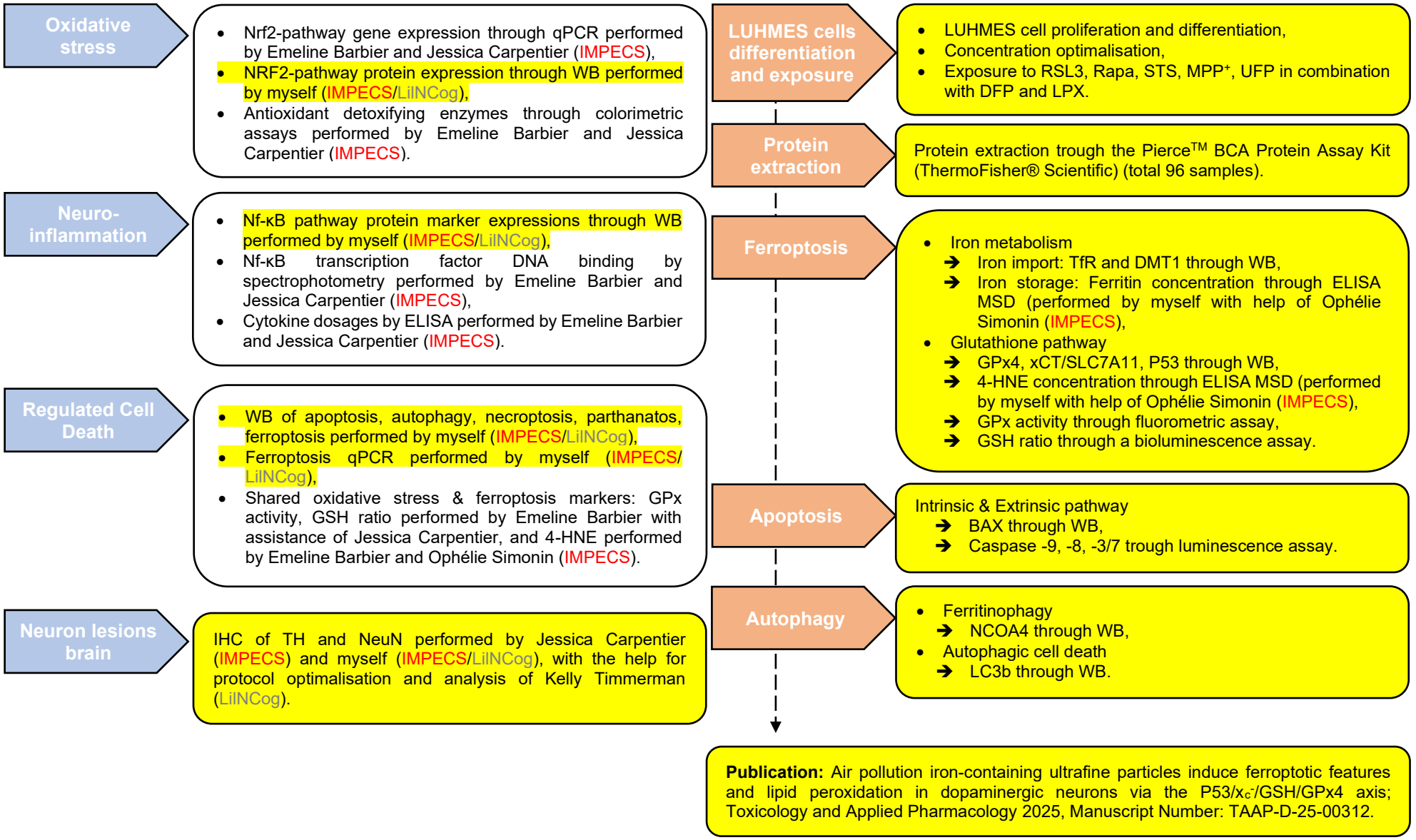

Figure 25: Overview of the experiments performed during this PhD project.

(Own creation)

The blue section outlines the chronological order of the PhD *in vivo* experiments as part of the PUF-EXPOmiR project, with attention on who performed each test. The orange section highlights the *in vitro* experiments, all of which were conducted by myself and therefore not repetitive indicated. To make it more clear, yellow indicates the experiments that I did by myself or where I was highly involved in.

Laboratory involvement

- **IMPECS** (PhD director Prof. Dr. G. Garçon, replaced by Dr. Lydia Nikasinovic): Briefly explained, oxidative stress markers were analyzed through Nrf2 activity (qPCR, WB), GSH levels (Fluorescence), lipid peroxidation markers (4-HNE ELISA), and oxidative DNA damage (8-OHdG ELISA). Inflammatory responses were assessed via cytokine panels (e.g., TNF-α, IL-1β, IL-6, MCP-1, TGF-β ELISA) in bronchoalveolar lavage fluid and target organs with Luminex® kits.

- **LilNCog** (PhD director Prof. Dr. D. Devos): *Direct translation of the project proposal ANSES (2018)*: "Types of cell death: To identify the type of cell death (i.e., apoptosis, ferroptosis, necrosis), in addition to electron microscopy observations, various biological markers specific to a given type of cell death will be studied.
  Apoptosis will be investigated through specific immunohistochemical staining (e.g., Annexin V) performed on tissue sections, as well as by analyzing cytochrome c, caspases 3, 8, and 9, and Bax/Bcl2 proteins using ELISA and Western blot techniques (Dagher *et al.*, 2006).
  Similarly, the investigation of ferroptosis mechanisms—a key focus of this project for the reasons detailed in the "1.-Context/Scientific Justifications" section of this document—will be conducted. In addition to iron quantification, analysis of the Nrf2 transcription factor, and lipid peroxidation, the specific determination of GPx4 through WB will demonstrate the presence of this type of cell death (Xie *et al.*, 2016). Finally, the identification of a necroptotic response in the various target organs will be established by analyzing ATP levels through chemiluminescence and RIP1 and RIP3 proteins via Western blotting (Xie *,* 2016)." **Indicating that Nrf2 and lipid peroxidation (4-HNE), as well the GSH/GPx4 pathway are common results of the oxidative stress and ferroptosis, concerning both PhDs, Emeline B. and myself, Emma T. as visualized in Fig. 24.** Not mentioned in detail in the project proposal where the neurological lesions, which were performed by Jessica Carpentier, Kelly Timmerman, and myself.

  Also the *in vitro* part is mostly conducted with LilNCog. Initially, as a Master's student (2020/2021 – LilNCog), I assisted former PhD student Hind Bouchaoui in characterizing ferroptotic markers (GSH, 4-HNE, C11-BODIPY$^{581/591}$) in RSL3-treated LUHMES cells, with results published in (Bouchaoui *et al.*, 2023). I used my knowledge about LUHMES cells to evaluate the UFP toxicity on dopaminergic neurons.

My contributions

In vivo

As indicated in Fig. 24, I had a central role in the PUF-EXPOmiR project, acting as a key link between both laboratories (IMPECS & LilNCog) and bridging the results generated during Emeline B.'s PhD with PD-features, such as disrupted brain metals, oxidative stress, and neuroinflammation, with neuronal RCD as potential endpoint. PUF-EXPOmiR served as a shared framework for both Emeline B.'s and my own PhD research.

However, as known, interpretating the results of exposed brain separately from the other organs is very useful, based on specific organ characterizations:

i) **Barrier**: The brain is protected by the BBB. Unlike the lungs, which are primary targets for airborne particles, or the heart, liver, and kidneys, which are highly exposed through circulation, the brain's unique barrier creates a distinct 'organ-environment'.

ii) **Anatomy:** The brain is anatomically strict divided in different regions. Whole brain analysis risk masking localized alterations that are critical in understanding region-specific pathological processes. This limitation can lead to false-negative results, complicating interpretation in the context of neurological diseases, such as PD.

iii) **Cellular composition:** The brain comprises highly specialized cells, including neurons, astrocytes, oligodendrocytes, and microglia, each with distinct functions. This diversity means that cellular responses to toxicants or stressors can vary significantly within the brain tissue, necessitating separate analyses, for example by IHC.

iv) **Non-regenerative:** Damage to the brain often results in long-lasting or irreversible functional deficits, such as cognitive impairment, motor dysfunction, or mood disorders. These outcomes are distinct from the reversible or regenerative capacities of other organs like the liver. Additionally, it makes it very important to concentrate on RCD, as the cells can poorly be replaced.

v) **Unique neuroinflammation:** Microglia, the brain's resident immune cells, play a central role in neuroinflammation, which operates differently compared to systemic inflammation. This makes it hard to compare neuroinflammation to inflammatory responses in other organs.

vi) **Neurotransmitter systems:** The brain has specialized neurotransmitter systems (e.g., dopamine, serotonin, acetylcholine) that are highly sensitive to disruption. Subtle alterations in these systems by toxins can significantly impact behavior and physiology.

vii) **Developmental and/or aging factors:** The brain's developmental stages and age-related changes, such as synaptic pruning or myelination, makes it uniquely vulnerable at certain life stages.

As shown in Fig. 25, before my arrival or while I focused on conducting the *in vitro* study, Emeline B. concentrated on multiorgan toxicity experiments, with significant assistance from lab technician Jessica Carpentier to ensure the timely progression of experiments. Additionally, it was more efficient, financially and timewise, to conduct experiments on all target organs simultaneously, and so not the brain alone.

Emeline B. would like to publish the multiorgan toxicity results in January 2025, while my work will focus on UFP brain detection and their neurotoxicological effects in the context of PD.

In vitro

The *in vitro* study represents an additionally project that was not initially part of PUF-EXPOmiR. I took the responsibility of that for my own, with the expertise obtained during my Master's two internship in the LilNCog lab. Fig. 25 shows the parallel work with the *in vivo* part, if not mentioned specific who performed the test, it was conducted by myself (colored in yellow). For the oxidative potential of the Dunkirk UFP, I worked together with Ophélie Simonin, as she plans to use the same UFP and protocol in future projects, she helped also with experiments performed by the MSD electrochemiluminescence detected ELISA tests (4-HNE, Ferritin). And if needed, I could rely on our cell culture coordinators, Aurélie Jonneaux (LilNCog) and Céline Grare (IMPECS).

This part is send for publication and will be the first publication of the PUF-EXPOmiR project, titled as 'Air pollution iron-containing ultrafine particles induce ferroptotic features and lipid peroxidation in dopaminergic neurons via the P53/x_c^-/GSH/GPx4 axis', published in Toxicology and Applied Pharmacology 2025, Manuscript Number: TAAP-D-25-00312.

IV. HYPOTHESIS

This research project was based on three main observations: i) epidemiological evidence, ii) the rising global prevalence of PD, and ii) toxicological findings.

As outlined in the Research Context, epidemiological studies suggest that exposure to $PM_{2.5}$ exacerbates PD symptoms and increases the risk of hospitalization. Population-based studies have reported a 3% increase in PD-related hospitalizations (Zanobetti *et al.*, 2014) and a 20% higher incidence of PD (Chen *et al.*, 2024) per 10 µg/m³ increase in $PM_{2.5}$ levels.

Since its first description by James Parkinson in 1817 — during the late industrial revolution — PD prevalence has risen dramatically, with the steepest increases observed in highly polluted regions such as China (E. Ray Dorsey *et al.*, 2018). These trends support the notion that environmental factors, particularly air pollution, may contribute significantly to the development of sporadic PD, which accounts for over 90% of cases.

Toxicological studies have linked $PM_{2.5}$ exposure to several neurological lesions, including oxidative stress (X. Chen *et al.*, 2018; Chu *et al.*, 2019; Koike *et al.*, 2002), brain metal dyshomeostasis (Calderón-Garcidueñas *et al.*, 2013; Chu *et al.*, 2019), unfolded protein response (α-synuclein) (Calderón-Garcidueñas *et al.*, 2010), and neuroinflammation (L. Chen *et al.*, 2018; Chu *et al.*, 2019; Finch *et al.*, 2002). However, the progressive and selective degeneration of dopaminergic neurons — the key hallmark of PD — has received limited attention in air pollution-related neurotoxicity research.

Together, these independent lines of evidence support the hypothesis that exposure to urban UFP can induce PD-related feature (oxidative stress, neuroinflammation, and RCD) in both murine and human dopaminergic cell models.

V. GENERAL GOAL OF THE PHD PROJECT

Limited evidence existed that UFP, as part of the PM fraction, could contribute to the pathoetiology of PD. Once UFP entered the CNS, their exact mechanisms of toxicity remained unclear. The main goal of this PhD research was to **determine the neurotoxic effects of UFP exposure, focusing on PD-related features** such as changes in motor and cognitive function, neuronal oxidative stress, brain metal alterations, neuroinflammation, and neurodegeneration, particularly through RCD pathways like ferroptosis, which has recently been recognized as a critical contributor to PD and linked to PM and nanoparticle exposure.

This PhD research consisted of two parts:

- ➔ **CHAPTER II:** In this *in vivo* study, male BALB/c mice were intranasally exposed to UFP to examine the effects on the brain, providing a comprehensive overview of PD-like symptoms and hallmarks. The study included behavioral tests, brain detection of UFP and metals, oxidative stress and neuroinflammation markers, alterations in RCD pathways using immunological and biochemical assays, and immunohistochemistry (IHC) of specific brain regions (i.e., prefrontal olfactory cortex, striatum, hippocampus, and SN). The goal was to evaluate the brain's susceptibility to developing a PD phenotype after UFP exposure. Key findings included UFP localization in the prefrontal cortex and SN, the involvement of cellular defenses such as NRF2 and GPx to mitigate oxidative stress, and neuroinflammation driven by Nf-κB. Additionally, the repression of RCD suggests the successfully activation of the brain's defensive mechanisms against UFP-induced cellular damage. These findings prompted further investigation into the effects on dopaminergic neurons, as primary target cells during PD, leading to the establishment of an *in vitro* study.

- ➔ **CHAPTER III:** This *in vitro* study on differentiated LUHMES cells focused on the responsiveness of dopaminergic neurons to acute UFP exposure and their vulnerability to RCD, particularly ferroptosis, but also apoptosis and autophagy. The central question was whether UFP exposure could induce a PD phenotype in these neurons. Several protein detections, focusing on x_c^-/GSH axis were conducted, along with examinations of both upstream (P53) and downstream (GPx4, 4-HNE) hallmarks. The results suggest that UFP exposure alter the P53/x_c^-/GSH/cGPx4 axis, potentially leading to ferroptosis.

CHAPTER II:
DOES SUBCHRONIC INHALATION TO ULTRAFINE PARTICLES INDUCE PARKINSON'S DISEASE-LIKE NEUROTOXICITY IN MICE?

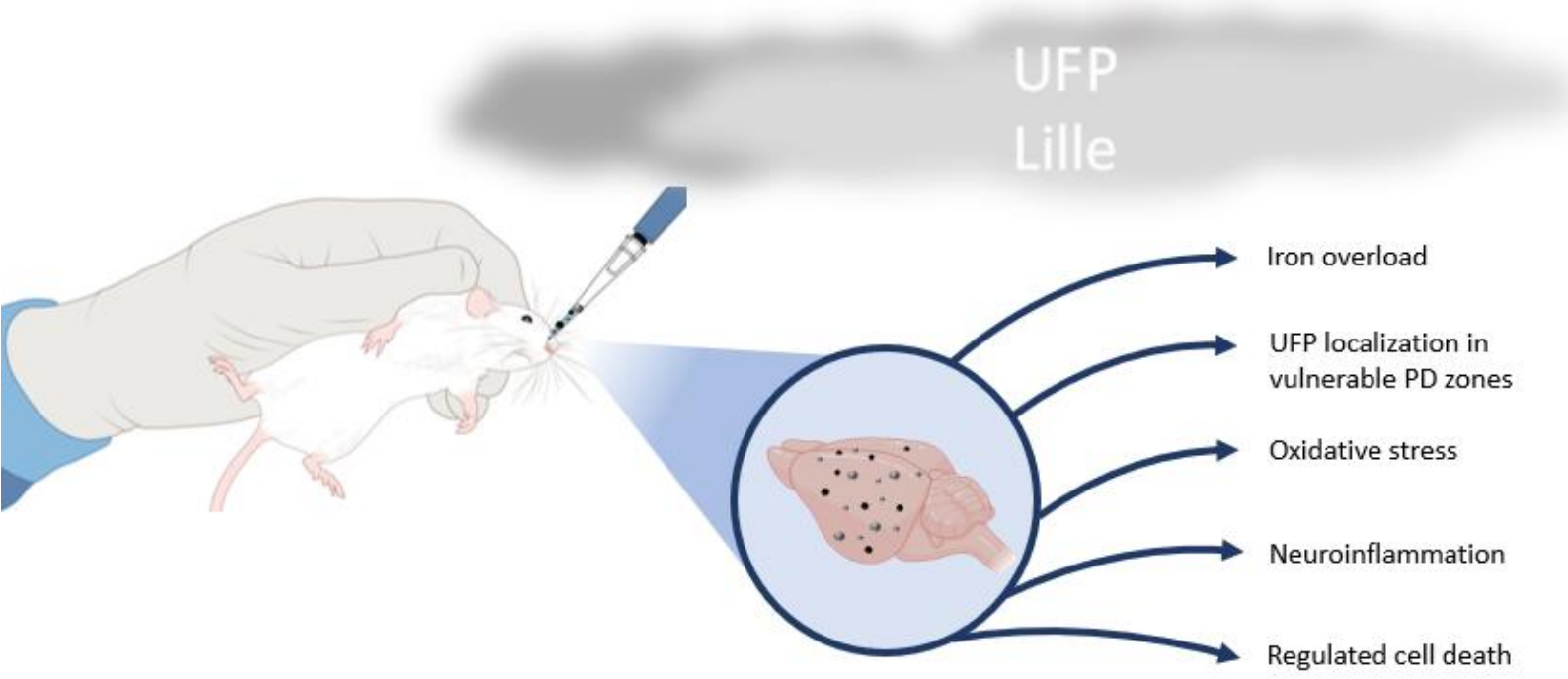

I. SPECIFIC GOALS

Thanks to growing epidemiological evidence and increasing knowledge about environmental triggers of PD, there is a high need for fundamental research to address specific questions regarding the role of ambient UFP as potential risk factor. To achieve this, the *in vivo* study provides a holistic view of UFP neurotoxicity, encompassing not only dopaminergic degeneration but also alterations in whole brain tissue, as well as UFP brain uptake and localization. This approach is considered to yield a more reliable understanding of UFP-induced neuropathological changes by encompassing oxidative stress markers, neuroinflammatory responses, and disruptions in cell death pathways associated with neurodegenerative processes.

In this study, ten-week-old male BALB/c mice were intranasally exposed to UFP at dosages of 0, 10, 30 µg/adm over a 12-week period, followed by an optional 12-week recovery to evaluate the potential reversibility of neurotoxic effects. This experimental design aims to address the following initial objectives:

1) **Can UFP alter mouse behavior?**
   To investigate if exposed UFP mice could induce alterations in motor function, anxiety or cognitive decline, they were exposed to a battery of behavioral tests.

2) **Is the brain capable of detoxifying metals and PAH originating from the UFP exposure?**
   By the use of the Inductively Coupled Plasma Mass Spectrometry (ICP-MS) we could better describe which (exchangeable) metals reaches the brain. Additionally, assess alterations in polycyclic aromatic hydrocarbon (PAH) and metal enzyme (metallothionein (Mt)) transcriptions through RT-qPCR gave a global view of brain metal and PAH detoxification after UFP exposure.

3) **Does UFP brain reach the brain?**
   Investigated whether UFP enter the brain, employ advanced microscopy techniques, such as femtosecond pulsed laser microscopy and Transmission Electron Microscopy (TEM), to provide direct evidence of UFP localization in neurons and specific brain regions.

4) **Can UFP exposure induce oxidative stress similar to that observed in PD?**
   Explore the induction of the Nrf2 antioxidant defense pathway via RT-qPCR and Western blot (WB), focusing on the transcription of downstream target genes involved in antioxidant proteins, detoxifying enzymes, and transport molecules to evaluate oxidative stress levels.

5) **Does UFP exposure trigger neuroinflammation as precursor of cell death?**
Examine neuroinflammatory responses by measuring the protein levels of Nf-κB-pathway by WB, the DNA binding activity of the Nf-κB transcription factor, followed by profiling proinflammatory cytokines using a cytokine panel.

6) **Do UFP influence RCD pathways, leading to neurodegeneration?**
Investigate the expression of proteins associated with various RCD pathways – ferroptosis, apoptosis, autophagy, necroptosis, and parthanatos – using WB and enzyme-linked immunosorbent assay (ELISA) protein analysis on whole brain tissue to gain insights into the overall neurodegenerative mechanisms.

7) **Which brain regions show neurodegeneration following UFP exposure?**
Detect markers of neurodegeneration using IHC to assess the lethal effects of UFP exposure on:
   - Nigrostriatal regions (Striatum, SN, VTA) using Tyrosine Hydroxylase (TH) as a marker for dopaminergic production.
   - The hippocampus using Neuronal-Nuclei (NeuN) as neuronal marker.

   These markers were evaluated after three months of UFP exposure and the recovery group, to assess the potential reversibility of neurodegenerative effects.

II. MATERIAL AND METHODS

II.1 Particle recovery in Lille and physico-chemical and biological characterization

Air pollution-derived UFP samples were systematically collected from May 6th to September 27th, 2019, by the *SAGE* (*Sciences de l'Atmosphère et Génie de l'Environnement*) department of the *Institut Mines Télécome (IMT)* Nord Europe, situated in Douai, France. As visualized in Fig. 26, the sampling regimen encompassed location within the southern part of Lille city, France, spanning an area of approximately 35 km^2 and hosting a resident populace numbering 238,104 individuals (density: 6,800 inhab/km^2). Additionally, the metropolitan expanse extended its reach to accommodate over 1.1 million inhabitants. The sampling site (50.612967, 3.037309), 1 Avenue Oscar Lambret, 59000 Lille, is surrounded by medium-sized buildings and is located less than 500 meters from a major road (A25) and the train station of the Lille Regional Hospital Center.

[1] [2] [3]

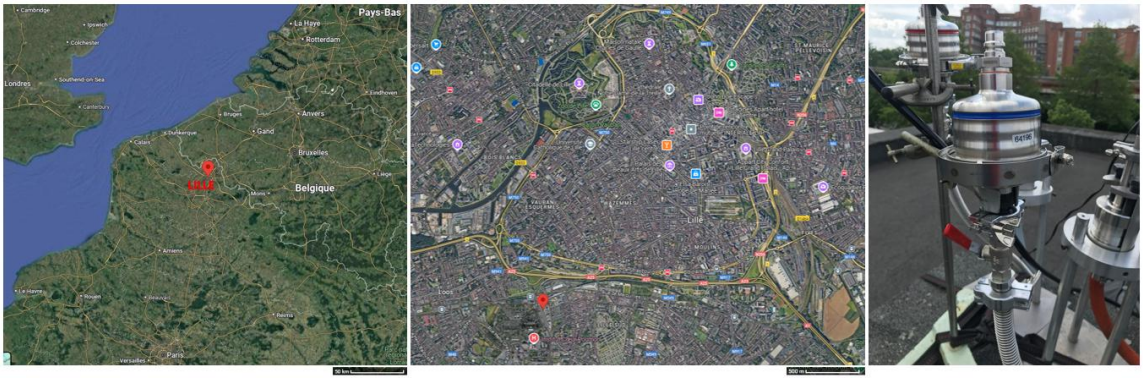

Figure 26: Visualization of the particle recovery site at Lille, France. (Own creation)

[1] Location of Lille: Lille is a city in the northern of France, located near the Belgian border. In a broader European context, Lille is situated in the northwestern part of Europe, within easy reach of several major cities: ± 90 km from Brussels, ± 225 km from Paris, and around 300 km from London, making it an important connection point in Western Europe, and therefore representative for realistic European inhalation of UFP. [2] The sampling location is located in the Lille-Sud district, located around 4 km from the city center (Grand Place). It is close to the *Centre Hospitalier Universitaire (CHU)*, also known as the University Hospital of Lille, forming a part of a large medical and academic complex. It is positioned close to the A25 and even A1 motorways, with public transportation options, including the Lille metro (Line1), connect the CHU to central Lille, and the Lille Regional Hopsital Center train station. [3] Picture of the Dekati DGI-1570 during sampling in 2019. This picture is taken from the roof of the particle recovery zone with in the background the *Pôle Recherche*, where both labs, IMPECS and LilNCog (-DVCD) are located.

Abbreviations: CHU: Centre Hospitalier Universitaire.

The UFP were captured using two-flow Dekati DGI-1570 cascade impactors (70 L/min), each equipped with four stages. These instruments facilitated the isolation of particles based on their aerodynamic diameters, affording access to specific cut-off dimensions of 2.5, 1.0, 0.5, and 0.2 µm, filtered by polycarbonate (PC) membranes, which underwent biweekly replacement. The final three stages of the impactors intercepted particles exhibiting aerodynamic equivalent diameters from 1.0 till 0.2 µm (i.e., referred as UFP in this paper) were amalgamated in MilliQ water. This extraction process was facilitated by a non-contact ultrasonic probe (Vibracell 75455, 500W, 20 KHz), maintained at a subdued temperature. Collected particles from all 130 filters were promptly weighed (total of 40 mg UFP), homogenized, and preserved at -20°C. The UFP samples were extracted and merged into a single comprehensive sample in MilliQ water, utilizing a non-contact ultrasonic probe (Vibracell 75455, 500W, 20 KHz) while keeping the temperature low. The granulometry, physico-chemical and biological characterization are performed in collaboration with IMT Nord-Europe and “Micropollutants Technologies” laboratory in Saint Julien Les Metz.

II.1.1 Granulometry

To analyze the particle size distribution of the collected UFP samples, they were suspended in sterile saline at a concentration of 1 mg/mL using a non-contact ultrasonic probe (Vibracell 75455, 500 W, 20 KHz) maintained at a low temperature. The samples were sonicated for 10 minutes and stirred to prevent aggregation and sedimentation. Laser diffraction, based on dynamic light scattering and the Stokes-Einstein relationship, was then employed to measure the particle sizes by assessing the rate of light diffusion, with smaller particles diffusing faster than larger ones. The amount of light scattered was measured twice within a brief interval of approximately 100 µs to analyze Brownian motion and deduce particle sizes.

II.1.2 Physico-chemical characterization

Analyses of metals and metalloids were performed in collaboration with the *SAGE* department at *IMT* Nord-Europe, measuring concentrations of seven major elements (Al, Ca, Fe, K, Mg, Na, and Si) and approximately thirty trace metals (including As, Ba, Be, Bi, Cd, Ce, Co, Cr, Cs, Cu, Hg, La, Li, Mn, Mo, Ni, Pb, Pd, Pt, Rb, Sb, Sc, Se, Sn, Sr, Th, Ti, Tl, U, V, and Zn) using ICP-MS (NeXion 300x, Perkin Elmer). Additionally, anions and cations were analyzed by ion chromatography, while organic and elemental carbon were quantified through thermal analysis using colorimetric detection. PAH, polybrominated dibenzo-p-dioxins and furans (PBDD/F), and polychlorinated biphenyls (PCB) were analyzed by the Micropolluants Technologies laboratory using high-

performance liquid chromatography (HPLC - Waters 2695 Alliance) and high-resolution gas chromatography/mass spectrometry (HRGC/HRMS).

II.1.3 Biological characterization (endotoxins quantification)

The Pierce™ Chromogenic Endotoxin Quant Kit (ThermoFisher®, Waltham, MA) was used according to the manufacturer's instructions to quantify lipopolysaccharide endotoxins in the UFP samples. When endotoxins interacts with the amebocyte lysate, it triggers a series of enzymatic reactions that activate factor C, factor B, and a pro-coagulant enzyme. This activated enzyme catalyzes the release of p-nitroaniline (pNA), resulting in a yellow color. After stopping the reaction, the released pNA is measured by spectrophotometry at 405 nm, with the absorbance corresponding to the endotoxin concentration in the UFP sample.

II.2 Oxidative potential of ultrafine particles

To give a complete overview of the test performed before exposure, the oxidative potential is included. Briefly, the measurement of the oxidative potential of UFP reflects their intrinsic ability to oxidize chemical compounds through the generation and/or action of ROS, was conducted using four complementary acellular methods: (a) the oxidation test using the ROS probe diacetate 2',7'-dichlorodihydrofluorescein (CM-H2DCFDA), (b) the depletion test of a reducing agent, dithiothreitol (DTT), (c) the measurement of GSH depletion, and (d) the measurement of ascorbate ion consumption, which are all proportional to the rate of ROS generation.
For all these tests, certified manufactured reference nanoparticles, including titanium dioxide (TiO_2), ZnO, and NIST 2584 (PM_4, indoor dust), along with a positive control (H_2O_2), were used as reference materials. Results are not included in the result section, but can be found in Supplemental Data, Fig. S2, p. 241.

II.3 *In vivo* mice model

Ten-week-old male specific pathogen-free BALB/cJRj mice (Janvier-Labs, Le Genest-Saint-Isle, France; weighing ± 30 g) (n = 120) were housed at room temperature (22 ± 2 °C) with a 12h alternating light/dark cycle, with food and water ad libitum. According to the Federation of European Laboratory Science Associations (FELASA) list, they had the sanitary status of specific opportunistic and pathogen free (SOPF). These animals were housed per 6 in a high-tech animal zone free from specific pathogenic organisms (EOPS) at the *Université de Lille (Faculté Médecine) – Pôle recherche*. Mice were acclimatized during one week to their new habitat, besides they were daily observed (weight, clinical examination, observation of any behavioral changes). Also when the

exposure protocol was started, the daily observation continued; special attention was devoted to the emergence of symptoms of discomfort for the animals. The local ethics committee authorized all animal experimental methods (N°: APAFIS#22734-201906070931570 v4).

This mouse model has been described as fairly susceptible to the development of diseases, notably malignancies, in response to chemical stress, making it indicative of persons' average susceptibility. This uniqueness explains why this model is so widely used in particle toxicology studies.

II.4 Exposure protocol

After light anesthesia with isoflurane (Zoétis, France) with induction at 3%, maintenance at 2.5 % at an air flow rate of 1 L/min, male BALB/cJRj mice (n = 36 / group) received by intranasal installation 40 µL of saline (control group) or different doses (10 or 30 µg) of urban UFP suspension in 40 µL of sterile normal saline, this at a rate of two exposures per week for 12 weeks (90 days) long. Meaning, a total of 24 intranasal installations, followed or not by a 12-week recovery period (Fig. 27). In order to evaluate the possible impact of the anesthesia, a control group of 12 mice that will not be anesthetized or infused will also be established. To reduce the formation of particle aggregates, the UFP suspension was ultrasonicated for 10 minutes before being administered to the animals. The mice were subsequently sacrificed with Dolethal 200 µL, followed by blood collection and extraction of the brain, as well as many other target organs, including lungs, heart, kidneys and liver for the PhD project of Emeline B., as colleague on the project PUF-EXPOmiR.

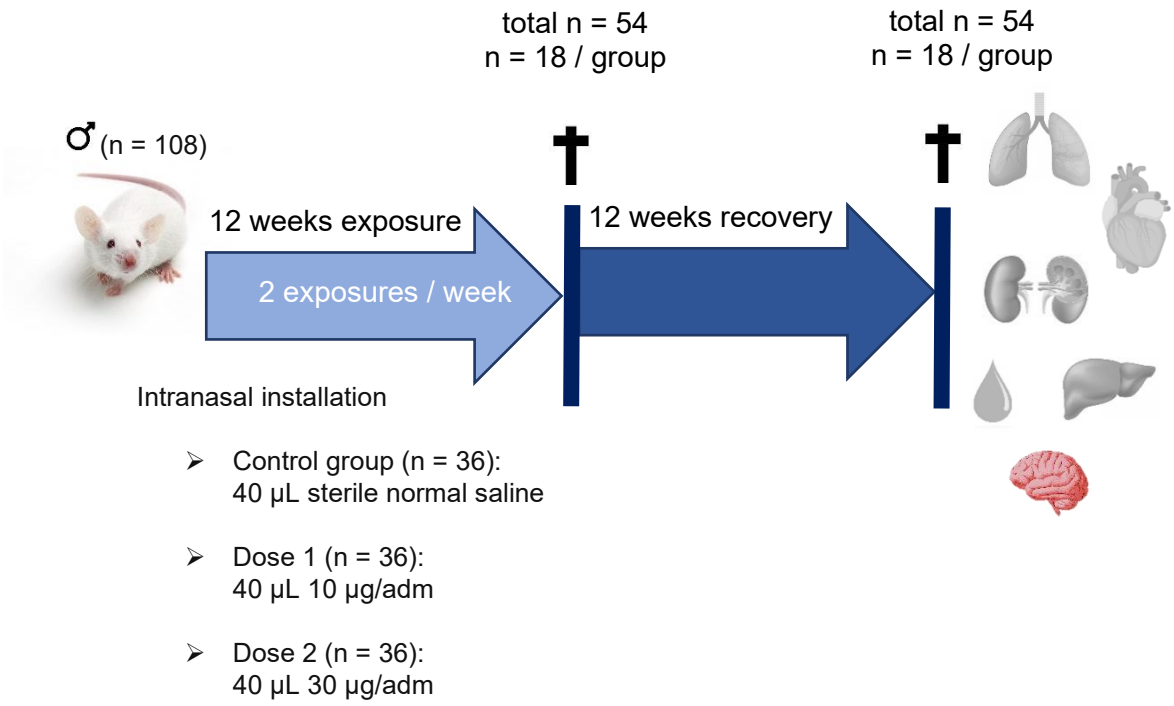

Figure 27: Visualization of exposure protocol. (Own creation)

In total 108 BALBcJRj mice were used in this project, from which 36 mice were only exposed to 40 µL sterile normal saline, 36 to Dose 1 (10 µg/adm) ultrafine particles (UFP) and the other 36 to Dose 2 (30 µg/adm) UFP, this with an exposure repeated twice a week for 12 weeks long. Thereafter, from each group 18 mice were sacrificed 24h after the latest exposure, followed by sample collection of lungs, hart, kidneys, liver, blood and brain. Additionally, the other half of each group (n = 18 / group) had a recovery period of 12 weeks without any exposure, followed as well by sample collection.

Abbreviations: UFP: Ultrafine particles.

II.5 Mouse behavioral tests

Mice that were not sacrificed following 12 weeks of exposure (n = 12/group, for a total of 36 mice) were subjected to a battery of behavioral tests designed to assess motor function (i.e. Open field test), anxiety (i.e. Elevated plus-maze) and cognition (i.e. Passive avoidance test, Y-maze, and Spontaneous alternation test). Behavioral tests were conducted within the *In vivo* imaging and functional exploration platform (LiiFFE) of health and biology platform unit of Lille (PLBS, France).

Before proceeding, the natural movement patterns and anxiety levels were examined to ensure that any potential motor impairment or anxiety-related issues would not disrupt the cognitive testing abilities of the animals.

II.5.1 Motor function

Open field test

The open field test was used to evaluate locomotion, but also anxiety and the general exploration habit. It was conducted in an infrared equipped actimeter (BIOSEB, Vitrolles, France) of 45 x 45 cm square arena, as shown in Fig. 28. The mouse was placed in the perimeter and allowed to explore the apparatus during 10 minutes, under a low light intensity of 20 lux. Average speed, total distance travelled, the number of rearing and resting moments, and the distinction between exploration by zones (center vs periphery) was measured by infrared detection beams system (Actitrack software).

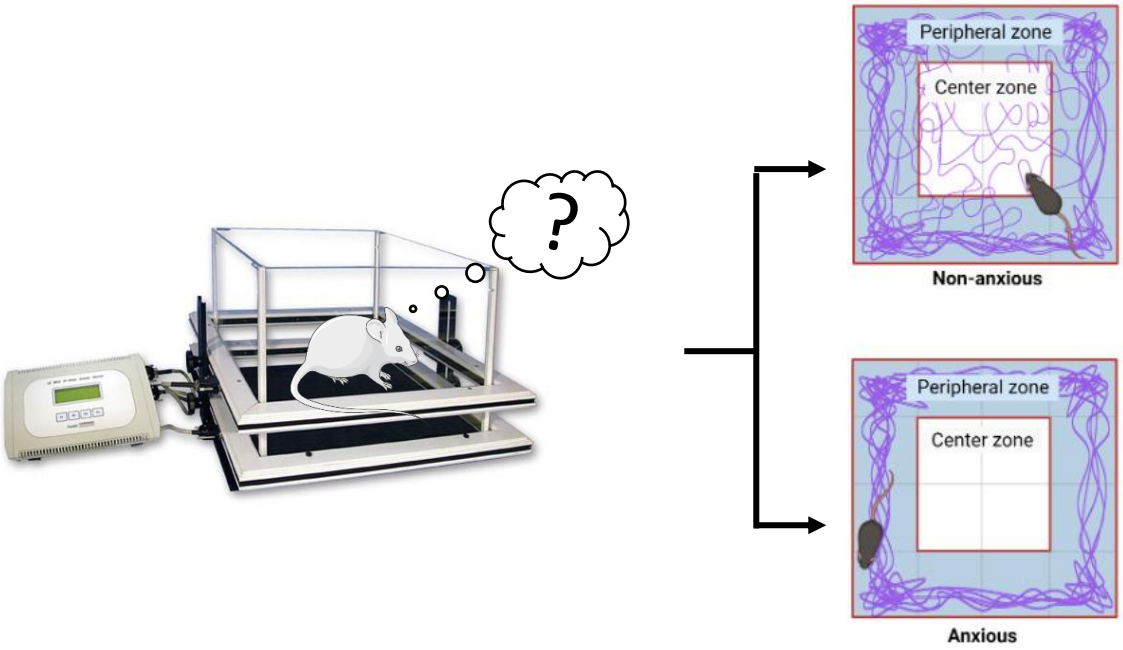

Figure 28: Open Field Test (Own creation)

The test typically involves placing the mouse in an open, enclosed squared arena with high walls to prevent escape. The floor is divided into zones, with a central zone and a peripheral zone along the edges. The animal is always placed at the same location and allowed to explore freely for 10 minutes. By video tracking is the behavior filmed whereafter patterns linked to locomotor activity and exploratory behavior are observed, such as the time spent in the central versus peripheral zones.

II.5.2 Anxiety

Elevated plus-maze (EPM)

The plexiglass cross maze labyrinth consisted of two open arms (150 lux) and two closed arms (40 lux) elevated 50 cm from the ground. The mouse was placed in the center of the maze, visualized in Fig. 29, and allowed to explore the apparatus for 10 minutes. Different arms visits, were measured by the video-tracking system (Ethovision XT 16, Noldus, Wageningen, Netherlands) and stretch posture, head dipping, grooming and rearing were manually scored.

Figure 29: Elevated plus-maze (Own creation)

The apparatus is made like a maze shaped in the form of a '+'-sign and elevated above the floor. It consists of four arms: two open arms without walls and two closed arms with high walls. The open arms are usually perceived as more aversive due to the lack of enclosure. The mouse was placed in the center of the maze where all four arms meet. During exploring the mice is filmed to mark specific anxiety-related behaviors.

II.5.3 Cognition

Y-maze test

The animal's spatial memory is measured by the use of a Y-shaped maze, with a light intensity of 20 lux in the 3-arms center. Each arm is L30 x W8 x H 15 cm, where the rodent could be video-tracked (Ethovision EVXT 16, Noldus, Wageningen, Netherlands) (Fig. 30). During the acquisition phase, which lasts 10 min, the mouse had free access to two of the three arms. After a break of 10 min, the mouse was placed back in the maze and had free access to three arms for 5 min. The test was predicated on the animal's preference for novelty, in this case the unknown arm. As a result, the parameters measured are the number of entries in the unknown arm reported in percentage, and the ratio between entries in the open arm compared to the total entry amount.

Figure 30: Y-maze test (Own creation)

A white polyvinyl chlore Y-shaped arranged maze with equal 120° angles is used to asses spatial memory and general exploration. Therefore, the mice is placed in one arm and can explore also another one, so, in total has access to two arms. After a break, the mice has access to the three arms where in normal conditions, he recognize the two previous ones, and will discover the new one.

Spontaneous alternation test

The spontaneous alternation test uses the same Y-maze equipment as described above (Cf. Y-maze test, p. 80) to asses working memory skills. When the animal is placed in the maze, it spontaneously explores the last recently visited arm, and exhibits a high degree of alternation of visits to the three arms. An alternation therefore corresponds to the succession of the three arms in a triplet of visits (Fig. 31). The parameter measured is the alternation score, which is equal to the number of alternations divided by (total number of visits - 2) multiplied by 100, expressed in %.

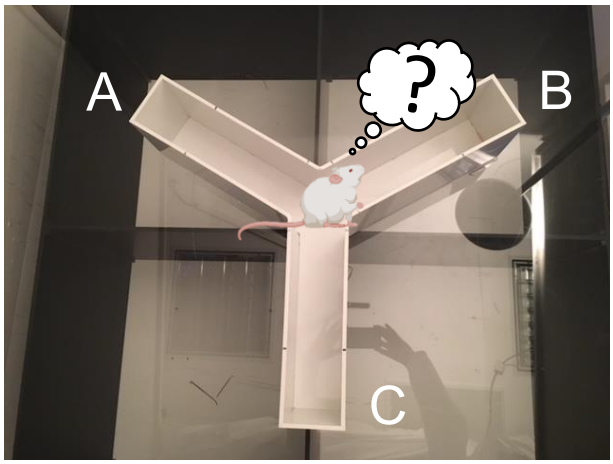

Figure 31: Spontaneous alternation test (Own creation)

For the spontaneous alternation test is again the Y-shaped maze used. This time, the animal's tendency to enter each of the three arms in sequence without repeating a recent arm (e.g., entering arms A-B-C instead of A-B-A) are measured. High alternation rates indicate good working memory.

Passive avoidance test

The passive avoidance arena (BIOSEB, Vitrolles, France) consists of a large, lighted compartment, and a small, dark compartment with weight sensors to detect the rodent's position. The test consisted of two phases, a habituation and the test itself, with a 24-hour difference. The first phase lasting a maximum of 1.5 minute, as the rodent is placed in the illuminated compartment (i.e., 3000 lux), after 10 seconds, the door separating the dark comportment opens. Once the animal has spontaneously entered the dark compartment, it received a mild electric shock (2 sec latency, 2 sec duration, 0.3 mA intensity footshock) (Fig. 32). If the animal has not entered the dark compartment within this time, it was excluded from the study. For the second stage, the animal is replaced during maximum 5 minutes. After the initial shock, the animal could associate entering the dark compartment with unpleased, therefore its latency to return there during the test (after 24 hours) could generally be increased. The acquisition and retention latency in the dark compartment were the measured metrics.

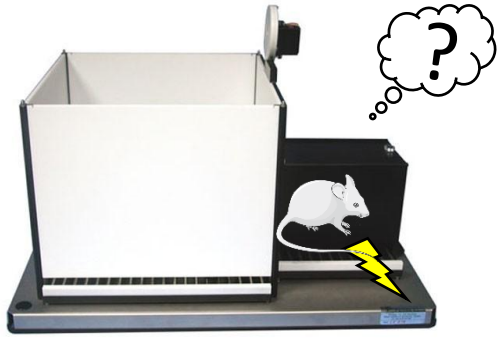

Figure 32: Passive avoidance test (Own creation)

The test involves a two-chamber box, with one brightly lit and the other dark. The chambers are connected by a door, and the dark chamber has a floor that can deliver a mild, brief electric shock. The test evaluate memory retention and is constructed by two phases, the training and testing phase. During the training phase will the mice learn that it gets a mild electric shock when entering the dark chamber. In the testing phase is a higher latency related to stronger memory of the aversive stimulus.

II.6 UFP detection

There are different methodologies for UFP localization. This indirect by searching for significant increases of metal concentrations originating from the outer layer of the particles, or observing expanded gene expression of detoxifying enzymes (i.e. AhR or Mt) as well as specific target gene expression (e.g. CYP oxidoreductases). Additionally, UFP are also directly localized by carbonaceous white light emission under femtosecond pulsed illumination in brain biopsies, and visualized on cellular level by the use of TEM.

II.6.1 Indirect UFP detection

Metal analysis in whole brain tissue

The concentration of seven major elements (i.e., Al, Ca, Fe, K, Mg, Na and Si) and approximately thirty trace metals (e.g., As, Ba, Be, Bi, Cd, Ce, Co, Cr, Cs, Cu, Hg, La, Li, Mn, Mo, Ni, Pb, Pd, Pt, Rb, Sb, Sc, Se, Sn, Sr, Th, Ti, Tl, U, V, and Zn) were measured in triplicate by the use of ICP-MS (NeXion 300x, Perkin Elmer, Waltham, MA). Therefore, brain biopsies were ground in 1 mL ultrapure water and analyzed through ICP-MS (NeXion 300x, Perkin Elmer, Waltham, MA) conducted by the Center for Energy and Environment, *IMT* Nord Europe, *Université de Lille*, France. The values acquired were then normalized to the respective total protein concentration of each sample, known by the Pierce™ BCA Protein Assay Kit (ThermoFisher® Scientific) measurement. Metals with a value higher than the threshold of 1.02 µg/µl are significative increased.

RT-qPCR gene expression of polycyclic aromatic hydrocarbon and metal metabolism enzymes in whole brain tissue

RNA extraction of brain samples was performed by the RNA extraction kit (AllPrep DNA/RNA/miRNA Universal Kit, QIAGEN, Hilden, Germany) and samples were stored in 2 mL RNA*later* Solutions (ThermoFisher®) at 4°C for 48 hours before being frozen at -20°C.

For measurement of genes expression of *AhR*, *Cyp1A1*, *Cyp1B1* cytochromes and *Mt1, Mt2, Mt3* and *Mt4,* approximately 20 mg of each sample was collected before being ground using the gentleMACS™ Dissociator in M tubes (gentleMACS™ M Tubes, Miltenyi Biotec) with 600 µL of RLT-Plus buffer supplemented with β-mercaptoethanol. Thereafter, centrifuged at 3000g for 10 min at room temperature (RT) and transferred to 2 mL safe-lock tubes and finalized by a centrifugation at 20,800g for 10 min. The extraction itself was done by using the protocols of the AllPrep® DNA/RNA/miRNA Universal Handbook from QIAGEN. Next, RNA reverse transcription was performed using the High-Capacity cDNA Reverse Transcription kit (ThermoFisher®), followed by qPCR analysis with the TaqMan™ Fast Advanced Master Mix (Applied Biosystems®). The housekeeping gene *Ppia* was used for normalization and validation.

II.6.2 Direct UFP detection

Transmission Electron Microscopy

After sacrificing due to an intraperitoneal injection of ketamine/xylazine mixture and an intracardiac blood collection, the brain was recuperated and fixated on the EPON technology where a piece of brain was cut-out and placed into 950 µL Papanicolaou's solution (haematoxylin) completed with 100 µL of 2.5% glutaraldehyde for 2 hours, whereafter it was transferred and incubated overnight into 1 mL 0.6% glutaraldehyde. After washing with cacodylate buffer 0.1 M, post-fixation in osmic acid, propylene oxide dehydration and a permeation with DMP-30 solution, the brain-pieces were included into plates and polymerizates. Followed by the TEM visualization in collaboration with the *Centre Biologie Pathologie*, *Centre Hospitalier Universitaire de Lille*, F-59000 Lille, France.

Label-free detection of carbon particles by femtosecond pulsed laser microscopy

In collaboration with the University of Hasselt (BE) is UFP-presence in four brain regions (i.e., Prefrontal Cortex, Striatum, Hippocampus and SN) analyzed by the use of a specific and sensitive detection technique based on non-incandescence related white light generation of carbonaceous particles (which is the core of the UFP) under femtosecond pulsed illumination, as previously reported (Bové *et al.*, 2016).

Therefore, mice (n = 6/group) were sacrificed by an intracardial perfusion with 0.9% NaCl / 0.4% heparin, followed by a fixation with 4% paraformaldehyde (PFA). Mice brains were recuperated and post-fixated in 4% PFA for 24 hours at 4°C. Followed by cryoprotection series with a range of 10% sucrose in 0.1 M PBS till 30% sucrose and a quick froze with -40°C isopentane solution. Brains were conservated at -80°C till needed for the cryostat sectioning. By comparison to the Paxinos Atlas (figures in Supplemental Data Fig. S3, p. 243), brain slices are sliced with a thickness of 20 µm and a minimum of 6 slices for each zone of interest, recuperated on Superfrost™ Plus Adhesion Microscope Slides.

Four zones of interest, mentioned by anterior/ventral to posterior/dorsal axis, are chosen based on specific research questions:

1) **Prefrontal cortex (olfactive / cortex)** → entering UFP by the olfactory bulb,
2) **Striatum** → major input nucleus of the basal ganglia, receives the densest dopaminergic innervation from the SN; dopaminergic loss linked to PD,
3) **Hippocampus** → neurodegeneration linked to AD, can be an indication for the behavioral/cognitive test outcomes,
4) **SN** → loss of dopaminergic neurons in the SN during PD.

In each brain region, UFP presence was assessed in both vehicle-treated mice as negative control (NC), and those exposed to 30 µg/adm UFP. The evaluations were conducted at two time points: 24 hours and 12 weeks post-final administration, with n=3 per group. Brain slices (20 µm) were analyzed using femtosecond pulsed laser technique (810 nm, 150 fs, 80 MHz) (Spectra-Physics), which generated label-free signals, including second harmonic generation (SHG) and two-photon excited autofluorescence (TPAF). Images were taken with a confocal microscope using a Plan-Neofluar 10x/0.3 objective (Carl Zeiss). Images of each 1615.37 µm by 1615.37 µm and 4676.06 µm by 4676.06 µm were taken of the tissue sections using a pixel dwell time of 2.05 µs. The biggest pictures to obtain an overview, from which the TPAF signal pictures can be found in Supplemental Data, Fig. S4, p. 246. The SHG signal, appearing as red light (emission filter 400-410 nm), originates from collagen type I, while the TPAF signal, shown in green (emission filter 450-650 nm), represents various structures, such as neurons. Both signals were produced simultaneously but were detected separately through spectral separation.

The label-free analysis used two properties of white light: (1) saturation of emission signals to establish a threshold for UFP detection in each channel, and (2) emission

across the full visible spectrum. Consequently, as demonstrated in Fig. 33, carbon particles were detected as overlapping pixels in both channels (i.e., green and red light) by the peak finding algorithm in MATLAB (version R2017b), resulting in white dots in merged images of TPAF and SHG signals. By using TPAF to outline entire brain slices, the particle count by ImageJ (Fiji Software) gave a number of particles per volume area of each slice.

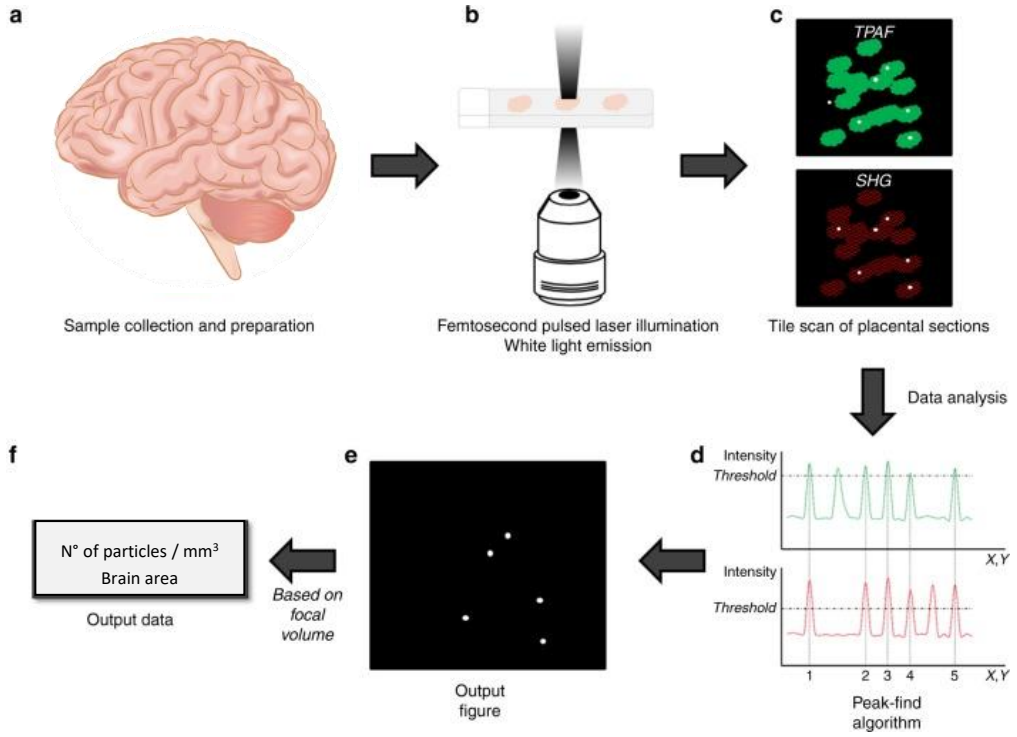

Figure 33: Flowchart of the experimental protocol for ultrafine particle detection in frozen brain slices.

[a] After brain fixation, 20 µm thick frozen slices are prepared using a cryostat. [b] Each section, representing a specific brain region, is illuminated using a two-photon femtosecond pulsed laser set to 810 nm (near-infrared), 150 fs, 80 MHz. [c] Emission from the black carbon core of the ultrafine particles (UFP), naturally present in the tissue (appearing as white dots), is detected alongside the simultaneous generation and detection of two-photon excited autofluorescence (TPAF) from cells (green) and second harmonic generation (SHG) from collagen (red). The image is visualized as a tile scan. [d] A peak-find algorithm is used to determine particle counts by identifying clusters of connected pixels above threshold values, specifically 0.5% and 45% below the maximum intensity values for the TPAF and SHG images, respectively. [e] The white dots in the resulting image represent saturated pixels detected in both the TPAF and SHG channels, identifying the particles. [f] Results are then expressed as the relative total count, or the number of detected UFP per cubic millimeter of brain tissue in each region (adapted figure to brain tissue, from (Bové *et al.*, 2019)).

Abbreviations: SHG: Second harmonic generation (SHG); TPAF: Two-photon excited autofluorescence; UFP: Ultrafine particles.

Additionally, two validation experiments are done based on separate questions:

1) Conformation of the carbon-like nature where the signals of our UFP were compared to those of a purchased reference DEP standard (Standard Reference Material® 1650b, National Institute of Standards & Technology, Gaithersburg, MD) to ensure the measured particles correspond to the exposed UFP.

2) Intra-tissue localization with Z-tag imaging to obtain the information that the UFP are embedded in the brain tissue. Approximately 100 images, each measuring 1024 by 1024 pixels with voxel dimensions of 425.1 x 425.1 x 70 µm, were captured across the tissue sections using a pixel dwell time of 2.05 µs. Orthogonal XZ- and YZ-projections were generated using Fiji software.

II.7 OXIDATIVE STRESS

II.7.1 Gene expression of the antioxidant Nrf2-pathway by RT-qPCR

Same RNA extraction samples are used as previously described (Cf. RT-qPCR gene expression of polycyclic aromatic hydrocarbon and metal metabolism enzymes in whole brain tissue, p. 84).

Gene expression of *Nrf2* and some of its target genes, namely *Keap1, Hmox1, Txn1, Gpx1, Gsr, Gclc, Gclm*, was quantified by real-time quantitative PCR (Polymerase Chain Reaction) using Taqman™ probes and primers (ThermoFisher® Scientific: Keap1 Mm00497268_m1; Hmox1 Mm00516005_m1; Txn1 Mm00726847_s1; Gpx1 Mm00656767_g1; Gsr Mm00439154_m1; Gclc Mm00802655_m1; Gclm Mm013224400_m1) and the TaqMan™ Fast advanced Master MIX (Applied Biosystems). Results are reported against expression of the *Ppia* housekeeping gene (ThermoFischer® Scientific Mm02342430_g1). The mRNAs are significantly over- or under-expressed, after normalization by the housekeeping gene expression with a threshold value of 2 (Fold-Change or FC > 2 or < 2).

II.7.2 Protein expression of the antioxidant NRF2-pathway by Western blot

For protein quantification, *in situ* tissue protein digestion is performed by adding 500 µL Radioimmunoprecipitation assay (RIBA) buffer (i.e., 142 mM KCl, 5 mM MgCl2, EDTA 1 mM, glycerol 5% v/v, SDS 0,1% v/v, NP40 1% v/v, HEPES 20 mM in ultrapure milliQ water) supplement with 1% protease- and phosphatase inhibitor (ThermoFisher® Scientific) to the brain biopsies, followed by mechanical dissociation using the gentleMACS™ Dissociator M tubes (gentleMACS™ M Tubes, Miltenyi Biotec, Bergisch

Gladbach, Germany) programmed for 5 min under shaking. Subjected to density gradient centrifugation, whereafter the supernatant fraction contained the protein extraction. Total protein concentration of each sample was analysed with the Pierce™ BCA Protein Assay Kit (ThermoFisher® Scientific). All following oxidative stress assays are measured in the same protein extract isolates.

Protein expression levels were measured by standard WB procedures. Samples were prepared containing 30 µg proteins, 4X tracking dye (bromophenol blue), 10X reducing agent (β-mercaptoethanol) and completed with H_2O to the according final well volume. For gel electrophoresis, premade polyacrylamide gels (NuPAGE gels - Bolt™ 4-12% Bis-Tris Plus (ThermoFisher®) were installed into Novex Mini Cell (ThermoFisher®) containers, filled with 1X MES SDS Running Buffer. After loading, samples and ladder (3.5 – 250 kDA Novex® Sharp Prestained LC5800), migrated for around 30 min at 200V/160mA, then transferred to nitrocellulose membranes by a classical sandwich semi-dry electroblotting (Trans-blot Turbo Transfer System, Biorad, Hercules, CA). To reduce nonspecific binding of antibodies, membranes were blocked before adding the primary antibody (Ab) (NRF2 (D1Z9C) XP®: 1/1000 Cell Signaling (Danvers, MA) #12721 (Mw 97-100 kDa); KEAP1 (D6B12): 1/1000 Cell Signaling #8047 (Mw 60-64 kDa); Thioredoxin 1 (C63C6): 1/1000 Cell Signaling #2429 (Mw 12 kDa); Thioredoxin 2 (D1C9L): 1/1000 Cell Signaling #14907 (Mw 13 kDa); TRXR1 (D1T3D): 1/1000 Cell Signaling #15140 (Mw 55 kDa); TXNIP (D5F3E): 1/1000 Cell Signaling #14715 (Mw 55 kDa); Prdx1 (D5G12): 1/1000 Cell Signaling #8499 (Mw 21 kDa); SCSTM1/p62 (D1Q5S): 1/1000 Cell Signaling #39749 (Mw 62 kDa); Phospho-SQSTM1/p62 (Ser349) (E7M1A): 1/1000 Cells Signaling #16177 (Mw 62 kDa). After overnight incubation and rinsing, membranes were exposed to the secondary Ab, whereafter signals could be detected by enhanced chemiluminescence using ECL Select™ Western Blotting Detection Reagent. Images were acquired using FUSION FX camera (Vilber - Lourmat®, Marne-la-Vallée, France). The optical density of each band was quantified and normalized to the intensity of calibration protein Actin-β* (1/50 000; R&D Systems® MAB8929), using the ImageJ Fiji Software.

* To avoid repetitive results, the Actin-β images are shown in Supplemental Data Fig. S5., p. 247.

II.8 NEUROINFLAMMATION

Oxidative stress and cellular ROS production induced by UFP exposure can disturb the Nf-κB mediated signaling cascade, resulting in gene expression of cell survival genes, pro-inflammatory enzymes and cytokines (Bhargava *et al.*, 2019).

II.8.1 Protein expression of NF-κB -pathway regulators by Western blot

Protein expression level of NF-κB-pathway regulators are analyzed using the WB protocol described in section II.7.2 Protein expression of the antioxidant NRF2-pathway by Western blot (Cf. p. 79).

Primary Ab specific to NF-κB-pathway regulators were selected as follows: positive regulator IKK (IκB Kinase) subunits IKKα (1/1000, Cell Signaling, clone D3W6N, #61294, Mw 85 kDa) and IKKβ (1/1000, Cell Signaling, clone D30C6, #8943, Mw 87 kDa), NF-κB inhibitor IκBα (1/1000, Cell Signaling, clone 44D4, #4812, Mw 39 kDa), and the NF-κB components itself, including p65 (RelA) (1/1000, Cell Signaling, clone D14E12 XP®, #8242, Mw 65 kDa), p50 and p105 (1/1000, Cell Signaling, clone D4P4D, #13586, Mw 50 and 120 kDa, respectively).

II.8.2 DNA affinity binding assay of transcription factor NF-κB trough spectrophotometry

The DNA affinity binding assay (DAPA) of NF-κB subunits p50 and p65 to an oligonucleotide sequence immobilized on a 96-well plate is the principle of the TransAM™ Flexi NF-κB Family Transcription Factor Assay Kit (Active Motif, La Hulpe, Belgium). For this assay, 20 µg of nuclear extract is added to each well and incubated for 30 min to allow binding to the sequence. After binding, the wells were washed, and the primary Ab specific for the NF-κB protein was added and incubated during 1 hour. This is followed by incubation with a horseradish peroxidase (HRP)-conjugated Ab (diluted 1/1000 in 1X Ab Binding Buffer) for another hour. A Developing Solution is then added to converted the colorimetric reaction. After 10 minutes at RT, Stop Solution containing acids turned the blue color in yellow. The reaction absorbance was measured at 450 nm using the Spark® multimode microplate reader (TECAN, Männedorf, Switzerland).

II.8.3 Cytokine dosages by electrochemiluminescence ELISA (MSD Technology)

The concentrations of 19 inflammation mediators were measured, including IFN-γ, IL-1β, 2, 4, 5, 6, 9, 10, 12p70, 15, 17 A/F, 27p28/IL-30, 33, Interferon Gamma-Induced Protein 10 (IP-10), Keratinocyte Chemoattractant/human Growth-Regulated Oncogene (KC/GRO-α), Monocyte Chemoattractant Protein (MCP-1), Macrophage Inflammatory Protein 1-α and 2 (MIP- 1α and MIP-2) and TNF-α.

These measurements were performed using two immunoassays, the V-PLEX Cytokine panel and V-Plex Proinflammatory Panel 1 Mouse kits (Meso Scale Discovery

(MSD) Technology, Rockville, USA), according to the manufacturer's instructions. The kits operate on the principle of a sandwich ELISA, where the 96-well plates are pre-coated with capture Ab specific to each inflammatory mediator.

For each assay, 50 µL of the protein extracts were added to the wells and incubated on a shaker for 2 hours, allowing the mediators in the samples to bind to their corresponding capture antibodies. After washing, 25 µL of Sulfo-Tag-labeled secondary detection Ab were added and incubated for another 2 hours. Electrochemiluminescence detection was performed by adding the Read Buffer, and signal intensities were calibrated using a standard curve. The interpolated data were analyzed using MESO QuickPlex SQ 120 instrument (MSD) with Recovery Workbench software.

II.9 Regulated Cell Death

RCD features were investigated through protein expression levels by WB, ELISA, or luminescence assays. For WB analysis the same protocol was used as described in section II.7.2 Protein expression of the antioxidant NRF2-pathway by Western blot (Cf. p. 87).

II.9.1 Apoptosis

Western Blot

Apoptosis was studied through WB by following primary Ab: Cleaved Casp-3 (Asp175): 1/1000, Cell Signaling, clone 5A1E, #9664 (Mw 17-19 kDa); BAD: 1/1000, Cell Signaling, clone D24A9, #9239 (Mw 23 kDa); p-BAD (Ser112): 1/1000, Cell Signaling, clone 40A9, #5284 (Mw 23 kDa).

II.9.2 Autophagy

Western Blot

For autophagy following primary Ab were used for WB analysis: LC3A/B: 1/1000, Cell Signaling, clone D3U4C XP®, #12741 (Mw 14-16); ATG5: 1/1000, Cell Signaling, clone D5F5U, #12994 (Mw 55 kDa); ATG16L1: 1/1000, Cell Signaling, clone D6D5, #8089 (Mw 66-68); ATG3: 1/1000, Cell Signaling, #3415 (Mw 40 kDa); LC3b: 1/1000, Novus Biologicals, NB100-2220 (Mw 15-17 kDa), ATG101: 1/1000, Cell Signaling, clone E1Z4W, #13492 (Mw 25 kDa), ATG13: 1/1000, Cell Signaling, clone D4P1K, #13273 (Mw 72 kDa), ATG12: 1/1000, Cell Signaling, clone D88H11, #4180 (Mw 16-55 kDa), ATG7: 1/1000, Cell Signaling, clone D12B11, #8558 (Mw 78); SCSTM1/p62 (D1Q5S): 1/1000 Cell Signaling #39749 (Mw 62 kDa).

II.9.3 Necroptosis

Western Blot

To investigate necroptosis, following primary Ab were used for WB analysis: RIP: 1/1000, Cell Signaling, clone D94C12 XP®, #3493 (Mw 78 kDa), p-RIP3 (Thr231/Ser232): 1/1000, Cell Signaling, clone E7S1R, #91702 (Mw 46-62 kDa); RIP3: 1/1000, Cell Signaling, clone E7S1R, #15828 (Mw 46-62 kDa); MLKL: 1/1000, Cell Signaling, clone D6W1K, #37705 (Mw 54 kDa); p-MLKL (Ser345): 1/1000, Cell Signaling, clone D6E3G, #37333 (Mw 54 kDa).

II.9.4 Parthanatos

Western Blot

Parthanatos is investigated through WB by following Ab: AIF: 1/1000, Cell Signaling, clone D39D2 XP®, #5318 (Mw 67 kDa); MIF: 1/1000, Cell Signaling, clone E8S8H, #75038 (Mw 12 kDa).

II.9.5 Ferroptosis

Western Blot

For WB analysis of ferroptotic markers, the following primary Ab were used: TFR: 1/1000 Abcam®, Ab84036 (Mw 84 kDa), FTH1: 1/1000 Cell Signaling D1D4, #4393 (Mw 21 kDa); GPx4: 1/1000 Cell Signaling, #52455 (Mw 20-22 kDa); SLC7A11/xCT: 1/1000 Novus NB300-318 (Mw 35 kDa).

Gene expression of SLC7A11/xCT by RT-qPCR

Again the same RNA extraction samples were used, the extraction protocol is described before (Cf. RT-qPCR gene expression of polycyclic aromatic hydrocarbon and metal metabolism enzymes in whole brain tissue, p. 84).

Gene expression of SLC7A11/xCT was quantified by RT-qPCR using Taqman™ probes (ThermoFisher® Scientific Mm00442530_m1) and primers, together with the TaqMan™ Fast advanced Master MIX (Applied Biosystems). Validation of significantly over- or underexpression was made, after normalization by the housekeeping gene expression (*Ppia*) (ThermoFischer® Scientific Mm02342430_g1) with a threshold value of 2 (Fold-Change or FC > 2 or < 2).

Glutathione peroxidase

The catalytic activity of two key enzymes involved (GPx and GR) in the GSH conversion which can be related to the ferroptotic pathway were investigated through

colorimetric assays in the same protein extraction samples as previously described (Cf. II.7.2 Protein expression of the antioxidant NRF2-pathway by Western blot, p. 87).

GPx activity was measurement using the Glutathione Peroxidase Cellular Activity Assay Kit (Sigma-Aldrich, Saint Louis, Mo), following the manufacturer's instructions. A standard curve was prepared according to the provided protocol. Protein and standard samples were dissolved in GPx Assay Buffer and supplemented with NADPH Reaction Mix. After a 15-minute incubation, the Oxidizing Reagent Working Solution was added to initiate the GPx reaction, and the samples were incubated at 25 °C. Absorbance at 340 nm (OD340) was measured every 5 minutes. The decrease in absorbance, indicative of NADPH oxidation to NAD^+, reflects GPx activity. The rate of the reaction was calculated as nmol/min/mg of proteins.

Glutathione reductase

GR activity is quantified with Glutathione Reductase Assay Kit (Sigma-Aldrich, Saint Louis, Mo), with a manual very similar to GPx activity. GR catalyzes the reduction of GSSG to GSH, using NADPH cofactor. Protein samples were mixed with Oxidized Glutathione Assay Buffer, along with 5,5'-dithiobis(2-nitrobenzoic acid) (DTNB) and NADPH. In the assay, GSSG was converted to GSH in the presence of GR. The measurement relies on the increase in absorbance at 340 nm caused by the reaction, wherein the reduced GSH spontaneously reacted with previously added DTNB, forming 5-thio(2-nitrobenzoic acid). From the every 5 minutes measurement, the reaction rate could be calculated as nmol/min/mg of proteins.

Oxidation of antioxidant glutathione

The GSH/GSSG ratio was determined using the GSH/GSSG-Glo™ Assay from Promega® (Madison, WI). Both, total and oxidized glutathione, were measured. Protein lysates were added to wells of a 96-well opaque white plate (25 µL per well) and combined with 25 µL of either Total Glutathione Reagent (containing 4% Luciferin-NT in RIPA buffer) or Oxidized Glutathione Reagent (containing 4% Luciferin-NT and 2% N-Ethylmaleimide (NEM) at 25 mM in RIPA buffer). The mixture was gently agitated on an orbital shaker for 5 minutes at room temperature. After incubation, 50 µL of Luciferin Generation Reagent was added and incubated for 30 minutes. Luciferin Detection Reagent (100 µL per well) was then added to all wells and allowed to equilibrate for 15 minutes at room temperature. Luminescence signals were then quantified using a Spark® multimode microplate reader (TECAN). GSH and GSSG levels were determined according to the manufacturer's instructions, normalized to protein concentrations, and expressed as the GSH (nmol/mg), GSSG (nmol/mg), and GSH/GSSG ratio.

4-hydroxynonenal adducts ELISA electrochemiluminescence analysis

Quantification of 4-HNE adducts in protein samples was conducted using an inverse competitive ELISA. Wells in a 96-well plate format were coated overnight with the antigen 4-HNE-bovine serum albumin (BSA) (2 µg/mL) (ab194193, Abcam® (Cambridge, UK)), followed by a blocking step with 3% BSA Blocking Solution. Either the sample or a standard solution was added along with an equal volume of the primary antibody (Ab) (Anti-4 Hydroxynonenal Rabbit polyclonal Antibody; concentration: 580 µg/mL; ab46545, Abcam®). The covered plate was subjected to orbital shaking (500 rpm) for 2 hours at room temperature to facilitate incubation, before washing steps to remove unbound 4-HNE-primary Ab. After three washes, the plate was incubated with the secondary antibody, anti-rabbit Antibody goat Sulfo-TAG labelled (R32AH, Mesoscale® Discovery – MSD, MD), for 1 hour. This was followed by the addition of 150 µL of MSD Gold Sulfo-TAG (R91AO, MSD). Due to the necessity for heightened detection sensitivity, the levels of 4-HNE adducts (pg/µg proteins) were measured by detecting electrochemiluminescence signals using the MESO QuickPlex SQ 120 instrument (MSD) with Recovery Workbench software.

II.10 BRAIN SECTIONS: IMMUNOHISTOCHEMISTRY ANALYSIS

To study cell death in specific neurons and brain regions, IHC was performed on the same frozen sample slices prepared in section II.6.2 Direct UFP detection (Cf. Label-free detection of carbon particles by femtosecond pulsed laser microscopy, p. 84).

Membrane permeabilization was achieved using PBS-triton 0.2% and endogenous peroxidase activity was inhibited with 3% H_20_2, during a 10 minutes incubation. Brain tissue sections were blocked with 10% normal goat or rabbit serum-PBS for 1 hour at RT. Primary Ab (TH: 1/1000 (24h) Cell Signaling 5884; NeuN: 1/400 (24h) Cell Signaling 24307) were then applied and incubated at 4°C for 24 hours. Following this, secondary Ab were applied and incubated for 2 hours at RT. The avidin-biotin-peroxidase complex method was used, employing peroxidase-conjugated streptavidin and the DAB substrate kit for detection. The sections were subsequently dehydrated using an alcohol series (70% to 100%) and cleared in xylene (5 min/step). Finally, the slices were prepared for microscopic observation.

An overview of the markers, brain region, indications, references, primary and secondary Ab dilutions, analysis methods can be find in Supplemental Data Table S5 (Cf. p. 248).

II.11 STATISTICAL ANALYSIS

Data are expressed as mean ± standard deviation (SD). For all experiments n= 6 biological replicates are investigated, except differently shown in figure legend. Significant differences between groups were evaluated using the non-parametric Mann-Whitney U test. Statistical significance was defined as *$p<0.05$, **$p<0.01$, and ***$p<0.001$. All statistical analyses were performed using GraphPad Prism 9 Software.

III. RESULTS

III.1 Characterization of UFP

III.1.1 Granulometry

There are three methods for describing granulometry results: 1) Size Distribution by Number, 2) Size Distribution by Intensity, and 3) Size Distribution by Volume. As discussed in the section I.2 Ultrafine particles and their brain translocation (Cf. p. 2), UFP have a significant proportion in terms of particle number. Therefore, only Size Distribution by Number is present below; descriptions using the other two methods can be found in Supplemental Data Fig. S6, p. 249.

As shown in Fig. 34, the Size Distribution by Number revealed two peaks: a major peak at 169.5 nm (78,7%), corresponding to UFP, and a minor peak at 622.1 nm (21.3%), likely indicating the formation of particle aggregates.

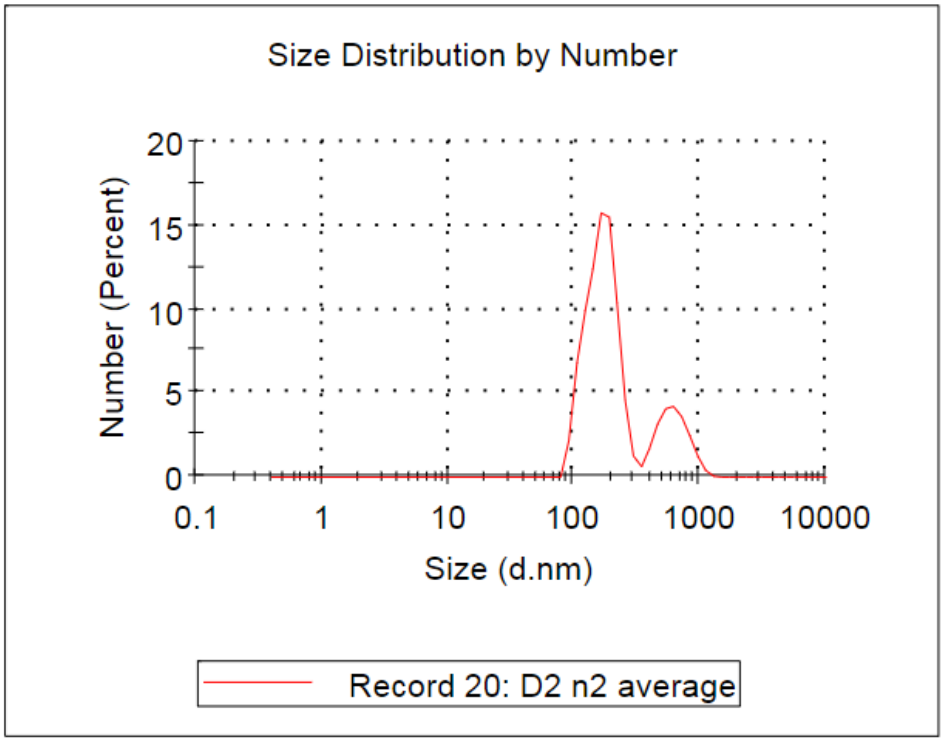

Figure 34 : Granulometry represented as Size Distribution by Number of ultrafine particle samples collected in Lille.

The Y-axis shows the percentage of UFP, and the X-axis shows particle diameter in nanometers (nm). A primary peak at 169.5 nm, representing 78.7% of the sample, corresponds to ultrafine particles (UFP). A secondary peak, indicating particle aggregates, accounts for 21.3% of the sample with a mean diameter of 622.1 nm.

Abbreviations: UFP: Ultrafine particles.

III.1.2 Physico-chemical characterization

Metal analysis

Trace metal analysis was performed using ICP-MS. A detailed overview of the elemental composition, along with their corresponding concentrations (µg/g), is provided in Supplemental Data Table S3, p. 239.

This data is also presented visually in a pie chart (Fig. 35). The three most abundant metals identified are calcium (Ca; 30.2%), silicon (Si; 23.9%), and iron (Fe; 10.1%).

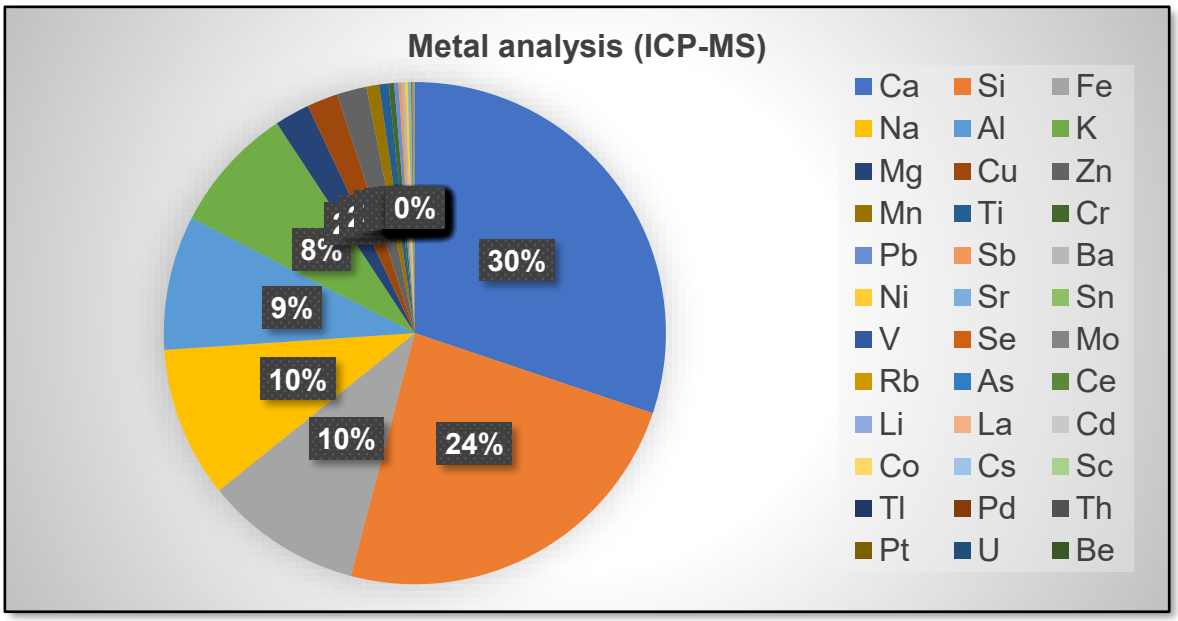

Figure 35: Percentage distribution of metals in ultrafine particle samples collected from Lille.

Pie chart showing metal composition in ultrafine particle (UFP) samples, analyzed by Inductively Coupled Plasma Mass Spectrometry (ICP-MS). Colors indicate each metal, with the highest concentration (Ca, 30.2%) in the legend on the upper left and the lowest concentration (Be, 0.0001%) in the lower right.

Abbreviations:

Elements: Al: aluminum; As: Arsenic; Ba: Barium; Be: Beryllium; Ca: Calcium; Cd: Cadmium; Ce: Cerium; Co: Cobalt; Cr: Chromium; Cs: Cesium; Cu: Copper; Fe: Iron; K: Potassium; La: Lanthanum; Li: Lithium; Mg: Magnesium; Mn: Manganese; Mo: Molybdenum; Na: Sodium; Ni: Nickel; Pb: Lead; Pd: Palladium; Pt: Platinum; Rb: Rubidium; Sb: Antimony; Sc: Scandium; Si: Silicon; Sn: Tin; Sr: Strontium; Th: Thorium; Ti: Titanium; Tl: Thallium; U: Uranium; V: Vanadium; Zn: Zinc,

ICP-MS: Inductively Coupled Plasma Mass Spectrometry; UFP: ultrafine particles.

PAH, dioxins, furans and PCB analysis

PAH concentrations were quantified by HPLC-Fluorimetry and are expressed as ng/mg of UFP. A detailed breakdown of PAH composition can be found in Supplemental Data Table S1 (Cf. p 236), with a total PAH concentration of 84.2 ng/mg UFP. This data is also represented in a pie chart (Fig. 36). The three most abundant PAH are Benzo[b]fluoranthene (BbF; 12.8%), Chrysene (CH; 11.9%), and Benzo[g,h,i]perylene (BghiP; 11.4%). Table S1 (Cf. p. 233) also includes Toxicity Equivalency Factor (TEF)

values from the EPA (US) to assess carcinogenic potential, expressed as benzo[a]pyrene equivalents, along with the calculated Toxicity Equivalent (TEQ).

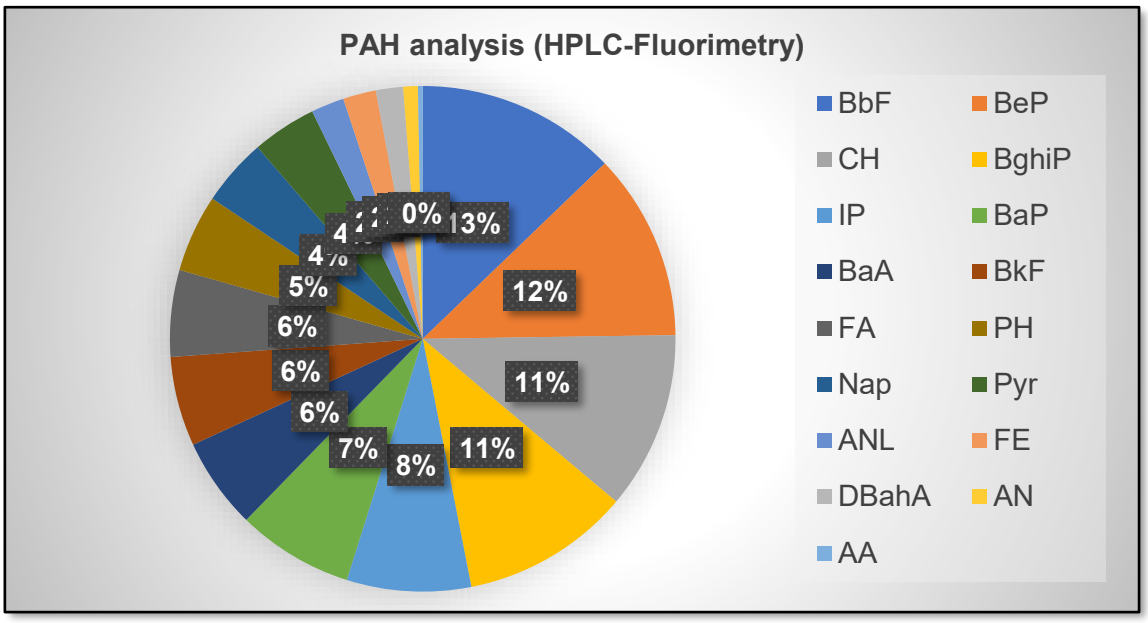

Figure 36: Percentage distribution of Polycyclic Aromatic Hydrocarbon in ultrafine particles samples collected from Lille.

Pie chart showing Polycyclic Aromatic Hydrocarbon (PAH) composition in ultrafine particles (UFP) samples, analyzed by high-performance liquid chromatography (HPLC)-Fluorimetry. Colors indicate each PAH, with the highest concentration (Benzo[b]fluoranthene (BbF), ~13%) in the upper left and the lowest (Anthracene (AA), 0.3%) in the lower left.

Abbreviations:

Polycyclic Aromatic Hydrocarbon (PAH): AN: Acenaphthene; ANL: Acenaphthylene; AA: Anthracene; BaA: Benzo[a]antracene; BaP: Benzo[a]pyrene; BbF: Benzo[b]fluoranthene; BeP: Benzo[e]pyrene; BghiP: Benzo[g,h,i]perylene; BkF: Benzo[k]fluoranthene; CH: Chrysene; DBahA: Dibenzo[a,h]anthracene; FA: Fluoranthene; FE: Fluorene; IP: Indeno[1,2,3-c,d]pyrene; Nap: Naphthalene; PH: Phenanthrene; Pyr: Pyrene.

HPLC: high-performance liquid chromatography; UFP: ultrafine particles.

HRGC/HRMS was used to quantify two groups (Cf. Supplemental Data Table S6, p. 250): Dioxins and Furans, both persistent organic pollutants that are chlorinated organic compounds. After decomposition of both in UFP samples, the dioxins highest concentration (Fig. 37) was octachlorodibenzodioxin (OCDD; 62,1%) and the lowest concentration for tetrachlorodibenzofuran (2,3,7,8-TCDD; 0.27%). Furans highest concentration octachlorodibenzofuran (OCDF; 56.5%), and the lowest concentration for tetrachlorodibenzofuran (2,3,7,8-TCDF; 1.1%).

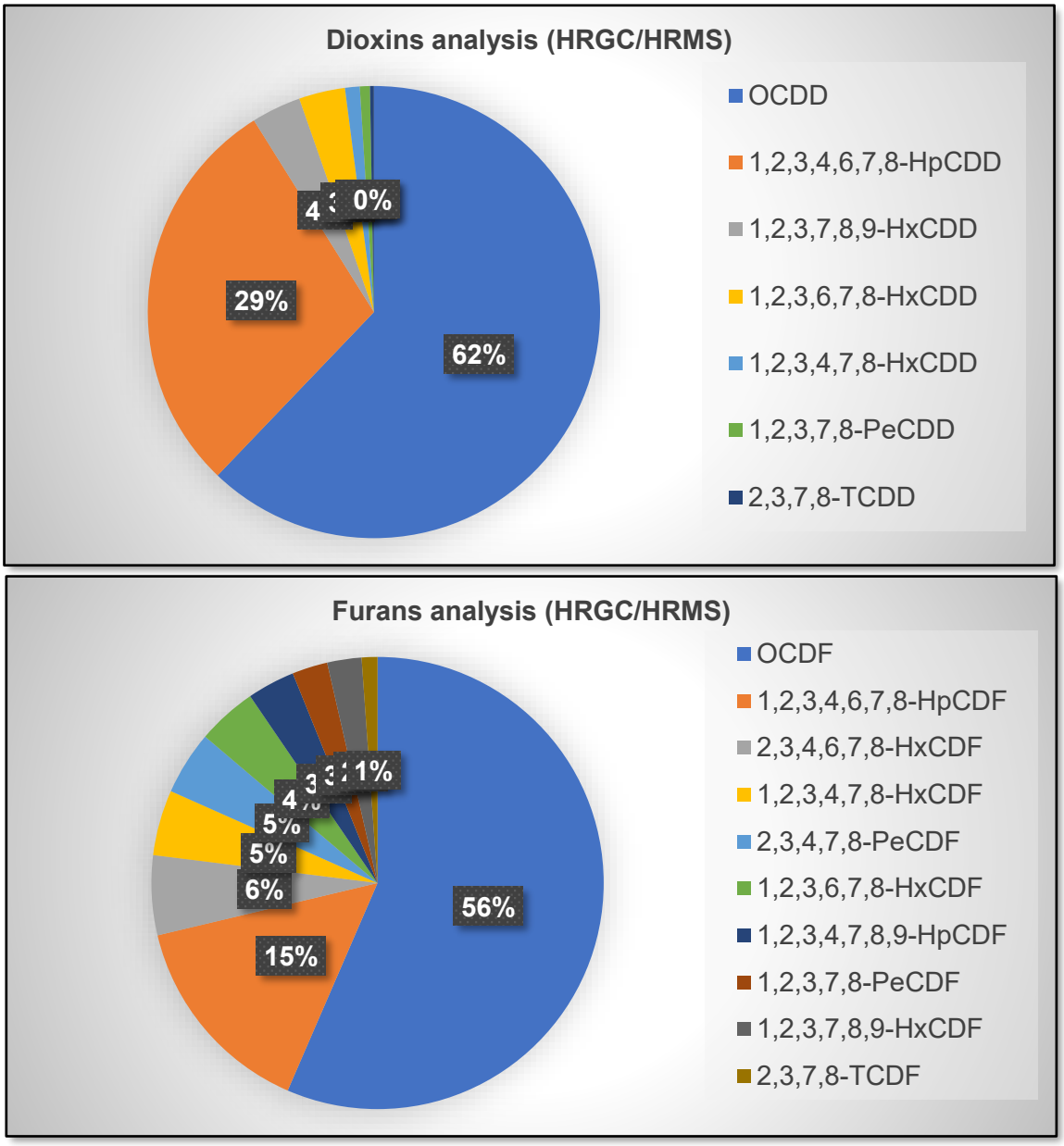

Figure 37: Pie chart showing percentage distribution of Dioxins and Furans in ultrafine particle samples collected from Lille.

First pie: Graph of the Dioxin analyzed through high-resolution gas chromatography/mass spectrometry (HRGC/HRMS). The legend indicates the color corresponding to each Dioxin, with the highest concentration (Octachlorodibenzodioxin (OCDD), 62,1 %) in the legend on top and the lowest concentration at last (Tetrachlorodibenzo-p-dioxin (2,3,7,8-TCDD), 0.27 %).

Second pie: Graph of the Furans analyzed through HRGC/HRMS. The legend indicates the color corresponding to each Furan, with the highest concentration (Octachlorodibenzofuran (OCDF), 56.5 %) as first indication and the lowest concentration (Tetrachlorodibenzofuran (2,3,7,8-TCDF), 1.1 %).

Abbreviations:

Dioxins: HpCDD: Heptachlorodibenzo-p-dioxin; HxCDD: Hexachlorodibenzo-p-dioxin; OCDD: Octachlorodibenzodioxin; PeCDD: Pentachlorodibenzo-p-dioxin; TCDD: Tetrachlorodibenzo-p-dioxin.

Furans: HpCDF: Heptachlorodibenzofuran; HxCDF: Hexachlorodibenzofuran; OCDF: Octachlorodibenzofuran; PeCDF: Pentachlorodibenzofuran; TCDF: Tetrachlorodibenzofuran.

HRGC/HRMS: high-resolution gas chromatography/mass spectrometry; UFP: ultrafine particles.

Polychlorinated biphenyls (PCB) (Supplemental Data Table S7, p. 251) are categorized into two main types: PCB dioxin-like and PCB indicators.

The dioxin-like PCB have structural and toxicological properties similar to dioxins and affect the body through the AhR pathway. They are classified by non-ortho and mono-ortho substituted PCB. Mono-ortho PCB have a greater dioxin-like activity and are therefore referred as more toxic. For the PCB indicators, the total amount of PCB is a reliable value to describe toxicity in environmental and biological samples. The concentrations are described in Fig. 38.

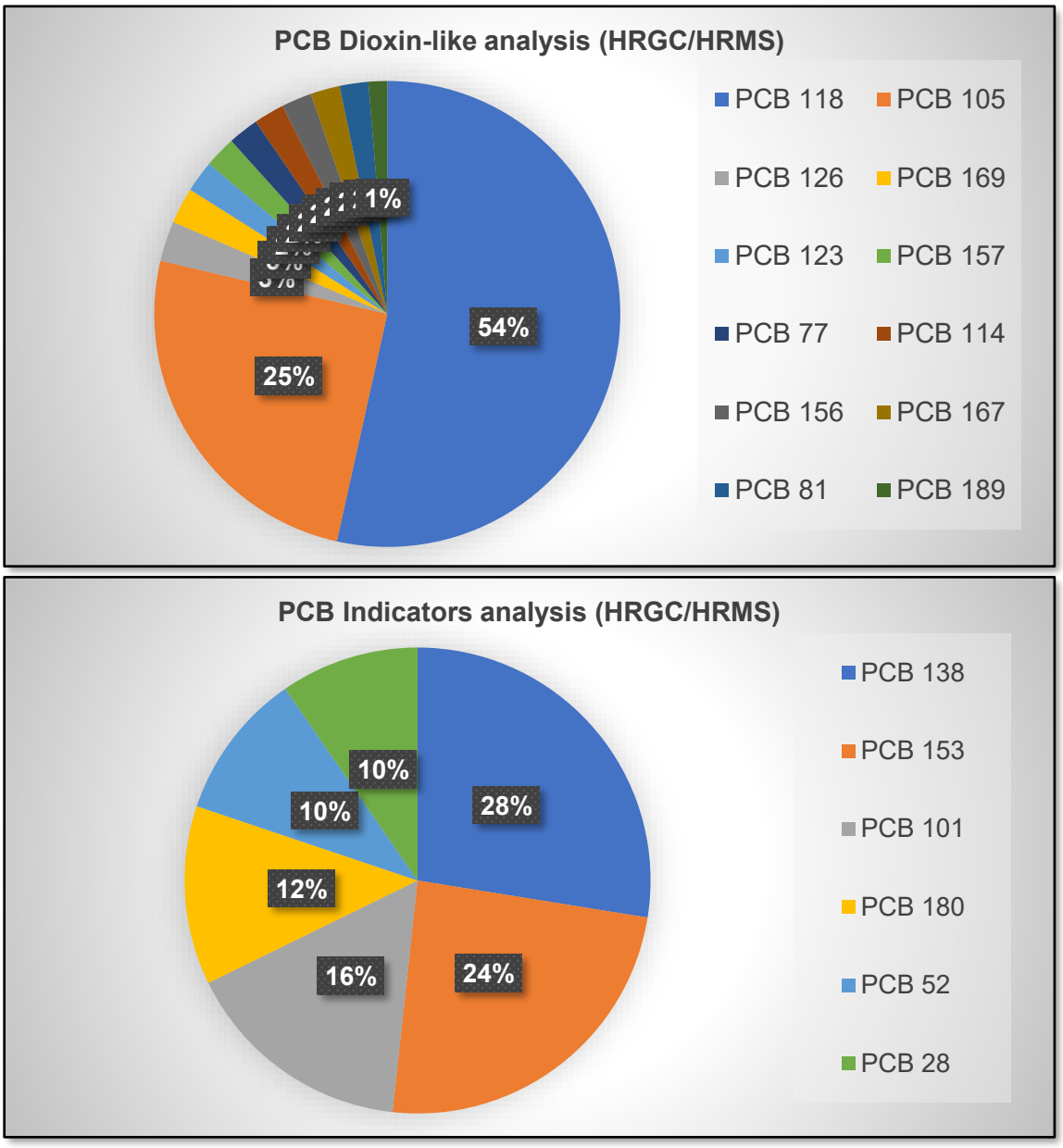

Figure 38: Pie chart showing percentage distribution of polychlorinated biphenyls in ultrafine particle samples collected from Lille.

First pie: Graph of the Dioxin-like PCB analyzed through high-resolution gas chromatography/mass spectrometry (HRGC/HRMS). The legend indicates the color corresponding to each Dioxin-like PCB, with the highest concentration (PCB 118; 53.5%) in the upper left corner and the lowest concentration (PCB 189; 1.3%) in the lower right corner.

Second pie: Graph of the PCB Indicators analyzed through HRGC/HRMS. The legend indicates the color corresponding to each PCB Indicator, with the highest concentration (PCB 138; 27.55%) and the lowest concentration (PCB 28, 9.61%).

Abbreviations: Polychlorinated biphenyls (PCB):

Non-ortho substituted PCB: 3,4,4',5-tetraCB (PCB 81), 3,3',4,4'-tetraCB (PCB 77), 3,3',4,4',5-pentaCB (PCB 126), 3,3',4,4',5,5'-hexaCB (PCB 169);

Mono-ortho substituted PCB: 2,3,3',4,4'-pentaCB (PCB 105), 2,3,4,4',5-pentaCB (PCB 114), 2,3',4,4',5-pentaCB (PCB 118), 2',3,4,4',5-penta (PCB 123), 2,3,3',4,4',5-hexaCB (PCB 156), 2,3,3',4,4',5'-hexa (PCB 157), 2,3',4,4',5,5'-hexaCB (PCB 167), 2,3,3',4,4',5,5'-heptaCB (PCB 189) HRGC/HRMS: high-resolution gas chromatography/mass spectrometry; UFP: ultrafine particles.

III.1.3 Biological characterization (endotoxins quantification)

The spectrophotometric analysis, using a typical chromogenic Limulus Amebocyte Lysate (LAL) assay, revealed a significantly higher level of Endotoxin Units per Milliliter (EUL/mL) in Dose 1 UFP (10 µg) with a mean of 2.11 EUL/mL. This level was approximately three times higher for Dose 2 (30 µg), with a mean of 6.72 EUL/mL, whereas the physiological serum had a mean value of 0.57 EUL/mL, as shown in Fig. 39.

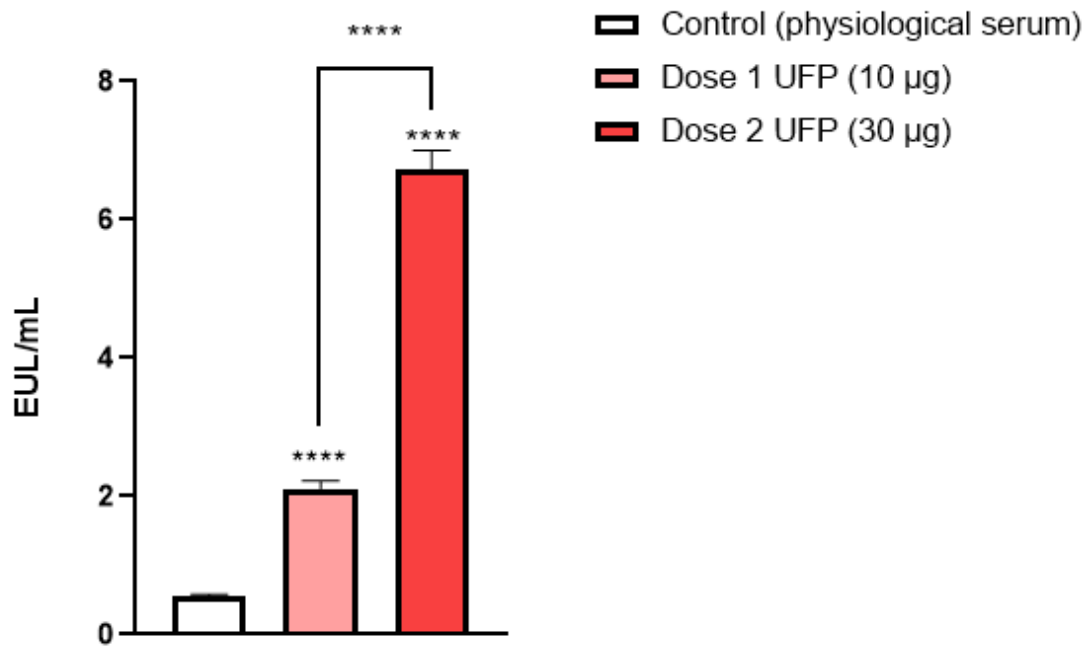

Figure 39: Endotoxins quantification of ultrafine particles.

Endotoxin levels (EUL/mL) measured using a chromogenic Limulus Amebocyte Lysate (LAL) assay for Dose 1 UFP (10 µg; mean: 2.11 EUL/mL) and Dose 2 UFP (30 µ; mean: 6.72 EUL/mL), showing a significant threefold increase in Dose 2 compared to Dose 1. The physiological serum control exhibited a mean value of 0.57 EUL/mL.

Control: physiological serum; Dose 1 UFP : 10 µg ; Dose 2: 30 µg

(n = 3; unpaired t-test (GraphPad Prism8); **** p<0.0001)

Abbreviations: EUL/mL: Endotoxin Units per Milliliter; LAL : Limulus Amebocyte Lysate ; UFP : Ultrafine particles.

III.2 Mouse behavioral tests

III.2.1 Open field test

Given the motor neurons are affected during the progression of PD, it was valuable to examine the impact of UFP exposure on motor function using the open field test. Under typical physiological conditions, mice tend to spend more time near the walls than in the center of the arena. Therefore, parameters such as means speed (V), total distance travelled, and the percentage of time spent in the center versus the periphery are

indicative of movement patterns in the arena. Additionally, behaviors like resting and rearing provide further insights into the rodent's motor activity. However, as shown in Fig. 40 none of the parameters was significative changed in UFP-exposed mice compared to the control group.

III.2.2 Elevated plus-maze test

During the EPM test, mice are examined for their well-being, which is related to the level of anxiety. In this study, we did not focus on the rodent's preference for the closed/dark arm compared to the open one, but instead, we investigated the direct effects on body position, such as head dipping, stretch posture, rearing, and grooming, as shown in Fig. 41. These behaviors provide insights into anxiety-like responses, which are associated with alterations in brain regions involved in emotional regulation and stress responses. In the context of PD or brain toxicity, anxiety-like behaviors observed by the EPM test are linked to dysfunction in brain regions such as the prefrontal cortex, amygdala, hippocampus, and even the dopaminergic system, particularly in the SN. The Dose 2 exposed group showed a higher level of head dipping compared to control, and the Dose 1 UFP-exposed group more rearing.

III.2.3 Y-maze test

Spatial memory was investigated using the Y-maze test. Mice are naturally curious and tend to explore new environments, which includes visiting the unknown arm among the three available arms during the test. This exploration behavior is used to assess the animals' spatial memory and cognitive flexibility. The parameters measured include the number of entries into the unknown arm, reported as a percentage, and the ratio of entries into the open arm compared to the total number of entries. These behaviors are primarily associated with brain regions involved in spatial memory and decision-making, such as the hippocampus and prefrontal cortex. As demonstrated by the graphs in Fig. 42, the percentage number of the entries in the unknown arm, as well as the ratio between entries of the open arm compared to the total amount did was not changed in the UFP-exposed groups compared to the control group.

III.2.4 Spontaneous alternation test

The spontaneous alternation test assess the exploratory behavior of mice to investigate working memory. Working memory is a critical component of cognition, as it enables the animal to hold and update information momentarily while making decisions. Spatial memory and cognitive flexibility are primarily associated with brain regions like

the hippocampus and prefrontal cortex. However, in PD, degeneration of dopaminergic neurons in the SN disrupts the balance of neurotransmitters, which can also impair cognitive functions. As shown in Fig. 43, we did not observe an altered alternation pattern among our groups.

III.2.5 Passive avoidance test

The passive avoidance test primarily evaluates fear-associated memory in mice, focusing on anxiety-related behavior outcomes. This test assesses emotional memory by measuring the latency before the mice re-enter the dark chamber where they previously received a mild electric shock. Parameters measured include the initial inquisition latency, retention latency, and the ratio between retention and acquisition. The initial acquisition represents the baseline time it takes for the animal to enter the dark compartment during the habituation phase, while the retention latency measures the time taken to enter the dark compartment during the test conducted 24 hours after training. As shown in Fig. 44 none of the three parameters gave a positive outcome, this can indicate that UFP, at the given doses of 10µg/adm and 30 µg/adm for a duration of 12 weeks, did not induce observable deficits in emotional memory or fear response, which are often impacted by alterations in the amygdala, hippocampus, or prefrontal cortex.

Open Field Test: Movement in the arena

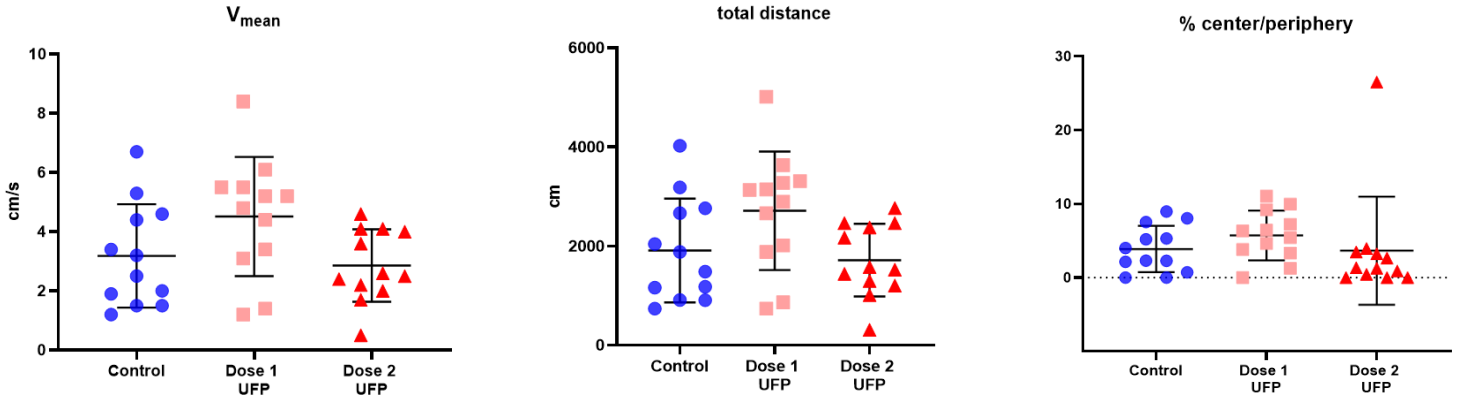

Open Field Test: Motor mice behavior

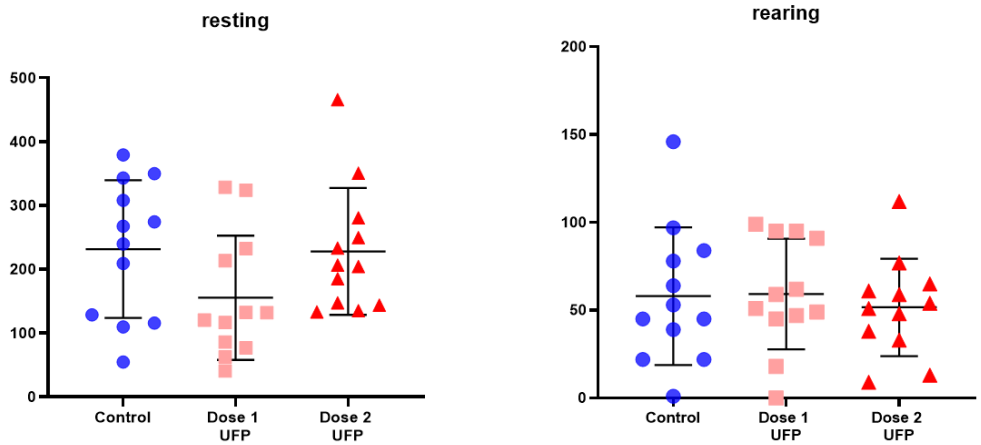

Figure 40: Locomotor activity results from the Open Field Test after three months of ultrafine particle exposure.

The open field test showed that mice exposed to Dose 1 (10 µg/adm) or Dose 2 (30 µg/adm) of ultrafine particles (UFP) exhibited locomotor activity similar to that of the control group. Parameters measuring movement in the arena included mean speed (V), represented in cm/s, total distance travelled, represented in cm, and the percentage of time spent in the center versus the periphery of the arena. Motor behavior was assessed by recording the frequency of resting and rearing behaviors of the mice.

Control: vehicle mice; Dose 1 UFP : 10 µg/adm ; Dose 2: 30 µg/adm

(n = 12; non-parametric Mann-Whitney U test (GraphPad Prism8)).

Abbreviations: UFP: Ultrafine particles; V: Speed

Elevated Plus-Maze test

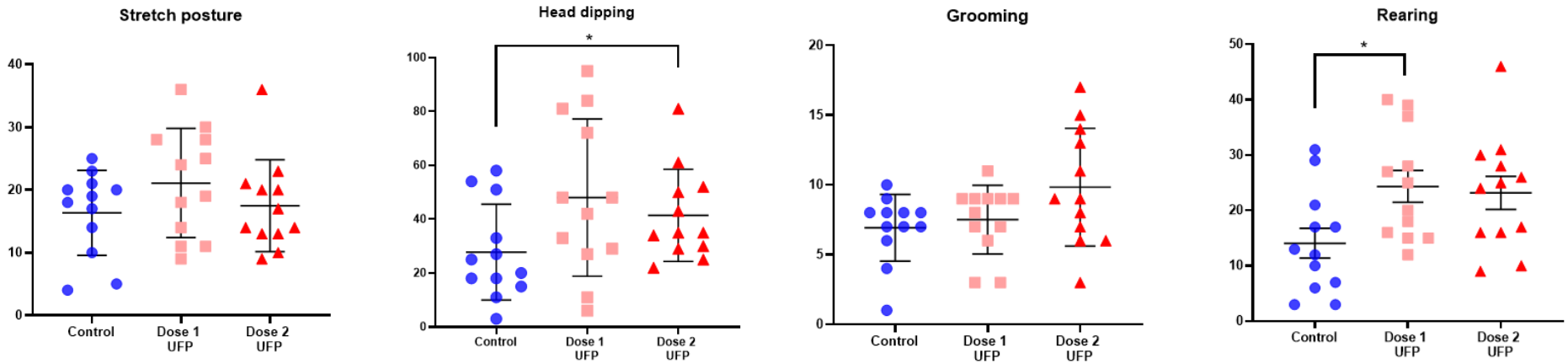

Figure 41: Anxiety results from the Elevated Plus-Maze test after three months of UFP exposure.

Mice exposed to the highest dose of 30 µg/adm ultrafine particles (UFP) for three months showed a significative number of head dipping behavior, while rearing was more frequently observed in mice exposed to 10 µg/adm UFP exposure compared to control mice. No significant effects were observed on the stretching of grooming behaviors of the mice.

Control: vehicle mice; Dose 1 UFP : 10 µg/adm ; Dose 2: 30 µg/adm

(n = 12; non-parametric Mann-Whitney U test (GraphPad Prism8); * $p<0.05$)

Abbreviations: UFP: Ultrafine particles.

Y-maze test

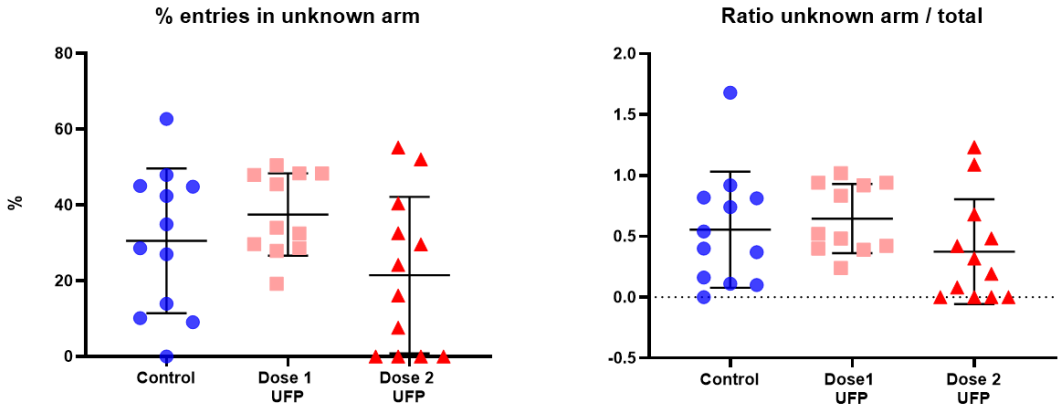

Figure 42: Spatial memory results from the Y maze test after three months of UFP exposure.

After replacing the mice in the Y-maze, no statistical difference were observed in the percentage of entries into the unknown arm, with an average of around 30% for all groups (i.e., control, exposed to 10 µg/adm and 30 µg/adm ultrafine particles (UFP)). This indicates that the mice explored the three arms of the maze almost equally. Similarly, the ratio of entries into the unknown arm compared to the total number of entries was not significantly different between the control and UFP-exposed mice.

Control: vehicle mice; Dose 1 UFP : 10 µg/adm ; Dose 2: 30 µg/adm

(n = 12; non-parametric Mann-Whitney U test (GraphPad Prism8))

Abbreviations: UFP: Ultrafine particles.

Spontaneous alternation test

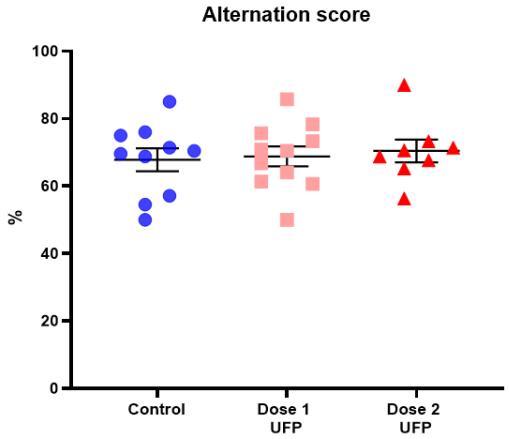

Figure 43: Working memory alternation score from the spontaneous alternation test after three months of UFP exposure.

The alternation score is calculated when the animal enters a new arm on each of three consecutive entries. Each set of three distinct, sequential arm entries counts as one alternation. The percentage of successful alternations was similar across all groups, indicating no significant cognitive decline in spatial memory in mice exposed to ultrafine particles (UFP) compared to the control group.

Control: vehicle mice; Dose 1 UFP : 10 µg/adm ; Dose 2: 30 µg/adm

(n = 12; non-parametric Mann-Whitney U test (GraphPad Prism8))

Abbreviations: UFP: Ultrafine particles.

Passive avoidance test

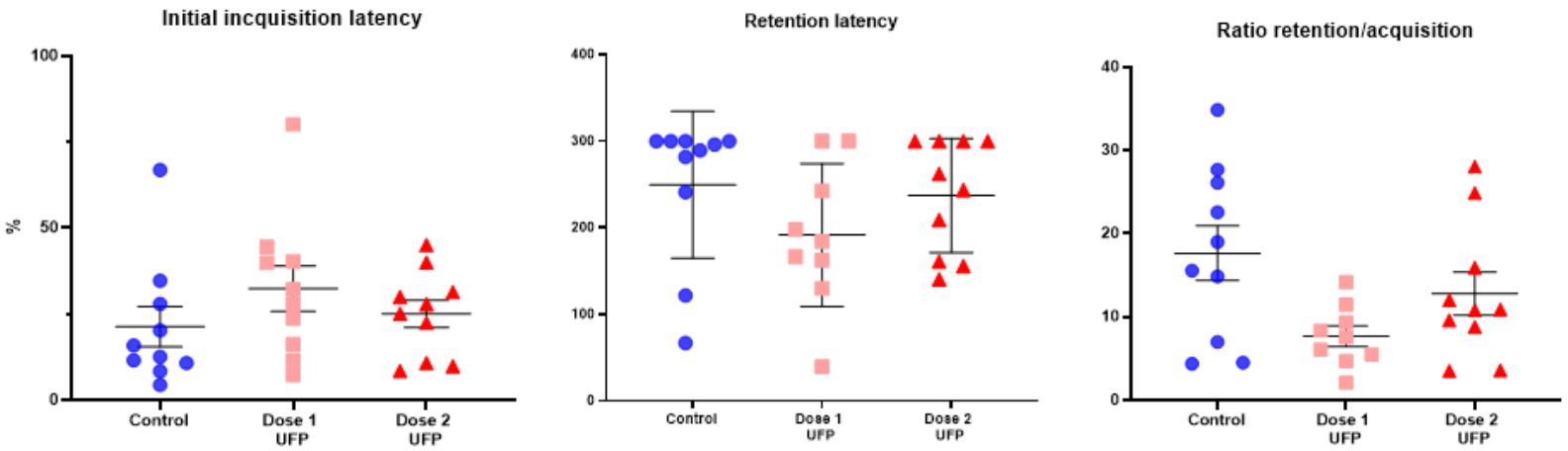

Figure 44: Fear-associated memory results from the passive avoidance test after three months of UFP exposure.

Th initial inquisition latency, retention latency and ratio of retention to acquisition latency did not show statistically significant differences between the control group and ultrafine particles (UFP)-exposed groups (Dose 1: 10 µg/adm; or Dose 2: 30 µg/adm).

Control: vehicle mice; Dose 1 UFP : 10 µg/adm ; Dose 2: 30 µg/adm

(n = 12; non-parametric Mann-Whitney U test (GraphPad Prism8))

Abbreviations: UFP: Ultrafine particles.

III.3 UFP detection

III.3.1 Indirect UFP detection

Metal analysis in whole brain tissue

Following exposure to UFP, metal analysis was conducted on blood and several organs, including the lungs, heart, liver, kidneys, and brain, using ICP-MS.

For the elements K, Fe, La, Mo, Rb, Sb, Se, Sn, and Zn, the measured concentrations were either too low or inconsistent with the expected organ levels. This inconsistency could be attributed to significant variability between individual mice or the intake of elements from other sources, such as dietary intake. Consequently, these elements are not discussed further in this study.

As shown in Table 5, indicating significant differences in metals between vehicle and 30 µg/adm exposed mice. Lungs were identified as the primary site of UFP deposition, with substantial accumulation of metals, including Cs, Mn, V, Cd, and Co. Blood concentrations of these metals remained low with minimal variability before and after exposure, suggesting a rapid transfer from systemic circulation to organs involved in detoxification, notably the liver and kidneys. This is reflected in the high metal concentrations observed in these organs, with Cr predominantly accumulating in the liver, and Cs, Cu and Mn found in both liver and kidneys. Notably, the brain, a protected organ by the BBB, exhibited elevated levels of Cu and Co, indicating metal infiltration into the CNS despite its protective mechanisms.

Table 5: Organs recuperated of Dose 2 (30 µg/adm) exposed mice in line with their significative metal values higher than the threshold of 1.02 µg/µl.

Metal	Lungs	Heart	Liver	Kidneys	Brain
Cr			X		
Cs	X		X	X	
Cu			X	X	X
Mn	X		X	X	
V	X				
Cd	X		X	X	
Co	X		X	X	X

RT-qPCR gene expression of polycyclic aromatic hydrocarbon and metal metabolism enzymes in whole brain tissue

Given that direct metal measurements in whole brain tissue may be shaded by intracellular presence and therefore hardly to interpretate, the focus of this analysis shifted to the metabolic pathways of metals in brain tissue, which Mt expression serving as an indirect marker for metal homeostasis and detoxification. Additionally, the transcript expression of several CYP enzymes, known to metabolize PAH into mutagenic diol epoxides, was investigated. The pathway begins with PAH binding to the AhR, which then triggers the transcription of CYP enzymes.

The gene expression of AhR, along with the downstream-regulated CYP enzymes CYP1A1 and CYP1B1, was significantly higher in the whole brain samples of UFP-exposed mice compared to vehicle-exposed mice, as shown in Fig. 45. Moreover, the gene expression of Mt1, Mt3, and Mt4, which are involved in brain metal detoxification, was also notably elevated in UFP-exposed mice relative to controls.

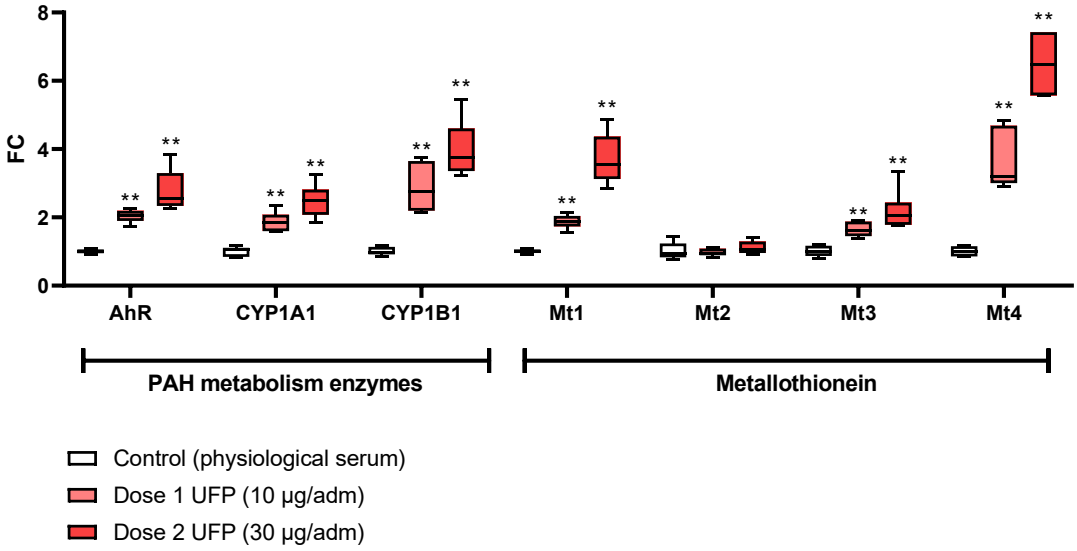

Figure 45: Gene expression of detoxification enzymes in whole brain tissue.

Gene expression levels measured through RT-qPCR of aryl hydrocarbon receptor (AhR), Cytochrome P450 (CYP)1A1 and CYP1B1 enzymes involved in PAH metabolism (left panel), and metallothionein (Mt), key proteins in metal detoxification (right panel), are shown. AhR, CYP1A1, CYP1B1, Mt1, Mt3 and Mt4 gene expression was significantly elevated in brain tissue following exposure to 10 µg/adm or 30 µg/adm UFP, compared to vehicle-exposed mice.

Control: vehicle mice; Dose 1 UFP : 10 µg/adm ; Dose 2: 30 µg/adm

(n = 6; Non-parametric Mann-Whitney U test (GraphPad Prism8); ** $p<0.01$)

Abbreviations: AhR: Aryl hydrocarbon receptor; CYP: Cytochrome P450 enzymes; Mt: Metallothionein; UFP: Ultrafine particles.

III.3.2 Direct UFP detection

Transmission Electron Microscopy (TEM)

The TEM assay provides detailed structural information and allows for the observation of subcellular structures where UFP may be localized. Due to the high resolution of TEM, it is particularly useful for detecting very tiny particles, such as UFP. Therefore, small biopsies (~ 1 mm^3) were used, which limits the sample detection representativeness for the whole organ. Fig. 46 shows TEM images obtained from brain tissue of the control group (Mouse 466), Dose 1 (Mouse 460), and Dose 2 (Mouse 418) exposed mice.

Interpreting these images is challenging, especially in the absence of contrast solutions or UFP-specific labelling. However, for Dose 1, some small electron-dense particles (dots) are observed within a neuronal axon and body. These could potentially be UFP, providing the first indication that UFP have reached the brain.

Control: Physiological Serum	Dose 1: 10 µg/adm UFP	Dose 2: 30 µg/adm UFP
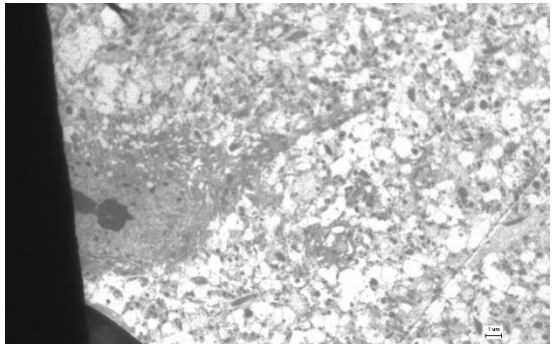 Mouse 466 brain neuron	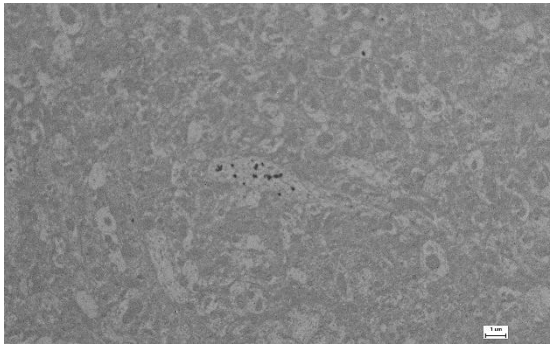 Mouse 460 brain axon with particles	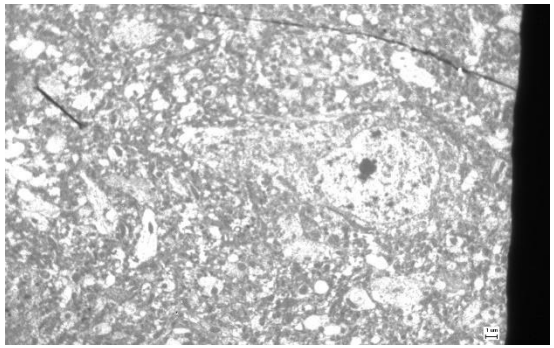 Mouse 418 brain neuron (without particles)
	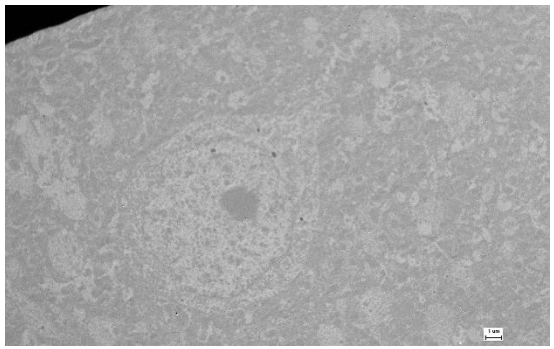 Mouse 460 brain neuronal body with particles	

Figure 46: Transmission Electron Microscopy images showing UFP brain localization.

The Transmission Electron Microscopy (TEM) images from the control group and the Dose 1 (10 µg/adm) and Dose 2 (30 µg/adm) UFP-exposed brains are inconclusive because of the bad resolution, and should ideally be redone. However, the black dots observed in the TEM images of the Dose 1 exposed brains, suggest particle presentation in a neuronal axon and cell body. These black dots are interpreted as UFP, providing preliminary evidence that UFP have reached the brain tissue in mice exposed to Dose 1 concentrations.

Abbreviations: TEM: Transmission Electron Microscopy; UFP: Ultrafine particles.

Label-free detection of carbon particles by femtosecond pulsed laser microscopy

TEM is a valuable tool for demonstrating that UFP translocate into the brain and even enter neurons, potentially leading to cellular alterations. However, the TEM methodology has several limitations: 1) no specific brain regions were targeted; 2) the accuracy of identifying UFP is compromised, as the dots could be mistaken for contaminants from reagents or other sources; and 3) a specific fixation protocol is required for optimal results.

To overcome these limitations, I established a collaboration with the Centre for Environmental Sciences (CMK, UHasselt, Belgium) to use a patented method based on femtosecond pulsed laser microscopy. This technique allows the visualization of UFP in frozen brain slices of our four brain regions (i.e., prefrontal cortex, striatum, hippocampus, SN).

Brain slice images obtained by the TPAF (green emission autofluorescence light) of vehicle and 30 µg/adm UFP-exposed mice, showing the background image can be found in Supplemental Data Fig. S4, p. 246.

The results of UFP detection in the prefrontal cortex, striatum, hippocampus, and SN are presented as the number of UFP per mm³ brain tissue (Fig. 47). Data are shown for mice after 3 months of exposure and after 3 months of exposure followed by a 3-month recovery period. Results for the vehicle group are represented as black dots, while red squares indicate the 30 µg/adm (Dose 2) group.

After 3 months exposure, vehicle mice showed a similar baseline UFP count of approximately 1000 UFP/mm³ across all four brain regions, reflecting exposure to particles from inhaled environmental air. In contrast, the Dose 2 group exhibited a significantly higher number of UFP in the prefrontal cortex and SN, suggesting that UFP accumulate in both anterior/ventral and posterior/dorsal brain regions following intranasal exposure.

After the 3-month recovery period, the baseline UFP count for the vehicle group remained at approximately 1000 UFP/mm³ in all brain regions. Interestingly, the UFP count in the Dose 2 group also returned to baseline levels, with no significant differences observed between the exposed and vehicle group. This suggest that the brain's UFP load may normalize after cessation of exposure.

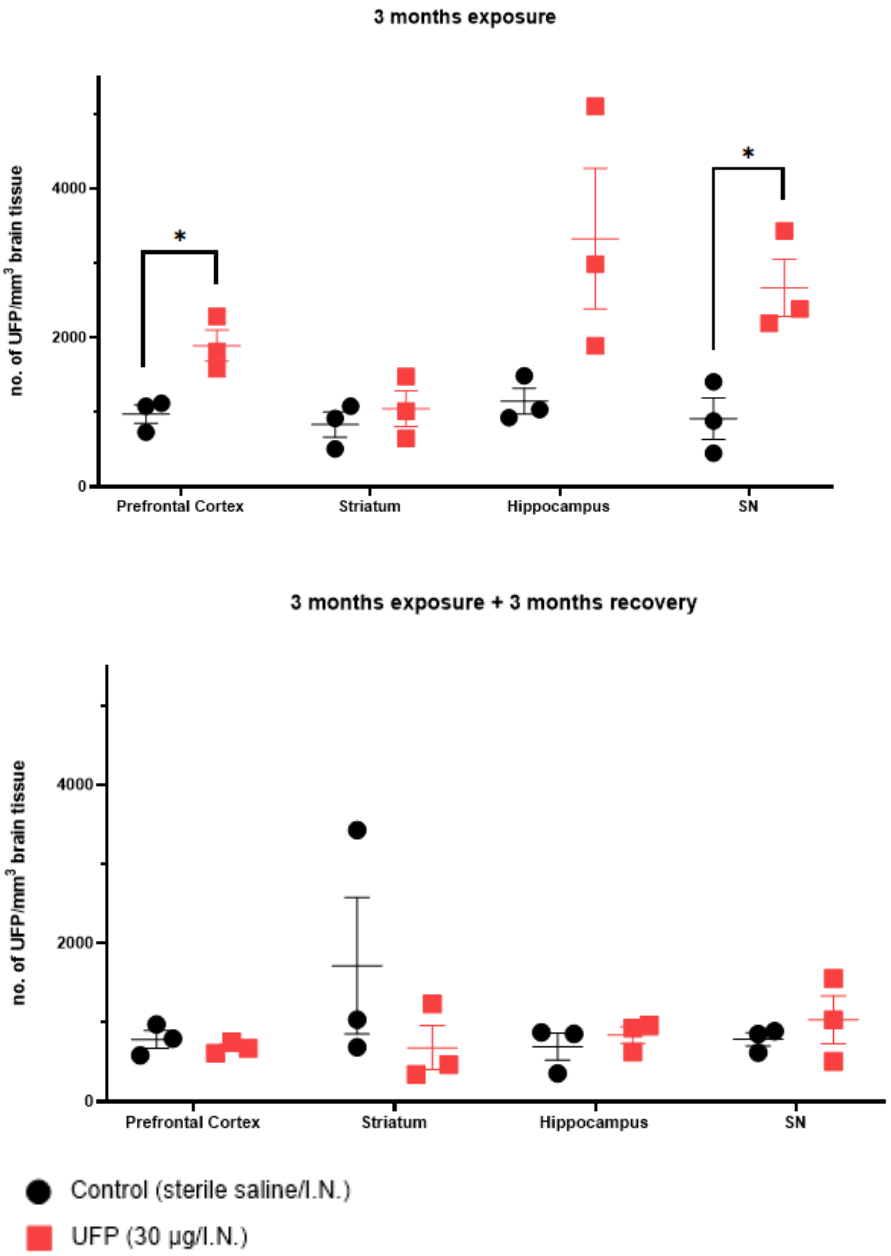

Figure 47: Ultrafine particle distribution in different brain regions of mice exposed to particles for 3 months, or 3 months with an additional 3-month recovery period.

This figure illustrates ultrafine particles (UFP) loading in four brain regions: the prefrontal cortex, striatum, hippocampus, and Substantia Nigra (SN). UFP were detected using a label-free method based on non-incandescence light generation under femtosecond-pulsed illumination. The first graph shows UFP detection after 3 months of exposure, while the second graph displays results from mice exposed for 3 months followed by a 3-month recovery period. Significant differences ($p < 0.05$) were observed between the vehicle-exposed group (Control) and the 30 µg/adm UFP-exposed group (Dose 2) in the prefrontal cortex and SN, indicating increased UFP accumulation in these regions.

Control (NC): vehicle mice; Dose 1 UFP : 10 µg/adm ; Dose 2: 30 µg/adm

(n = 3; unpaired t-test (GraphPad Prism8); * $p<0.05$)

Abbreviations: Substantia Nigra (SN); UFP: ultrafine particles.

Additional results not shown in Fig. 47: Significant differences were also observed in the prefrontal cortex and SN when comparing the 30 µg/adm UFP-exposed mice without recovery to those with the 3-month recovery period.

Validation test confirmed the identified particles inside the brain as our exposed UFP:

1) To verify the carbonaceous composition of the UFP, the emitted white light from the UFP within the brain tissue showed a characteristic fingerprint with a broad range of emission wavelengths. This profile closely matched the signal observed for commercially recovered DEP (Fig. 48). Conversely, the autofluorescence signals from brain tissue presented a distinct peak, with the highest intensity around 500-550 nm (green light), which did not extend across all wavelengths.

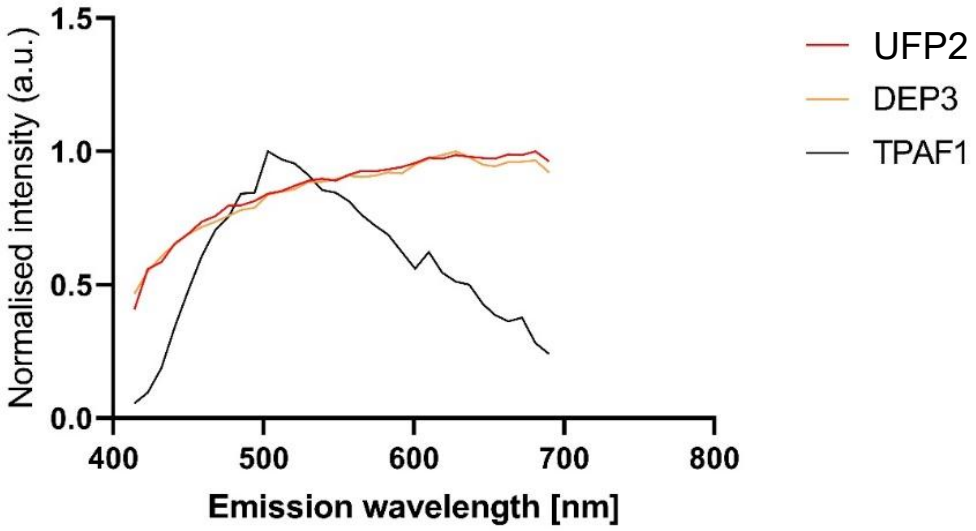

Figure 48: Emission spectrum of ultrafine particle validation.

The graphs shows the normalized intensity values of emission wavelengths (in nm) for our ultrafine particles (UFP), compared to reference diesel exhaust particles (DEP) and two-photon excited autofluorescence signals from brain tissue (TPAF - green background). Under femtosecond pulsed illumination, the emission spectrum of UFP closely matches that of DEP, confirming the particles' environmental anthropogenic origin. The carbon core of UFP, characterized by its wide range of emission wavelengths, allows for clear distinction from the background autofluorescence signals, which exhibit a narrower green emission peak.

Abbreviations: DEP: diesel exhaust particles; TPAF: two-photon excited autofluorescence signals from brain tissue; UFP: ultrafine particles.

2) Optical sectioning along the Z-axis (perpendicular to the plane of the brain slice) and the corresponding orthogonal projections revealed that the UFP were embedded within the brain tissue. This indicates that the particles were not a result of external contamination during sample preparation (Fig. 49).

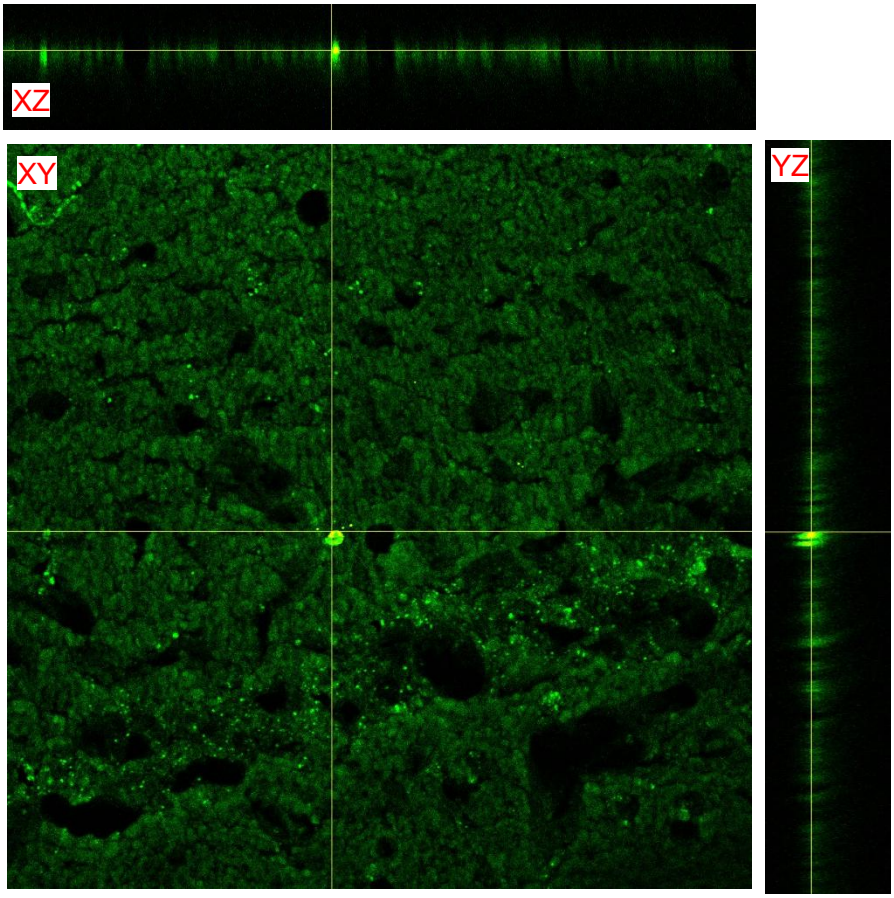

Figure 49: Confirmation intra-tissue localization of ultrafine particles.

XY-images acquired throughout a brain section in the Z-direction, along with corresponding orthogonal XZ- and YZ-projections, showing an ultrafine particles (UFP) (yellow/light green) located within the brain tissue (green). This confirms that the observed particle is an exposed particle and not an artifact.

Abbreviations: UFP: ultrafine particles.

III.4 Oxidative Stress

III.4.1 Gene and protein expression of NRF2-patwhay markers

Gene expression Nrf2-pathway

To assess the impact of UFP exposure on the transcriptional regulation of *Nrf2* and its downstream target genes, RT-qPCR analyses were performed. After three months of exposure to UFP at concentrations of 10 µg/adm and 30 µg/adm, *Nrf2*, a key antioxidant transcription factor, was significantly induced, as shown in Fig. 50. Subsequently, the expression of *Nrf2* downstream genes involved in cellular detoxification and stabilization,

including *Hmox1, Txn1, Gpx1, Gsr,* and *Gclc* (only for 30 µg/adm) were upregulated in response to both UFP doses, while the modifier subunit of GCL, namely *Gclm* was downregulated. Significant differences were observed between the two doses, with the higher dose resulting in approximately a two-fold increase in gene expression compared to vehicle-exposed mice. In contrast, no significant differences were detected in the expression of *Keap1*, a negative regulator of the NRF2 signaling pathway, contributing to cellular defense mechanisms against oxidative stress.

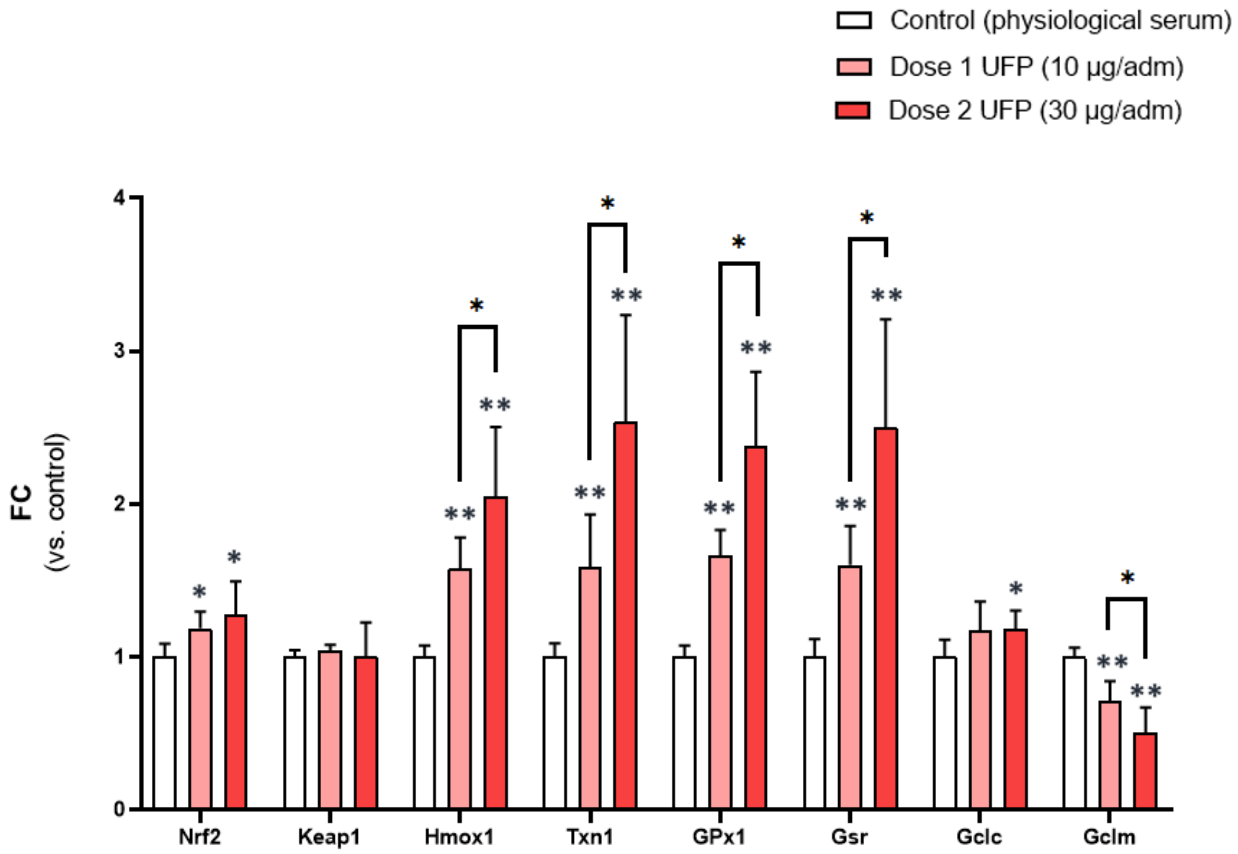

Figure 50: RT-qPCR analysis of *Nrf2* and its downstream target genes in mice exposed to ultrafine particles.

Mice were exposed to ultrafine particles (UFP) at doses of 0 (vehicle), 10 or 30 µg/adm for three months. Fold changes (FC) in gene expression relative to vehicle-exposed mice is shown. *Nrf2* and its target genes involved in detoxification (*Hmox, Txn1, GPx1, Gsr,* and *Gclc*) were significantly upregulated at both exposure doses (except for *Gclc* only in the highest condition). *Gclm* was significant downexpressed in both exposed conditions. No significant change in Keap1 expression was observed.

Control (NC): vehicle mice; Dose 1 UFP : 10 µg/adm ; Dose 2: 30 µg/adm

(FC: Fold changes; n = 6; non-parametric Mann-Whitney U test (GraphPad Prism8); * $p < 0.05$, ** $p < 0.01$)

Abbreviations: Gclc: Glutamate-cysteine ligase catalytic subunit; Gclm: Glutamate-cysteine ligase modifier subunit; Gpx1: Glutathione peroxidase 1; Hmox: Heme oxygenase; Keap1: Kelch-like ECH-associated protein 1; Nqo1: NAD(P)H quinone oxidoreductase 1; Nrf2: Nuclear factor erythroid 2-related factor 2; Sod1: Superoxide dismutase 1; Txn1: Thioredoxin 1, UFP: Ultrafine particles.

Protein expression Nrf2-pathway

The activated NRF2 is detached from KEAP1 (~ 70 kDa), which normally function to sequester and degrade NRF2 under non-stress conditions. To confirm that KEAP1 is not bound to NRF2 at protein level, WB analysis are assed for KEAP1, NRF2 and downstream regulated gene protein HO-1.

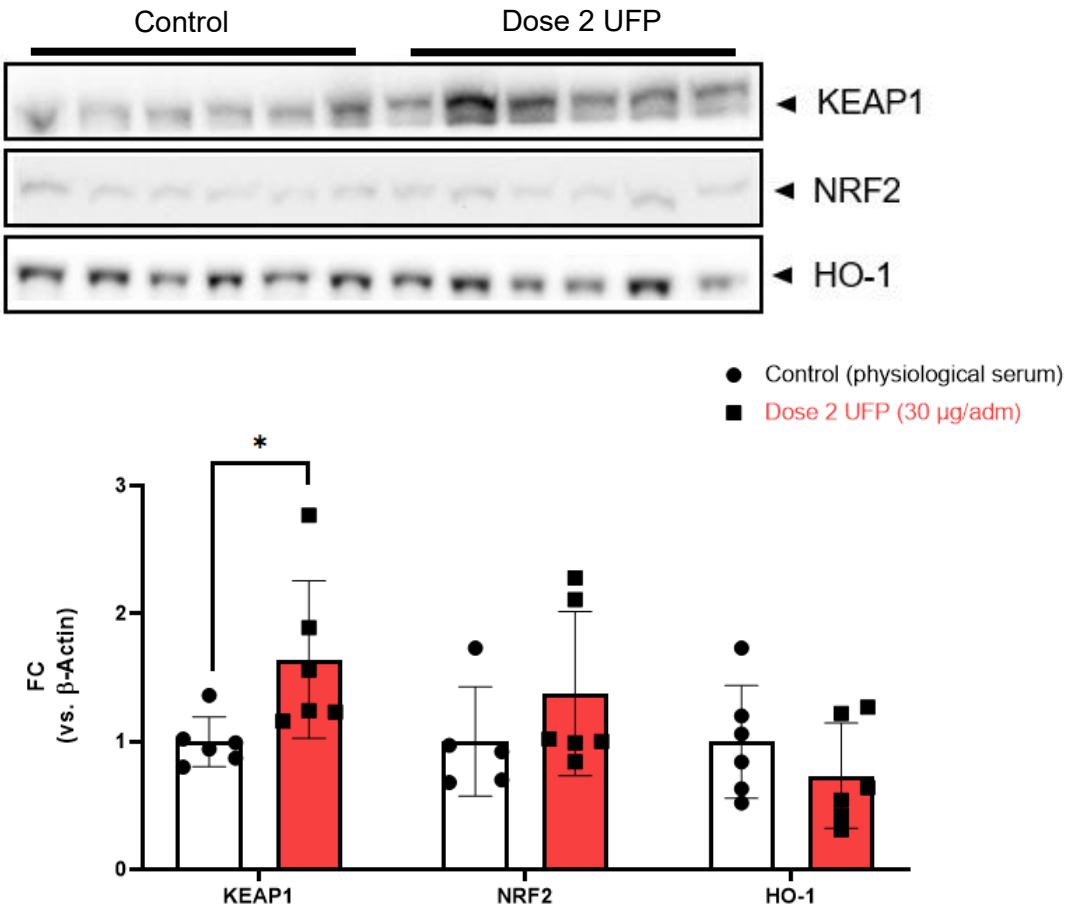

Figure 51: Protein quantification of KEAP, NRF2, and HO-1 in control and Dose 2 whole brain tissue.

In brain samples of Dose 2 ultrafine particles (UFP)-exposed mice is the Kelch-like ECH-associated protein 1 (KEAP1) level, the unbounded protein, significantly elevated. For both Nuclear factor erythroid 2-related factor 2 (NRF2) and Heme oxygenase-1 (HO-1) are there no differences between control and UFP-exposed mice.

Control (NC): vehicle mice; Dose 2: 30 µg/adm

(FC: Fold changes; n = 6; non-parametric Mann-Whitney U test (GraphPad Prism8); * $p < 0.05$)

Abbreviations: HO-1: Heme oxygenase-1; KEAP1: Kelch-like ECH-associated protein 1; NRF2: Nuclear factor erythroid 2-related factor 2; UFP: Ultrafine particles.

As shown in Fig. 51, we observed a significantly higher level of unbound KEAP1. Looking upstream in the pathway, under oxidative stress or cellular damage, p62 (SQSTM1) becomes phosphorylated at Ser349 (p-p62), which enhances its interaction with KEAP1 and promotes its sequestration. This interaction prevents KEAP1 from

binding to NRF2, thus inhibiting NRF2 degradation through ubiquitination. As a result, NRF2 is stabilized, translocate to the nucleus, and functions as a transcription factor. To validate that the activation of p62 leading to the dissociation of KEAP1 from NRF2, we quantified the ratio of p-p62 to total p62. Fig. 52 shows an induced ratio p-p62/p62 level after UFP exposure, compared to control brain samples.

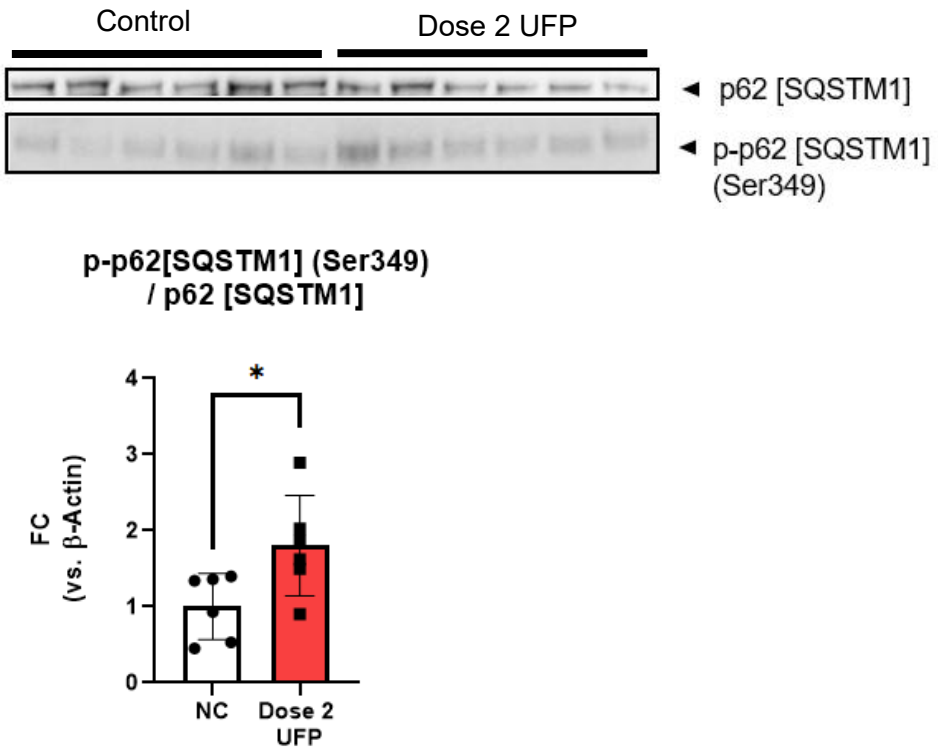

Figure 52: Activation of p62 shown as p-p62 onto p62 ratio in control and Dose 2 exposed brains.

In whole brain tissue of Dose 2 ultrafine particle (UFP)-exposed mice, a higher level of phosphorylated p62 (p-p62) at Ser 349 was detected relative to the total amount of p62, indicating the activation of p62 in response to exposure.

Control (NC): vehicle mice; Dose 2: 30 µg/adm

(FC: Fold changes; n = 6; non-parametric Mann-Whitney U test (GraphPad Prism8); * $p<0.05$)

Abbreviations: p-p62: Phosphorylated p62 at Ser 349; UFP: Ultrafine particles.

III.4.2 Protein expression levels of two central nervous system thiol-dependent redox systems: thioredoxin (Trx) and glutathione (GSH)

In this section, only results related to the thioredoxin system are discussed. The analysis of proteins and enzymes associated with the GSH system are presented in the context of ferroptosis (Cf. III.6.2 Additional ferroptotic hallmarks, p. 131).

A briefly chronological explanation of the investigated markers: Thioredoxin-Interacting Protein (TXNIP): acts as an inhibitor of thioredoxin (TXN); the mitochondrial thioredoxin (TXN2); the downstream antioxidant enzyme Peroxiredoxin 1 (Prdx1) that

uses reduced TXN as an electron donor to neutralize H_2O_2 and other ROS; the Thioredoxin Reductase 1 (TRXR1) to catalyze the reduction of oxidized TXN back to its active, reduced form using NADPH as an electron source. As shown in Fig. 53, none of them were significative changed in whole brain tissue of control mice compared to Dose 2 exposed mice.

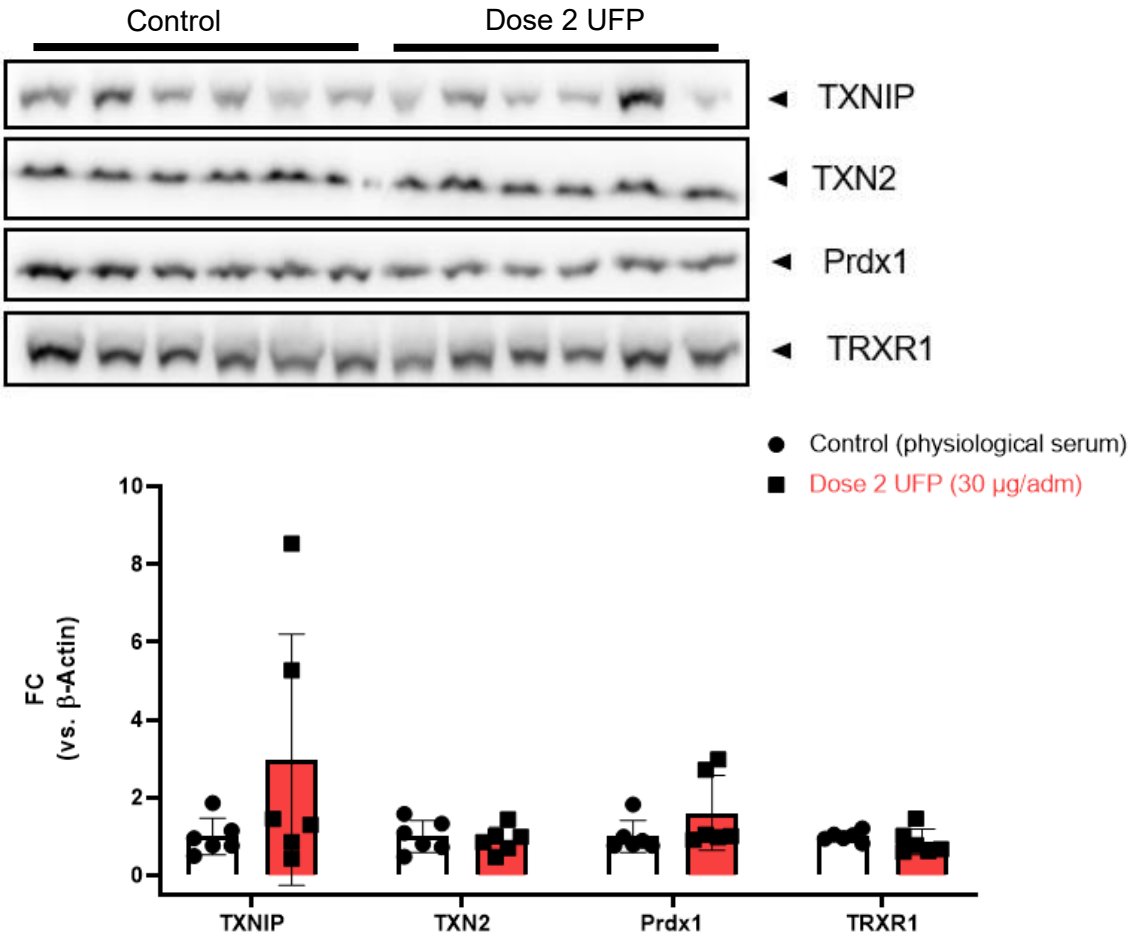

Figure 53: Hallmarks of the thioredoxin system reducing H_2O_2 and ROS, in control and Dose 2 brain samples.

The protein expression levels of TXNIP, TXN2, Prdx1, and TRXR1 in whole brain tissue of ultrafine particle (UFP)-exposed mice were not significantly different compared to control samples.

Control: vehicle mice; Dose 2: 30 µg/adm

(n = 6; non-parametric Mann-Whitney U test (GraphPad Prism8))

Abbreviations: FC: Fold changes; UFP: ultrafine particles.

III.5 Neuroinflammation

III.5.1 Protein expression of NF-κB-pathway markers

In the CNS, the resident immune cells microglia and astrocytes are the primary cell types involved in neuroinflammation. However, other cell types, including neurons, can

also activate the NF-κB pathway in response to various pro-inflammatory signals such as cytokines (TNF-α, IL-1β) or DAMP. The assess NF-κB activation following UFP-exposure, we investigated key proteins of the NF-κB-pathway through WB analysis, as shown in Fig. 54. In whole brain tissue of Dose 2 (30 µg/adm) UFP exposed mice, a notable decrease in IKK_{β} and an increase In $I\kappa B_{\alpha}$ expression were detected. The other markers, including NF-κB p105, along with the NF-κB p50 and NF-κB p65 subunits, showed no significant changes between UFP exposed and non-exposed brain tissue.

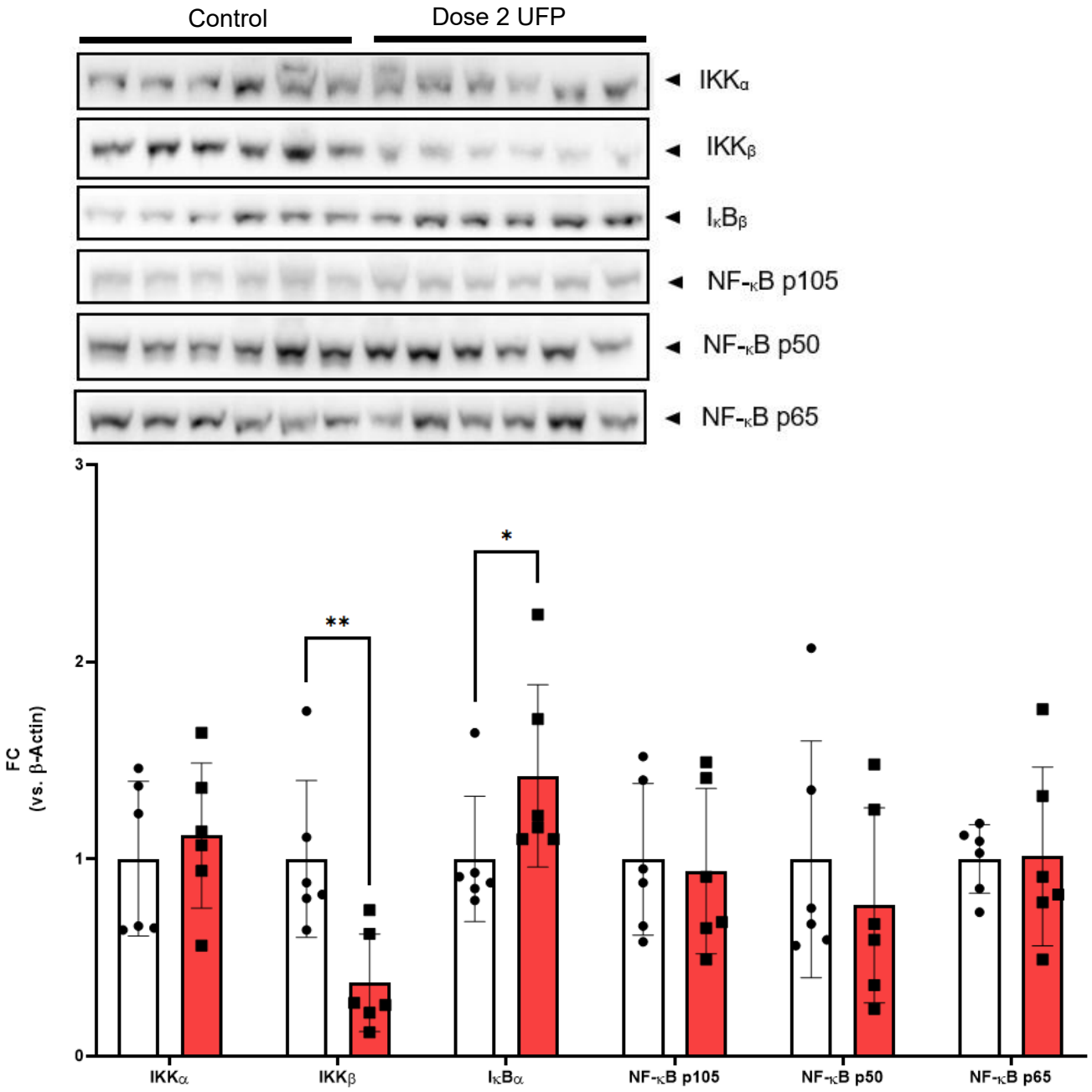

Figure 54: Key proteins of the NF-κB pathway involved in initiation, translocation and activation of NF-κB in whole brain tissue from ultrafine particle-exposed mice.

The analysis includes two IKK subunit proteins, IKK_{α} and IKK_{β}, which are responsible for the phosphorylation and subsequent degradation of $I_{\kappa}B$. A significant downregulation of IKK_{β} and an elevation of $I_{\kappa}B_{\alpha}$ were observed after Dose 2 (30 µg/adm) ultrafine particle (UFP) exposure. In contrast, the precursor protein NF-κB p105 and the subunits NF-κB p50 and NF-κB p65 remained unchanged compared to control brain tissue.

Control: vehicle mice; Dose 2: 30 µg/adm

(FC: Fold Changes; n = 6; non-parametric Mann-Whitney U test (GraphPad Prism8); * $p<0.05$; ** $p<0.01$)

Abbreviations: UFP: Ultrafine particles

III.5.2 DAPA of NF-κB transcription factor

The colorimetric reaction, which reflects the presence of NF-κB subunits (p50 and p65) bound to the DNA sequence, showed a significantly higher signal in whole brain tissue of mice exposed to Dose 2 (30 µg/adm) of UFP compared to the vehicle-exposed control group (physiological serum) (Fig. 55). In contrast, no significant differences were observed in the brain tissue of mice exposed to Dose 1 (10 µg/adm) when compared to the control group. Additionally, the signal from Dose 1 exposure was significantly lower than that observed in the highest exposure group (Dose 2).

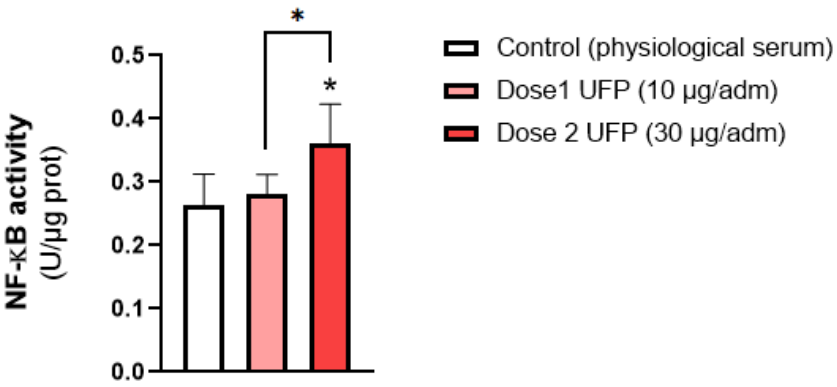

Figure 55: NF-κB activity measurement by colorimetric assay with higher activity in whole brain tissue of 30 µg/adm ultrafine particle-exposed mice compared to controls.

A significantly higher signal for NF-κB subunits binding to DNA was observed in mice exposed to Dose 2 (30 µg/adm) compared to the vehicle control. No significant difference was found between Dose 1 (10 µg/adm) and control, with Dose 1 showing a significant lower signal than Dose 2.

Control: vehicle mice; Dose 1: 10 µg/adm; Dose 2: 30 µg/adm

(n = 6; non-parametric Mann-Whitney U test (GraphPad Prism8); * $p<0.05$)

Abbreviations: NF-κB: Nuclear Factor kappa-light-chain-enhancer of activated B cells; UFP: Ultrafine particles.

III.5.3 Cytokine dosages

The cytokine profiling of whole brain tissue revealed significant changes in inflammatory markers in response to UFP exposure. A total of 19 cytokines were analyzed (Fig. 56), from which MCP-1 levels were significantly elevated in both exposure groups (10 µg/adm and 30 µg/adm), with a dose-dependent increase observed. IL-5 showed a significant depletion in the 10 µg/adm group, while KC/GRO-α and IL-33 were markedly increased in the 30 µg/adm group. These findings highlight alterations in cytokine expression, suggesting a potential link between UFP exposure and neuroinflammatory processes.

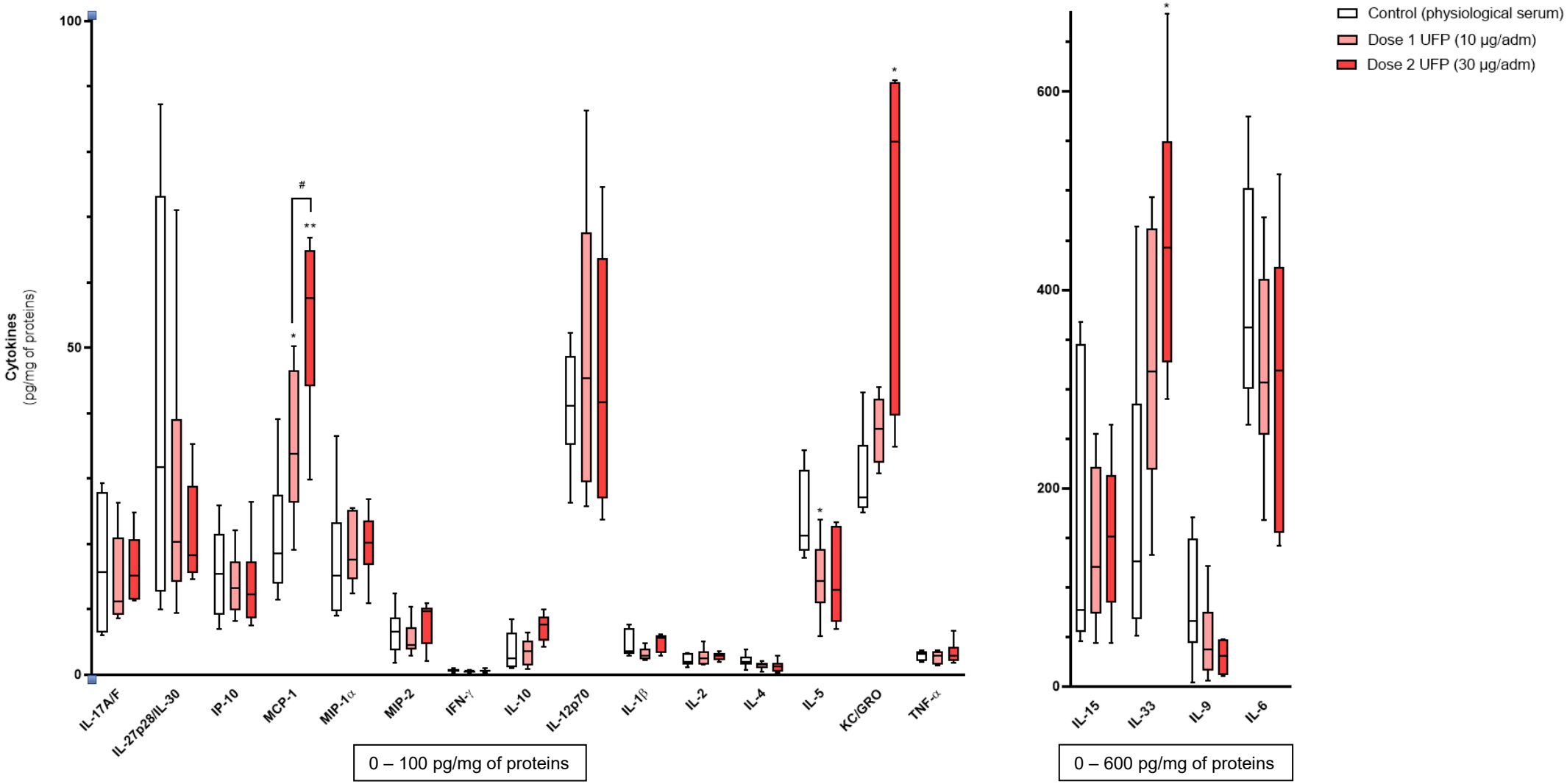

Figure 56: Cytokine profiling in the control group and the ultrafine particle-exposed groups (10 µg/adm and 30 µg/adm) in whole brain tissue.

The analysis includes 19 cytokines presented in two graphs: cytokines with levels below 100 pg/mg of proteins and those above 100 pg/mg proteins. The investigated cytokines are IL-17A/F, IL-27p28/IL-30, IP-10, MCP-1, MIP- 1α, MIP-2, IFN-γ, IL-10, IL-12p70, IL-1β, IL-2, IL-4, KC/GRO-α, TNF-α, IL-15, IL-33, IL-9, and IL-6. The black line inside the boxes represents the median, the edges of the boxes correspond to the first and third quartiles, and the whiskers indicate the largest and smallest values. Statistical analysis reveals that MCP-1 is significantly elevated in the 10 µg/adm group (* $p<0.05$), the 30 µg/adm group (** $p<0.01$), and between the two doses (# $p<0.05$). Additionally, IL-5 is significantly decreased in the 10 µg/adm group compared to controls (* $p<0.05$), while KC/GRO-α and IL-33 are significantly elevated in the 30 µg/adm group compared to controls (** $p<0.01$).

Control: vehicle mice; Dose 1: 10 µg/adm; Dose 2: 30 µg/adm

(n = 6; non-parametric Mann-Whitney U test (GraphPad Prism8); * $p<0.05$; ** $p<0.01$)

Abbreviations: IP-10: Interferon Gamma-Induced Protein 10; IFN-γ: Interferon γ; IL: Interleukins; KC/GRO-α: Keratinocyte Chemoattractant/human Growth-Regulated Oncogene; MIP: Macrophage Inflammatory Protein; MCP-1: Monocyte Chemoattractant Protein; TNF-α: Tumor Necrosis Factor α.

III.6 Whole brain regulated cell death markers

III.6.1 Western Blot analysis Apoptosis, Autophagy, Necroptosis, Parthanatos, and Ferroptosis

Given the evidence that UFP enters the brain and induce oxidative stress, we investigated whether they provoked RCD. WB analysis was performed to assess the expression levels of key protein markers associated with apoptosis (Fig. 57), autophagy (Fig. 58), necroptosis (Fig. 59), parthanatos (Fig. 60) ferroptosis (Fig. 51-66), in control and D2 (30 µg/adm)-exposed mice in whole brain tissue after three months of exposure.

Apoptosis

To evaluated apoptosis, we examined the expression of pro-apoptotic proteins (BAD, BIM, BAK) and assessed the activation of the caspase cascade via caspase 3 cleavage (Fig. 57).

The analysis of pro-apoptotic and caspase protein expression revealed no significant differences in the levels of BAD, phospho-BAD (Ser 112), BIM, BAK, and full or cleaved caspase 3 between the vehicle-exposed (NC) group and the UFP-exposed group (30 µg/adm). However, key functional indicators showed significant changes. The ratio of phosphorylated BAD (p-BAD) to total BAD, a marker of cell survival, was significantly altered, suggesting a shift in BAD activation dynamics. Furthermore, the ratio of cleaved caspase 3 (17 kDa) to full caspase 3 was significantly reduced, indicating that caspase 3 predominantly remains in its inactive form, which may reflect a suppression of apoptosis in the exposed group.

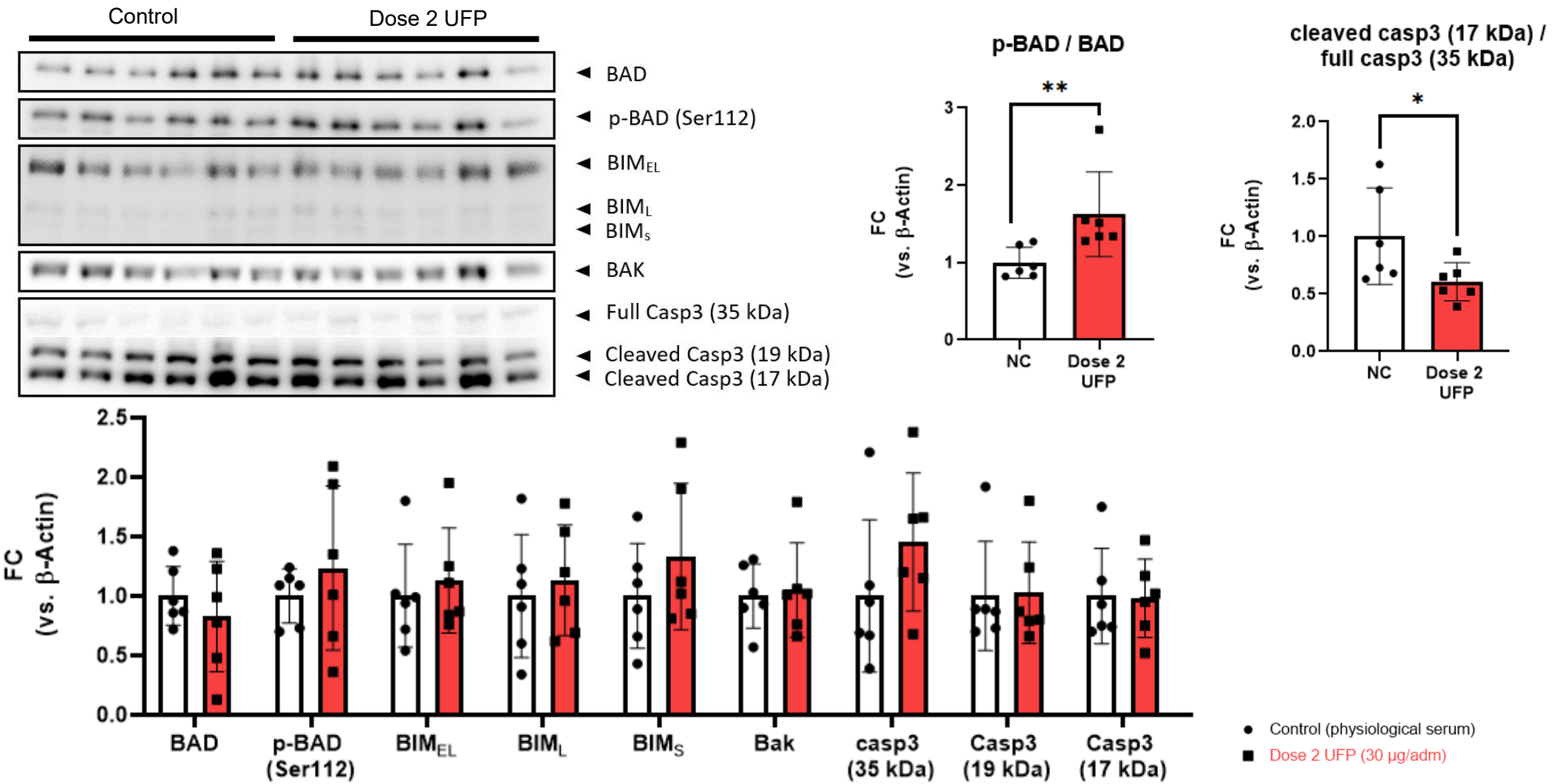

Figure 57: Protein expression levels of pro-apoptotic and caspase proteins.

The expression levels of Bcl-2-associated death promoter (BAD), phospho-BAD (Ser 112), Bcl-2 interacting mediator of cell death (BIM), Bcl-2 homologous antagonist/killer (BAK), and full and cleaved caspase 3 showed no significant differences between the NC (vehicle-exposed) and Dose 2 (30 µg/adm UFP-exposed) groups. However, BAD activation depends on its dephosphorylation, and the ratio of phosphorylated BAD (p-BAD) to total BAD, indicating cell survival, was significantly altered. Additionally, the ratio of cleaved caspase 3 (17 kDa) to full caspase 3 was significantly reduced, suggesting that caspase 3 is predominantly in its inactive full form.

Control (NC): vehicle mice; Dose 2: 30 µg/adm

(FC: Fold Changes; n = 6; Non-parametric Mann-Whitney U test (GraphPad Prism8); * p<0.05, ** p<0.01))

Abbreviations: BAD: Bcl-2-associated death promoter; BAK: Bcl-2 homologous antagonist/killer; BIM: Bcl-2 interacting mediator of cell death; p-BAD: Phosphorylated BAD (Ser 112); UFP: Ultrafine particles.

Autophagy

WB analysis was performed to examine key autophagic parameters involved in autophagosome formation and degradation, focusing on initiation (Beclin-1, ATG13, ATG101), membrane expansion and maturation (ATG7, ATG12, ATG5, ATG16L1(β)), autophagosome completion (ATG3, LC3), and cargo degradation (P62/SQSTM1) (Fig. 58).

Comparisons between vehicle-exposed (NC) and UFP-exposed (30 μg/adm) mice revealed no significant disruptions in the autophagic process. Therefore, ATG13, critical for the initiation of autophagy, and ATG7, essential for autophagosome maturation, were downregulated in the UFP-exposed group. This impairment was reflected in defective LC3 activation, where only a single band was detected despite testing with two different primary antibodies, indicating hindered autophagic flux following UFP exposure.

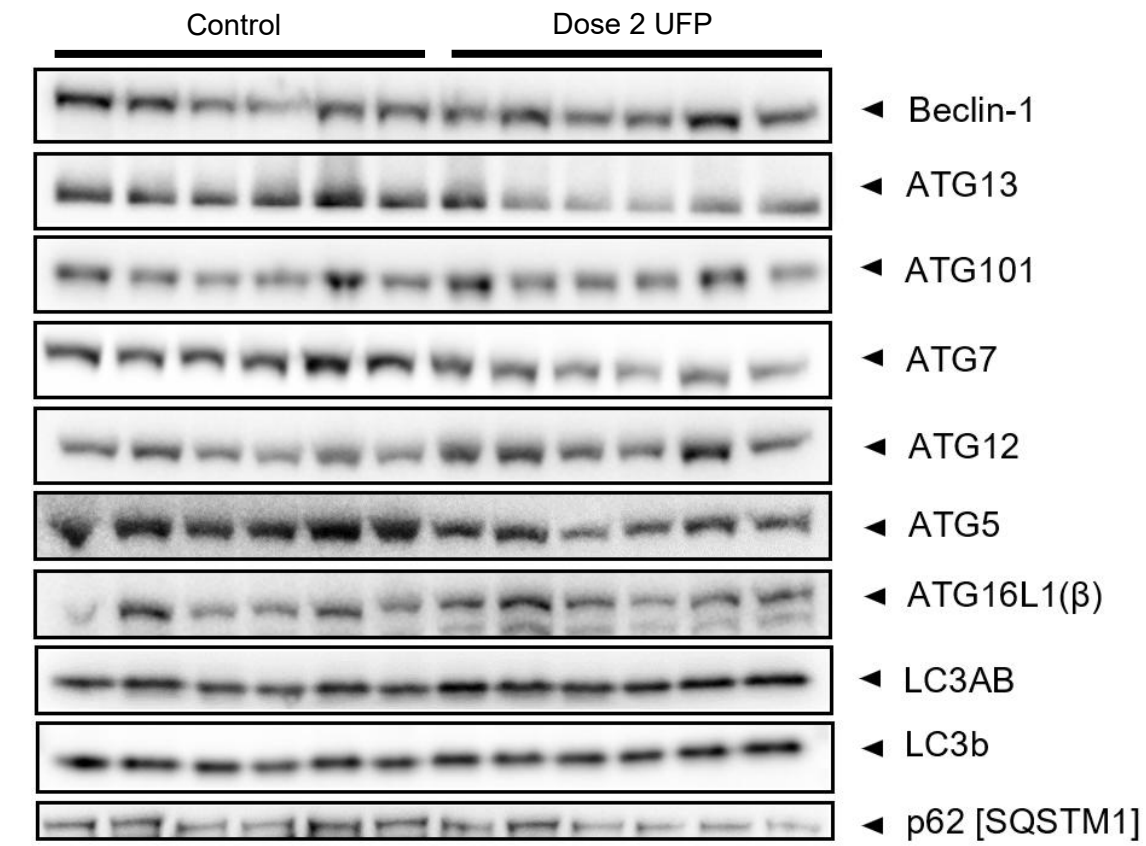

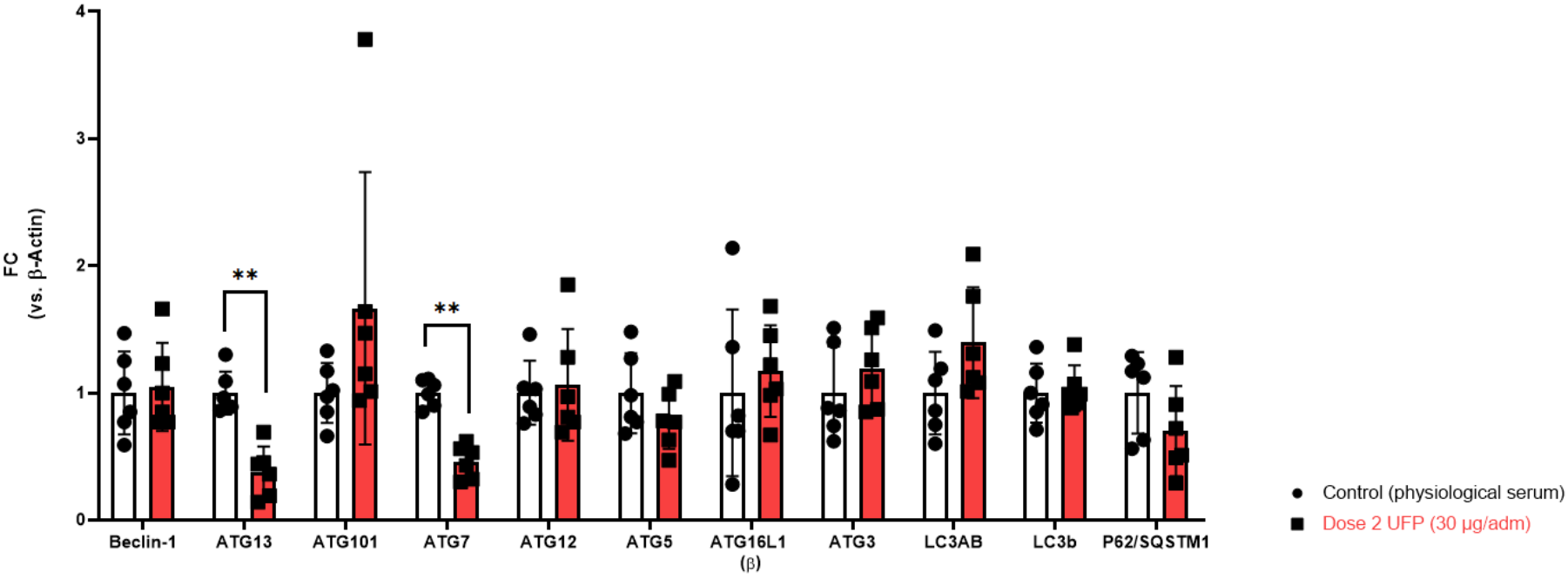

Figure 58: Autophagic parameters involved in autophagosome formation and degradation

Comparison was made between vehicle-exposed mice and Dose 2 (30 µg/adm ultrafine particles (UFP)-exposed mice). The results show that Autophagy-related protein (ATG)13 (involved in the initiation step) and ATG7 (involved in the autophagosome maturation) were downregulated after UFP exposure, resulting in impaired Microtubule-associated protein 1 light chain 3 (LC3) activation, as only one band was visible, and therefore tested with 2 different primary antibodies.

Control: vehicle mice; Dose 2: 30 µg/adm

(FC: Fold Changes; n = 6; non-parametric Mann-Whitney U test (GraphPad Prism8); ** p<0.01)

Abbreviations: ATG: Autophagy-related protein; LC3: Microtubule-associated protein 1 light chain 3; UFP: Ultrafine particles.

Necroptosis

During necroptosis, the RIP1-RIP3 necrosome forms via the activation of RIP1, which phosphorylates RIP3 (p-RIP3). Subsequently, the effector protein MLKL becomes phosphorylated, oligomerizes, and translocate to the plasma membrane, disrupting its integrity and leading to cell death.

To investigate necroptosis, we assessed key components and activation markers of the pathway: RIP and RIP3 as initiators, p-RIP3 as an indicator of necrosome activation, and MLKL and its phosphorylated form (p-MLKL) as markers of necroptotic execution.

As visualized in Fig. 59, In the UFP-exposed group (30 µg/adm), the expression levels of RIP and MLKL were significantly downregulated compared to controls. Despite this, the ratio of phosphorylated RIP3 (p-RIP3) to total RIP3 remained unchanged, suggesting no activation of RIP3. Interestingly, the small amount of MLKL present in UFP-exposed cells was predominantly in its phosphorylated form (p-MLKL).

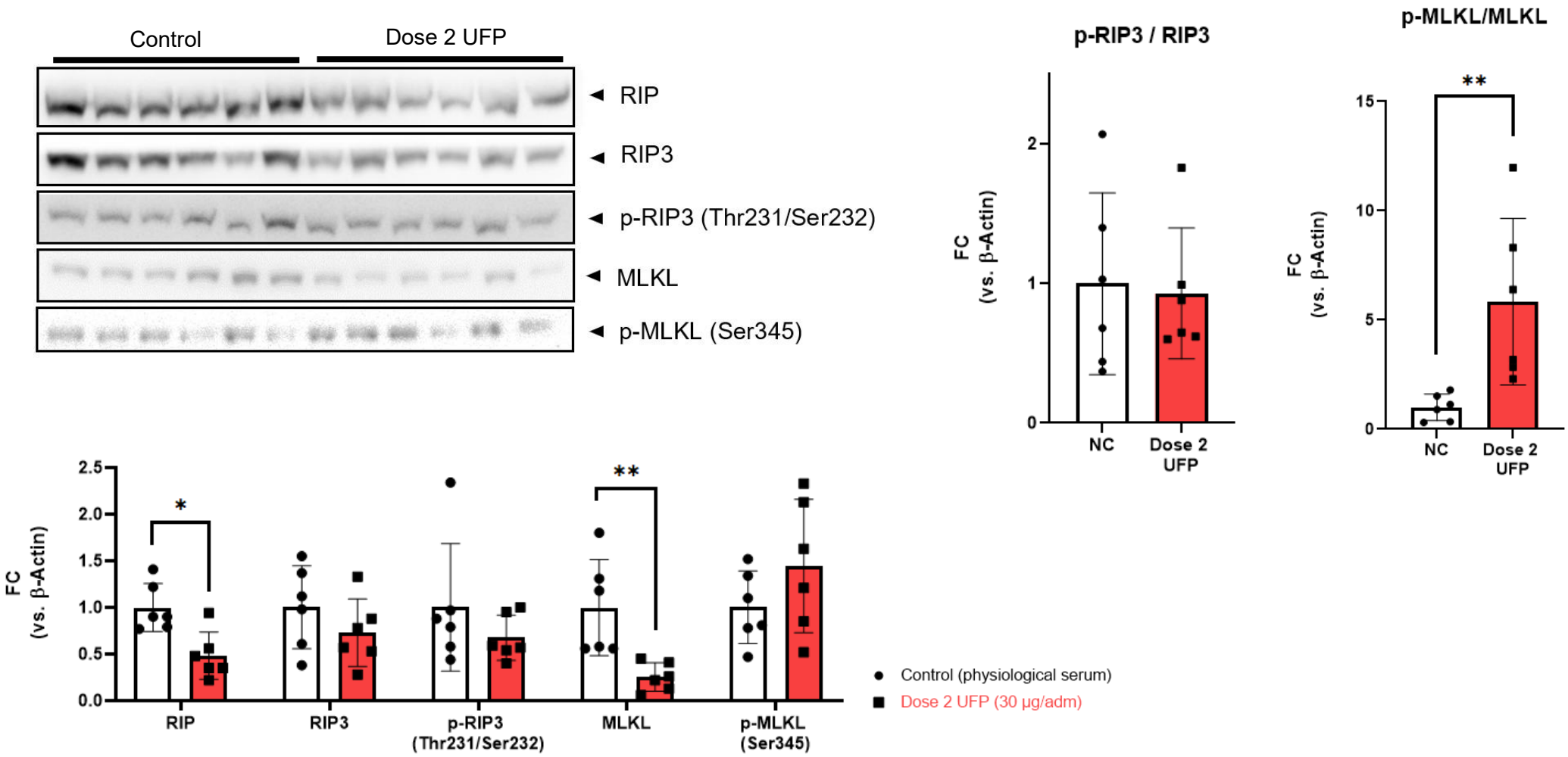

Figure 59: Necroptosis after ultrafine particle-exposure, investigation of activation and progression.

Western blot analysis revealed that the protein expression levels Receptor-interacting protein (RIP) and Mixed lineage kinase domain-like protein (MLKL) were downregulated following Dose 2 (30 µg/adm) ultrafine particles (UFP) exposure. The ratio of (Phosphorylated receptor-interacting protein kinase 3) p-RIP3 to total Receptor-interacting protein kinase 3 (RIP3) remained unchanged, indicating no activation of RIP3. However, the small amount of MLKL present in the UFP-exposed cells are most abundant in the phosphorylated form (p-MLKL).

Control: vehicle mice; Dose 2: 30 µg/adm

(FC: Fold Changes; n = 6; Non-parametric Mann-Whitney U test (GraphPad Prism8); * $p<0.05$, ** $p<0.01$)

Abbreviations: MLKL: Mixed lineage kinase domain-like protein; p-MLKL: Phosphorylated mixed lineage kinase domain-like protein; p-RIP3: Phosphorylated receptor-interacting protein kinase 3; RIP: Receptor-interacting protein; RIP3: Receptor-interacting protein kinase 3; UFP: Ultrafine particles.

Parthanatos

Parthanatos is primarily driven by the hyperactivation of poly(ADP-ribose) polymerase-1 (PARP-1), a key enzyme involved in DNA damage repair. Under conditions of severe DNA damage, excessive PAR polymers migrate from the nucleus to the mitochondria. This disrupts mitochondrial membrane integrity, leading to the release of Apoptosis-Inducing Factor (AIF) into the cytoplasm. AIF induces large-scale DNA fragmentation by activating endonucleases. Upon interacting with Macrophage Migration Inhibitory Factor (MIF), AIF forms a complex that translocate to the nucleus, where the nuclease activity of MIF cleaves genomic DNA, ultimately resulting in cell death. The activation of this AIF/MIF complex is essential for parthanatos, and its formation depends on the expression levels of both proteins. Therefore, we quantified these protein levels in brain tissue following UFP exposure, comparing them to control samples; shown in Fig. 60, and as observed, no differences are found in AIF and MIF protein amount between the control mice and Dose 2 UFP group.

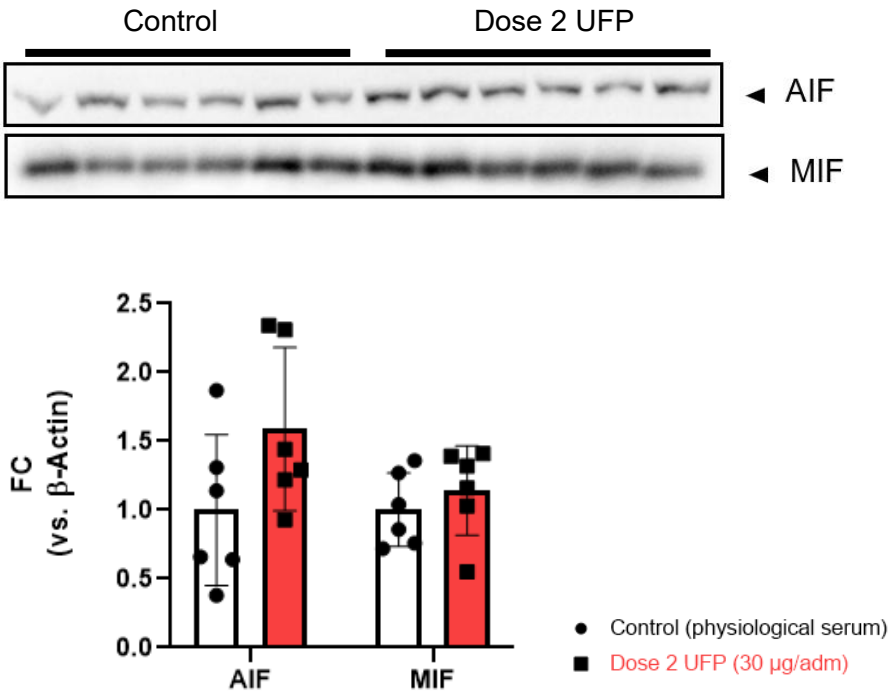

Figure 60: Determination of parthanatos in response to excessive DNA damage of ultrafine particle exposure.

After UFP-exposure, there is a trend towards elevated Apoptosis-inducing factor (AIF) protein levels, tough this change did not reach statistical significance. In contrast, Macrophage migration inhibitory factor (MIF) protein levels remained unchanged when comparing the prevalence in brain tissue of control (vehicle exposed) mice and UFP (Dose 2 – 30 µg/adm) exposed mice.

Control: vehicle mice; Dose 2: 30 µg/adm

(FC: Fold Changes; n = 6; Non-parametric Mann-Whitney U test (GraphPad Prism8))

Abbreviations: AIF: Apoptosis-inducing factor; MIF: Macrophage migration inhibitory factor; UFP: Ultrafine particles.

Ferroptosis

The investigation of ferroptotic hallmarks in Dose 2 (30 µg/adm UFP-exposed) mice compared to controls (NC) showed that iron homeostasis, as measured by TfR and FTH1, remained unaffected. Also the main enzyme involved in ferroptosis, cGPx4, did not show significant changes. On the other hand, xCT protein levels were elevated in the UFP-exposed mice compared to controls, indicating altered cystine/glutamate antiporter activity associated with anti-ferroptotic mechanism.

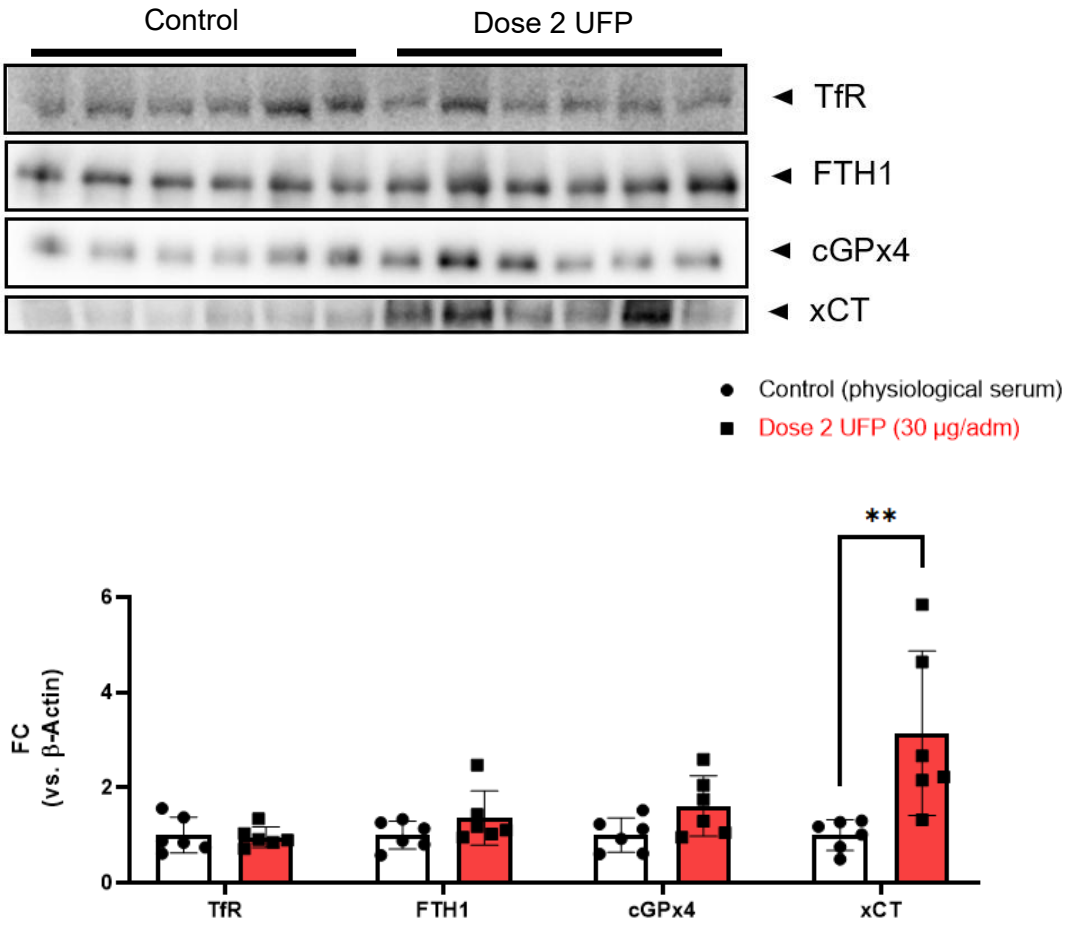

Figure 61: Ferroptotic hallmarks investigating iron imbalance and glutathione axis.

Iron homeostasis, assessed by transferrin receptor (TfR) and ferritin heavy chain 1 (FTH1), was not disturbed in Dose 2 group compared to negative control (NC) mice. However, the main enzyme involved in ferroptosis, glutathione peroxidase 4 (GPx4) showed no significant changes. The cystine/glutamate antiporter (xCT; Solute carrier family 7 member 11 (SLC7A11)) protein levels were higher in the Dose 2 exposed mice compared to controls.

Control: vehicle mice; Dose 2: 30 µg/adm

(FC: Fold Changes; n = 6; Non-parametric Mann-Whitney U test (GraphPad Prism8); ** p<0.01)

Abbreviations: FTH1: Ferritin heavy chain 1; GPx4: Glutathione peroxidase 4; GSH: Glutathione; NC: Negative control; SLC7A11: Solute carrier family 7 member 11 (xCT, cystine/glutamate antiporter); TfR: Transferrin receptor; UFP: Ultrafine particles.

III.6.2 Additional ferroptotic hallmarks

To dig deeper on the potential inducement of ferroptosis upon UFP-exposure in whole brain tissue, several key features are additionally investigated, such as xCT gene expression (Fig. 62), GPx activity (Fig. 63), GR activity (Fig. 64), GSH imbalance (Fig. 65) and 4-HNE adducts (Fig. 66).

SLC7A11 gene expression

The gene expression of SLC7A11 (xCT) was not upregulated in whole brain tissue following either Dose 1 (10µg/adm) or Dose 2 (30 µg/adm) UFP exposure.

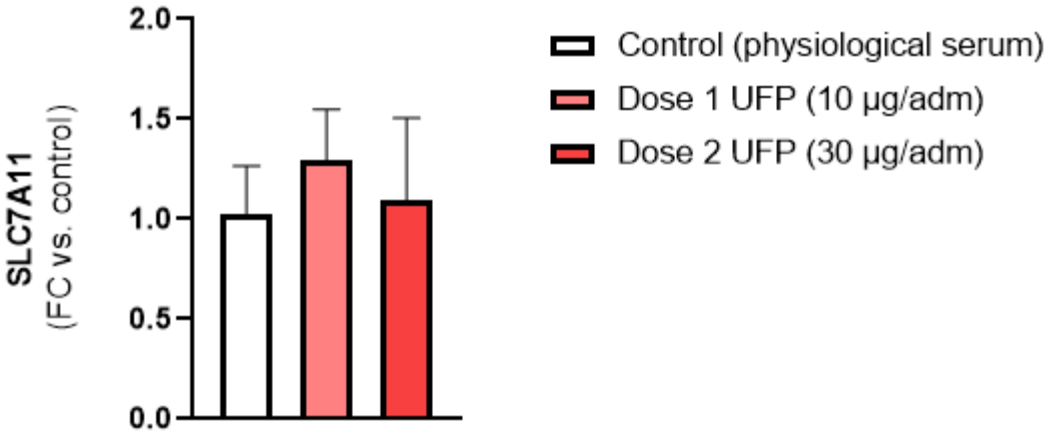

Figure 62: No significant changes in SLC7A11 gene expression after UFP-exposure.

The gene expression levels, presented as fold change relative to control, did not show a significant increase in SLC7A11 (also known as xCT) expression following UFP-exposure.

Control: vehicle mice; Dose 1: 10 µg/adm; Dose 2: 30 µg/adm
(FC: Fold Changes; n = 6; Non-parametric Mann-Whitney U test (GraphPad Prism8))

Abbreviations: SLC7A11: Solute carrier family 7 member 11 (xCT, cystine/glutamate antiporter); UFP: Ultrafine particles.

GPx activity

GPx activity is a critical marker of oxidative stress, though it is not specific to ferroptosis. Since no specific assay exists to measure GPx4 activity directly overall GPx activity is assessed as a proxy to understand its contribution to cellular antioxidant defenses.

The GPx activity in brain samples from control mice (vehicle-exposed) was approximately 15 nmol/min/mg. Following UFP exposure, the activity increased significantly, till 43.32 nmol/min/mg for Dose 1 UFP exposure and 62.33 nmol/min/mg for Dose 2 UFP exposure.

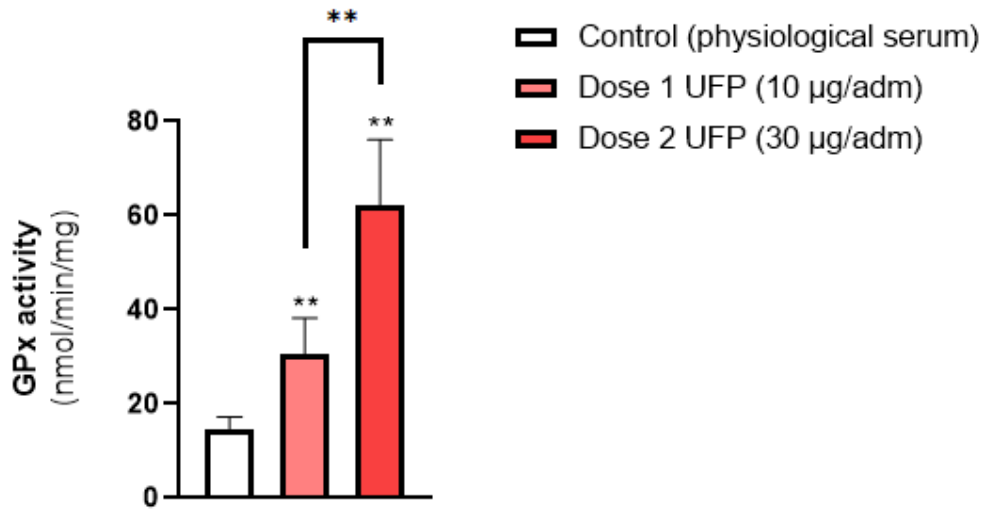

Figure 63: Increased glutathione peroxidase (GPx) activity in whole brain tissue after Dose 1 and Dose 2 ultrafine particles-exposure (10 and 30 µg/adm, respectively).

The mean glutathione peroxidase (GPx) activity in control brain samples from vehicle-exposed mice was approximately 15 nmol/min/mg, which was increased to a three-fold after Dose 1 (to 43.32 nmol/min/mg) and four-fold after Dose 2 (to 62.33 nmol/min/mg).

Control: vehicle mice; Dose 1: 10 µg/adm; Dose 2: 30 µg/adm

(n = 6; Non-parametric Mann-Whitney U test (GraphPad Prism8); ** $p<0.01$)

Abbreviations: GPx: Glutathione peroxidase; UFP: Ultrafine particles.

GR activity

In brain samples from control mice (vehicle-exposed), GR activity was approximately 1.64 nmol/min/mg. Upon UFP exposure, this activity increased significantly, reaching 3.65 nmol/min/mg for Dose 1 and 5.21 nmol/min/mg for Dose 2 UFP exposures. Furthermore, GR activity differed significantly between Dose 1 and Dose 2.

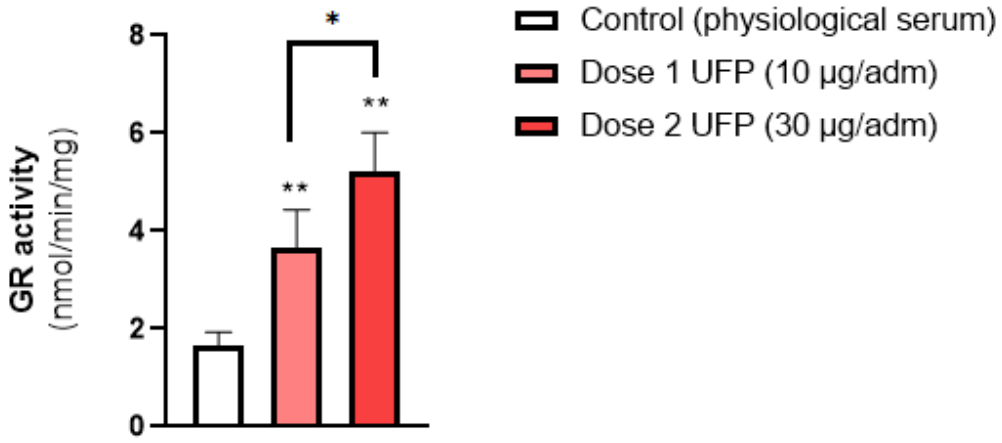

Figure 64: Glutathione reductase (GR) activity in whole brain tissue increases following ultrafine particle exposure at Dose 1 (10 µg/adm) and Dose 2 (30 µg/adm).

Glutathione reductase (GR) activity in control brain samples from vehicle-exposed mice was approximately 1.64 nmol/min/mg. Exposure to Dose 1 elevated GR activity to 3.65 nmol/min/mg, while Dose 2 further increased it to 5.21 nmol/min/mg.

Control: vehicle mice; Dose 1: 10 µg/adm; Dose 2: 30 µg/adm
(n = 6; Non-parametric Mann-Whitney U test (GraphPad Prism8); * $p<0.05$, ** $p<0.01$)

Abbreviations: GR: Glutathione reductase; UFP: Ultrafine particles.

Glutathione ratio

GSH serves as the essential cofactor of GPx enzymes, being oxidized to GSSG in the process. To assess the availability of GSH, its levels are directly measured, while the activity and utilization of GSH by GPx enzymes are inferred from the GSH/GSSG ratio.

Reduced GSH levels showed a downward trend following UFP exposure. While Dose 1 does not show a significant reduction compared to controls, GSH levels were significantly decreased in Dose 2. Additionally, there is a statistically significant difference between Dose 1 and Dose 2. On the other hand, its oxidized form, GSSG, were significantly elevated after UFP exposure in both Dose 1 and Dose 2. And at least, the GSH/GSSG ratio, which indicates the balance between reduced and oxidized GSH, is significantly reduced in UFP-exposed samples compared to controls.

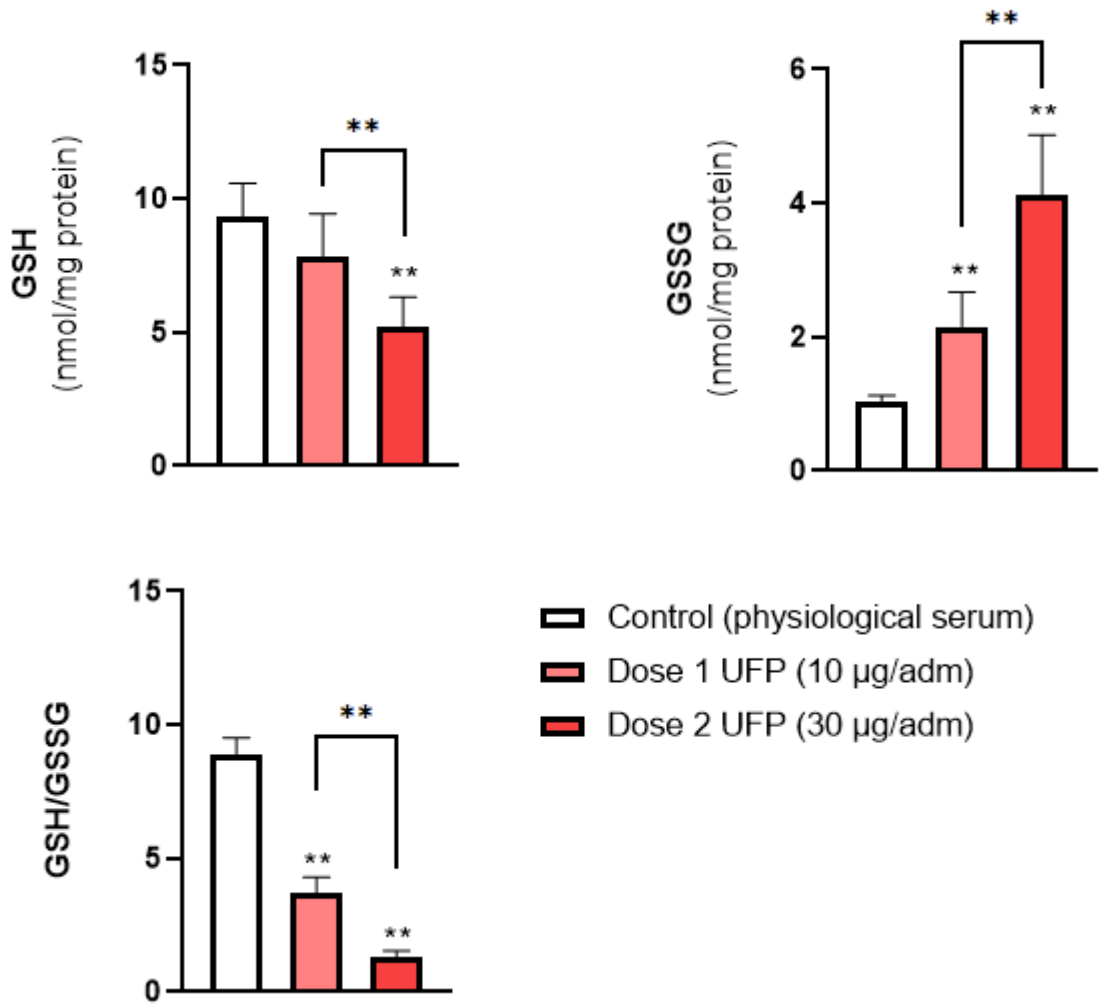

Figure 65: Glutathione, oxidized glutathione and the reduced on oxidized glutathione ratio in whole brain tissue of control, Dose 1 and Dose 2 ultrafine particles-exposed mice.

A downward trend in glutathione (GSH) levels is noticeable after ultrafine particles (UFP) exposure. While GSH levels in Dose 1 are not significantly reduced compared to controls, they are significantly decreased in Dose 2. Moreover, the differences between Dose 1 and Dose 2 are statistically significative. Conversely, oxidized GSH (GSSG) shows an increase after UFP exposure, with significant elevations in both Dose 1 and Dose2. The GSH/GSSG ratio, reflecting the balance between reduced and oxidized GSH, is significantly decreased in UFP-exposed samples compared to controls.

Control: vehicle mice; Dose 1: 10 µg/adm; Dose 2: 30 µg/adm

(FC: Fold Changes; n = 6; Non-parametric Mann-Whitney U test (GraphPad Prism8); ** p<0.01)

Abbreviations: GSH: glutathione; GSSG: oxidized glutathione; UFP: Ultrafine particles.

4-HNE adduct quantification

4-HNE is a lipid peroxidation byproduct and marker of ferroptosis, reflecting the accumulation of oxidative damage due to impaired antioxidant defenses such as GPx4. In both conditions, Dose 1 and Dose 2, were 4-HNE adducts depleted compared to control brain samples.

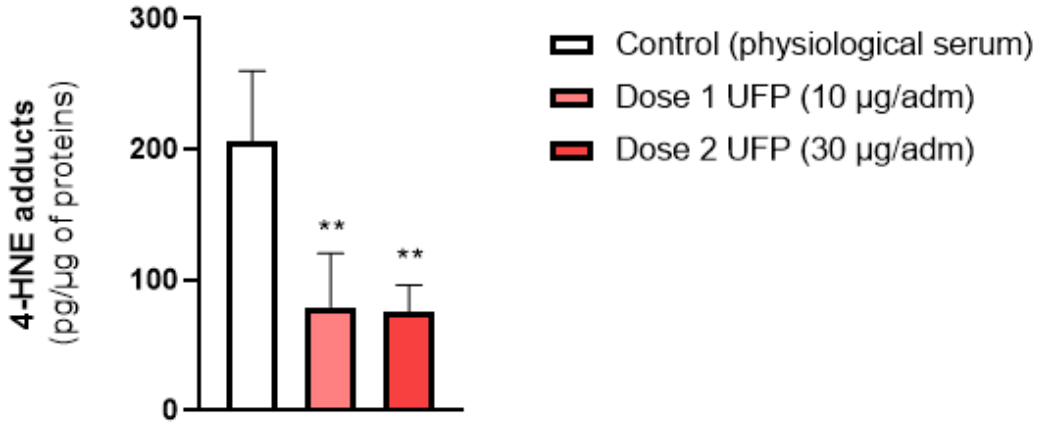

Figure 66: Reduced 4-hydrosynonenal (4-HNE) adducts reflecting decreased lipid peroxidation in whole brain tissue of Dose 1 and Dose 2 ultrafine particle-exposed mice compared to control.

4-HNE adducts measurement by ELISA-MSD shows a significant reduction in ultrafine particles (UFP) exposed mice (Dose 1 and Dose 2) compared to control mice.

Control: vehicle mice; Dose 1: 10 µg/adm; Dose 2: 30 µg/adm

(FC: Fold Changes; n = 6; non-parametric Mann-Whitney U test (GraphPad Prism8); ** $p<0.01$))

Abbreviations: 4-HNE: 4-hydrosynonenal; UFP: Ultrafine particles.

III.7 Brain sections

III.7.1 IHC analysis TH, and NeuN

The markers selected for immunohistochemical (IHC) analysis —TH and NeuN — were chosen based on their relevance to neurodegenerative processes in regions typically affected by these diseases. TH, a key enzyme in dopaminergic neurons essential for dopamine synthesis, is particularly relevant for studies on PD and other neurodegenerative disorders (Fig. 67). NeuN, a marker of mature neurons, is commonly used to evaluate neuronal integrity (Fig. 68).

None of the staining's (TH: Striatum, SN, and VTA, and NeuN: Hippocampus) revealed changes between the control group and the UFP-exposed group. However, only TH staining of the Striatum revealed a significant down expression in the UFP-exposed group comparing with and without the three month recovery period. However, as the control group also exhibited a downregulation (which was not significant), and there was no significant difference in TH staining between control and UFP-exposed samples after the three-month recovery. This raises the question of whether the decreased TH levels were due to a depletion in TH-fiber signal or if the recovery group in general exhibited less TH staining.

Other staining's did not reveal any signs of neuronal death in the key brain regions (TH: SN, and VTA, and NeuN: Hippocampus).

TH staining in Striatum, SN, and VTA

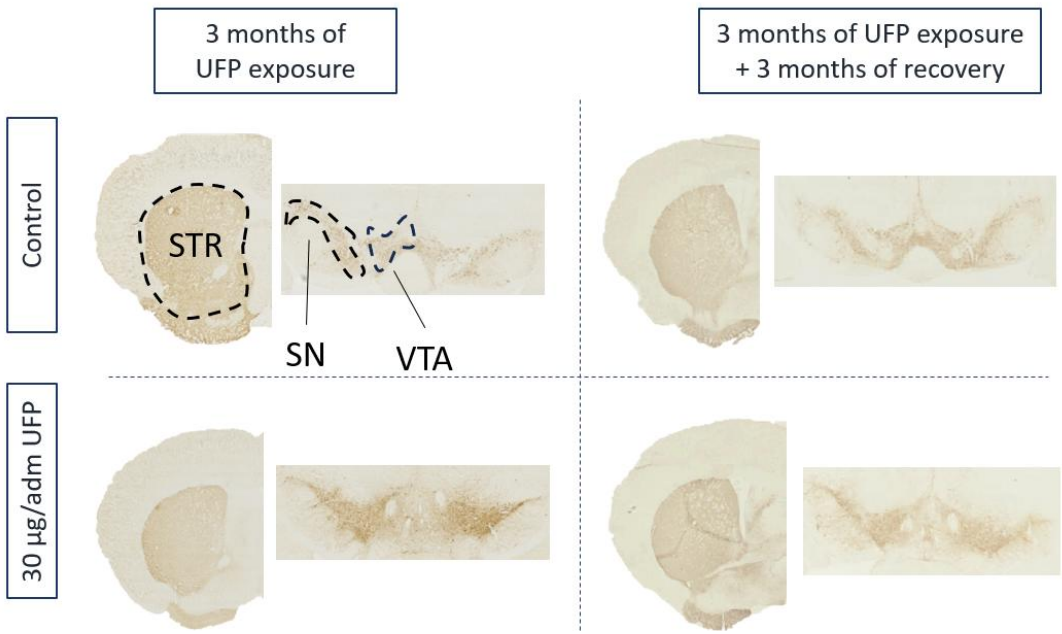

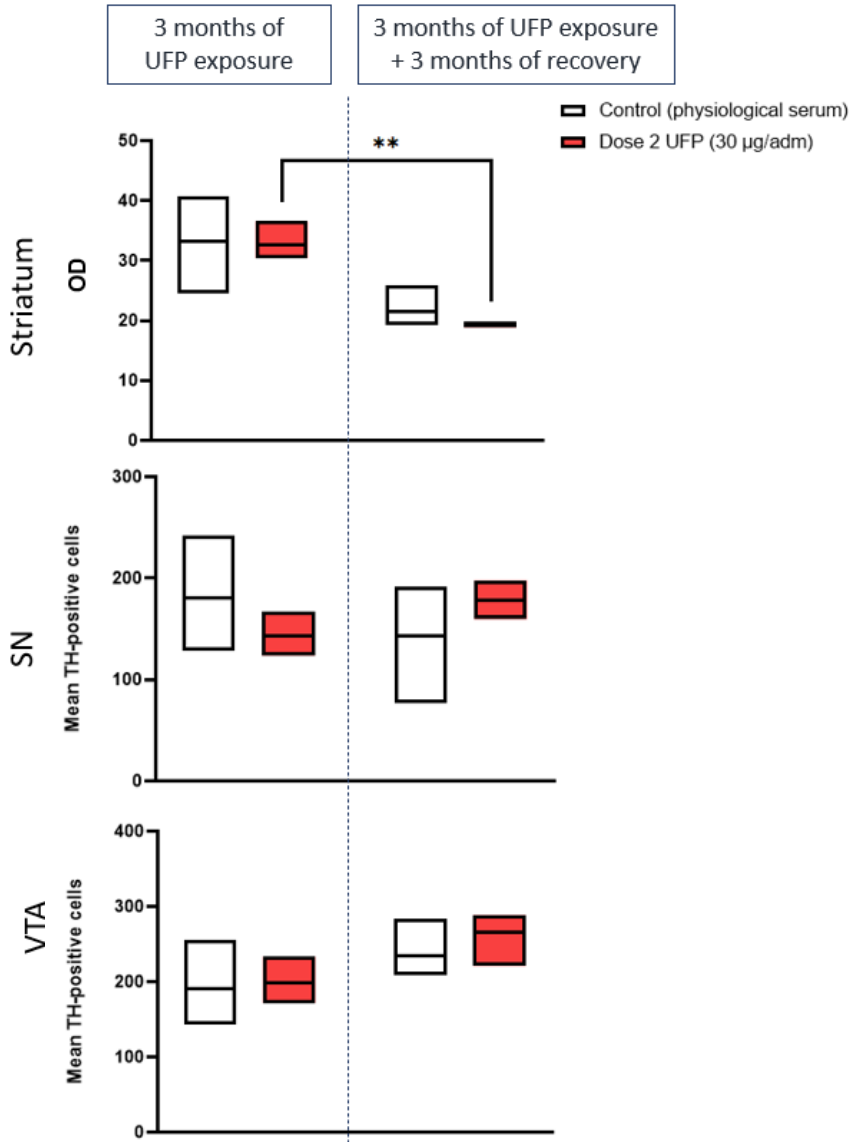

Figure 67: Immunohistochemistry analysis of tyrosine hydroxylase expression in the Striatum, Substantia Nigra, and ventral tegmental area in control and ultrafine particles-exposed (30 µg/adm, Dose 2) mice.

Floating bars represent the minimum and maximum values, with the lower and upper bounds denoting the respective walls, and the middle line indicating the mean. tyrosine hydroxylase (TH) staining was assessed in three different regions associated with Parkinson's disease (PD). In the striatum, TH expression was quantified by optical density. No significant differences were observed between control mice and Dose 2-exposed mice. However, a significant decrease in TH staining was detected in mice exposed to ultrafine particles (UFP) for 3 months compared to those exposed for 3 months followed by a 3-month recovery period. In the substantia nigra (SN) and ventral tegmental area (VTA), TH-positive were quantified as TH-positive cells, and no differences were observed either between control mice and exposed mice, or between 3 months of exposure and the 3 months of exposure with recovery.

Control: vehicle mice; Dose 2: 30 µg/adm
(n = 3; unpaired t-test (GraphPad Prism8); ** $p<0.01$)

Abbreviations: PD: Parkinson's disease; SN: Substantia nigra; TH: Tyrosine hydroxylase; UFP: Ultrafine particles; VTA: Ventral tegmental area.

NeuN in Hippocampus

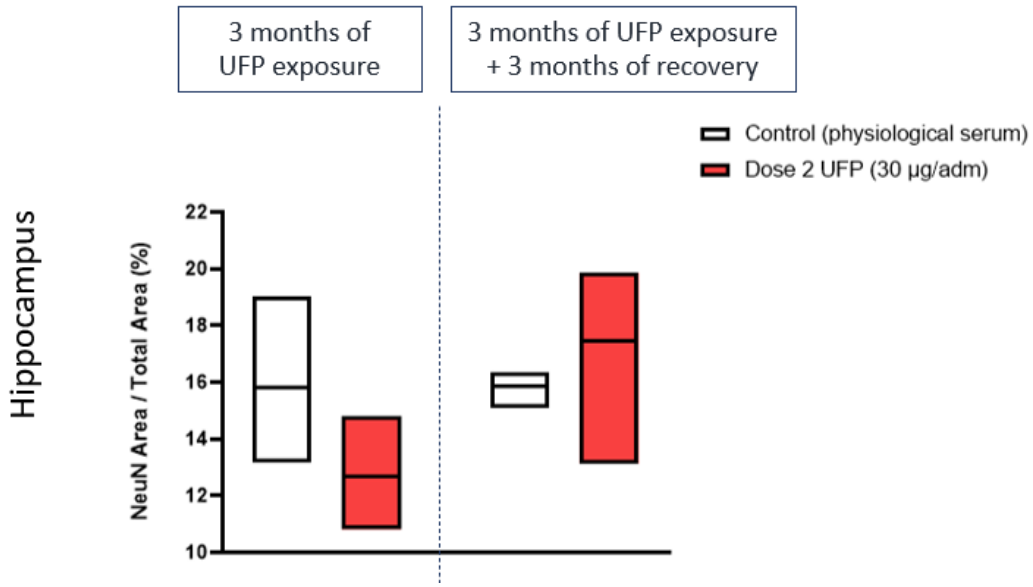

Figure 68: Immunohistochemistry analysis of neuronal nuclear expression in the Hippocampus of control and ultrafine particle-exposed (30 µg/adm, Dose 2) mice.

No significant differences in (Neuronal Nuclear) NeuN expression, as measured by percentage of NeuN-positive cells, were observed between control and Dose 2 ultrafine particles (UFP)-exposed mice, either after three months of UFP exposure or after three months of exposure followed by a 3-month recovery period.

Control: vehicle mice; Dose 2: 30 µg/adm
(n = 3; unpaired t-test (GraphPad Prism8); ** $p<0.01$)

Abbreviations: NeuN: Neuronal nuclear antigen; UFP: Ultrafine particles.

IV. DISCUSSION AND LIMITS

The key findings of this *in vivo* study are that UFP can reach the brain, as evidenced by their detection using TEM and femtosecond pulsed laser microscopy. Elevated metal concentrations (i.e., Cu and Co) and increased metabolic enzyme activity further confirm that UFP successfully target the brain. Despite this, the behavioral assessments (open field test, EPM, passive avoidance, Y-maze, and spontaneous alternation) revealed no significant changes in motor activity, anxiety, or cognitive function. Our findings suggest that UFP exposure induces oxidative stress and neuroinflammation, primarily mediated through NRF2 pathway activation and GSH-dependent antioxidant defenses. The cytokine profile, including MCP-1, CXCL1, and IL-33, highlights a dynamic interplay between redox imbalance and inflammatory signaling of Nf-κB. In the brain, cells appear to activate protective mechanisms, such as GPx activity, to counteract cell death. Immunological and biochemical analyses indicated suppression of RCD pathways across whole-brain tissue and specific regions, including the Prefrontal Cortex, Striatum, Hippocampus and SN, after UFP exposure.

Air pollution remains a major public health challenge. According to the WHO, 91% of the global population resides in areas where air quality exceeds WHO recommended guidelines (Copernicus & Programme). Furthermore, the Global Burden of Disease study identified air pollution as a leading risk factor for conditions such as stroke, heart disease, lung cancer, and respiratory infections, and contributing to approximately 7 million premature deaths annually (Kuehn, 2014). This health burden also has significant economic consequences. A World Bank report from 2016 estimated that air pollution costs the global economy over $5 trillion each year in welfare losses, largely driven by health-related issues (Development & Bank, 2020).

The choice of the city of Lille for UFP collection is particularly relevant given this PhD's affiliation with the University of Lille. Lille represents an ideal urban environment to study the impact of air pollution, with characteristic emission sources such as transportation, residential heating, and tertiary activities. Urban areas are particularly affected by air pollution, indicating that pollution levels in cities often exceed those in rural areas by more than double, disproportionately impacting urban populations (Hulin *et al.*, 2010; Matz *et al.*, 2015). This makes the study of UFP in Lille highly pertinent to understand air pollution's health effects in urban settings.

Due to an insufficient quantity of UFP collected for our initial research design – where the highest intended intranasal exposure dose was set at 50 µg/adm – we adjusted the

exposure protocol. Consequently, mice were subchronically exposed to reduced doses of 10 µg/adm and 30 µg/adm, administered twice weekly over 12 weeks, and part of the mice followed an optional 12-week recovery phase. This mandatory adjustment raises the question of whether alternative particle recovery methods could have enhanced collection efficiency. For example, instead of the Dekati DGI-1570 cascade impactor, the Versatile Ambient Particle Enrichment System (VACES) could be considered for future studies. VACES employs a multi-step process, concentrating particles via condensation and preserving their physical integrity while operating at higher flow rates for faster sampling. This system, already used in environmental monitoring and toxicology studies (Freney *et al.*, 2006; Viana *et al.*, 2021), offers the flexibility to target specific particle sizes and minimizes alterations caused by membrane contact, making it a potentially superior choice for UFP collection. Given the limitations faced in this study, adopting such methods in the future would likely improve the efficiency and reliability of UFP recovery.

Characterization of the UFP confirmed our hypothesis of their significant heterogeneity, encompassing elements typical for urban pollution, such as PAH and metals, alongside naturally derived endotoxins. These particles demonstrated notable oxidative potential, correlating with their toxicity and capacity to induce oxidative stress. This suggests that UFP exposure generates conditions conducive to a redox imbalance.

This supports the decision to expose our BALB/c mice to representative urban UFP. As mentioned earlier, the selection of the BALB/c strain is based on its well-documented suitability for investigating moderate toxicity levels, as evidenced by its use in various toxicity studies conducted within our lab, including research on the effects of electronic and conventional cigarettes (Djouina *et al.*, 2024). Additionally, the use of male mice aligns with prior research protocols in our laboratory (Barbier *et al.*, 2023). However, attributing the choice of male mice solely to the avoidance of hormonal fluctuations would be an oversimplification. UFP exposure has demonstrated sex-dependent effects. For example, Woodward (2019) observed that male mice exposed to UFP exhibited increased adiposity and weight, while females showed no significant changes in metabolic homeostasis compared to controls (Woodward *et al.*, 2019). Similarly, Ehsanifar and colleagues (Ehsanifar *et al.*, 2021) reported that diesel UFP exposure (350-400 µg/m^3, 6 h/day, 5 days/week for 14 weeks) induced higher levels of pro-inflammatory cytokines (IL-1α, IL-1β, IL-6, TNF-α), oxidative stress markers (nNOS, HO1, MDA), and altered neurotransmitter receptor subunits (NR2A, and NR2B) in the hippocampus and olfactory bulb of male mice, with males exhibiting stronger neuroinflammatory responses compared to females. (Cory-Slechta *et al.*, 2019) also

found that male C57BL6/J mice exposed to concentrated ambient ultrafine particles (CAP) had significantly increased neuronal cell death in the nucleus accumbens and reduced live cell numbers, effects that were less pronounced in females, suggesting a potential delayed neurotoxic effect of UFP exposure in females. One hypothesis for these differences may lie in the trajectory of microglial activation. During early postnatal development, males exhibit higher numbers of activated microglia, which may influence early neurogenesis, oligodendrogenesis, and neuronal susceptibility to later damage (Schwarz *et al.*, 2012). In the context of PD, studying male mice is particularly relevant, as observational studies have shown that the risk of PD is approximately twice as high in men compared to women (Cerri *et al.*, 2019; E Ray Dorsey *et al.*, 2018; Ma *et al.*, 2014; Pringsheim *et al.*, 2014; Riccò *et al.*, 2020).

However, it is worth noting that the BALB/c strain may not be the most appropriate model for investigating UFP-induced brain toxicity. Most studies examining the effects of UFP on the brain have used the C57BL/6 strain (Cory-Slechta *et al.*, 2019; Ji *et al.*, 2022; Vanbrabant, Rasking, *et al.*, 2024). Comparing the BALB/c strain to C57BL/6, research suggest that C57B/L6 mice are less susceptible to stress-induced behavioral impairment (Garcia & Esquivel, 2018), likely due to differences in corticosterone response (Balogh & Wehner, 2003; Brinks *et al.*, 2008). Regarding our behavioral tasks assessing motor activity, anxiety, and cognition (attention, learning, and memory), overall, no significant differences were observed between control and UFP-exposed BALB/c mice. Of course, it is important to note that our small sample size (n= 12) may have limited the statistical power to detect subtle effects. Another possible explanation is that BALB/c mice exhibit high baseline fear levels, which may mask the effects of UFP exposure. For instance, during the passive avoidance task, BALB/c mice demonstrate heightened sensitivity to electric shocks compared to C57BL/6 mice (Garcia & Esquivel, 2018), often leading even control mice to avoid re-entering the dark compartment. Another difference comparing C57BL/6 and BALB/c strains is that BALB/c mice exhibit lower exploratory behavior in the novel arm of the Y-maze (Garcia & Esquivel, 2018). This could explain the absence of significant differences between control and UFP-exposed mice in our Y-maze test. Similarly, the Novel Object Recognition (NOR) test was excluded from our study based on findings highlighting the strain-specific object exploration preferences: BALB/c mice favor plastic caps of volumetric flask, while C57BL/6 are more drawn to plastic cylinders (Garcia & Esquivel, 2018). In our case, the objects used were not adapted to the preferences of the BALB/c strain, which may have influenced the outcome of these cognitive assessments. Moreover, the decision to include behavioral analyses was made spontaneously, and the tests themselves may not have been optimally adapted to the BALB/c model. On a molecular and biochemical level, however, BALB/c mice present certain advantages over C57BL/6 mice in toxicological studies. For example, BALB/c

mice exhibit an earlier and more pronounced inflammatory response, marked by rapid cytokine release, which enhances the likelihood of detecting subtle cellular alterations (Ferreira *et al.*, 2018).

Given the absence of significant results in the behavioral tests, it was important to verify whether UFP had actually reached the brain. To address this, we first performed an indirect UFP detection via metal analysis of brain tissue using ICP-MS, although the results were not as expected. While Cu and Co levels in whole brain tissue were significantly elevated after UFP exposure, the sample preparation method may not have been optimal. Previous studies (Bai *et al.*, 2014; Chu *et al.*, 2019) have demonstrated reliable brain metal detection following nanoparticle and PM exposure using ICP-MS, employing protocols similar to those used in this study for UFP characterization (Cf. II.1 Particle recovery in Lille and physico-chemical and biological characterization, p. 74). These protocols include critical steps such as adding 1 mL of 30% H_2O_2 to ~ 100 mg PM or tissue samples to oxidize organic matter and break down the matrix, facilitating metal release, and improving the detection accuracy. The samples are then digested with 5 mL of concentrated HNO_3 in a closed-vessel microwave-assisted reaction system to dissolve minerals and metal oxides, ensuring that metals are in ionic form for detection. After digestion, the mixture is diluted to 2 mL with 2% HNO_3 prior to ICP-MS analysis. Using this optimized protocol, Chu (2019) reported elevated levels of metals, including Li, Be, Al, Cr, Co, Ni, Se, Cd, Ba, Ti, and Pb, in rodent brains after $PM_{2.5}$ exposure. Interpreting our results, however, remains challenging, as the brain is inherently rich in metals. Concentrations of transition metals in brain tissue can be up to 10,000 times higher than those of common neurotransmitters and neuropeptides, and are often considered as essential brain nutrients (Que *et al.*, 2008). This background concentration may limit the ability to detect additional metals beyond a certain threshold. Nevertheless, the observed increase in Cu and Co levels is noteworthy. This elevation was further confirmed by **increased gene expression of Mt**, highlighting a potential neurotoxicological role. Mt proteins are primarily expressed in the cytoplasm, mitochondria, and lysosomes, were they regulate metal homeostasis and oxidative stress. Among the four isoforms, Mt1, Mt2, and Mt3 are localized in the CNS, while Mt4 is typically restricted to epithelial tissues. Neuroinflammation, injury, or heavy metal exposure can induce Mt4 expression in the brain, possibly explaining its upregulation after UFP exposure. Mt1 and Mt2 are primarily expressed in astrocytes, where they protect neurons and regulate metal homeostasis under pathological and inflammatory conditions. Mt3, the most brain-specific isoform, is found in Zn^{2+}-containing neurons in the hippocampus, amygdala, and cerebral cortex (Juárez-Rebollar *et al.*, 2017). The elevated Mt expression observed in our study is consistent with findings in PD models

and post-mortem brains, where increased megalin (a neuronal Mt receptor) and Mt levels in reactive astrocytes in the SN supports their neuroprotective roles (Michael *et al.*, 2011). Experimental studies on Mt1 and Mt2 KO mice have demonstrated that these isoforms protect against damage caused by dopamine quinones (Miyazaki *et al.*, 2007). Additionally, in 6-OHDA-induced parkinsonian rats, Levodopa treatment significantly increased Mt3 mRNA expression in the striatum (Miyazaki *et al.*, 2000). Studies using KO PD models have further highlighted Mt's neuroprotective roles in dopaminergic neurons, including enhancing coenzyme Q10 synthesis, attenuating α-synuclein nitration, preserving GSH, promoting neuromelanin synthesis, preserving ferritin, preventing metal ion accumulation, and scavenging free radicals. As a result, it may be relevant to consider Mt as a potential biomarker for PD (Sharma & Ebadi, 2014; Sharma *et al.*, 2013). The lack of increased Mt2 expression after UFP exposure remains unclear, but it may be linked to the expression degree of astrocytes, as Mt1 is already overexpressed, cells do not increase Mt2 transcription.

AhR activation was next assessed via RT-qPCR, as it is a well-established marker for UFP exposure (reviewed by (Vogel *et al.*, 2020). AhR is expressed in various brain regions, including the Olfactory bulb, Striatum, Cerebral cortex, Hippocampus, and Cerebellum (Petersen *et al.*, 2000). Emerging evidence suggest that AhR plays complex roles in neurodegenerative diseases, with its activation exhibiting both anti- and pro-inflammatory effects depending on environmental conditions (Lee *et al.*, 2015; Piper *et al.*, 2019; Rothhammer *et al.*, 2016; Wang *et al.*, 2018; J. Zhu *et al.*, 2018). However, its specific involvement in PD remains poorly defined. In an *in vivo* PD mouse model, increased phosphorylated AhR (p-AhR) was observed in the SN*pc* and Striatum after MPTP treatment. This was accompanied by a significant rise in p-AhR-positive IBA1- and GFAP-expressing cells, implicating AhR activation in promoting pro-inflammatory responses in reactive glial cells during PD progression (Zhou *et al.*, 2021). Our results align with this hypothesis, showing **significantly elevated levels of AhR** and its downstream target genes, CYP1A1 and CYP1B1, indicating its activation as transcription factor. This is associated with **PAH detoxification pathways** and provides indirect evidence supporting the translocation of UFP into the brain.

To directly visualize UFP, we collaborated with *the Centre Biologie et Pathologie, Centre Hospitalier Universitaire de Lille*, F-59000, France, using TEM. As hypothesized, UFP were detected in axons within brain tissue exposed to 10 µg/adm (Dose 1). This aligns with previous reports associating air pollution-derived PM exposure with excess myelination, referred to as hypermyelination or white matter overgrowth (Klocke *et al.*, 2018). To further explore UFP localization, I initiated a collaboration with the University

of Hasselt at the Centre of Environmental Science (*Centrum voor Milieukunde – CMK*), where I worked during three months as a guest-researcher. During that stay, I could employ the femtosecond pulsed laser microscopy technique to quantify UFP presence in specific brain regions. Analysis of the Prefrontal cortex, Striatum, Hippocampus, and SN revealed significant **UFP accumulation**, particularly in the **prefrontal cortex** (1895 UFP/mm³) **and SN** (2670 UFP/mm³) after 12 weeks of exposure (30 µg/adm, twice per week). The hippocampus showed the highest UFP density, averaging 3327 UFP/mm³, compared to approximately 1000 UFP/mm³ in vehicle-exposed mice, though this difference was not statistically significant (n=3, p=0.08). To context, recent findings in post-mortem brain tissue from AD patients report mean particle densities between 200 and 500 particles/mm^3 (Vanbrabant, Van Dam, *et al.*, 2024). These results underscore the importance of considering interspecies differences when interpreting data. Notably, a resting mouse use up to 3.5 mL of oxygen/gram/hour, compared to 0.25 mL of oxygen/gram/hour in humans (Kling, 2011). This difference may partly explain the higher UFP levels observed in vehicle-exposed mice compared to human brain tissue. To be critical, while intranasal exposure is feasible in the mouse model, it is not a natural route of inhalation, potentially leading to an artificial overdosage of UFP in the brain. Besides, structural differences in the nasal olfactory mucosa further complicate direct comparisons; in humans, this mucosa accounts for only 5-10% of the nasal cavity, compared to 50% in rodents (Facciolà *et al.*, 2019). While this anatomical variation likely reduces humans susceptibility to UFP translocation via the nasal-neuronal pathway compared to our mice model, the neurotoxic effects upon UFP accumulation in the CNS through subchronic or chronic exposure are expected to remain similar. Of course, mimicking natural inhalation processes in mice without the need for sedation and minimal stress can achieved through whole-body or nose-only exposure systems. However, in these both methods, factors such as animal activity, respiratory rate, and individual physiology influence the exact amount of inhaled UFP (Cheng *et al.*, 2010). To reduce those counteracts, and to be sure to have the UFP in our organ of interest, the brain, we choose to expose mice intranasally.

After three months of recovery, UFP levels normalized, indicating effective clearance or potential dissolution. Complementary research using isotope-labeled UFP and intratracheal installation showed prolonged retention of inhaled particles in the brain compared to metabolic organs like the spleen, liver, and kidney. Notably, the brain exhibited significantly longer half-life values ($t_{1/2}$ of 2.822 days) for exogenous particles, whereas other tissues had $t_{1/2}$ of less than 1.5 days. Besides, particle aggregates were visualized in brain regions such as the Cerebral cortex, Hippocampus, and Cerebellum, highlighting the brain's unique susceptibility to prolonged UFP retention (Qi *et al.*, 2022).

The UFP are well distributed throughout the brain tissue, raising concerns about their potential to induce whole-brain neurotoxicity. A key mechanisms by which UFP exert their effects, is through the overproduction of ROS, which disrupts cellular redox balance. Restoring equilibrium requires activation of homeostatic pathways, such as the NRF2 redox system. Cell culture and animal studies on various UFP sources, including DEP, urban air pollution, and engineered nanoparticles, have consistently shown **NRF2 pathway activation** as defense mechanism (Li *et al.*, 2004; Xu *et al.*, 2022). In our whole-brain tissue study, UFP exposure significantly upregulated *Nrf2* gene expression, triggering downstream transcription of cytoprotective genes such as *Keap1, Hmox1, Txn1, Gpx1, Gsr, and Gclc*. However, the gene expression of *Gclm* was downregulated. WB analysis of KEAP1 monomers and the dissociation regulator p-p62 confirmed that release of KEAP1 from NRF2, enabling NRF2 activation, meaning that cells are fighting against an overall oxidative stress environment. This followed enhanced vital enzyme activity of GPx and GR, signifying effective neutralization of ROS and repair of oxidative damage caused by UFP exposure. Looking deeper on the GSH-axis, GPx and GR refer to the excessive use of GSH, while GSR and GCLC will support GSH recycling and production, however, the lack of Gclm gene expression could result in a lower than expected increase in GSH levels. This disruption in homeostasis makes cells more susceptible for oxidative damage, with a higher chance to develop in more pronounced effects such as lipid peroxidation or RCD.

Both the **TRX and the GSH pathways** are crucial for maintaining redox balance. While gene expression analysis revealed upregulation of both pathways, our protein level findings indicated no differences in TXNIP, TXN2, Prdx1, and TRXR1 in whole brain tissue of UFP- and vehicle-exposed mice. This discrepancy contrasts with previous studies where exposure to pollutants like cigarette smoke, DEP, and airborne PM particles activated the TRX system through downregulation of TXNIP and upregulation of TXN and TXNR in lung tissues and airway epithelial or alveolar cell lines (BEAS-2B, MLE-12, L-132) (Abiko *et al.*, 2022; Son *et al.*, 2020; Zhongyin *et al.*, 2022). Interestingly, the GSH and TRX systems overlap in function and often compensate for one another when one pathway is impaired (Du *et al.*, 2012). However, they have distinct functions and target different types of oxidative damage: the TRX system reduces protein disulfides, playing a critical role in redox signaling and protein repair, whereas the GSH system detoxifies ROS, lipid peroxides, and xenobiotics (Go *et al.*, 2013; Jones & Go, 2010). Given the brain's high oxygen consumption (~20% of the body's total) (Tavares *et al.*, 2023), significant ROS production, and vulnerability to lipid peroxidation, it suggest that GSH pathway predominates in maintaining brain redox homeostasis after UFP exposure, which probably explains are negative results concerning the TRX system.

Oxidative stress is closely linked to neuroinflammation. To evaluate the functional state of brain cells, we focused on dynamic inflammatory markers rather than static structural markers like GFAP for astrocytes and Iba1 for microglia. Notably, Nf-κB activity is an early and dynamic event that precedes the appearance of structural or cytoskeletal markers. However, the results regarding **Nf-κB** activation are contradictory. WB analysis comparing control and high UFP exposure (Dose 2, 30 µg/adm) showed a decrease in IKKβ and an increase in IκBα in whole brain tissue, crucial proteins of the canonical Nf-κB pathway. Additionally, no differences was found in subunit p65 or p50 on protein expression. However, consistent with previous studies (Bhargava *et al.*, 2019; Li *et al.*, 2013), high UFP exposure **significantly increased Nf-κB binding to DNA, upregulating pro-inflammatory mediators such as MCP-1 (CCL2), KC/GRO-α (CXCL1), and IL-33, and downregulation of IL-5.** Interestingly, our hypothesis was that the BBB will be damaged during UFP-exposure, especially to destroy tight junctions between the endothelial cells to restrict blood-borne substances from entering the brain. MCP-1, a monocyte chemoattractant, known to compromise BBB integrity by affecting pericytes, astrocytes, neurons, and basement membrane (Yao & Tsirka, 2014), was upregulated following UFP-exposure. Moreover, elevated MCP-1 levels have been observed in CSF of PD patients and correlate with disease severity, promising to become potential prognostic biomarker (Santaella *et al.*, 2020). CXCL1/Gro-α, is on its turn expressed in multiple brain regions, including the ventral midbrain, and it has been implicated in dopaminergic nerve regeneration and inflammatory response after brain injury (Edman *et al.*, 2008; Jiang *et al.*, 2023). IL-33 exhibits both pro- and anti-inflammatory properties, influencing neuroinflammation, apoptosis, and synaptic plasticity. Excessive IL-33 expression has been linked to cognitive decline and PD. Astrocytes in the midbrain and Striatum of PD patients show elevated IL-33 levels (Kempuraj *et al.*, 2019), and in *in vitro* studies with MPP^+ treatment (Kempuraj *et al.*, 2015). IL-5, a Th2-response cytokine, is upregulated in PD patients, with higher levels detected in those with longer disease durations (> 8 years) compared to shorter durations (< 5 years) (Di Lazzaro *et al.*, 2024). Interestingly, IL-5 was downregulated in the brain tissue of UFP-exposed mice, this may reflect a shift toward an M1-dominant state. Until now, no clear distinction has been made between the classical M1 and alternative M2 microglia phenotypes. The panel of significant cytokines analyzed in this study provides no conclusive evidence, and the lack of investigation into microglial polarization (M1/M2 balance) remains a limitation of this study. However, regarding our results, among the 19 inflammatory mediators analyzed, four showed significant changes, including the downregulation of the M2 marker IL-5. These findings suggests a potential shift toward neuroinflammation. However, the dynamic and spectrum-like nature of microglial activation complicates definitive interpretation of the M1/M2 balance. Our results likely

represent the initial stages of neuroinflammation, with more pronounced effects potentially emerging following chronic UFP exposure or in the advanced stages of PD.

Given that the release of inflammatory factors – primarily cytokines and chemokines – can contribute to neurodegeneration, we investigated several hallmarks under the RCD umbrella in Dose 2 UFP-exposed whole brain tissue compared to control samples. These included apoptosis, autophagy, necroptosis, parthanatos, and ferroptosis.

The first set of analyzed proteins was related to **apoptosis**, including pro-apoptotic markers such as BAD, BIM, and BAK, and the apoptotic endpoint marker, Caspase-3. BAD is a key regulator balancing cell survival and apoptosis through post-translational modifications. In our study, we observed a higher p-BAD/BAD ratio in UFP-exposed brain tissue, indicating a compensatory mechanism to counteract UFP toxicity. If cells fail to compensate, BAD can trigger MOMP, leading to Cytochrome C release and the irreversible activation of the caspase cascade, ultimately resulting in cell death (Ohi *et al.*, 2006). However, other markers supporting mitochondrial apoptotic activity, such as BIM and BAK, were not significantly upregulated. Similarly, the ratio of cleaved caspase-3 to total caspase-3, which reflects caspase activity, was decreased in UFP-exposed brain tissue. These findings suggest that apoptosis does not occur in whole brain tissue following UFP exposure under the conditions of this study.

Autophagy, another RCD pathway, was investigated trough the activation of ATG proteins, LC3, and p62 (Luo *et al.*, 2020). In our study, the protein levels of key ATG proteins such as ATG13 and ATG7 were significantly downregulated, likely impairing LC3 activation and explaining the observed WB results where only the non-activated LC3-I band was present and no changes in cargo degradation protein p62 expression.

Necroptosis, a more inflammatory RCD form, is primary mediated by protein kinases RIP and RIP3, and the downstream effect MLKL. WB analysis showed reduced levels of RIP and MLKL, with RIP3 not found in its activated, phosphorylated form. Most MLKL proteins were phosphorylated, but their low concentration suggests they do not induce membrane rupture or release of DAMP, indicating that necroptosis did not occur in UFP-exposed brains.

Parthanatos, another subtle RCD pathway, was investigated using MIF and AIF markers. However, no positive outcomes were observed, suggesting that parthanatos was not induced upon UFP exposure.

Ferroptosis, likely the predominant RCD mechanism in PD and particle-induced toxicity, was examined by assessing iron homeostasis (TfR and FTH1), GSH-antioxidant defense (GPx4 and xCT), overall GPx activity (colorimetric tests), GSH ratio (bioluminescence), and lipid peroxidation (4-HNE adducts via ELISA). Protein levels of

iron import (TfR) and iron storage (FTH1) showed no significant changes in UFP-exposed samples compared to controls. As highlighted in the introduction, this aligns with previous findings suggesting that particle exposure does not always disturb the iron balance to induce ferroptosis (C. Zhang *et al.*, 2020). Similarly, GPx4 protein levels remained unchanged; however, overall GPx activity was significantly elevated, consistent with the observed depletion of the GSH/GSSG ratio upon UFP-exposure. A significant dose-dependent effect was noted: low-dose UFP exposure (10 µg/adm) did not reduce GSH levels in whole brain tissue, but it significantly increased GSSG. In contrast, high dose-exposure (D2, 30 µg/adm) led to pronounced GSH depletion. Investigating this ferroptotic marked response, SLC7A11 (xCT) protein levels were measured in D2 exposed mice and were unexpectedly found to be significantly elevated, suggesting a feedback mechanism aimed at restoring antioxidant capacity. This response likely reflects the depletion of GSH triggering increased xCT expression to counter oxidative stress. Notably, despite elevated xCT protein levels, SLC7A11 gene expression was not upregulated, contradicting expectations based on recent findings that activated AhR signaling regulates ferroptosis via SLC7A11 transcription (Kou *et al.*, 2024). Moreover, NRF2, known to bind directly to the ARE in the SLC7A11 promoter, typically drives transcriptional upregulation (Sasaki *et al.*, 2002). This discrepancy suggests alternative regulatory mechanisms may be involved, as the gene expression remained unchanged. In amyotrophic lateral sclerosis (ALS), another motor neurodegenerative disease, x_c^- contributes to microglial-derived glutamate release, influencing microglial reactivity and motor neuron degeneration (Mesci *et al.*, 2015). The observed divergence between xCT protein and gene expression levels could be attributed to post-transcriptional or post-translational regulation. A possible explanation, is related to reduced miRNA-mediated silencing of SLC7A11 mRNA, regulated by miR-26b, miR-27a, and miR-375 (Drayton *et al.*, 2014; Liu *et al.*, 2011; Wu *et al.*, 2017). At the post-translationally level, the stability of the SLC7A11 (xCT) protein is influenced by interactions with CD44v and SLC3A2, which help stabilize it at the plasma membrane (T. Liu *et al.*, 2019). Additionally, SLC7A11 may be stored near the plasma membrane and rapidly mobilized in response to increase GSH synthesis demands. This suggests that assessing gene or protein expression alone may not provide a definitive understanding of SLC7A11 activity. Instead, functional assays, such as measuring x_c^- system activation through glutamate release, could offer more conclusive insights (Beckers *et al.*, 2024). All those anti-ferroptotic markers, associated with NRF2 pathway activation, upregulation of xCT and activation of GPx enzymes, likely contributed to the reduction of toxic 4-HNE adducts in brain tissue following UFP exposure. These findings suggests that the brain's defense mechanisms, particularly NRF2 signaling, were activated to maintain cellular integrity and mitigate RCD, such as ferroptosis.

Consistent with these observations, no morphological evidence of cell death was detected in target brain regions linked to neurodegeneration. IHC results for **TH** in the Striatum, SN, and VTA, as well as **NeuN** in the Hippocampus, revealed no differences between control and UFP-exposed mice, either immediately after 12 weeks of exposure or following a 12-week recovery period without further exposure.

Overall, no RCD forms were observed in brain tissue after 12 weeks of subchronic intranasal exposure to urban UFP. The outcome suggests that brains adapt to the exposure by activating defense mechanisms, such as the NRF2 pathway. The specific downstream effects of NRF2 and/or other oxidative stress related mechanisms depend on the xenobiotic trigger, in this case, UFP exposure. These adaptations can manifest in three key ways:

- **Variable reactivity:**
  Depending on the xenobiotic, for us UFP, different kind of ROS will be produced that vary in reactivity. For example, $^{\bullet}OH$ react rapidly with guanine, leading to DNA oxidation, whereas $O_2^{\bullet -}$ is less relative with guanine.
- **Specific enzyme transcription:**
  The type of ROS produced determines which Phase II metabolic enzymes are transcribed via NRF2 signaling. In this study, *Hmox1*, *Txn1*, *Gpx1*, *Gsr*, and *Gclc* were upregulated to mitigate oxidative stress.
- **Subcellular and neuronal heterogeneity:**
  Neuronal susceptibility to oxidative stress varies across subcellular domains (e.g., synaptic mitochondria vs. synaptic membranes) and within compartments (e.g., soma vs synapse). Neuronal types, such as dopaminergic vs catecholaminergic neurons, also differ in function, location, connectivity, myelination, and axon length. This can lead to other reactions on oxidative stress. RCD form hallmarks can therefore be hidden in whole brain tissue analysis.

Despite the significant oxidative stress observed, the lack of RCD induction and even depletion of key RCD hallmarks was unexpected. Possible explanations include:

1) **Insufficient UFP exposure intensity:**
   The oxidative stress induced by UFP may not have been severe enough to overwhelm neuronal defenses. Consequently, neurons effectively managed ROS levels through NRF2-mediated transcription of Phase II metabolic enzymes.

2) **Adaptive immune responses:**

Immune cells, such as microglia, may have developed an adaptative immune response, creating immunological memory to efficiently address subsequent UFP exposures. Although the speed of UFP clearance was not directly assessed, brain UFP levels normalized to control levels after a three-month recovery period.

3) **Neuronal exposure history:**

Repeated sub-lethal UFP exposures may have triggered coordinated adaptive responses in neurons. For example, high oxidative stress activated GSH antioxidant defenses and GPx activity, both resulting in GSH depletion. Neurons have an adaptation on their history, they probably recognized the following UFP exposures (twice/weekly), whereafter they adapted, for example through a feedback loop involving the x_c^- mechanism, as evidenced leading to reduced 4-HNE adducts. This adaptation lowered peroxidized lipid load, moving cells further from the ferroptotic threshold, as shown in Fig. 69 (Cobley , 2018).

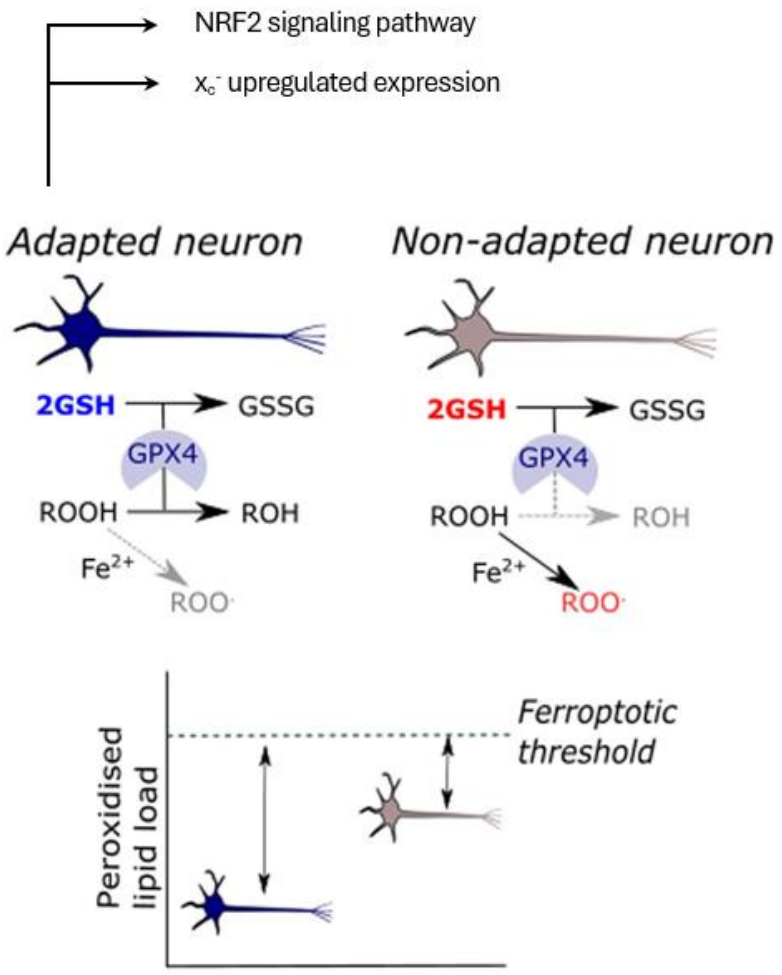

Figure 69: Adapted neurons under oxidative stress move further away from the ferroptotic threshold.

Neurons repeatedly exposed to xenobiotics, develop an adaptive memory based on prior exposure history. This adaptation enables a more consistent, rapid, and targeted activation of defense mechanisms, such as the nuclear factor erythroid 2-related factor 2 (NRF2) pathway, leading to the downstream expression of detoxifying enzymes. In response to increase glutathione (GSH) consumption, the cystine/glutamate antiporter system (x_c^-) may be upregulated as a compensatory mechanism to restore GSH levels. GSH serves as a co-substrate for glutathione peroxidase 4 (GPx4), counteracting lipid peroxides. Consequently, the peroxidized lipid load decreases, moving these neurons further from the ferroptotic threshold (Cobley *et al.*, 2018).

Abbreviations: GPx4: Glutathione peroxidase 4; GSH: Glutathione; NRF2: Nuclear factor erythroid 2-related factor 2; x_c^-: Cystine/glutamate antiporter system.

V. CONCLUSION AND PERSPECTIVES

Mice exposed to UFP (10 µg/adm or 30 µg/adm) during a sub-chronic three-month exposure exhibited UFP localization in brain regions linked to PD (prefrontal cortex and SN), accompanied by overall elevated metal concentrations and increased detoxification enzymes, including AhR and Mt. Despite these changes, no significant motor activity, anxiety or cognitive impairments were observed in behavioral tests. Oxidative stress, indicated by NRF2 activation and the upregulation of related antioxidant enzymes, was insufficient to fully counteract neuroinflammation, as evidenced by Nf-κB activation and pro-inflammatory cytokines release. However, this antioxidant response appeared effective in preventing RCD (apoptosis, autophagy, ferroptosis, necroptosis, parthanatos) and neuronal loss in key brain regions, including the SN, VTA, striatum, and hippocampus. These findings highlight the brain's remarkable resilience and adaptive capacity to counteract toxic insults. Nevertheless, the cumulative and chronic nature of environmental exposures, such as air pollution, may contribute to the progressive onset of clinical manifestations in neurodegenerative diseases like PD, emphasizing the need for long-term studies on the interplay between environmental factors and disease progression.

Long-term exposure models can introduce us the better understanding of the kinetics of UFP neurotoxicity. One promising approach is the two-hit hypothesis, where acute prenatal maternal immune activation (MIA) is followed by low-dose postnatal UFP exposure to assess synergistic effects on neurological development or later on in the offspring life age-related neurodegenerative diseases. Alternatively, incorporating UFP exposure into established PD models (e.g., subthreshold doses of 6-OHDA, MPTP, or Rotenone) could reveal whether UFP exacerbate PD-related features or accelerate disease onset.

In chronical order of this present study, is the NF-κB activity and the release of neuroinflammatory mediators the last positive target related to PD. It would be useful that perspectives starts were this study ended. While this study provides evidence of an inflammatory response, further investigations are needed to delineate its chronicity and phenotypic polarization of microglia. Future work could use markers such as Iba1 and GFAP through IHC in the four brain regions, as well as mRNA and protein analysis to characterize the potential excessive activation of glial cells, including microglia and astrocytes. Chronic inflammation may also contribute to synaptopathology, characterized by dyshomeostasis of synaptic proteins, structural alterations, and disrupted neuronal communication. As synaptic dysfunction often precedes

neurodegeneration, it would be valuable to investigate markers such as synaptophysin (all synapses), vGLUT (Vesicular Glutamate Transporter; Glutamatergic), GAD (Glutamic Acid Decarboxylase; GABAergic), MAP2 (Microtubule-Associated Protein 2; dendritic integrity), Olig2 (Oligodendrocyte Transcription Factor 2; oligodendrocytes), MBP (Myelin Basic Protein), and NfL (Neurofilament Light Chain; axonal damage). Moreover, knowing that we found UFP in axons, by the use of TEM, it would be valuable to explore more the branching neuronal structures related to this stressor, like shown in Fig. 70.

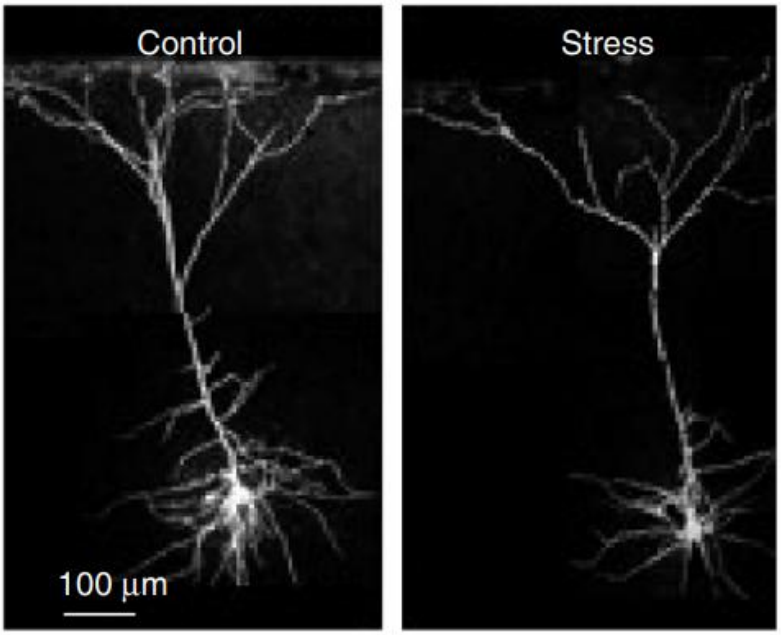

Figure 70: Chronic stress leads to neuronal process atrophy and a reduction in synapse density.

This image, obtained using two-photon laser-scanning microscopy, highlights pyramidal neurons labeled with neurobiotin. The visualization reveals that stress results in shortened and fewer apical dendrites (Duman *et al.*, 2016).

As previously mentioned, greater focus should be placed on neuronal inactivity, particularly in determining the specific time point (the kinetical time, denoted as *t* in Fig. 71) at which the disruption of intraneuronal communication, caused by chronical UFP-induced stress, triggers neurodegeneration associated with PD.

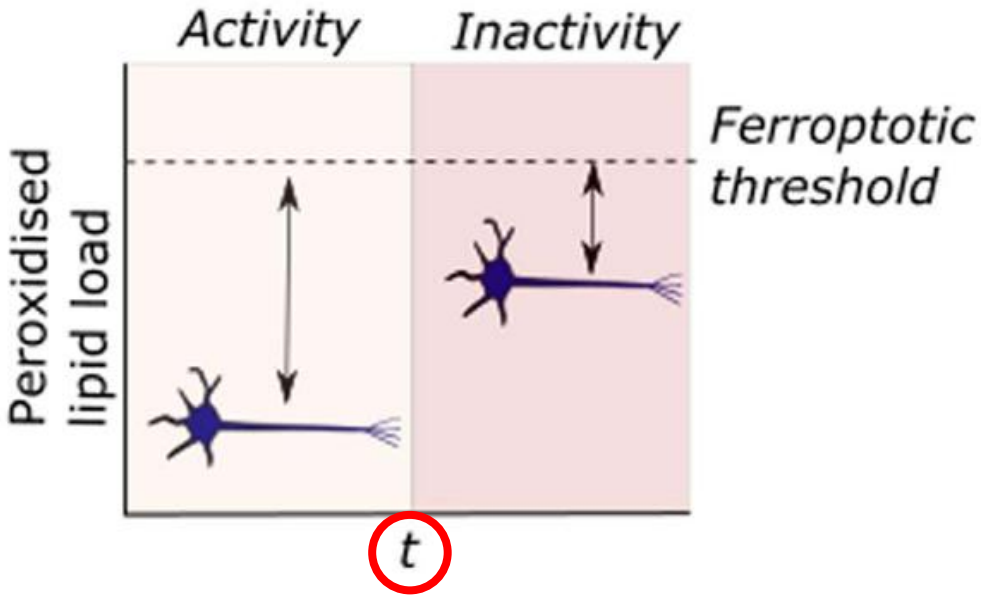

Figure 71: 'Use it or lose it' idea about neuronal network.

According to a theoretical threshold model, a neuron's resistance to ferroptosis decreases with prolonged inactivity. This suggests that the absence of synaptic or neurotransmitter stimuli, and the resulting reduction in neuronal activity, gradually weakens this resistance to ferroptosis, ultimately contributing to neurodegeneration (Cobley *et al.*, 2018).

As confirmed through this PhD study, neurons are highly adaptative cells, capable of activating robust defense mechanisms against UFP-induced stress. However, these findings also suggest that this resilience has limits. Persistent exposure to UFP, with a prolonged accumulation of harmful compounds (such as ROS or lipid peroxides), may eventually overwhelm these protective mechanisms, pushing neurons past their adaptative capacity and triggering cell death.

CHAPTER III:
DOES AIR POLLUTION-DERIVED ULTRAFINE PARTICLES INDUCE FERROPTOSIS IN DIFFERENTIATED HUMAN DOPAMINERGIC NEURONAL LUHMES CELLS?

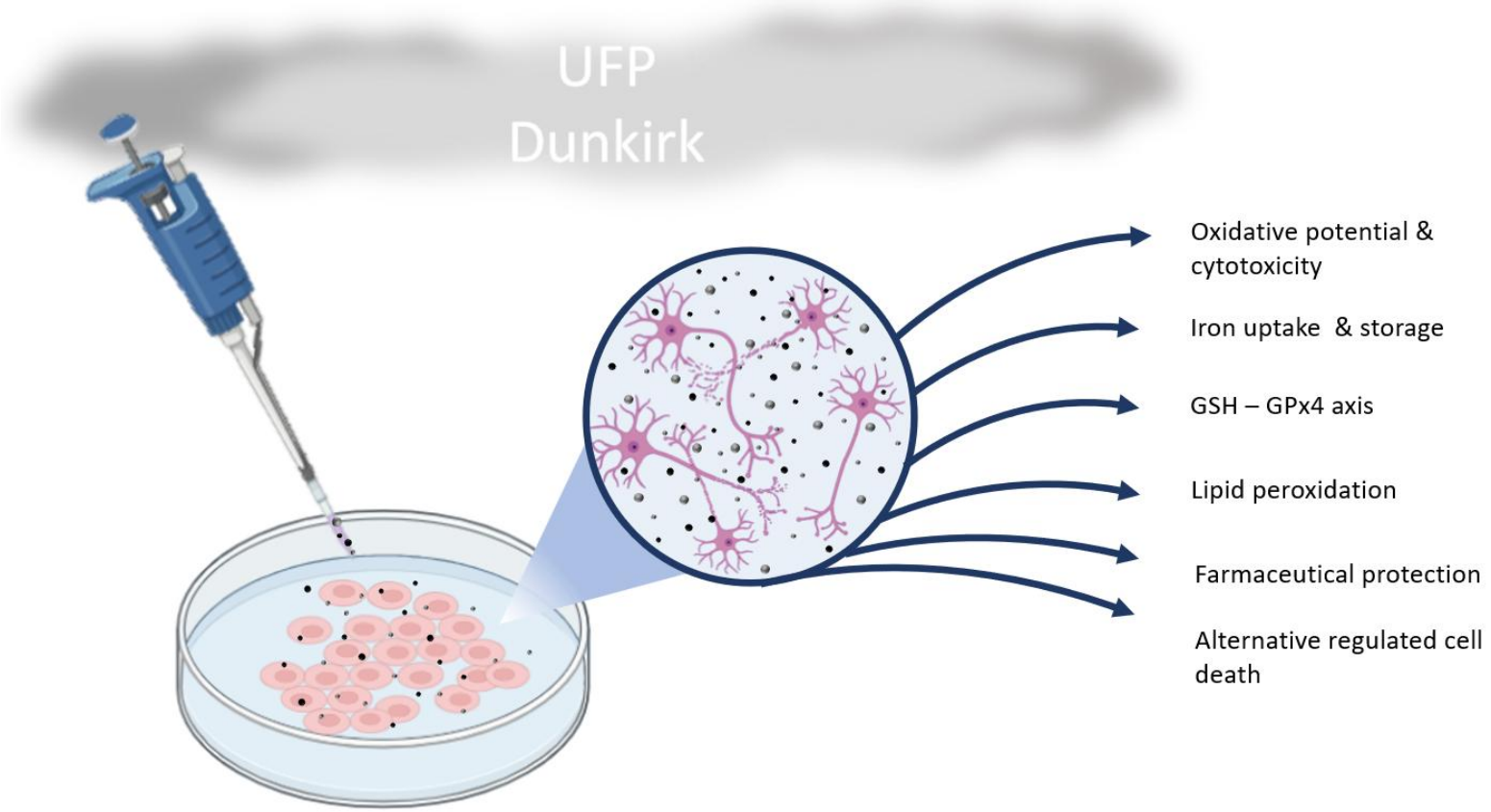

I. SPECIFIC GOALS

This *in vitro* study aimed to evaluate the toxicity of UFP on dopaminergic neurons, focusing on UFP with high iron content from an industrial region (Dunkirk, France), their potential to induce ferroptosis, and the underlying mechanisms.

The following objectives were set:

1) **Can UFP generate ROS?**
   The oxidative potential of UFP is assessed using the DTT-assay.

2) **Cytotoxicity evaluation**:
   What are the effects of UFP exposure on LUHMES cells viability and metabolism? Therefore, differentiated LUHMES cells were exposed to concentrations of 0, 2, 5, 10, 20, 30, and 40 µg/cm² UFP and thereafter monitored by the fluorescence-based G6PD release and Resazurin assays.

Realistic exposure scenarios focused on UFP concentrations of 2 and 10 µg/cm² with a 24-hour acute exposure period.

Investigating ferroptosis

3) **Will UFP result in iron uptake and storage?**
   - Iron uptake was assessed via transferrin receptor (TfR) and divalent metal transporter (DMT) expression (Western blot).
   - Intracellular iron storage was measured through ferritin levels (ELISA-MSD).

4) **Is the glutathione pathway altered upon UFP exposure, leading to lipid peroxidation?**
   Several markers are investigated through corresponding assays to obtain a global idea:
   - Glutathione status: GSH/GSSG ratio (bioluminescence).
   - Glutathione peroxidase: GPx activity (fluorescence) and GPx4 protein levels (Western blot)
   - GSH depletion mechanisms: Protein levels of xCT/SLC7A11 and p53 (Western blot).
   - Lipid peroxidation: 4-HNE adducts (ELISA-MSD).

5) **Can anti-ferroptotic drugs prevent ferroptosis when exposed to UFP?**
   Testing the protective effects of the radical-trapping antioxidants liproxstatin-1 (LPX) and the iron chelator DFP by pre-treating cells for 1 hour before UFP exposure.

6) **Does UFP lead to a PD-phenotype?**
   Comparing ferropotitc hallmarks of UFP exposure on dopaminergic neurons to a well-established PD-model, 1-methyl-4-phenylpyridinium (MPP^+), to assess the relative toxicity of UFP.

After a 24-hour exposure to 2 or 10 µg/cm² UFP, it is unlikely that only ferroptosis will occur. Consequently, additional RCD pathways relevant to PD and/or cross-talk with ferroptosis were investigated.

Broader context of RCD

7) **What if alternative RCD form also occur in the context of UFP-toxicity?**
   - Assessed intrinsic **apoptosis** markers, including BAX (Western blot) and caspase-9 activity (bioluminescence), as well as extrinsic apoptosis markers, such as caspase-8 activity (bioluminescence).
   - Measured the end-point caspase activity: caspase-3/7 (bioluminescence).
   - Investigated **(selective) autophagy** markers, such as NCOA4 and LC3b-II/I (Western blot).

8) **Is it possible that preventing ferroptosis, leads to cross-talk with other RCD pathways?**
   Evaluated whether pharmacological prevention of ferroptosis with LPX would still result in cell death via alternative RCD pathways (apoptosis or autophagy) following UFP exposure.

II. MATERIAL AND METHODS

II.1 Particle recovery in Dunkirk and physico-chemical characterization

Particle sampling, size distribution and physico-chemical analyses have been published previously (Platel *et al.*, 2020; Saleh *et al.*, 2019; Sotty *et al.*, 2019; Sotty *et al.*, 2020). Briefly, UFP were collected in Dunkirk, a French coastal city known for its industrial and traffic-related air pollution. Sampling of UFP (aerodynamic equivalent diameter ≤ 180 nm) was performed using a High-Volume Impactor Sampler (HVIS, flow rate of 400 L/min) with filtration on an 8" × 10" PC membrane. All PC membranes used to collect UFP were weighed and then transferred to a Hank's Balanced Salt Solution (HBSS) by three successive water-cooled ultrasonic extractions (Vibracell 75455, 500 W, 20 KHz). All extracts were pooled to a final concentration of 2.7 µg/µL. The UFP suspensions were then aliquoted and stored at -20°C until use.

The hydrodynamic diameter of UFP was measured after suspending the particles in HBSS (1 mg/mL) using a Dynamic Light Scattering (DLS) Zetasizer nano ZS (Malvern Instruments, Orsay, France). Two peaks were observed at 188.0 ± 39.9 nm (71.9%) and 1078 ± 305 nm (28.1%), the major peak corresponding to the presence of UFP and the minor peak to the formation of particle aggregates. The zeta potential measured at 25°C showed negative values of -17.1 ± 0.3mV. Chemical analyses were performed directly on the HBSS aliquots. Therefore, trace elements (including Al, As, Ba, Be, Ca, Cd, Ce, Co, Cr, Cs, Cu, Fe, K, La, Mg, Mn, Mo, Na, Ni, Pb, Rb, Sb, Sn, Sr, Tl, V, Zn) were analyzed by ICP-MS (NeXion 300x, Perkin Elmer, Waltham, MA). PAH (including Fluoranthene, Pyrene, Benzo(c)phenanthrene, Benzo(a)anthracene, Chrysene, 5-Methylchrysene, Benzo(e)pyrene, Benzo(b)fluoranthene, Benzo(j)fluoranthene, Benzo(k)fluoranthene, Benzo(a)pyrene, Dibenzo(a,l)pyrene, Dibenzo(a,h)anthracene, Benzo(g,h,i)perylene, Indeno(1,2,3-c,d)pyrene, Dibenzo(a,e)pyrene, Anthanthrene and Coronene) extracted by a Dionex ASE 200 instrument (ThermoFisher® Scientific) were analyzed by high-pressure liquid chromatography (HPLC) consisting of a Waters 2695 Alliance system (Waters SA, Saint-Quentin-en-Yvelines, France) coupled to an on-line 996-photodiode array and a 2475-fluorimetric detector. An overview of both, the elemental (Table S4) and PAH (Table S2) composition, can be found in the Supplementary data (p. 237, 235).

II.2 Oxidative potential analysis

A dithiothreitol (DTT) depletion assay was used to assess the oxidative capacity of previously collected and stored UFP. Despite prolonged storage of aliquoted particles at -20°C, it was necessary to assess their intrinsic ability to oxidize chemical compounds via the generation or action of Reactive Oxygen Species (ROS). The assay was adapted from the protocol described by Crobeddu (Crobeddu *et al.*, 2017) and used as a cell-free method to detect oxidative potential. Briefly, UFP samples at concentrations of 0, 2, 10, 40, and 80 µg/cm² were dissolved in phosphate-buffered saline (PBS) and incubated with an equal volume of DTT (400 µM in 30 mM degassed 4-(2-hydroxyethyl)-1-piperazineethanesulfonic acid [HEPES] buffer) in a 96-well plate. Incubation was carried out at 37°C for 1 hour. Whereafter, the plate was centrifuged at 3500 g for 15 minutes at 4°C. After centrifugation, 100 µL of the supernatant from each well was transferred and mixed with an equal volume of 2.5 mM 5,5'-dithiobis-(2-nitrobenzoic acid) (DTNB). The absorbance of the resulting reaction was measured at 405 nm using a Spark® multimode microplate reader (TECAN, Männedorf, Switzerland). The percentage of DTT consumption was calculated as $100-(OD_{sample}/OD_{N.C.})x100$, which is proportional to the generation of ROS, where OD refers to the optical density measured for each sample and the negative control (PBS + 30 mM HEPES).

II.3 Cellular model: Differentiated Lund Human Mesencephalic (LUHMES) cells

LUHMES (CRL-2927™) cells were obtained from the In vitro Toxicology and Biomedicine Laboratory, University of Konstanz, Germany. The LUHMES subclone has been immortalised by transfection with a tetracycline-regulated v-*myc*-vector.

Proliferated cells were cultured in Nunclon® plastic, coated with 50 µg/mL poly-L-Ornithine and 1 µg/mL fibronectin dissolved in water. They were maintained in coated T75 flasks at 3 million cells with advanced DMEM/F-12 medium (Gibco, Waltham, MA) (1% Penicillin-Streptomycin), supplemented by 1X N2 (Gibco), 2 mM L-Glutamine (Gibco) and 40 ng/mL basic fibroblast growth factor (bFGF) (Miltenyi, Bergish Gladbach, Germany) under growth conditions (37°C, 95 % humidified atmosphere, 5 % CO_2). For differentiation into postmitotic human mature dopaminergic neurons, a previous published protocol was followed (Scholz *et al.*, 2011), which is already widely used in our laboratory (Bonte *et al.*, 2024; Bouchaoui *et al.*, 2023; Do Van *et al.*, 2016; Mahoney-Sanchez *et al.*, 2022). The differentiation medium contained advanced DMEM/F-12 medium, 1X N2, 2 mM L-Glutamine, 1 mM cAMP (Sigma-Aldrich, St Quentin Fallavier, France), 1 µg/mL tetracycline (Sigma Aldrich) and 2 ng/mL recombinant human GDNF (Bio-Techne, Minneapolis, MN). These differentiated cells express key markers of dopaminergic neurons and exhibit many of the functional properties of neurons found in

the SN*pc*, including dopamine synthesis, release, and uptake. As shown in Fig. 72, proliferating LUHMES cells appeared spherical, when fully differentiated, at day 5 (D5), it formed a web of axons and dendrites.

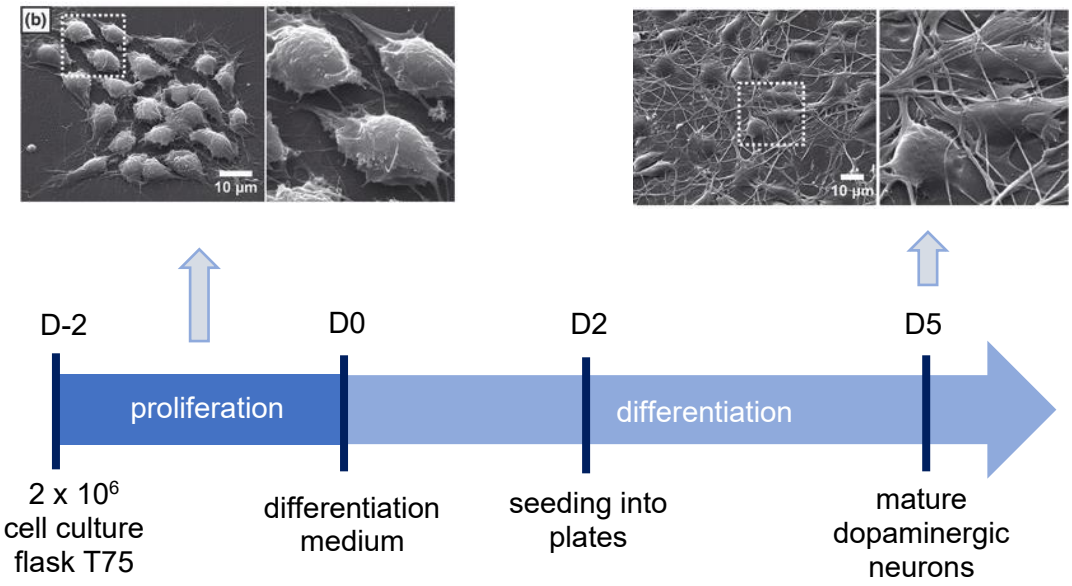

Figure 72: Schematic overview of proliferation and cell differentiation of LUHMES cells.

Starting on day 0 (D0) cells are maintained in differentiation medium (advanced DMEM/F-12 medium (1% Penicillin-Streptomycin), 1X N2, 2 mM L-Glutamine and 40 ng/mL basic fibroblast growth factor (bFGF); 37°C, 95 % humidified atmosphere, 5 % CO_2) and fully differentiated into mature dopaminergic-like neurons on day 5 (D5). On day 2 (D2) they are cultured in a poly-lornithine/fibronectin-coated Nunclon® plate. Fully differentiated cells are exposed at D5, and on day 6 (D6) the cells/proteins are investigated/harvested for specific characteristics (Scholz *et al.*, 2011).

Abbreviations: bFGF: Basic Fibroblast Growth Factor; DMEM/F-12: Dulbecco's Modified Eagle Medium/Nutrient Mixture F-12; LUHMES: Lund Human Mesencephalic.

II.4 Cytotoxicity

Differentiated LUHMES cells were cultured in 96-well plates at a seeding density of 40,000 cells/well. Following exposure to UFP in the range of 0 to 40 µg/cm², both metabolism and viability were assessed 24 hours post-exposure.

Cell Metabolism Assay

The resazurin assay is a widely used protocol to investigate cell metabolism and frequently applied on LUHMES cells (Bonte *et al.*, 2024; Bouchaoui *et al.*, 2023; Mahoney-Sanchez *et al.*, 2022). Cells were incubated with resazurin (100 µg/mL) for 2 hours at 37°C, protected from light. Fluorescence intensity was measured (Ex: 560 nm; Em: 600 nm) using a Spark® multimode microplate reader (TECAN, Männedorf, Switzerland), and normalized to control wells, representing 100% cell metabolism.

Cell Viability Assay

Cell viability was assessed by measuring G6PD Release using the CyQUANT™ Cytotoxicity Assay Kit (ThermoFisher®, Waltham, MA). Equal volumes of cell supernatant and 2X resazurin/reaction mixture were added to a black 96-well plate. The assay is based on the detection of glucose-6-phosphate dehydrogenase (G6PD) released from damaged or dying cells in the medium. A two-step enzymatic process occurs, in which oxidation of glucose 6-phosphate by G6PD generates nicotinamide adenine dinucleotide phosphate (NADPH), which subsequently leads to the reduction of resazurin to fluorescent resorufin by the enzyme diaphorase. The fluorescence of resorufin was measured (Ex: 563 nm; Em: 587 nm) using the Spark® multimode microplate reader (TECAN). Higher fluorescence signals corresponded to increased cell death. Results were compared to the control and expressed inversely as a percentage of cell viability.

II.5 Cell lysis, protein extraction and quantitation of total protein amount

The cytotoxicity assay results (Cf. III.1.2 Resazurin and G6PD Release Fluorescence Assay, p. 167) determined that UFP concentrations of 2 µg/cm² and 10 µg/cm² would be used for further experiments.

On D5, differentiated LUHMES cells were exposed to six treatment conditions, as outlined in Table 6, following the schedule of Fig. 73. To evaluate pharmaceutical ferroptotic protection, cells were pre-treated for one hour with two anti-ferroptotic drugs: the radical-trapping antioxidants liproxstatin-1 (LPX) (SML1414, Sigma-Aldrich) and iron chelator deferiprone (DFP) (379409, Sigma-Aldrich). This was followed by a 24-hour exposure to the respective treatments. Additionally, a well-established model, 1-methyl-4-phenylpyridinium (MPP^+) (D048, Sigma-Aldrich), was used to assess the relative toxicity of UFP in the context of PD.

Table 6: Six working conditions, all with the first post-treatment for 1h, followed by a 24h-treatment.

N°	Condition	First treatment (1h)	Second treatment (24h)
1	Negative control (NC)	Medium	Medium
2	Positive control PD-like phenotype	Medium	5 µM MPP^+
3	Low dose UFP	Medium	2 µg/cm²
4	High dose UFP	Medium	10 µg/cm²
5	Ferroptotic protection (iron chelator) + high dose of UFP	100 µM DFP	10 µg/cm²
6	Ferroptotic protection (lipid ROS-protection) + high dose of UFP	2 µM LPX*	10 µg/cm²

*LPX was dissolved in a final concentrations of 0.004% DMSO. To ensure that this concentration did not induce molecular alterations, a specific NC for LPX was set up by exposing LUHMES cells to 0.004% DMSO for 24 hours. Results from these controls consistently showed no significant effects on metabolism (Cf. Supplemental Data Fig. S7, p. 252), the morphology of the cells were normal, and are therefore not described further in this document.

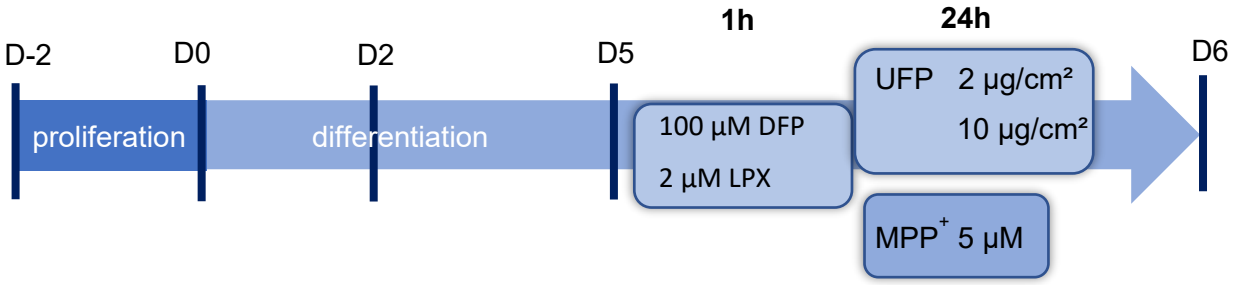

Figure 73: Exposure scheme of LUHMES cells.

At day 5, mature dopaminergic neurons are exposed to their corresponding exposure treatment for 24h (UFP or MPP^+), with or without a pre-treatment of anti-ferroptotic drugs (100 µM DFP or 2µM LPX) for one hour.

Abbreviations: DFP: Deferiprone; LPX: Liproxstatin-1; MPP^+: 1-Methyl-4-phenylpyridinium; UFP: Ultrafine Particles.

Depending on the research assay and the targeted RCD pathway, specific inducers were used as positive controls, as listed in Table 7. The concentrations and incubation times were determined based on previously published results from our lab (Do Van *et al.*, 2016) and dose-response experiments conducted in-house.

Table 7: Three different positive controls depending on the regulated cell death investigation.

N°	RCD-form	Treatment	Incubation time
7	Ferroptosis	20 nM RSL3** (Ref: S8155, Selleckhem)	6h
8	Apoptosis	0.5 and 1 µM Staurosporine (STS) (Ref: S4400, Sigma-Aldrich)	24h
9	Autophagy	15 µM Rapamycin (Rapa) (Ref: S1039, Selleckhem)	24h

** RSL3 was dissolved in a final concentrations of 0.0002% DMSO. To ensure that this concentration did not induce molecular alterations, a specific NC for RSL3 was set up by exposing LUHMES cells to 0.0002% DMSO for 6 hours. Results from these controls consistently showed no significant effects on metabolism (Cf. Supplemental Data Fig. S7, p. 252), the morphology of the cells were normal, and are therefore not described further in this document.

For protein recuperation, cells were scratched with 150 µL/well of Radio-Immunoprecipitation Assay (RIPA) lysis buffer completed with 1% protease-phosphatase inhibitor, sonicated for 20 seconds, then subjected to a final differential centrifugation. The total protein fraction of the supernatant was quantified using the BCA Protein Assay kit (ThermoFisher®, Waltham, MA).

II.6 Analyzing cell death

II.6.1 Ferroptosis

Ferritin quantification

Ferritin, the primary intracellular iron-storage protein, was measured using the MSD® R-PLEX Antibody Sets & Singleplex Assays (K151ADAR-2), in a classical ELISA-based microarray format according to the kit instructions. The 96-well R-PLEX plate was coated with a streptavidin-biotinylated captured primary antibody. Subsequently, standard or sample protein extracts (1:1000 dilution) were added. After washing, the sandwich was completed with an electrochemical detection antibody. Measurements were performed by adding the reading buffers and using the MESO QuickPlex SQ 120 instrument (MSD) with Recovery Workbench software. The Ferritin levels (pg/mL) were normalized to protein concentrations.

4-HNE quantification

Quantification of 4-HNE adducts in cell lysates is performed using the same protocol as in 4-hydroxynonenal adducts ELISA electrochemiluminescence analysis (Cf. p. 93).

GPx activity

The Glutathione Peroxidase Activity Assay kit (Fluorometric) from Abcam® (# ab219926) provides a method for measuring GPx activity in cell lysates. The kit is based on the two redox reactions of GSH. While GPx is active and oxidizes GSH, there is a counter-reaction of glutathione reductase (GR), which reduces GSSG and oxidizes NADPH into $NADP^+$. $NADP^+$ levels are directly related to GPx activity. The assay is based on a $NADP^+$ probe which generates a fluorescent product. The presence of fluorescence is monitored by a kinetic fluorescence measurement at 420/480 nm (Ex/Em), every 2 min for a total of 60 min. The elevated presence of the fluorescent product is proportional to the GPx activity presented in samples. The reaction rate (ΔRFU/min) was first calculated, and then interpolated onto the standard curve to determine the GPx activity.

Glutathione assay

The GSH, GSSG and GSH/GSSG ratio was determined using the same Promega® bioluminescence kit as described in section II.9.5 Ferroptosis (Cf. p. 92).

Protein expression of xCT/SLC7A11, cGPx4, TfR, DMT1, P53

Protein expression levels of specific ferroptotic biomarkers were measured using standard WB procedures, as already mentioned in II.7.2 Protein expression of the antioxidant NRF2-pathway by Western blot (Cf. p. 87).

This with adapted primary Ab (SLC7A11/xCT: 1/1000 Cell Signaling, #12691 (Mw 35 kDa); cGPx4: 1/1000 Cell Signaling #52455 (Mw 20 kDa); TfR: 1/1000 Abcam #Ab84036 (Mw 98 kDa); DMT1/SLC11A2 (D3V8G): 1/1000 Cell Signaling #15083 (Mw 70-100 kDa); P53: 1/1000 R&D Systems (Minneapolis, MN) #MAB1746 (Mw 53 kDa)).

II.6.2 Apoptosis

Protein expression of BAX

To investigate BAX by WB analysis, the protocol of II.7.2 Protein expression of the antioxidant NRF2-pathway by Western blot (Cf. p. 87), was slightly adapted by changing the primary Ab, in BAX (1/1000 Cell Signaling #2772 (Mw 20 kDa)).

Caspase-3/7, -8, and -9 activity

Caspase activity was measured using three independent luminescence-based assays: Caspase-Glo® 3/7 (G8091, Promega); Caspase- Glo® 8 (G8201, Promega), Caspase- Glo® 9 (G8211, Promega) Assay System. For each assay, specific Caspase-Glo reagents were prepared according to the manufacturer's instructions. Equal volumes of caspase-specific reagent (Caspase-3/7 activity was assessed using DEVD-aminoluciferin; Caspase-8 using LETD-aminoluciferin, and Caspase-9 using LEHD-aminoluciferin) and protein sample were mixed and incubated for 20 minutes at room temperature. After incubation, bioluminescence was measured using the Spark® multimode microplate reader (TECAN).

II.6.3 Autophagy

Protein expression of NCOA4 and LC3b-II/I

The Western blot protocol for NCOA4 detection followed the methodology outlined for ferroptotic markers (Cf. II.7.2 Protein expression of the antioxidant NRF2-pathway by Western blot, p. 87), adapted with the primary Ab for NCOA4 detection, namely Cell Signaling #66849 (1/1000; Mw 80 kDa)).

However, the protocol for LC3b-II/I required additional adjustments due to the close proximity of the molecular weights of LC3b-II (17 kDa) and LC3b-I (19 kDa). To achieve better protein separation between the 10 and 20 kDa range, the Novex Mini Cell (ThermoFisher®) was used with 1X MES SDS Running Buffer. The primary antibody used for LC3b detection was Novus Biologicals NB100-2220 (1/1000; Mw 17-19 kDa).

II.7 Statistical analysis

Data are presented as mean ± standard deviation (SD). Normality of data distribution was assessed using the Shapiro-Wilk test prior to statistical analysis.
For oxidative potential, assessed by the DTT test (n=4 replicates), data were normally distributed, and ANOVA was performed. Cell metabolism and viability were evaluated based on the percentage of fluorescence signal relative to UFP concentration (n=6 biological replicates). As data were not normally distributed, statistical comparisons

across UFP concentration ranges were conducted using the Kruskal-Wallis test, as detailed in the figure legends.

For all other experiments (except Western Blot analysis), n=3 biological replicates and n=2 technical repeats were included (total of n=6 replicates). Group comparisons were performed using the non-parametric Mann-Whitney U test. In case of Western Blot analysis (n=3 replicates), data were normally distributed, and unpaired t-test was applied. Statistical significance was defined as *$p<0.05$, **$p<0.01$, ***$p<0.001$, and ****$p<0.0001$. All statistical analyses were performed using GraphPad Prism 9 Software.

III. RESULTS

III.1 Concentration-related effects of UFP on oxidative potential do not alter cell metabolism or viability in differentiated LUHMES cells after 24 hours of exposure

III.1.1 DTT-assay

All UFP conditions (i.e., 2, 10, 40, 80 µg/cm²) exhibited a significant dose-dependent increase in DTT oxidation. At 2 µg/cm², the average DTT consumption was 9.73% ($p<0.001$), while at 10 µg/cm², it reached 21.10% ($p<0.0001$) (Fig. 74).

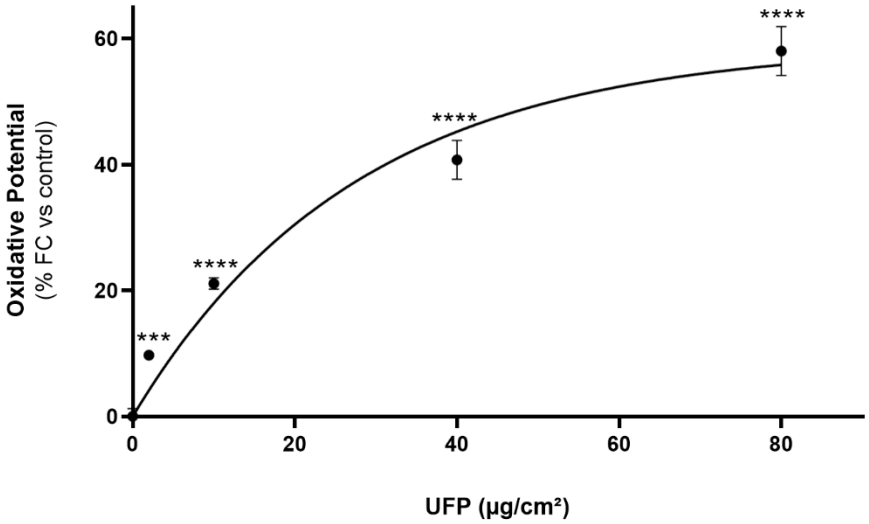

Figure 74: Oxidative potential increases by increased ultrafine particle concentrations (µg/cm²).

The rate of Reactive Oxygen Species (ROS) generation catalyzed by ambient ultrafine particles (UFP) is measured by the dithiothreitol (DTT) assay. Our conditions include a negative control, containing 0 µg/cm² particles, and a range of UFP concentrations (2, 10, 40, and 80 µg/cm²). For UFP compared to control, we observed a dose-dependent trend in oxidative potential.

(FC: Fold Change; n=4; mean ± SD; ANOVA, ***p<0.001, ****p<0.0001)

Abbreviations: DTT: Dithiothreitol; ROS: Reactive Oxygen Species; UFP: Ultrafine Particles.

III.1.2 Resazurin and G6PD Release Fluorescence Assays

After differentiation, LUHMES cells were exposed to a range of UFP concentrations, namely 0, 2, 5, 10, 20, 30, 40 µg/cm² for 24 hours, after which cell metabolism was assessed using the Resazurin Fluorescence Assay, and viability was determined using the G6PD Release Assay. Neither significant changes in fluorescence were observed in

the Cell Viability nor in the Metabolism Assay following UFP exposure, except for the 40 µg/cm² condition in the Cell Viability Assay (Fig. 75).

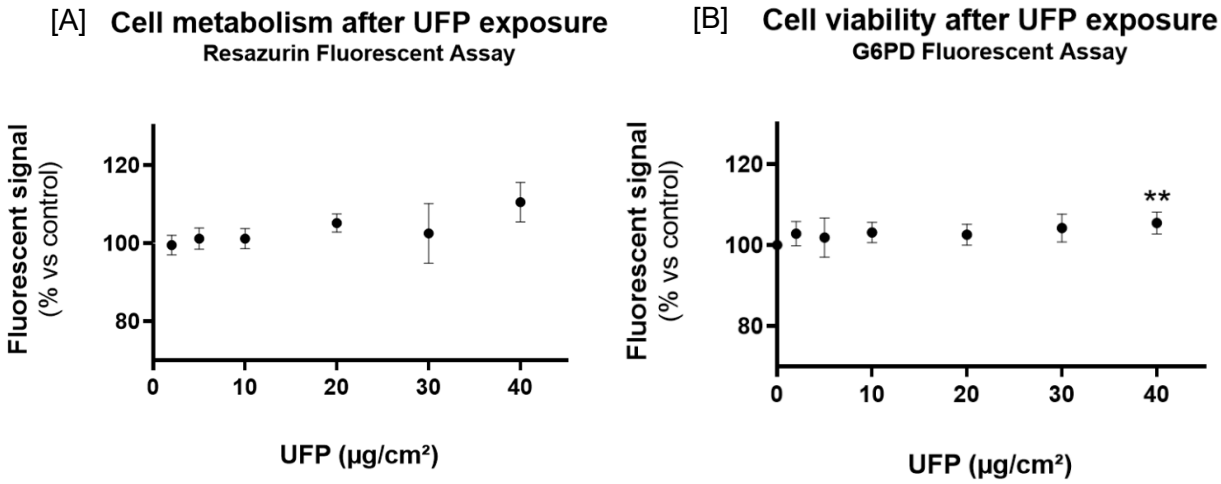

Figure 75: Metabolic activity and cell viability of LUHMES cells exposed to a range of UFP concentrations (0-40 µg/cm²).

[A] After 24-hour exposure, metabolic activity assessed using Resazurin Fluorescence Assay revealed no significative changes. [B] Cell Viability evaluated via the G6PD Fluorescent Assay had only a significant difference after 40 µg/cm².
All results are described in % of Fluorescent signal compared to control cells (0 µg/cm² UFP).

(n=6; mean ± SD; Kruskal-Wallis test, **p<0.01)

Abbreviations: G6PD: Glucose-6-Phosphate Dehydrogenase; UFP: Ultrafine Particles.

III.2 Ferroptotic markers in SN neuronal dopamine-like LUHMES cells

Due to the heterogeneity observed in resazurin assay results at higher UFP exposure concentrations and to expose to more realistic exposure scenarios, we focused on **UFP** concentrations of **2 and 10 µg/cm²** for subsequent experiments, maintaining a 24-hour exposure period.

For comparative purposes, cells were also treated with **MPP^+**, a well-characterized neurotoxin that selectively targets dopaminergic neurons, to mimic a PD-phenotype. This comparison provided insights into the relative toxicity of UFP.

To explore ferroptosis, we evaluated the protective effects of two ferroptosis inhibitors, **LPX or DFP**, on LUHMES cells exposed to 10 µg/cm². LPX acts by inhibiting lipid peroxide propagation, while DFP chelates free cellular iron, both of which are key mediators of ferroptosis, but acts in a different way.

As a positive control for ferroptosis, cells were treated for 6 hours with 20 nM **RSL3**, a potent inhibitor of GPx4 that binds its selenium co-factor, inducing ferroptotic cell death.

III.2.1 Intracellular iron homeostasis is not disturbed after 24 hours iron-containing UFP exposure.

Cellular iron import

To assess the levels of TfR and DMT1/SLC11A2, we performed WB analysis on samples from eight experimental groups: the 6-hour control (NC (6h)), the 6-hour RSL3 treatment, the 24-hour control (NC (24h)), the MPP^+ treatment, the UFP exposed groups (2 and 10 µg/cm^2), the DFP-treated group with 10 µg/cm² UFP, and the LPX-treated group with 10 µg/cm² UFP.

As shown in Fig. 76, no statistically significant changes in TfR and DMT1 expression levels were observed between the MPP^+ and the UFP treatment groups compared to the controls ($p > 0.05$). This indicates that neither MPP^+ nor UFP treatments altered the expression of those iron import proteins. As a positive control for ferroptosis, TfR expression was reduced in the RSL3 condition ($p < 0.05$), but no significant changes were detected in DMT1 levels. For the anti-ferroptotic drug co-treatment, DFP significantly increased TfR ($p < 0.05$), but this effect was not observed for DMT1. In contrast, LPX in combination with 10 µg/cm² UFP, did not alter TfR or DMT1 levels.

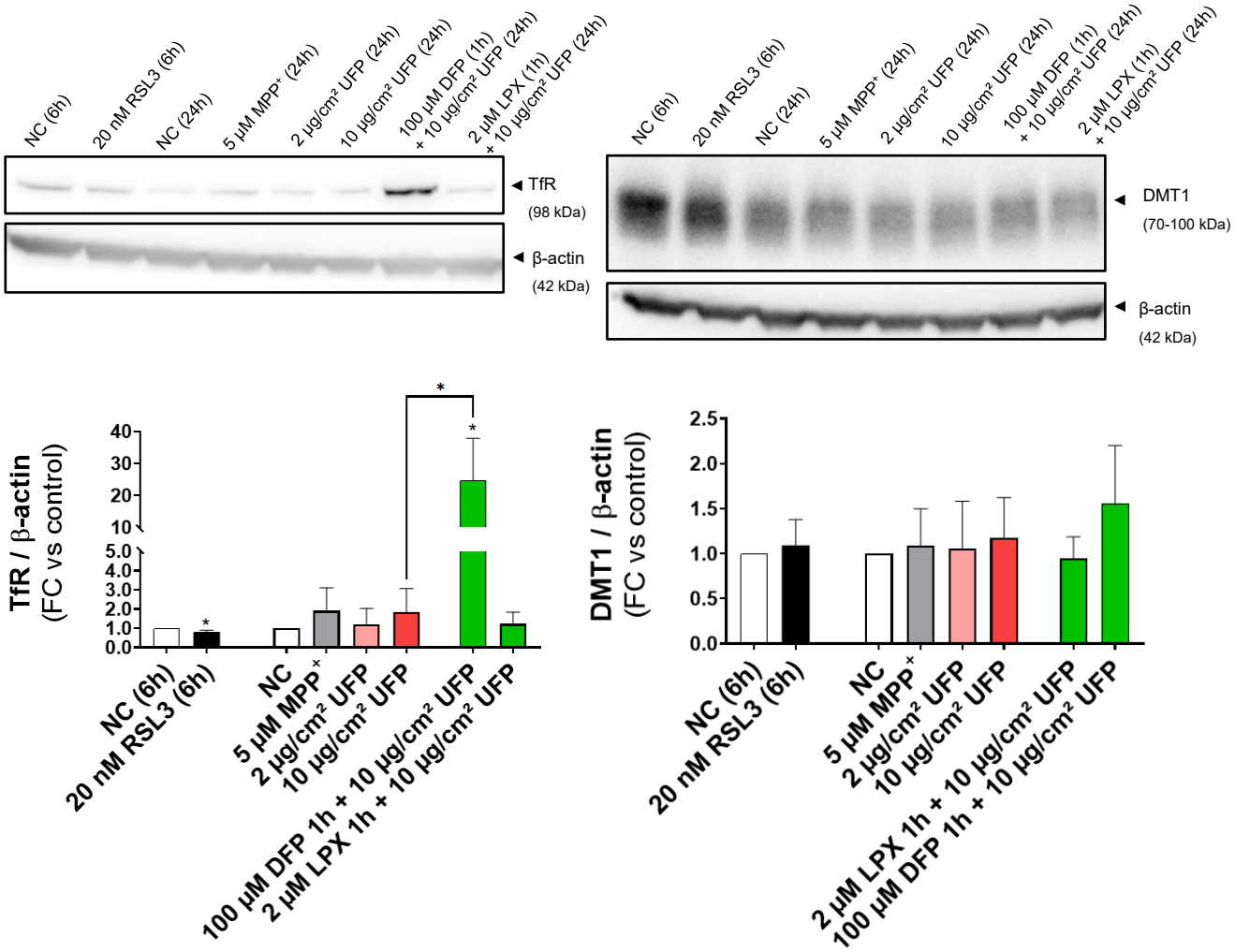

Figure 76: No significant cellular iron import by Transferrin Receptor (TfR) and Divalent Metal Transporter 1 (DMT1) after UFP exposure or MPP⁺ treatment.

Western blot analysis of TfR and DMT1 expressed as fold change, showed no significant changes after 2 or 10 µg/cm² UFP or 5 µM MPP⁺ exposure for 24 hours in differentiated LUHMES cells. TfR was slightly but significantly decreased in the RSL3 treatment group. LPX was unchanged, but DFP exposure elevated TfR protein expression approximately 25-fold compared to controls, without statistical differences for DMT1 levels.

(FC: Fold Changes; n=3; mean ± SD; unpaired t-test, *p<0.05)

Abbreviations: DMT1: Divalent Metal Transporter 1; DFP: Deferiprone; LPX: Liproxstatin-1; LUHMES: Lund Human Mesencephalic Cells; MPP⁺: 1-Methyl-4-phenylpyridinium; RSL3: Ras-Selective Lethal; TfR: Transferrin Receptor; UFP: Ultrafine Particles.

Intracellular iron storage

The ELISA analysis of ferritin concentrations in LUHMES cells exposed to UFP (2 and 10 µg/cm²) and MPP^+ revealed distinct effects on intracellular iron storage. In graph of Fig. 77, it is demonstrated that UFP exposure did not result in statistically significant changes in ferritin levels compared to the control group ($p > 0.05$). However, exposure to MPP^+ significantly reduced ferritin concentrations ($p < 0.05$). Similarly, RSL3, a ferroptotic inducer, caused significant decrease in ferritin levels ($p < 0.05$). Among the ferroptotic inhibitors, DFP treatment drastically lowered ferritin concentrations (14.08 ±4.6; $p < 0.01$), while LPX co-treatment with UFP did not alter ferritin levels ($p > 0.05$).

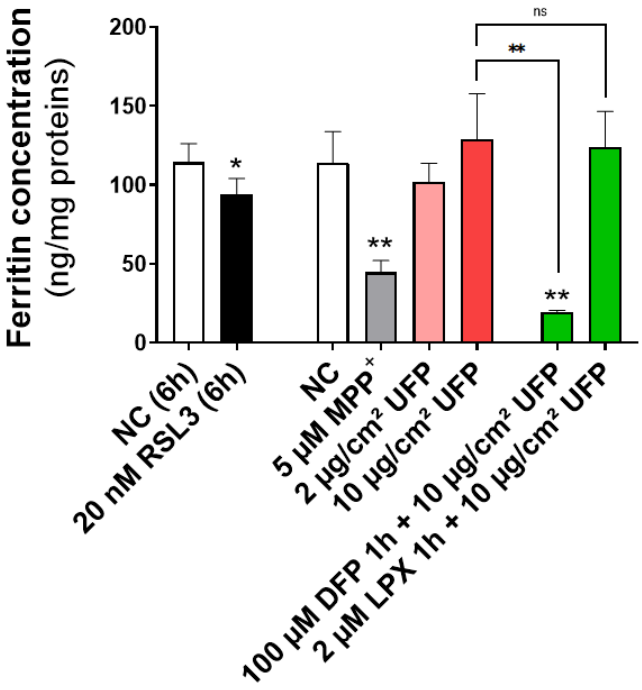

Figure 77: Ferritin levels remain unaffected by ultrafine particle exposure, but decreased in MPP^+ conditions.

Ferritin concentration (ng/mg of total protein) were assessed by ELISA under various conditions of exposed differentiated LUHMES cells. Ultrafine particles (UFP) exposure (with and without Liproxstatin-1 (LPX) co-treatment) did not significantly alter ferritin levels compared to negative control (NC). In contrast, 1-Methyl-4-phenylpyridinium (MPP^+) treatment (5 µM) and Ras-Selective Lethal (RSL3) (20 nM) significantly reduced ferritin concentrations. Deferiprone (DFP) treatment led to a marked decrease in ferritin levels.

(n=6; mean ± SD; non-parametric Mann-Whitney U test, *p<0.05; **p<0.01)

Abbreviations: DFP: Deferiprone; LPX: Liproxstatin-1; LUHMES: Lund Human Mesencephalic Cells; MPP^+: 1-Methyl-4-phenylpyridinium; NC: Negative Control; RSL3: Ras-Selective Lethal; UFP: Ultrafine Particles.

NB: The results suggest that concentration of DFP is too high, leading to excessive iron depletion, which is also toxic for dopaminergic neurons. UFP from Dunkirk contain a high level of iron comparing other sourced urban UFP, however, the iron amount is generally

small (10,267.0 µg/g), and the calculated total iron derived from 10 µg/cm² UFP in a 6-well plate is approximately 0.985 µg. The strong chelating effect of DFP likely exceeds the amount of external iron provided by UFP, potentially disrupting intracellular iron storage in organelles such as the mitochondria or lysosomes. This disruption might contribute to cellular toxicity, thereby diminishing DFP's protective effects. Consequently, the condition of 100 µM DFP (1h) combined with 10 µg/cm² UFP was excluded from further experiments.

III.2.2 Cytosolic GPx4 depletion and elevated lipid peroxidation following UFP exposure

Cytosolic GPx4 main enzyme during ferroptosis

The cGPx4 isoform, which is crucial for preventing lipid peroxidation, investigated by Western blot, was downregulated after high UFP exposure (significant at 10 µg/cm²; $p < 0.05$), as shown in Fig. 78. When 10 µg/cm² UFP is combined to pre-treatment of LPX, no significant level of decreased cGPX4 is measured, suggesting a protective effect of LPX against lipid peroxidation. Quantitative analysis showed that RSL3 or MPP^+ did not significantly affect cGPx4 levels compared to the control group ($p > 0.05$).

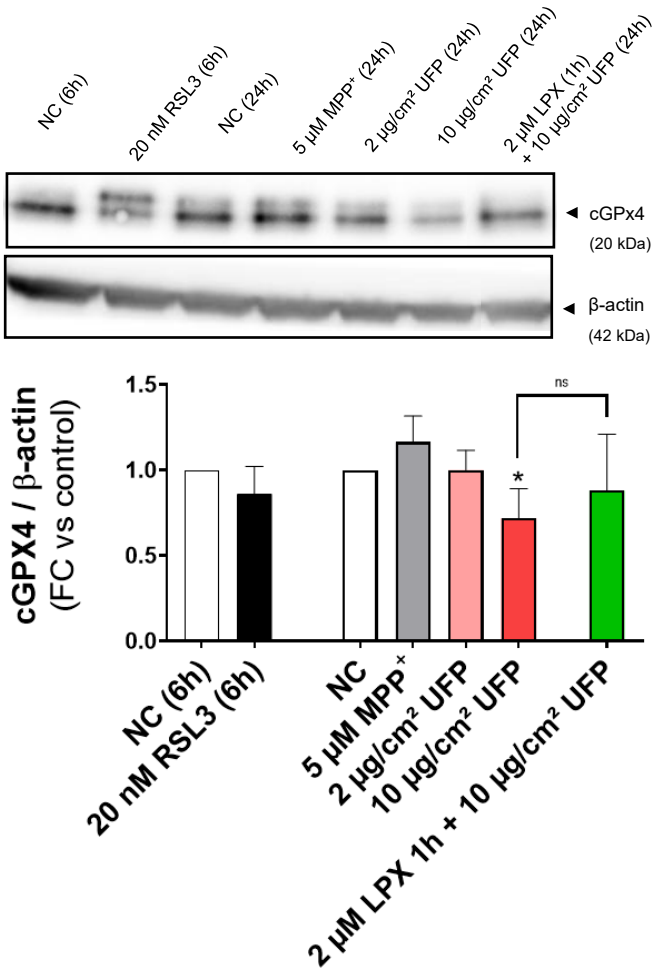

Figure 78: Cytosolic GPx4 (cGPx4) decreased in differentiated LUHMES cells exposed to 10 µg/cm² ultrafine particles.

Western Blot analysis of cGPx4, the main enzyme for reducing lipid peroxides in the cellular membrane. Ras-Selective Lethal (RSL3), 1-Methyl-4-phenylpyridinium (MPP^+), and 2 µg/cm² ultrafine particles (UFP) did not change the amount of cGPX4, whereas 10 µg/cm² UFP significantly depleted cGPx4. The combination of 2 µM LPX with 10 µg/cm² UFP had the physiological amount of cGPx4.

(FC: Fold Changes; n=3; mean ± SD; unpaired t-test, *p<0.05)

Abbreviations: cGPx4: cytosolic GPx4; LPX: Liproxstatin-1; LUHMES: Lund Human Mesencephalic Cells; MPP^+: 1-Methyl-4-phenylpyridinium; RSL3: Ras-Selective Lethal; UFP: Ultrafine Particles.

4-HNE adducts, lipid peroxidation marker

In mono-culture conditions, the lipid peroxidation marker 4-HNE adducts was significantly elevated only after exposure to 2 µg/cm² UFP. Although, MPP^+ and 10 µg/cm² UFP showed a tendency toward increased levels, the high variability (large SD) prevented statistical significance. The RSL3 condition did not differ significantly from the control ($p > 0.05$), as illustrated in the graph of Fig. 79.

Additionally, while the comparison of 10 µg/cm² UFP exposure with and without LPX co-treatment was not significant, however, there was a noticeable trend suggesting that LPX could mitigate 4-HNE adducts in the presence of UFP.

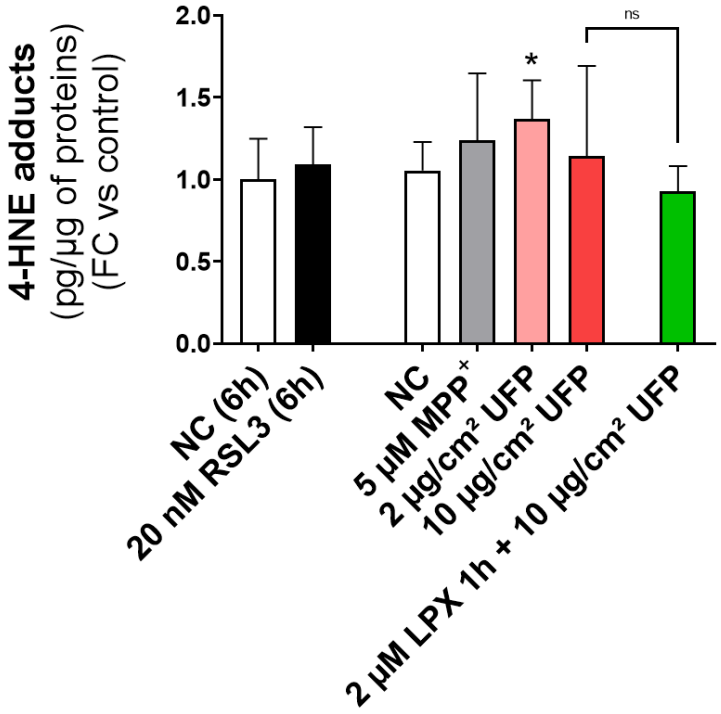

Figure 79: 4-hydroxynonenal (4-HNE) adducts level to reflect the amount of lipid peroxidation.

No significant results are observed after Ras-Selective Lethal (RSL3), 1-Methyl-4-phenylpyridinium (MPP^+) and 10 µg/cm² Ultrafine particles (UFP) in differentiated Lund Human Mesencephalic Cells (LUHMES) cells, probably due to the high variation. But exposure to 2 µg/cm² UFP led to a significative increase of 4-HNE adducts.
The differences between 10 µg/cm² UFP exposure and LPX in combination with 10 µg/cm² was also not significative.

(n=6; mean ± SD; non-parametric Mann-Withney U test; *p<0.05, **p<0.01)

Abbreviations: 4-HNE: 4-hydroxynonenal; LPX: Liproxstatin-1; LUHMES: Lund Human Mesencephalic Cells; MPP^+: 1-Methyl-4-phenylpyridinium; RSL3: Ras-Selective Lethal; UFP: Ultrafine Particles.

III.2.3 Downstream compensatory response of MPP^+ and UFP exposure: Activation of Gpx enzymes, GSH-ratio depletion, reduced x_c^- levels and increased p53 protein levels.

Overall GPx activity

As shown in Fig. 80, the overall GPx activity did not changed after RSL3 treatment compared to NC. But following exposure to MPP^+, and 2 µg/cm² and 10 µg/cm² UFP, an increase in GPx activity was detected (MPP^+: $p < 0.05$; 2 µg/cm² and 10 µg/cm²: $p <$

0.01). The co-treatment of 2 µM LPX in combination with 10 µg/cm² led to significant less activated GPx's ($p < 0.01$), and there was also a difference between 10 µg/cm² alone and in combination with LPX ($p < 0.01$).

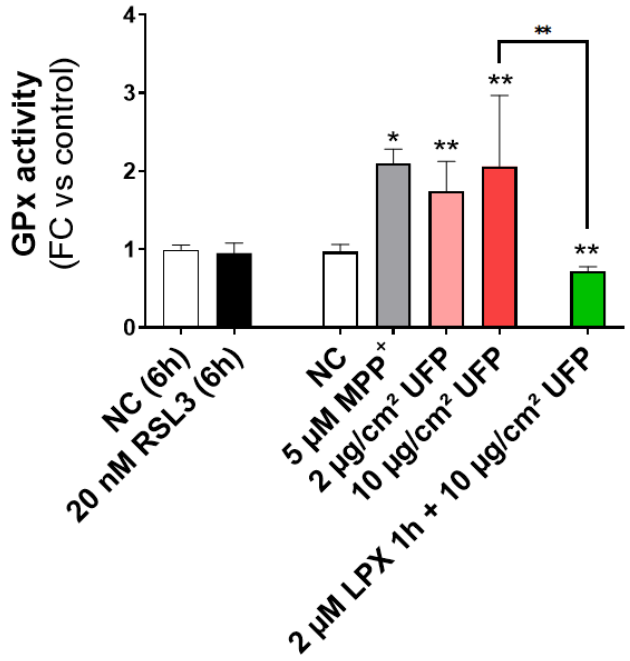

Figure 80: Glutathione Peroxidase (GPx) activity is increased after ultrafine particles exposure and MPP^+ treatment, and decreased upon co-treatment with LPX.

Oxidative stress led to the activation of GPx enzymes to counteract intracellular Reactive Oxygen Species (ROS). Total GPx activity is significantly induced after 5 µM 1-Methyl-4-phenylpyridinium (MPP^+) and 2 or 10 µg/cm² Ultrafine Particles (UFP), and downregulated when differentiated LUHMES cells are co-exposed to LPX before 10 µg/cm² UFP.

(n=6; mean ± SD; non-parametric Mann-Whitney U test, *p<0.05; **p<0.01)

Abbreviations: GPx: Glutathione Peroxidase LPX: Liproxstatin-1; LUHMES: Lund Human Mesencephalic Cells; MPP^+: 1-Methyl-4-phenylpyridinium; RSL3: Ras-Selective Lethal; ROS: Reactive Oxygen Species; UFP: Ultrafine Particles.

Three key results of the Glutathione (GSH) assay: GSH, GSSG, and GSH/GSSG

GSH acts as an antioxidant and is a key component of the non-enzymatic defense against oxidative stress. In cells exposed to UFP, both concentrations 2 µg/cm² ($p < 0.05$) and 10 µg/cm² ($p < 0.01$) resulted in a depletion in GSH amount. GSSG was significantly elevated after MPP^+ ($p < 0.01$) and remained unchanged in UFP-exposed conditions ($p > 0.05$). The glutathione ratio is expressed in reduced GSH to its oxidized form, GSSG. The GSH/GSSG ratio was decreased in differentiated LUHMES cells exposed to 5 µM MPP^+ or 2 and 10 µg/cm² UFP (MPP^+: $p < 0.01$; 2 µg/cm² and 10 µg/cm²: $p < 0.05$). No statistical differences were observed in cells post-exposed to 2 µM

LPX followed by 10 µg/cm² UFP or in the RSL3 treated condition ($p > 0.05$). Graphs are represented in Fig. 81.

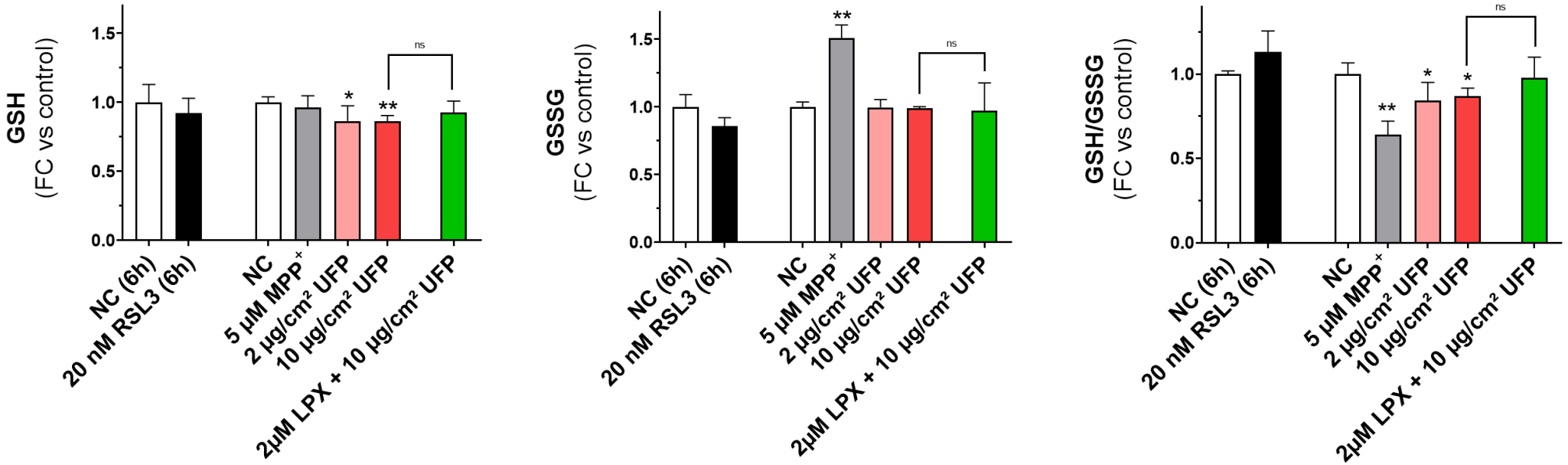

Figure 81: Reduced glutathione (GSH), Oxidized glutathione (GSSG), and the Glutathione ratio (GSH/GSSG) revealed the level of oxidative stress in MPP^+ and ultrafine particles conditions.

Through bioluminescence assays it was found that reduced GSH decreased in UFP-exposed LUHMES cells (2 µg/cm², $p < 0.05$; 10 µg/cm², $p < 0.01$). Oxidized GSSG increased after MPP^+ exposure ($p < 0.01$) but remained stable in UFP conditions ($p > 0.05$). The GSH/GSSG ratio was reduced in differentiated LUHMES cells exposed to 5 µM MPP^+ or 2 and 10 µg/cm² UFP (MPP^+: $p < 0.01$; 2 µg/cm² and 10 µg/cm²: $p < 0.05$). No differences were observed with 2 µM LPX in combination with 10 µg/cm² UFP, or after RSL3 treatment.

(FC: Fold Changes; n=6; mean ± SD; non-parametric Mann-Whitney U test, *p<0.05; **p<0.01)

Abbreviations: GSH: Glutathione (Reduced), GSSG: Oxidized Glutathione: GSH/GSSG: Glutathione Ratio; LPX: Liproxstatin-1; LUHMES: Lund Human Mesencephalic Cells; MPP^+: 1-Methyl-4-phenylpyridinium; RSL3: Ras-Selective Lethal; UFP: Ultrafine Particles.

xCT/SLC7A11 subunit responsible for substrate-specific transport of x_c^-

The expression of SLC7A11 (xCT), a subunit of the cystine/glutamate antiporter x_c^- essential for GSH synthesis, was significantly reduced following exposure to MPP^+ ($p < 0.01$) and UFP (2 µg/cm² ($p < 0.01$), respectively). LPX treatment mitigated the reduction, increasing SLC7A11 expression by approximately 1.5-fold compared to the standard amount ($p < 0.01$). RSL3 and 10 µg/cm² UFP did not significantly change the levels of SLC7A11 ($p > 0.05$). Fig. 82 represents the WB image and graphical visualization.

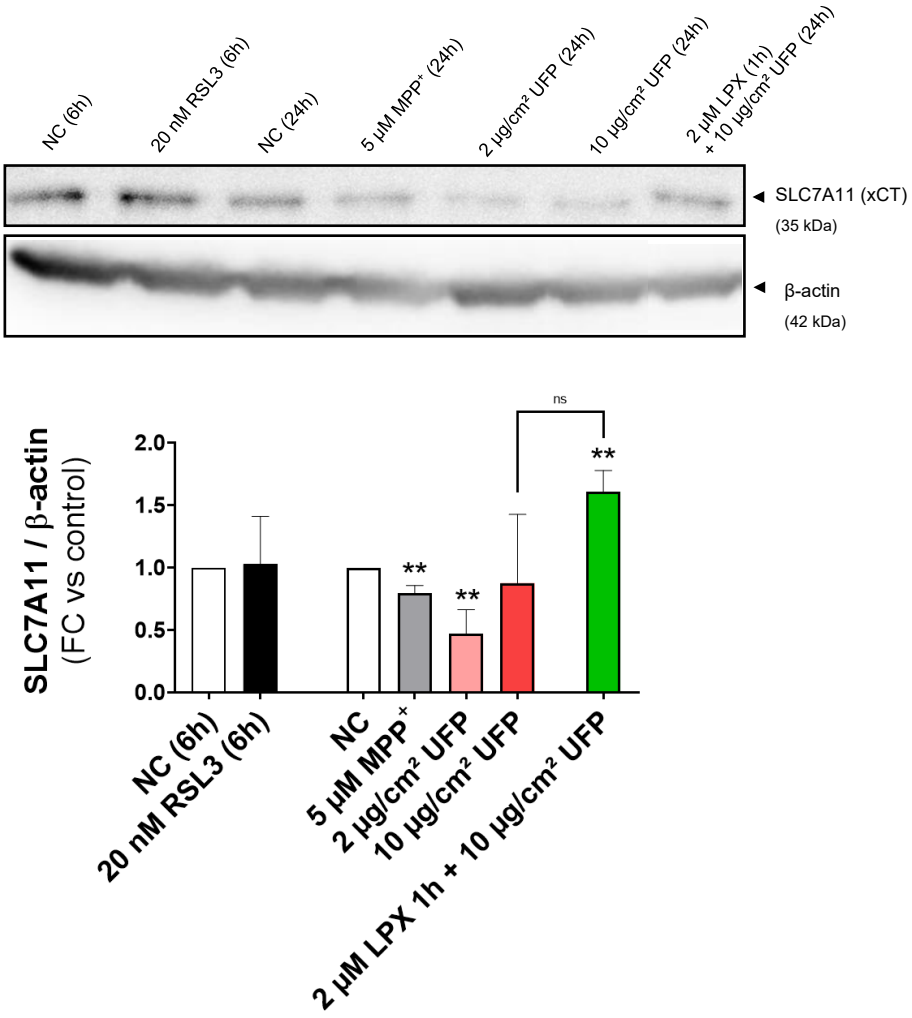

Figure 82: Protein expression of SLC7A11 was downregulated after MPP^+ and 2 µg/cm² UFP, but showed a significant elevation when co-treated with LPX.

The lipid membrane-incorporated cystine/glutamate antiporter x_c^- is composed of a heavy chain (4F2hc, SLC3A2) and a light chain (xCT, SLC7A11). Quantification revealed reduced SLC7A11 in mono-treated LUHMES cells with 5 µM MPP^+ and 2 µg/cm² UFP. Co-treatment with the anti-ferroptotic drug LPX (2 µM) in combination with 10 µg/cm² UFP resulted in increased SLC7A11 protein levels, although there was no significant difference compared to 10 µg/cm² UFP alone. Cells treated with RSL3 did not change significantly the amount of SLC7A11.

(FC: Fold Changes; n=3; mean ± SD; unpaired t-test, **p<0.01)

Abbreviations: LPX: Liproxstatin-1; LUHMES: Lund Human Mesencephalic Cells; MPP+: 1-Methyl-4-phenylpyridinium; RSL3: Ras-Selective Lethal; UFP: Ultrafine Particles.

p53, not only a tumor suppressor protein or involved in apoptosis, there is more

Demonstrated in Fig. 83, p53 protein expression was significantly elevated after exposure to 10 µg/cm² UFP ($p < 0.05$). The response at 2 µg/cm² exhibited greater variation, making it not statistically significant. LPX treatment significantly reduced p53 expression ($p < 0.05$). Neither MPP+ nor RSL3 conditions altered p53 levels ($p > 0.05$).

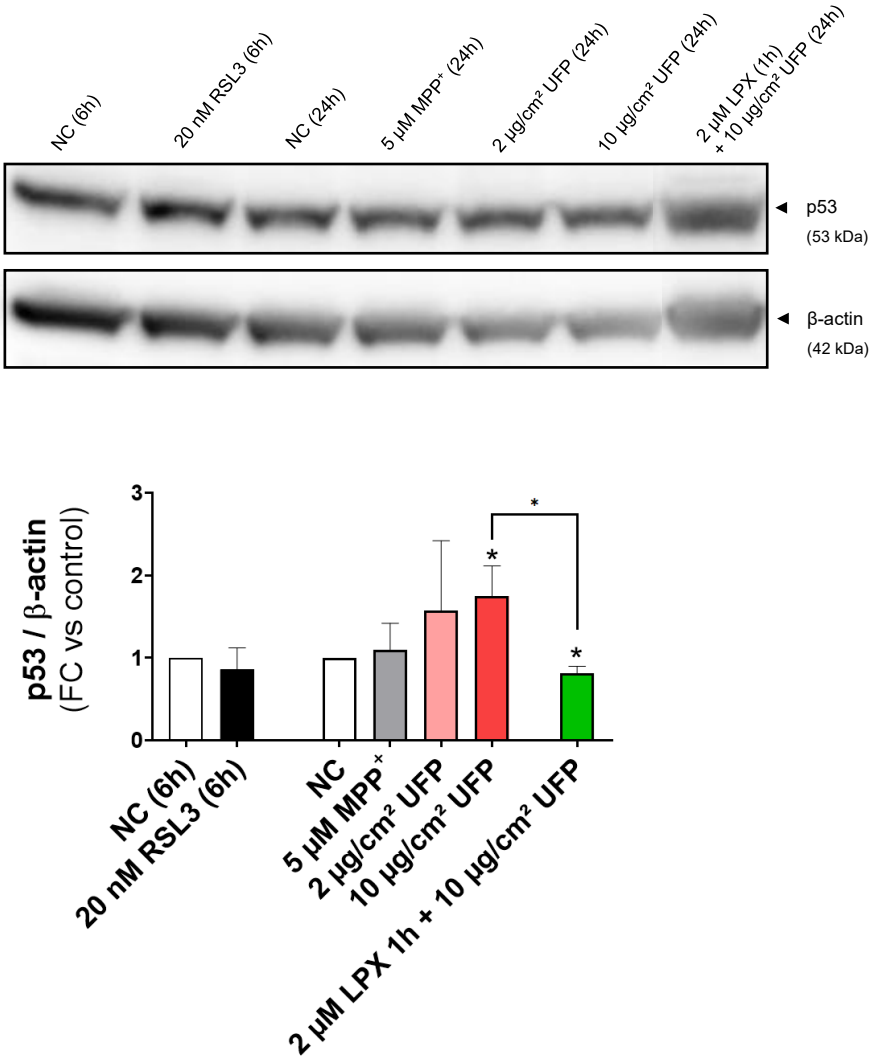

Figure 83: p53 increased upon exposure to UFP, with a significant result after 10 µg/cm² UFP exposure and a significative decrease with LPX co-treatment.

p53, a tumor suppressor protein, is not only involved in the intrinsic apoptosis pathway, but also negatively regulates SLC7A11. By Western blot, p53 protein was significantly elevated in cells exposed to 10 µg/cm² UFP, and decreased when LPX was co-treated with 10 µg/cm² UFP. The differences between UFP exposure alone and LPX co-treatment are statistically significant. RSL3, MPP+, and 2µg/cm² UFP did not significantly alter p53 levels, though there was an increase observed at 2 µg/cm² UFP exposure.

(FC: Fold Changes; n=3; mean ± SD; unpaired t-test, *p<0.05)

Abbreviations: LPX: Liproxstatin-1; LUHMES: Lund Human Mesencephalic Cells; MPP+: 1-Methyl-4-phenylpyridinium; RSL3: Ras-Selective Lethal; UFP: Ultrafine Particles.

III.3 Apoptotic markers in SN neuronal dopamine-like LUHMES cells

III.3.1 MPP^+ exposed neuronal dopamine-like LUHMES cells induce intrinsic and extrinsic apoptosis, which is not significant after UFP exposure.

Bcl-2-associated X protein (BAX) indicator of intrinsic pathway

p53 is known to be a regulator of the intrinsic pathway of apoptosis in response to cellular damage, including DNA damage or oxidative stress. When activated, it acts as a transcription factor for pro-apoptotic genes, such as BAX, after which it can promote MOMP, leading to the release of cytochrome C and activation of caspase-9.

Using WB demonstrated in Fig. 84, our results indicate a significantly higher amount of BAX after exposure to 5 µM MPP^+ ($p < 0.05$). Moreover, the results of UFP-exposures were not significant, but show a dose-dependent tendency ($p > 0.05$).

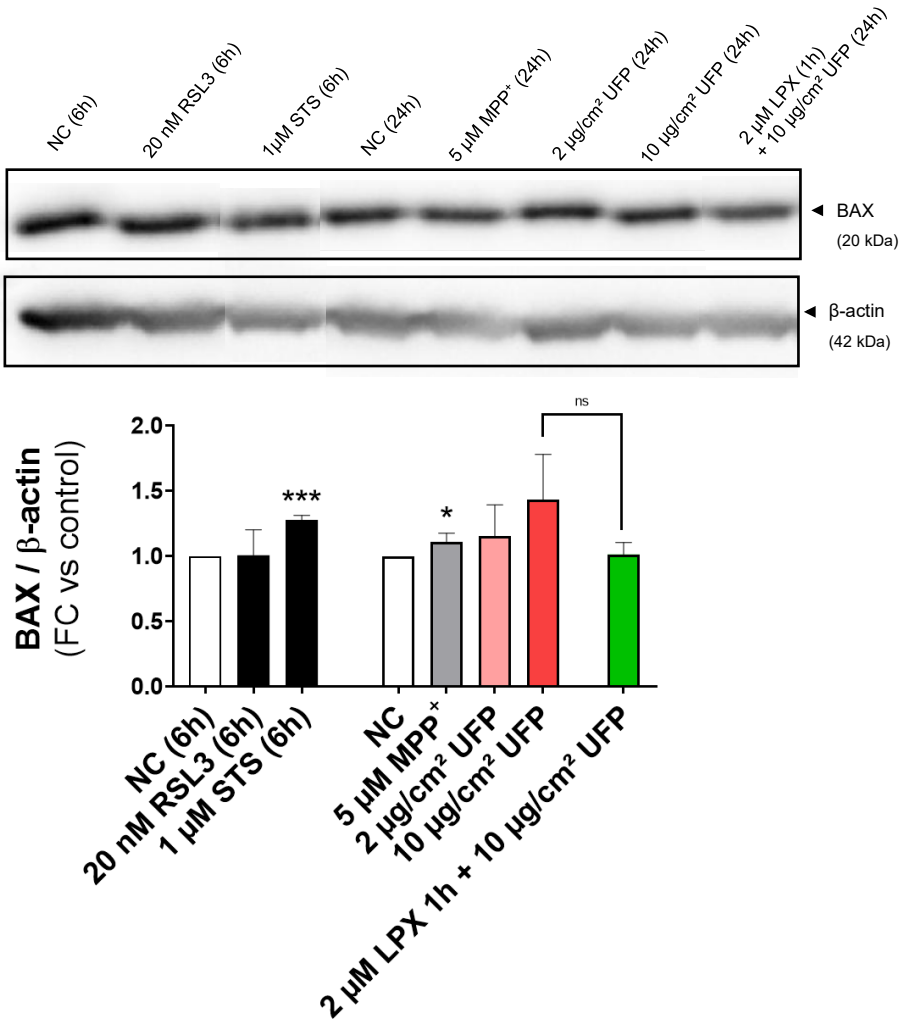

Figure 84: Intrinsic apoptotic Bcl-2-associated X protein (BAX) protein significantly elevated upon MPP⁺ exposure.

BAX is a p53-dependent pro-apoptotic protein that promotes cell death by permeabilizing the mitochondrial membrane, making it a key marker for the initiation of intrinsic apoptosis. However, while exposure to UFP (2 µg/cm² and 10 µg/cm²) gave a trend of elevated BAX protein levels, only 5 µM MPP⁺ differentiated LUHMES cells resulted in significantly higher BAX protein levels. The ferroptotic inducer RSL3 did not led to an increase of BAX, but as normal, the 6-hour treatment with 1µM STS did.

(FC: Fold Changes; n=3; mean ± SD; unpaired t-test, *p<0.05, ***p<0.001)

Abbreviations: LPX: Liproxstatin-1; LUHMES: Lund Human Mesencephalic Cells; MPP⁺: 1-Methyl-4-phenylpyridinium; RSL3: Ras-Selective Lethal; STS: Staurosporine; UFP: Ultrafine Particles.

Caspase cascade

The result of BAX only includes the intrinsic pathway of apoptosis; in order to consider both pathways, also extrinsic, the measurement of several caspase activities was investigated by a luminescence assay. Fig. 85 shows the results, and all measured caspases (-3/7, -8, and -9) were high significantly increased after MPP⁺ treatment ($p < 0.01$). This was not observed after UFP exposure (2 µg/cm² and 10 µg/cm²), nor in combination with LPX.

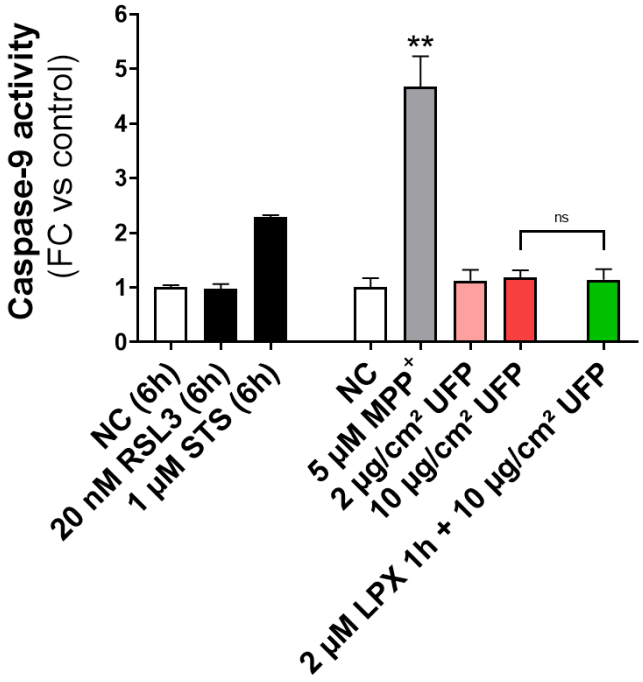

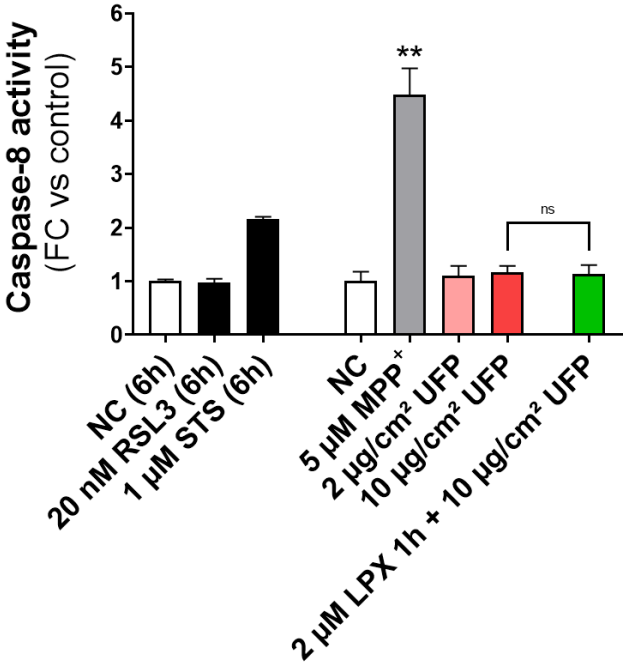

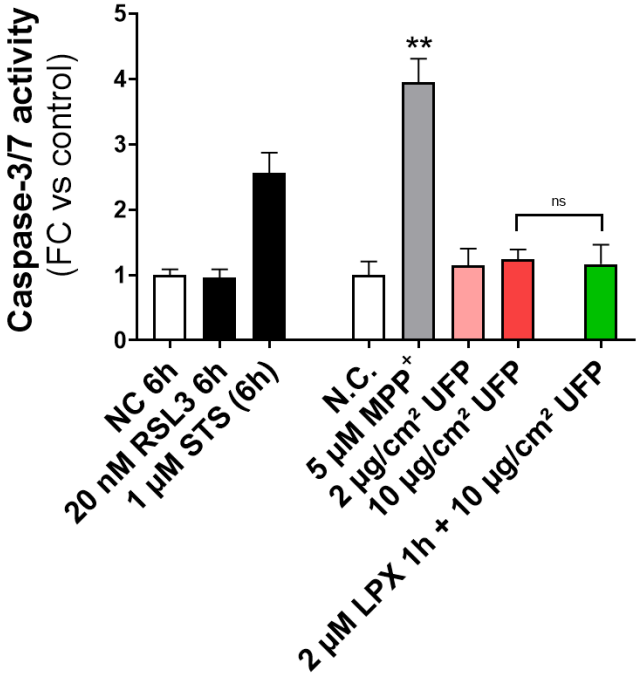

Figure 85: Caspase cascade is activated in cells exposed to MPP⁺.

Both intrinsic (Caspase-9) and extrinsic (Caspase-8) apoptotic pathways end up with downstream activity of caspase-3/7. Surprisingly, exposure to 5 µM MPP⁺ produces approximately a four-fold larger signal of caspase-9, -8 and -3/7 activity compared to NC, and no significant results were observed after UFP (respectively 2 and 10 µg/cm²), nor when 10 µg/cm² was combined with LPX.

(FC: Fold Changes; n=6; mean ± SD; non-parametric Mann-Whitney U test, **p<0.01)

Abbreviations: LPX: Liproxstatin-1; LUHMES: Lund Human Mesencephalic Cells; MPP⁺: 1-Methyl-4-phenylpyridinium; RSL3: Ras-Selective Lethal; STS: Staurosporine; UFP: Ultrafine Particles.

III.4 Ferritinophagy and autophagy markers in SN neuronal dopamine-like LUHMES cells

III.4.1 NCOA4 indicated reduced Ferritinophagy specifically in MPP^+ treated cells, while LC3b activity suggests autophagic cell death in low UFP exposure.

NCOA4 key regulator of ferritinophagy

NCOA4 (Nuclear Receptor Coactivator 4) is a well-established marker of ferritinophagy, the selective autophagic degradation of ferritin. This process releases iron stored in ferritin, contributing to cellular iron homeostasis.

While NCOA4 protein expression was investigated as part of this study, the Western blots produced inconsistent and heterogeneous results, with a poor photographic quality, as illustrated in Fig. 86. Due to the variability in detection and suboptimal signal quality, NCOA4 is present here as a qualitative observation rather than a quantitative result. Except, MPP^+ condition showing reproducible results, with a highly significant decrease in NCOA4 levels compared to the NC ($p < 0.0001$).

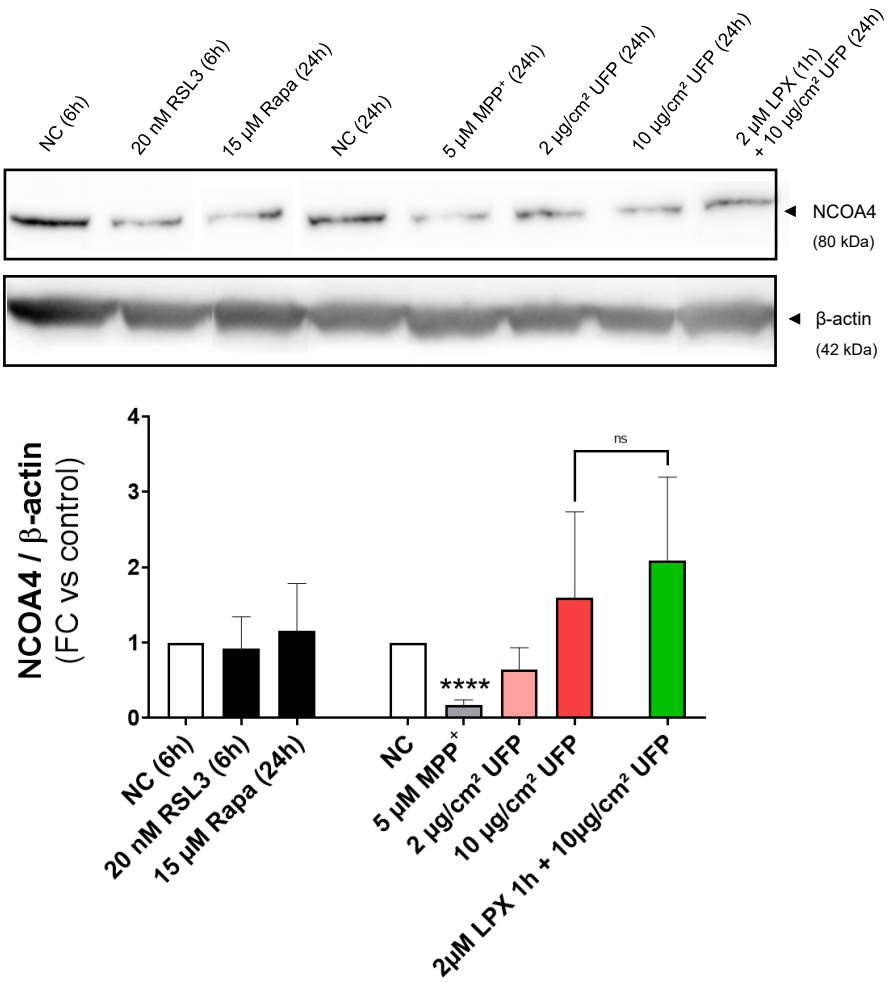

Figure 86: Representative Western blot analysis of NCOA4 expression, with significant depletion observed after MPP⁺ treatment.

While most conditions showed high variability, preventing statistical significance, the positive controls for ferroptosis (RSL3) and autophagy (Rapa) and treatments with UFP (2 and 10 µg/cm²), with or without 2 µM LPX co-treatment, did not yield consistent results compared to the negative control. In contrast, MPP⁺ treated LUHMES cells consistently and significantly reduced NCOA4 expression across three independent Western blot analyses, indicating a reproducible overall depletion.

(FC: Fold Changes; n=3; mean ± SD; unpaired t-test, *p<0.05, ****p<0.0001)

Abbreviations: LPX: Liproxstatin-1; LUHMES: Lund Human Mesencephalic Cells; MPP⁺: 1-Methyl-4-phenylpyridinium; Rapa: Rapamycin; RSL3: Ras-Selective Lethal; UFP: Ultrafine Particles.

LC3b

Autophagy was assessed by analyzing the ratio of LC3b-II (the active, lipidated form) to LC3b-I (the inactive form), which serves as a reliable indicator of autophagic activity. A significant increase in this ratio confirms autophagic activation. The positive control, 15 µM Rapa, demonstrated increased LC3b-II levels ($p < 0.05$), validating the assay. Interestingly, 2 µg/cm² UFP exposure was the only experimental condition to induce LC3b activation ($p < 0.01$). Other conditions, including RSL3, MPP⁺, 10 µg/cm² UFP, and

10 µg/cm² with LPX co-treatment, did not show significant activation of LC3b ($p > 0.05$) (Fig. 87), suggesting minimal involvement of autophagy under these treatments.

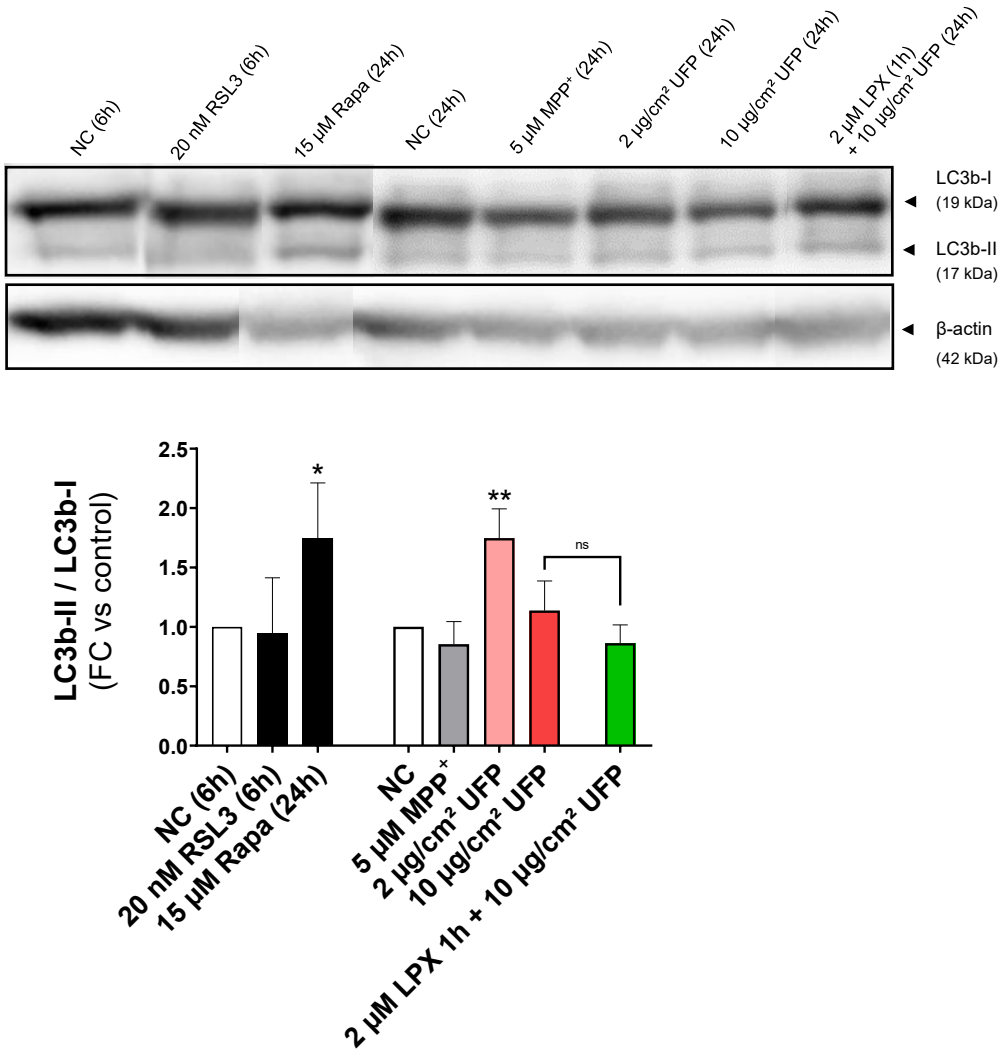

Figure 87: Analysis of autophagy trough the LC3b-II/LC3b-I ratio.

A significant increase in LC3b-II levels was observed with the positive control, 15 µM Rapamycin (Rapa) for 24 hours, as investigated by Western blotting. Among experimental conditions, 2 µg/cm² UFP exposure resulted in a significant LC3b-II/LC3b-I increase. The others, RLS3, MPP+, and 10 µg/cm², with or without co-treatment with 2 µM LPX, did not induce significant LC3b activation.

(FC: Fold Changes; n=3; mean ± SD; unpaired t-test, *p<0.05, **p<0.01)

Abbreviations: LPX: Liproxstatin-1; LUHMES: Lund Human Mesencephalic Cells; MPP^+: 1-Methyl-4-phenylpyridinium; Rapa: Rapamycin; RSL3: Ras-Selective Lethal; UFP: Ultrafine Particles.

IV. DISCUSSION AND LIMITS

Our study demonstrates that differentiated LUHMES cells, cultured into dopaminergic neurons, do not undergo immediate cell death following exposure to UFP. However, after 24 hours exposure, we observed significant alterations in the antioxidant defense system, including increased GPx enzyme activity, depletion of GSH, and reduced expression of SLC7A11 (x_c^- subunit) and GPx4 proteins. Additionally, UFP exposure led to elevated levels of p53 and 4-HNE adduct proteins. Although intracellular iron homeostasis remained unchanged after 24 hours of UFP exposure, these findings suggest that UFP exposure favors ferroptosis as a form of RCD in differentiated LUHMES cells. The absence of severe viability impairment following acute UFP exposure is quite logical, and echoes epidemiological studies suggesting that prolonged exposure may contribute to the etiopathogenesis of neurodegenerative diseases. Although there is an initial antiferroptotic response, indicating some resistance to cell death, UFP still possess toxic potential, particularly over the long term, as they may gradually deplete antiferroptotic defenses.

Among environmental PD-factors, exposure to UFP has emerged as a significant area of concern due to mounting evidence suggesting a potential link between UFP exposure and neurodegenerative diseases, including PD (You *et al.*, 2022). While the most recent studies have primarily focused on brain particle localization (Vanbrabant, Van Dam, *et al.*, 2024), mitochondrial dysfunction (Mussalo *et al.*, 2024) and disruption of neurotransmission (Cory-Slechta *et al.*, 2024), the relationship between urban UFP and regulated neuronal cell death mechanisms such as ferroptosis is still in its infancy.

To replicate the specific target cells of PD, namely the dopaminergic neurons of the SN*pc*, we used the human-derived neuronal cell line LUHMES, which has been differentiated into dopaminergic-like neurons. Differentiated LUHMES cells express key dopaminergic markers and functional properties, making them a valuable tool for PD research. Additionally, their healthy donor origin makes LUHMES cells a reliable and attractive model. Other cell lines such as hESC and induced pluripotent stem cells (iPSC) are on the rise and hold promise for studying neurotoxicity and neurodegeneration, but their differentiation process is long, the protocols are demanding with strict ethical and culture conditions, and the cost is prohibitive. While alternative cell lines, such as the SH-SY5Y human dopaminergic neuroblastoma cells used in the context of air pollution neuronal toxicity (Xiong *et al.*, 2022), are cancer-derived and may undergo genotypic and phenotypic drift. Overall, while this study demonstrates a link between UFP-induced toxicity and dopaminergic ferroptosis, these findings should be interpreted with certain

limitations in mind. As an exploratory study with a small sample size, our results provide a foundation for future research. Further studies could extend these findings by involving larger sample sizes, subchronic exposure models, and employing more complex systems such as advanced co-cultures (*in vitro*), brain organotypic cultures (*ex vivo*), or *in vivo* models. These approaches could provide a more comprehensive understanding of the neurotoxic impacts of UFP.

To evaluate UFP oxidative potential, the acellular **DTT assay** revealed a dose-dependent response, likely due to DTT-active PAH-derived quinones. This cell-free test relies on redox-active species in PM donating electrons to dissolved molecular oxygen, forming superoxide ($O^{2.-}$), which generates other ROS such as hydrogen peroxide (H_2O_2) and hydroxyl radical ($^{\cdot}OH$) in the presence of metals (Kumagai *et al.*, 2002), and all three ROS types contribute to DTT oxidation (Chung *et al.*, 2006; Kumagai *et al.*, 2002; Park *et al.*, 2005; Wang *et al.*, 2010). Moreover, H_2O_2 and $^{\cdot}OH$ are both contributors of ferroptosis, explaining the importance to perform a DTT assay. However, not all UFP components are DTT-active; for instance, while many PAH of our UFP are not inherently redox-active, some can oxidize to form quinones, such as Benzo(a)pyrene (BaP), Chrysene (CHR), Benzo(k)fluoranthene (BkF), Benzo(b)fluoranthene (BbF), Dibenzo(a,h)anthracene (DahA), 5-Methylchrysene (5MCHR), and Indeno(1,2,3-c,d)pyrene (IP) (listed in Supplementary Data Table S2, p. 235). These quinones are crucial contributors to ROS production. Although quinones are more effective oxidizers of DTT than metals, the high levels of transition metals in UFP, including Co, Cu, Mn, Mo, Ni, Zn, Cr, V, Fe (Table S4 Supplementary Data, p. 237), play also a dominant role in the DTT response (Charrier & Anastasio, 2012). This suggests that UFP samples, likely enriched with metals from industrial combustion processes, originated from fossil fuel emissions (Maciejczyk *et al.*, 2021; Vouk & Piver, 1983). Interestingly, the DTT oxidation efficiency decreased at higher concentrations. This trend may reflect interactions between DTT and certain metals within UFP, like Cu and Mn, reducing their availability and underestimating of redox activity (Charrier & Anastasio, 2012). Other oxidative processes, such as biological transformations via cytochrome P450 enzymes or antioxidant evaluations using ascorbate or GSH measurements, provide additional insights into cellular redox status. It is important to be cautious when comparing oxidative potential to cellular metabolism and viability, as these relationships are naturally complex.

The potential link between air-pollutant UFP and PD represents a critical research area with significant implications for public health and disease prevention. Given the vulnerability of the SN*pc* to oxidative stress, selecting an appropriate model to mimic PD-

like phenotypes was crucial. Environmental toxins that selectively degenerate dopaminergic neurons and replicate PD-like behavioral outcomes provide valuable insights into disease mechanisms.

In this study, MPP^+, a mitochondrial respiratory chain (complex I) inhibitor, was chosen as a positive control due to its well-established ability to induce dopaminergic neurotoxicity. MPP^+ is particularly relevant because it not only replicates a PD-associated phenotype but also contributes to oxidative stress-related pathways, including ferroptosis, through ROS and GSH depletion. To ensure accurate modeling of disease-relevant processes, determining optimal exposure conditions was critical. Based on previous studies, a MPP^+ concentration of 5 µM or 10 µM MPP^+ with a 24-hour exposure was ideal, avoiding confounding effects observed under other conditions, and are therefore frequently used in our laboratory (Bonte *et al.*, 2024; Do Van *et al.*, 2016). Lower concentrations (< 5 µM) prompted an overactivation of cellular defense systems, including a ~10% increase in GSH levels in LUHMES cells, which could obscure ferroptotic-related mechanisms. Conversely, prolonged exposures (> 24 hours), even at low concentrations (e.g., 1 µM), also led to elevated GSH levels (Krug *et al.*, 2014). To maintain consistency across all experimental conditions, a 24-hour exposure period was selected to represent acute neurotoxic stress. Consequently, the optimal MPP^+ concentration for this research had to be determined a priori. As explained, GSH was previously used as parameter for exposure optimalization. To compare MPP^+ and UFP exposure, we validated this approach by comparing the effects of 5 and 10 µM MPP^+ concentrations on the GSH/GSSG ratio (Cf. Supplemental Data, Fig. S8, p. 253). Treatment with 5 µM MPP^+ for 24 hours induced an imbalance in the GSH/GSSG ratio comparable to that observed following UFP exposure. Based on this validation, we investigated whether acute (24-hour) exposure to 5 µM MPP^+ and 2 and 10 µg/cm² UFP could induce RCD pathways, with a particular focus on both shared and distinct mechanisms. This comparative approach provided critical insights into the respective neurotoxic profiles of UFP compared to MPP^+ in dopaminergic-like neurons.

In this study, we examined the neurotoxicological effects of urban UFP with relative high iron content, sourced from the highly industrial area of Dunkirk, on differentiated dopaminergic-like neurons. Recognizing the potential of UFP to directly access the brain via the olfactory route, we used direct UFP exposure on neuronal cultures ranging from 2 to 40 µg/cm². Notably, **cytotoxicity effects** were absent across all conditions (except for cell viability at 40 µg/cm² UFP). This is consistent with a prior *in vitro* study showing that diesel exhaust PM does not induce neuronal cell death up to concentrations six times higher than our 10 µg/cm² exposure. Interestingly, toxicity was mediated by microglial neuroinflammation in co-culture conditions (Roqué *et al.*, 2016).

Throughout this study, certain observed trends lacked statistical significance, often due to high variations. This variability can be attributed to the inherent heterogeneity of urban UFP, which contrasts with the uniformity of engineered nanoparticles (e.g., TiO_2 or SiO_2) or next-generation nanomaterials (e.g., carbon nanotubes, fullerenes, or quantum dots). To address this variability (e.g., at high levels in the resazurin assay) and to simulate more realistic exposure scenarios, we focused subsequent experiments on UFP concentrations of 2 and 10 µg/cm², maintaining a 24-hour exposure period. Finally, we assessed also the protective effects of LPX, a ferroptosis inhibitor, on LUHMES cells subjected to high levels of UFP (10 µg/cm²). LPX is known to inhibit lipid peroxide propagation, a key mediator of ferroptosis. However, before discussing the RCD features of treated LUHMES cells, it must be noted that the results of RSL3 were disappointing. The concentration of 20 nM and 6-hour exposure is based on previous published data of our lab (Bouchaoui *et al.*, 2023). Unfortunately, and surprisingly, similar results were not found in this study. In the previous paper, there was a 5-fold increase in 4-HNE adducts in RSL3-treated cells (20 nM, 6h) compared to controls, which also impacted the GSH axis with a depletion approximately five times for GH and three times for the GSH/GSSG ratio. Since the results of RSL3 were not reproducible in this study – despite being tested in two biologically independent studies with different cells but the same lot of RSL3 – the issue appears to be with the function of RSL3, prompting its exclusion from further discussion.

Digging deeper into the forms of RCD, we assessed the first critical ferroptotic factor: iron homeostasis. We analyzed **TfR and ferritin levels**, both of which are transcriptional regulated by the iron regulatory element/iron regulatory protein (IRE/IRP) system (Wilkinson & Pantopoulos, 2014). After UFP exposure, no significant changes were observed. In contrast, MPP^+-exposed cells exhibited reduced ferritin levels, indicating decreased iron storage and potentially elevated intracellular iron content. This prompted an investigation into ferritinophagy, the autophagic degradation of ferritin. **NCOA4**, the cargo receptor responsible for transporting ferritin to the autophagosome for breakdown, mediates ferroptosis in lung tissue exposed to cigarette smoke. Moreover, inhibition of NCOA4 shows promising potential for COPD treatment (J. Liu *et al.*, 2022). Surprisingly, NCOA4 was also significant downregulated in MPP^+ conditions, suggesting it may not be responsible for the observed reduction in ferritin levels. Interpreting NCOA4 data is challenging, as it involves not only iron content but also post-translational modifications including the E3 ubiquitin protein ligase antibody (HERC2)-mediated proteolysis of NCOA4 (Mancias *et al.*, 2015). Given that NRF2 regulates HERC2, which controls

NCOA4, high levels of oxidative stress likely lead to the ubiquitination of NCOA4 (Wang *et al.*, 2023), as seen in MPP^+ treated cells, reducing its potential to create ferroptosis.

In addition to iron, UFP contain other transition metals, such as Cu, Mn, and Co, which can catalyze ROS formation via Fenton-like reactions. Their uptake, mediated by **DMT1**, differs from receptor-mediated endocytosis by TfR (Canonne-Hergaux *et al.*, 2001; Foot *et al.*, 2008). In PD models, DMT1 upregulation correlates with increased neurotoxin susceptibility, suggesting that DMT1-mediated iron influx may enhance toxicity (Bai *et al.*, 2021; Sun *et al.*, 2018). However, in our study, DMT1 levels did not increase following MPP^+ or UFP exposure, indicating that exposure to iron-containing UFP did not disrupt iron homeostasis. This finding is consistent with studies indicating that nanoparticles disrupt lysosomal or mitochondrial iron stores, or release iron from heme breakdown by Hmox1, thereby increasing labile iron pools (Wei *et al.*, 2024; C. Zhang *et al.*, 2020). A study of 21 nanomaterials ranging in size from 5 to 200 nm (10 µg/mL, 24 hours) exposed in HUVEC cells showed that all upregulated ACSL4 mRNA levels, and 19 resulted in higher PGTS2 or reduced GPx4 mRNA levels. Only four nanomaterials (i.e., carbon nanotubes, α-Fe_2O_3, Co_3O_4, WO_3) resulted in significant divalent iron staining. Surprisingly, some of these materials lacked inherent iron content, suggesting that the iron originated internally (C. Zhang *et al.*, 2020). In our study, direct measurement of iron levels (e.g., by FerroOrange) was not the focus, as we aimed to assess the dynamics and regulation of iron homeostasis, which is disrupted in both ferroptosis and PD.

The second critical factor in ferroptosis is the activity of **GPx4**, a lipid hydroperoxide-reducing enzyme. In our study, high UFP exposure (10 µg/cm²) resulted in decreased GPx4 protein expression, providing a novel link between UFP exposure and ferroptosis. A recent study in $PM_{2.5}$-treated neuronal Neuro-2a (N2A) and SH-SY5Y cells also reported a significant decrease in x_c^- (SLC7A11) and GPx4 expression, with bioinformatic analysis suggesting that CREB regulates GPx4 via downregulation of the ERK pathway. Interestingly, activation of ERK1/2 agonist post-$PM_{2.5}$ treatment restored GPx4 expression, inhibiting ferroptosis (Xiong *et al.*, 2022). In the present study, co-treatment of LPX with 10 µg/cm² UFP did not alter GPx4 expression, suggesting a ferroptotic protective effect. Besides, the reduction of cytosolic GPx4 led to lipid peroxidation, as indicated by increased **4-HNE** adducts after 2 µg/cm² UFP.

As the primary antioxidant in the brain and critical co-factor for GPx4, measurement of the **GSH ratio** is of particular relevance. More than thirty years ago, Sofic (1992) reported significant GSH depletion in the SN of post-mortem PD patients. Following MPP^+ or UFP (2 µg/cm² and 10 µg/cm²) exposure, we observed a reduced GSH/GSSG ratio, indicating a more oxidized cellular environment. Notably, the mechanisms

underlying the disruption of this ratio differ between the two treatments. After MPP^+ treatment, no significant differences were observed in GSH levels, but GSSG levels were significantly increased, reflecting the well-known inhibition of mitochondrial complex I by MPP^+, promoting ROS production, and subsequent oxidation of GSH into GSSG. In contrast, after UFP exposure, GSSG levels remained unchanged, while GSH levels were significantly decreased. This suggests that the decline in the ratio may be due to impaired GSH synthesis, reduced GR activity, or insufficient NADPH, rather than direct oxidation by ROS, potentially indicating a different oxidative stress profile compared to MPP^+ treatment. These aligns with the findings of Sofic (1992), where GSH decreased without corresponding changes in GSSG levels in the SN of PD patients. Remarkably, when looking at the results of UFP in combination with LPX, no significant differences in the ratio, GSH or GSSG were observed, further supporting the potential of LPX to counteract the ferroptotic features induced by UFP. GSH synthesis is closely linked to the activity of **x_c^- (encoded by SLC7A11)**, which transports cystine, a GSH precursor. Unlike the *in vivo* study, it was necessary to first verify whether our cell culture medium (DMEM/F-12) contained cystine, as the x_c^- antiporter cannot function properly without it. The amino acid L-Cystine 2HCl was present at a concentration of 0.1 mM in the cellular medium. In the context of PD, recent studies have linked DNA methylation changes in *SLC7A11* to an increased risk of the disease (C. L. Vallerga *et al.*, 2020). Consistent with these findings, our study demonstrates that exposure to MPP^+ and UFP significantly reduced SLC7A11 protein levels, while co-treatment with LPX and UFP resulted in a notable increase in SLC7A11 expression. LPX appears to neutralize lipid peroxidation-derived ROS, protecting the integrity of cellular membranes, including x_c^- proteins, and helping to maintain GSH levels.

Recent research has highlighted the significant role of the tumor suppressor **P53** in regulating ferroptosis (Jiang, Kon, *et al.*, 2015). The role of P53 is complex, bidirectional, and context-dependent, as it can both promote and inhibit ferroptosis. Under mild or transient oxidative stress, P53 restrains ferroptosis, whereas under severe oxidative damage, it can induce ferroptosis by coordinating with downstream target genes, including *SAT1, GLS2, and PTGS2* (Gao *et al.*, 2015; Hu *et al.*, 2010; Ou *et al.*, 2016; Yang *et al.*, 2014). *SLC7A11* is also a target; P53 reduces x_c^- system activity, decreases GSH levels and increases oxidative stress susceptibility (Jiang, Hickman, *et al.*, 2015; Jiang, Kon, *et al.*, 2015). Our findings are consistent with this model, showing elevated P53 levels following UFP exposure and suppression of SLC7A11. This was also previously observed following zinc oxide nanoparticle (ZnO) and zinc ion (Zn^{2+}) treatment (C. Zhang *et al.*, 2020). Notably, co-treatment with LPX and UFP exposure resulted in opposing effects on P53 and SLC7A1, suggesting that UFP can induce ferroptosis in

differentiated LUHMES cells through the P53/SLC7A11/GSH/cGPX4 signaling pathway, and that LPX modulates P53 activity and its suppression of SLC7A11.

Prolonged oxidative stress may initial apoptosis instead of ferroptosis, preventing the proliferation of damaged cells. Hydrophobic 4-HNE can diffuse into cellular compartments, forming DNA-adducts (Pizzimenti *et al.*, 2013), cleaving PARP to induce DNA fragmentation, and activating caspases-8, -9, and -3 (Liu *et al.*, 2000; Ruef *et al.*, 2001). This cross-talk suggests that ferroptotic conditions can ultimately lead to apoptosis. Moreover, P53 regulates both ferroptosis and apoptosis by targeting SLC7A11 and pro-apoptotic genes like **BAX**, which disrupt mitochondrial integrity and activate caspases in the intrinsic pathway. While the intrinsic pathway involves cytochrome C and **caspase-9**, the extrinsic pathway activates **caspase-8** through death receptors, both converging on **caspase-3/7**. Our study revealed that UFP exposure did not activate intrinsic (i.e., BAX, caspase-9) or extrinsic (i.e., caspase-8) apoptotic pathways, resulting in the absence of caspase-3/7 activity. In contrast, MPP^+ exposure increased BAX and all measured caspase (i.e., -9, -8, and -3/7) activities, even surpassing the positive control STS, highlighting its potency as a neurotoxin for dopaminergic neurons. These results align with previous findings in differentiated LUHMES cells exposed to 80 µM MPP^+ for 48h (Zhang *et al.*, 2014), although our study achieved similar results using only 5 µM MPP^+ for 24h. Additionally, MPP^+ decreased the GSH/GSSG ratio and extensive thiol oxidation, reflected in elevated GSSG levels, suggesting that MPP^+ treated cells undergo oxidative damage, potentially leading to apoptosis.

Regarding autophagy, our lab previously showed that LUHMES cells exhibit limited susceptibility to autophagy, with only high doses (> 5 µM) of Rapa reducing viability (Do Van *et al.*, 2016). Therefore, the positive control in our study used 15 µM Rapa for 24h. The **LC3b-II/-I protein expression** ratio indicated that UFP at 2 µg/cm² activated autophagy, likely playing a protective role trough (as mentioned in introduction, Cf. I.6.1 Autophagy and its potential implication in PD, p. 43) or inducement to selective autophagy mechanisms (e.g., lipophagy, clockophagy, and chaperone-mediated autophagy (CMA)), as precursor of ferroptosis (Lee *et al.*, 2023). At 10 µg/cm², UFP may overwhelm these protective effects, inducing directly ferroptosis.

An overview of how RCD crosstalk due to common features, can be found in Fig. 88.

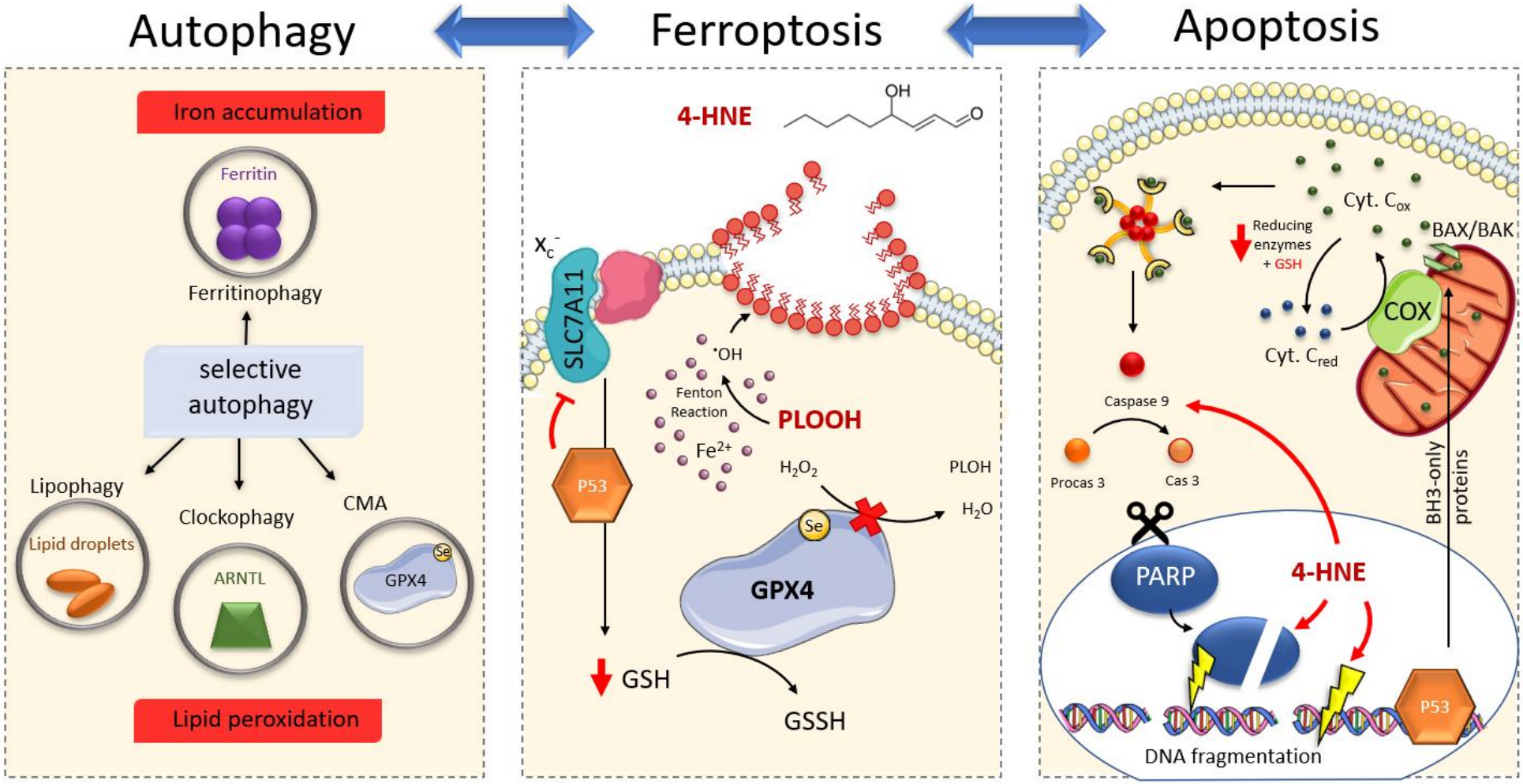

Figure 88: Crosstalk between three Regulated Cell Death (RCD) forms, Autophagy, Ferroptosis, and Apoptosis. (Own creation)

The first box illustrates pre-ferroptotic mechanisms involving selective autophagy, including ferritinophagy (leading to iron accumulation) and lipophagy, clockophagy, and CMA (contributing to lipid peroxidation). The second box highlights ferroptosis, emphasizing the role of P53 in inhibiting SLC7A11, which reduces GSH levels and promotes lipid peroxidation, as reflected by increased 4-HNE adducts. The final box depicts apoptosis, showing how 4-HNE can induce DNA damage directly or through PARP inactivation, leading to DNA fragmentation. P53-driven transcription of BH3-only proteins (BAX/BAK) triggers Cytochrome C release and the activation of the caspase cascade. Additionally, 4-HNE can also directly activate caspases-8, -9, and -3.

Abbreviations: 4-HNE: 4-Hydroxy-2-nonenal; BAK: BCL-2 Antagonist/Killer; BAX: BCL-2 Associated X Protein; BH3: BCL-2 Homology Domain 3; CMA: Chaperone-Mediated Autophagy; ; GSH: Glutathione; PARP: Poly(ADP-Ribose) Polymerase; P53: Tumor Protein P53; RCD: Regulated Cell Death; SLC7A11: Solute Carrier Family 7 Member 11.

V. CONCLUSION AND PERSPECTIVES

This study is the first to demonstrate that acute exposure (24 h) to iron-containing urban-industrial UFP leads to dopaminergic cell alterations via the P53/x_c^-/GSH/cGPx4 axis. Importantly, the ability of LPX to mitigate these ferroptotic changes supports the hypothesis that chronic exposure might lead to neurodegeneration.

Both MPP^+ and UFP exposures produced similar outcomes, particularly in terms of increased oxidative stress, disruption of the GSH/GSSG balance, and GPx activation. While environmental exposure to MPP^+ is extremely rare, this well-established model allowed us to explore the degree of toxicity of UFP on dopaminergic neurons. Our results show that MPP^+ exposure induces cell death via apoptosis, whereas UFP exposure triggered acute milder alterations linked to ferroptosis, which might become detrimental at long term.

With growing evidence linking UFP exposure to neurodegenerative features, further investigation is critical. Taken the limitations discussed earlier (Cf. IV. Discussion and Limits, p. 186) into account, it would advantageous to include direct iron analysis in future studies. As shown in Fig. 89, I have already started optimizing the protocol for FerroOrange staining to visualize intracellular ferrous iron levels through live cell fluorescence imaging. Additionally, the direct measurement of C11-$BODIPY^{581/591}$ for lipid peroxidation, CellROX Deep Red for oxidative stress, and LysoTracker for autophagosome formation could provide valuable insights into the cellular processes affected by UFP or MPP^+ treatments.

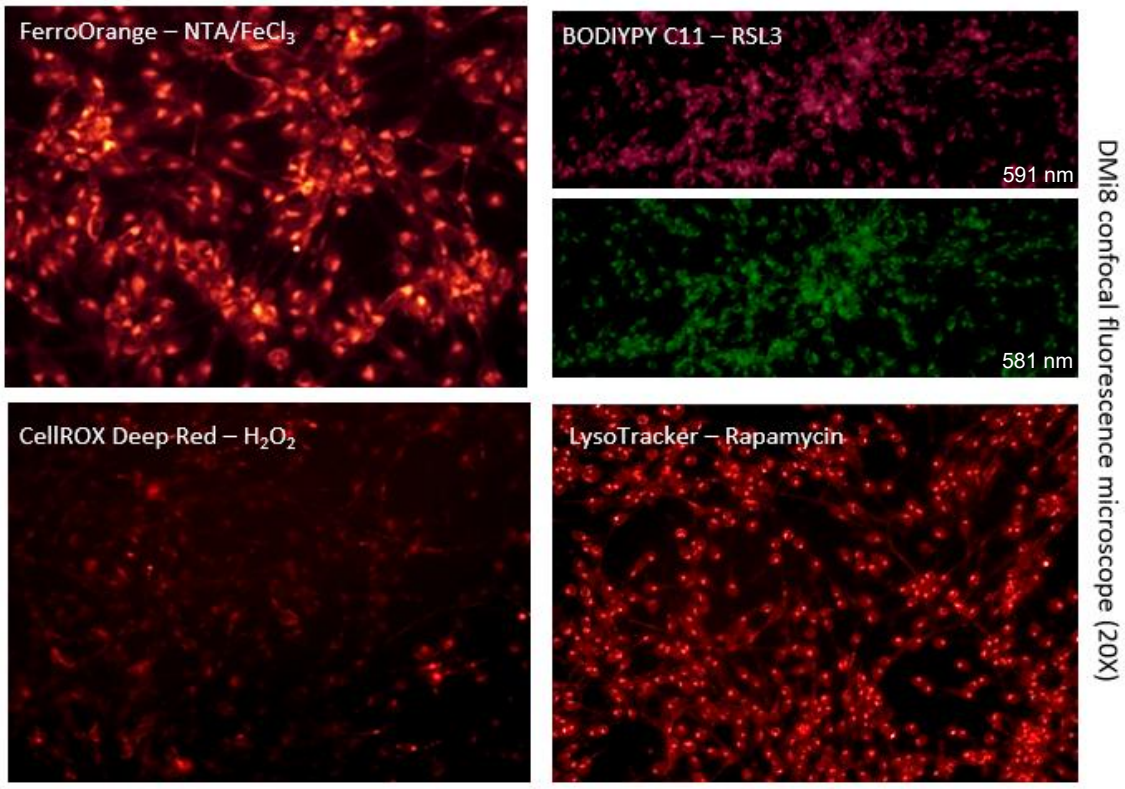

Figure 89: Immunofluorescence markers FerroOrange, C11-BODIPY$^{581/591}$, CellROX, and LysoTracker induced by positive controls for protocol optimalization.

Representative immunofluorescence images illustrates four makers, each induced by their positive control for validation: NTA/$FeCl_3$ for FerroOrange, RSL3 for BODIPY$^{581/591}$, H_2O_2 for CellROX, and Rapamycin for LysoTracker. Images were captured using a DMi8 confocal fluorescence microscope (20X magnification).

The results of this project indicated significant changes in GPx4 levels and GSH status, from which the synthesis depends on GCL and GSS enzymes, both regulated by NRF2. Further investigation into the NRF2 signaling pathway could enhance our understanding of the relationship between oxidative stress an ferroptosis induction upon UFP exposure. But, also taken into account that NRF2 acts as a “double-edged sword”. For instance, while NRF2 downregulates TfR, reducing iron uptake, it also induces HO-1, breaking down heme into Fe, CO, and biliverdin, thereby contributing to the Labile Iron Pool. Moreover, NRF2 influences lipid metabolism, for example, by upregulating the incorporation of PUFA into membranes, through the induction of ACSL4, making them more susceptible to lipid peroxidation (Song & Long, 2020).

Another important aspect of neurotoxicity in the context of ferroptosis is the role of mitochondria, which serve as central organelles for iron storage and are enriched with PUFA in their membranes. The PhD study from a formal colleague, using the same Dunkirk recovered UFP as used in this study, but exposed BEAS-2B cells, identified

mitochondrial alterations (Sotty *et al.*, 2020). Dysregulation of mitochondrial dynamics, such as excessive fission (via DRP1) or fusion (via OPA1), can impact mitochondrial health and contribute to ferroptotic cell death. Increased fission is often associated with elevated mitochondrial ROS (mtROS) and reduced mitochondrial membrane potential (Δψm), which can be assessed using a TMRM- SYTOX Blue flow cytometry assay.

With the results of the *in vitro* part of this PhD, we can conclude that:

Given the increasing incidence of PD, particularly in highly polluted urban areas, the lack of effective therapies, and the absence of policy on UFP, this study underscores the need for greater awareness of UFP neurotoxicity, even at low doses.

REFERENCES

Abiko, Y., Taguchi, K., Hisamori, M., Hiyoshi-Arai, K., Luong, N. C., Toriba, A., & Kumagai, Y. (2022). Redox Homeostasis is Disturbed by Redox Cycling between Reactive Cysteines of Thioredoxin 1 and 9,10-Phenanthrenequinone, an Atmospheric Electron Acceptor. *Chemical research in toxicology.*, *35*(8), 1425-1432. https://doi.org/10.1021/acs.chemrestox.2c00174

Ahn, H. J., Hernandez, C. M., Levenson, J. M., Lubin, F. D., Liou, H.-C., & Sweatt, J. D. (2008). c-Rel, an NF-kappaB family transcription factor, is required for hippocampal long-term synaptic plasticity and memory formation. *Learn Mem*, *15*(7), 539-549. https://doi.org/10.1101/lm.866408

Ahn, K. S., & Aggarwal, B. B. (2005). Transcription factor NF-kappaB: a sensor for smoke and stress signals. *Annals of the New York Academy of sciences*, *1056*, 218-233. https://doi.org/10.1196/annals.1352.026

Ailshire, J. A., & Crimmins, E. M. (2014). Fine particulate matter air pollution and cognitive function among older US adults. *Am J Epidemiol*, *180*(4), 359-366. https://doi.org/10.1093/aje/kwu155

Air pollution accounted for 8.1 million deaths globally in 2021, becoming the second leading risk factor for death, including for children under five years. (**2024**). Unicef. https://www.unicef.org/press-releases/air-pollution-accounted-81-million-deaths-globally-2021-becoming-second-leading-risk

Ajmani, G. S., Suh, H. H., & Pinto, J. M. (2016). Effects of Ambient Air Pollution Exposure on Olfaction: A Review. *Environmental health perspectives : EHP.*, *124*(11), 1683-1693. https://doi.org/10.1289/EHP136

American neurological, a. (2013). Ceruloplasmin dysfunction and therapeutic potential for Parkinson disease. *Annals of neurology*, *73*(4), 554-559. https://doi.org/10.1002/ana.23817

Anglade, P., Vyas, S., Javoy-Agid, F., Herrero, M. T., Michel, P. P., Marquez, J.,…Agid, Y. (1997). Apoptosis and autophagy in nigral neurons of patients with Parkinson's disease. *Histol Histopathol*.

Antony, P. M. A., Diederich, N. J., Krüger, R., & Balling, R. (2013). The hallmarks of Parkinson's disease. *FEBS journal.*, *280*(23), 5981-5993. https://doi.org/10.1111/febs.12335

Aoki, Y., Sato, H., Nishimura, N., Takahashi, S., Itoh, K., & Yamamoto, M. (2001). Accelerated DNA adduct formation in the lung of the Nrf2 knockout mouse exposed to diesel exhaust. *Toxicology and applied pharmacology.*, *173*(3), 154-160. https://doi.org/10.1006/taap.2001.9176

Ariya, P. A., & Amyot, M. (2004). New Directions: The role of bioaerosols in atmospheric chemistry and physics. *Atmospheric Environment*, *38*(8), 1231-1232. https://doi.org/https://doi.org/10.1016/j.atmosenv.2003.12.006

Ayton, S., & Lei, P. (2014). Nigral iron elevation is an invariable feature of Parkinson's disease and is a sufficient cause of neurodegeneration. *BioMed research international.*, *2014*, 581256. https://doi.org/10.1155/2014/581256

Bagley, S., Winthrop, W., Johnson, J., Kittelson, D., Johnson, J., & Schauer, J. (2002). Impact of Low-Emission Diesel Engines on Underground Mine Air Quality.

Bai, L., Yan, F., Deng, R., Gu, R., Zhang, X., & Bai, J. (2021). Thioredoxin-1 Rescues MPP+/MPTP-Induced Ferroptosis by Increasing Glutathione Peroxidase 4. *Molecular neurobiology.*, *58*(7), 3187-3197. https://doi.org/10.1007/s12035-021-02320-1

Bai, R., Zhang, L., Liu, Y., Li, B., Wang, L., Wang, P.,…Chen, C. (2014). Integrated analytical techniques with high sensitivity for studying brain translocation and potential impairment induced by intranasally instilled copper nanoparticles. *Toxicology letters.*, *226*(1), 70-80. https://doi.org/10.1016/j.toxlet.2014.01.041

Ball, N., Teo, W.-P., Chandra, S., & Chapman, J. (2019). Parkinson's Disease and the Environment. *Frontiers in neurology.*, *10*, 218. https://doi.org/10.3389/fneur.2019.00218

Balogh, S. A., & Wehner, J. M. (2003). Inbred mouse strain differences in the establishment of long-term fear memory. *Behavioural brain research.*, *140*(1-2), 97-106. https://doi.org/10.1016/s0166-4328(02)00279-6

Banati, R. B., Daniel, S. E., & Blunt, S. B. (1998). Glial pathology but absence of apoptotic nigral neurons in long-standing Parkinson's disease. https://doi.org/10.1002/mds.870130205

Banerjee, M., Siddique, S., Dutta, A., Mukherjee, B., & Ranjan Ray, M. (2012). Cooking with biomass increases the risk of depression in pre-menopausal women in India. *Social science & medicine.*, *75*(3), 565-572. https://doi.org/10.1016/j.socscimed.2012.03.021

Barbier, E., Carpentier, J., Simonin, O., Gosset, P., Platel, A., Happillon, M.,…Garçon, G. (2023). Oxidative stress and inflammation induced by air pollution-derived PM2.5 persist in the lungs of mice after cessation of their sub-chronic exposure. *Environment international*, *181*, 108248. https://doi.org/10.1016/j.envint.2023.108248

Bayo Jimenez, M. T., Frenis, K., Hahad, O., Steven, S., Cohen, G., Cuadrado, A.,…Daiber, A. (2022). Protective actions of nuclear factor erythroid 2-related factor 2 (NRF2) and downstream pathways against environmental stressors. *Free radical biology & medicine.*, *187*, 72-91. https://doi.org/10.1016/j.freeradbiomed.2022.05.016

Beckers, P., Belo Do Nascimento, I., Charlier, M., Desmet, N., Massie, A., & Hermans, E. (2024). Implication of system xc- in neuroinflammation during the onset and maintenance of neuropathic pain. *Journal of neuroinflammation.*, *21*(1), 117. https://doi.org/10.1186/s12974-024-03112-9

Bhargava, A., Shukla, A., Bunkar, N., Shandilya, R., Lodhi, L., Kumari, R.,…Mishra, P. K. (2019). Exposure to ultrafine particulate matter induces NF-κβ mediated epigenetic modifications. *Environmental pollution.*, *252*(Pt A), 39-50. https://doi.org/10.1016/j.envpol.2019.05.065

Bhat, A. H., Dar, K. B., Anees, S., Zargar, M. A., Masood, A., Sofi, M. A., & Ganie, S. A. (2015). Oxidative stress, mitochondrial dysfunction and neurodegenerative diseases; a mechanistic insight. *Biomedicine & pharmacotherapy.*, *74*, 101-110. https://doi.org/10.1016/j.biopha.2015.07.025

Billions of people still breathe unhealthy air: new WHO data. (2022). Wolrd Health Organization (WHO). https://www.who.int/news/item/04-04-2022-billions-of-people-still-breathe-unhealthy-air-new-who-data

Bjørklund, G., Peana, M., Maes, M., Dadar, M., & Severin, B. (2021). The glutathione system in Parkinson's disease and its progression. *Neuroscience and biobehavioral reviews.*, *120*, 470-478. https://doi.org/10.1016/j.neubiorev.2020.10.004

Block, M. L., & Calderón-Garcidueñas, L. (2009). Air pollution: mechanisms of neuroinflammation and CNS disease. *Trends Neurosci*, *32*(9), 506-516. https://doi.org/10.1016/j.tins.2009.05.009

Block, M. L., Wu, X., Pei, Z., Li, G., Wang, T., Qin, L.,…Veronesi, B. (2004). Nanometer size diesel exhaust particles are selectively toxic to dopaminergic neurons: the role of microglia, phagocytosis, and NADPH oxidase. *The FASEB journal.*, *18*(13), 1618-1620. https://doi.org/10.1096/fj.04-1945fje

Bonte, M.-A., Gouel, F., Jonneaux, A., Belarbi, K., Devos, D., & Devedjian, J.-C. (2024). Long-term inhibition of lysosomal glucocerebrosidase activity promotes GPX4 stability and inhibits ferroptosis in a Parkinson's model. https://doi.org/10.21203/rs.3.rs-3879123/v1

Borie, C., Gasparini, F., Verpillat, P., Bonnet, A.-M., Agid, Y., Hetet, G.,…Grandchamp, B. (2002). Association study between iron-related genes polymorphisms and Parkinson's disease. *Journal of neurology.*, *249*(7), 801-804. https://doi.org/10.1007/s00415-002-0704-6

Bouchaoui, H., Mahoney-Sanchez, L., Garçon, G., Berdeaux, O., Alleman, L. Y., Devos, D.,…Devedjian, J.-C. (2023). ACSL4 and the lipoxygenases 15/15B are pivotal for ferroptosis induced by iron and PUFA dyshomeostasis in dopaminergic neurons. *Free radical biology & medicine.*, *195*, 145-157. https://doi.org/10.1016/j.freeradbiomed.2022.12.086

Boulard, M., Blume, K. G., & Beutler, E. (1972). The effect of copper on red cell enzyme activities. *J Clin Invest*, *51*(2), 459-461. https://doi.org/10.1172/JCI106833

Bové, H., Bongaerts, E., Slenders, E., Bijnens, E. M., Saenen, N. D., Gyselaers, W.,…Nawrot, T. S. (2019). Ambient black carbon particles reach the fetal side of human placenta. *Nat Commun*, *10*(1), 3866. https://doi.org/10.1038/s41467-019-11654-3

Bové, H., Steuwe, C., Fron, E., Slenders, E., D'Haen, J., Fujita, Y.,…Ameloot, M. (2016). Biocompatible Label-Free Detection of Carbon Black Particles by Femtosecond Pulsed Laser Microscopy. *Nano Lett*, *16*(5), 3173-3178. https://doi.org/10.1021/acs.nanolett.6b00502

Brinks, V., de Kloet, E. R., & Oitzl, M. S. (2008). Strain specific fear behaviour and glucocorticoid response to aversive events: modelling PTSD in mice. *Prog Brain Res*, *167*, 257-261. https://doi.org/10.1016/S0079-6123(07)67019-8

Broersen, K., van den Brink, D., Fraser, G., Goedert, M., & Davletov, B. (2006). Alpha-synuclein adopts an alpha-helical conformation in the presence of polyunsaturated fatty acids to hinder micelle formation. *Biochemistry.*, *45*(51), 15610-15616. https://doi.org/10.1021/bi061743l

Cai, H., Bao, Y., Cheng, H., Ge, X., Zhang, M., Feng, X.,…Yang, X. (2023). Zinc homeostasis may reverse the synergistic neurotoxicity of heavy metal mixtures in Caenorhabditis elegans. *The science of the total environment.*, *868*, 161699. https://doi.org/10.1016/j.scitotenv.2023.161699

Calderón-Garcidueñas, L., Azzarelli, B., Acuna, H., Garcia, R., Gambling, T. M., Osnaya, N.,…Rewcastle, B. (2002). Air pollution and brain damage. *Toxicologic pathology.*, *30*(3), 373-389. https://doi.org/10.1080/01926230252929954

Calderón-Garcidueñas, L., Franco-Lira, M., Henríquez-Roldán, C., Osnaya, N., González-Maciel, A., Reynoso-Robles, R.,…Doty, R. L. (2010). Urban air pollution: influences on olfactory function and pathology in exposed children and young adults. *Experimental and toxicologic pathology.*, *62*(1), 91-102. https://doi.org/10.1016/j.etp.2009.02.117

Calderón-Garcidueñas, L., Mora-Tiscareño, A., Ontiveros, E., Gómez-Garza, G., Barragán-Mejía, G., Broadway, J.,…Solt, A. C. (2008). Air pollution, cognitive deficits and brain abnormalities: a pilot study with children and dogs. *Brain and cognition.*, *68*(2), 117-127. https://doi.org/10.1016/j.bandc.2008.04.008

Calderón-Garcidueñas, L., Reed, W., Maronpot, R. R., Henríquez-Roldán, C., Delgado-Chavez, R., Calderón-Garcidueñas, A.,…Swenberg, J. A. Brain inflammation and Alzheimer's-like pathology in individuals exposed to severe air pollution. *Toxicologic pathology.*, *32*(6), 650-658. https://doi.org/10.1080/01926230490520232

Calderón-Garcidueñas, L., Serrano-Sierra, A., Torres-Jardón, R., Zhu, H., Yuan, Y., Smith, D.,…Guilarte, T. R. (2013). The impact of environmental metals in young urbanites' brains. *Experimental and toxicologic pathology.*, *65*(5), 503-511. https://doi.org/10.1016/j.etp.2012.02.006

Calderón-Garcidueñas, L., Solt, A. C., Henríquez-Roldán, C., Torres-Jardón, R., Nuse, B., Herritt, L.,…Reed, W. (2008). Long-term air pollution exposure is associated with neuroinflammation, an altered innate immune response, disruption of the blood-brain barrier, ultrafine particulate deposition, and accumulation of amyloid beta-42 and alpha-synuclein in children and young adults. *Toxicologic pathology.*, *36*(2), 289-310. https://doi.org/10.1177/0192623307313011

Campbell, A., Oldham, M., Becaria, A., Bondy, S. C., Meacher, D., Sioutas, C.,…Kleinman, M. (2005). Particulate matter in polluted air may increase biomarkers of inflammation in mouse brain. *Neurotoxicology.*, *26*(1), 133-140. https://doi.org/10.1016/j.neuro.2004.08.003

Canonne-Hergaux, F., Zhang, A. S., Ponka, P., & Gros, P. (2001). Characterization of the iron transporter DMT1 (NRAMP2/DCT1) in red blood cells of normal and anemic mk/mk mice. *Blood*, *98*(13), 3823-3830. https://doi.org/10.1182/blood.v98.13.3823

Cao, Z., Yuan, Y., White, A. J., Li, C., Luo, Z., D'Aloisio, A. A.,…Chen, H. (2024). Air Pollutants and Risk of Parkinson's Disease among Women in the Sister Study. *Environmental health perspectives : EHP.*, *132*(1), 17001. https://doi.org/10.1289/EHP13009

Castellani, R. J., Perry, G., Siedlak, S. L., Nunomura, A., Shimohama, S., Zhang, J.,…Smith, M. A. (2002). Hydroxynonenal adducts indicate a role for lipid

peroxidation in neocortical and brainstem Lewy bodies in humans. *Neuroscience letters*, *319*(1), 25-28. https://doi.org/10.1016/s0304-3940(01)02514-9

Cathryn Tonne , J. D. Y., Sean Beevers , Paul Wilkinson , Frank J Kelly. (2012). PM mass concentration and PM oxidative potential in relation to carotid intima-media thickness. *Epidemiology*, *23*(3), 486-494. https://doi.org/10.1097/EDE.0b013e31824e613e

Cerri, S., Mus, L., & Blandini, F. (2019). Parkinson's Disease in Women and Men: What's the Difference? *J Parkinsons Dis*, *9*(3), 501-515. https://doi.org/10.3233/JPD-191683

Chang, K.-H., & Chen, C.-M. (2020). The Role of Oxidative Stress in Parkinson's Disease. *Antioxidants.*, *9*(7). https://doi.org/10.3390/antiox9070597

Chang-fu Wu , I.-C. K., Ta-Chen Su , Ya-Ru Li , Lian-Yu Lin , Chang-Chuan Chan , Shih-Chieh Hsu. (2010). Effects of personal exposure to particulate matter and ozone on arterial stiffness and heart rate variability in healthy adults. *American journal of epidemiology*, *171*(12), 1299-1309. https://doi.org/10.1093/aje/kwq060

Charitidis, C. A., Georgiou, P., Koklioti, M. A., Trompeta, A.-F., & Markakis, V. (2014). Manufacturing nanomaterials: from research to industry. *Manufacturing Rev.*, *1*, 11. https://doi.org/10.1051/mfreview/2014009

Charrier, J. G., & Anastasio, C. (2012). On dithiothreitol (DTT) as a measure of oxidative potential for ambient particles: evidence for the importance of soluble transition metals. *Atmos Chem Phys*, *12*(5), 11317-11350. https://doi.org/10.5194/acpd-12-11317-2012

Chen, C., Shen, J., Yang, L., Zhang, W., Xia, R., Huan, F.,…Wang, S.-L. (2021). Identification of structural properties influencing the metabolism of polycyclic aromatic hydrocarbons by cytochrome P450 1A1. *The science of the total environment.*, *758*, 143997. https://doi.org/10.1016/j.scitotenv.2020.143997

Chen, G., Canonaco, F., Tobler, A., Aas, W., Alastuey, A., Allan, J.,…Font, A. (2022). European aerosol phenomenology - 8: Harmonised source apportionment of organic aerosol using 22 Year-long ACSM/AMS datasets. *Environment international*, *166*, 107325. https://doi.org/10.1016/j.envint.2022.107325

Chen, H., Kwong, J. C., Copes, R., Hystad, P., van Donkelaar, A., Tu, K.,…Burnett, R. T. (2017). Exposure to ambient air pollution and the incidence of dementia: A population-based cohort study. *Environment international*, *108*, 271-277. https://doi.org/10.1016/j.envint.2017.08.020

Chen, H., Kwong, J. C., Copes, R., Tu, K., Villeneuve, P. J., van Donkelaar, A.,…Burnett, R. T. (2017). Living near major roads and the incidence of dementia, Parkinson's disease, and multiple sclerosis: a population-based cohort study. *Lancet*, *389*(10070), 718-726. https://doi.org/10.1016/S0140-6736(16)32399-6

Chen, J., Liu, G., Kang, Y., Wu, B., Sun, R., Zhou, C., & Wu, D. (2014). Coal utilization in China: environmental impacts and human health. *Environmental geochemistry and health.*, *36*(4), 735-753. https://doi.org/10.1007/s10653-013-9592-1

Chen, L., Deng, H., Cui, H., Fang, J., Zuo, Z., Deng, J.,…Zhao, L. (2018). Inflammatory responses and inflammation-associated diseases in organs. *Oncotarget.*, *9*(6), 7204-7218. https://doi.org/10.18632/oncotarget.23208

Chen, L., Hambright, W. S., Na, R., & Ran, Q. (2015). Ablation of the Ferroptosis Inhibitor Glutathione Peroxidase 4 in Neurons Results in Rapid Motor Neuron Degeneration and Paralysis. *J Biol Chem*, *290*(47), 28097-28106. https://doi.org/10.1074/jbc.M115.680090

Chen, M., Li, B., & Sang, N. (2017). Particulate matter (PM2.5) exposure season-dependently induces neuronal apoptosis and synaptic injuries. *Journal of environmental sciences (China).* *54*, 336-345. https://doi.org/10.1016/j.jes.2016.10.013

Chen, T.-B., Liang, C.-S., Chang, C.-M., Yang, C.-C., Yu, H.-L., Wu, Y.-S.,…Yang, C.-P. (2024). Association Between Exposure to Particulate Matter and the Incidence of Parkinson's Disease: A Nationwide Cohort Study in Taiwan. *Journal of movement disorders*, *17*(3), 313-321. https://doi.org/10.14802/jmd.24003

Chen, X., Liu, S., Zhang, W., Wu, C., Liu, H., Zhang, F.,…Ding, W. (2018). Nrf2 deficiency exacerbates PM2.5-induced olfactory bulb injury. *Biochemical and biophysical research communications*, *505*(4), 1154-1160. https://doi.org/10.1016/j.bbrc.2018.10.057

Chen, Y., Shertzer, H. G., Schneider, S. N., Nebert, D. W., & Dalton, T. P. (2005). Glutamate cysteine ligase catalysis: dependence on ATP and modifier subunit for regulation of tissue glutathione levels. *J Biol Chem*, *280*(40), 33766-33774. https://doi.org/10.1074/jbc.M504604200

Cheng, Y. S., Bowen, L., Rando, R. J., Postlethwait, E. M., Squadrito, G. L., & Matalon, S. (2010). Exposing animals to oxidant gases: nose only vs. whole body. *Proc Am Thorac Soc*, *7*(4), 264-268. https://doi.org/10.1513/pats.201001-001SM

Chu, C., Zhang, H., Cui, S., Han, B., Zhou, L., Zhang, N.,…Zheng, Y. (2019). Ambient PM2.5 caused depressive-like responses through Nrf2/NLRP3 signaling pathway modulating inflammation. *Journal of hazardous materials.*, *369*, 180-190. https://doi.org/10.1016/j.jhazmat.2019.02.026

Chung, M. Y., Rick A Lazaro , D. L., Joscelyne Jackson , J. L., & Dora Rendulic , A. S. H. (2006). Aerosol-borne quinones and reactive oxygen species generation by particulate matter extracts. *Environmental science & technology*, *40*(16), 4880-4886. https://doi.org/10.1021/es0515957

Cobley, J. N., Fiorello, M. L., & Bailey, D. M. (2018). 13 reasons why the brain is susceptible to oxidative stress. *Redox Biol*, *15*, 490-503. https://doi.org/10.1016/j.redox.2018.01.008

Cohen, A. J., Brauer, M., Burnett, R., Anderson, H. R., Frostad, J., Estep, K.,…Shin, H. (2017). Estimates and 25-year trends of the global burden of disease attributable to ambient air pollution: an analysis of data from the Global Burden of Diseases Study 2015. *Lancet*, *389*(10082), 1907-1918. https://doi.org/10.1016/S0140-6736(17)30505-6

Copernicus, & Programme, E. U. s. E. O. *Why we investigate the composition of the atmosphere*. European Union's Earth Observation Programme. https://atmosphere.copernicus.eu/why-we-investigate-composition-

atmosphere#:~:text=According%20to%20the%20World%20Health,quality%20exceeds%20WHO%20guideline%20limits.

Cory-Slechta, D. A., Marvin, E., Welle, K., Goeke, C., Chalupa, D., Oberdörster, G., & Sobolewski, M. (2024). Male-biased vulnerability of mouse brain tryptophan/kynurenine and glutamate systems to adolescent exposures to concentrated ambient ultrafine particle air pollution. *Neurotoxicology.*, *104*, 20-35. https://doi.org/10.1016/j.neuro.2024.07.004

Cory-Slechta, D. A., Sobolewski, M., Marvin, E., Conrad, K., Merrill, A., Anderson, T.,…Oberdorster, G. (2019). The Impact of Inhaled Ambient Ultrafine Particulate Matter on Developing Brain: Potential Importance of Elemental Contaminants. *Toxicologic pathology.*, *47*(8), 976-992. https://doi.org/10.1177/0192623319878400

Cox, A. G., Winterbourn, C. C., & Hampton, M. B. (2009). Mitochondrial peroxiredoxin involvement in antioxidant defence and redox signalling. *The biochemical journal.*, *425*(2), 313-325. https://doi.org/10.1042/BJ20091541

Crobeddu, B., Aragao-Santiago, L., Bui, L.-C., Boland, S., & Baeza Squiban, A. (2017). Oxidative potential of particulate matter 2.5 as predictive indicator of cellular stress. *Environmental pollution.*, *230*, 125-133. https://doi.org/10.1016/j.envpol.2017.06.051

Dagher, Z., Garçon, G., Billet, S., Gosset, P., Ledoux, F., Courcot, D.,…Shirali, P. (2006). Activation of different pathways of apoptosis by air pollution particulate matter (PM2.5) in human epithelial lung cells (L132) in culture. *Toxicology*, *225*(1), 12-24. https://doi.org/10.1016/j.tox.2006.04.038

Dashtipour, K., Liu, M., Kani, C., Dalaie, P., Obenaus, A., Simmons, D.,…Zarifi, M. (2015). Iron Accumulation Is Not Homogenous among Patients with Parkinson's Disease. *Parkinson's disease.*, *2015*, 324843. https://doi.org/10.1155/2015/324843

Dauer, W., & Przedborski, S. (2003). Parkinson's disease: mechanisms and models. *Neuron.*, *39*(6), 889-909. https://doi.org/10.1016/s0896-6273(03)00568-3

Davies, K. M., Bohic, S., Carmona, A., Ortega, R., Cottam, V., Hare, D. J.,…Double, K. L. (2014). Copper pathology in vulnerable brain regions in Parkinson's disease. *Neurobiology of aging.*, *35*(4), 858-866. https://doi.org/10.1016/j.neurobiolaging.2013.09.034

Davies, K. M., Hare, D. J., Bohic, S., James, S. A., Billings, J. L., Finkelstein, D. I.,…Double, K. L. (2015). Comparative Study of Metal Quantification in Neurological Tissue Using Laser Ablation-Inductively Coupled Plasma-Mass Spectrometry Imaging and X-ray Fluorescence Microscopy. *Anal Chem*, *87*(13), 6639-6645. https://doi.org/10.1021/acs.analchem.5b01454

Davis, G. C., Williams, A. C., Markey, S. P., Ebert, M. H., Caine, E. D., Reichert, C. M., & Kopin, I. J. (1979). Chronic Parkinsonism secondary to intravenous injection of meperidine analogues. *Psychiatry research.*, *1*(3), 249-254. https://doi.org/10.1016/0165-1781(79)90006-4

de Farias, C. C., Maes, M., Bonifácio, K. L., Bortolasci, C. C., de Souza Nogueira, A., Brinholi, F. F.,…Barbosa, D. S. (2016). Highly specific changes in antioxidant levels and lipid peroxidation in Parkinson's disease and its progression: Disease

and staging biomarkers and new drug targets. *Neuroscience letters*, *617*, 66-71. https://doi.org/10.1016/j.neulet.2016.02.011

De Franceschi, G., Frare, E., Bubacco, L., Mammi, S., Fontana, A., & de Laureto, P. P. (2009). Molecular insights into the interaction between alpha-synuclein and docosahexaenoic acid. *Journal of Molecular Biology*, *394*(1), 94-107. https://doi.org/10.1016/j.jmb.2009.09.008

De Volder, M. F. L., Tawfick, S. H., Baughman, R. H., & Hart, A. J. (2013). Carbon nanotubes: present and future commercial applications. *Science.*, *339*(6119), 535-539. https://doi.org/10.1126/science.1222453

Dehay, B., Ramirez, A., Martinez-Vicente, M., Perier, C., Canron, M.-H., Doudnikoff, E.,…Bezard, E. (2012). Loss of P-type ATPase ATP13A2/PARK9 function induces general lysosomal deficiency and leads to Parkinson disease neurodegeneration. *Proc Natl Acad Sci U S A*, *109*(24), 9611-9616. https://doi.org/10.1073/pnas.1112368109

Deng, X., Feng, N., Zheng, M., Ye, X., Lin, H., Yu, X.,…Qian, B. (2017). PM2.5 exposure-induced autophagy is mediated by lncRNA loc146880 which also promotes the migration and invasion of lung cancer cells. *Biochimica et biophysica acta . General subjects*, *1861*(2), 112-125. https://doi.org/10.1016/j.bbagen.2016.11.009

Deng, X., Luan, Q., Chen, W., Wang, Y., Wu, M., Zhang, H., & Jiao, Z. (2009). Nanosized zinc oxide particles induce neural stem cell apoptosis. *Nanotechnology.*, *20*(11), 115101. https://doi.org/10.1088/0957-4484/20/11/115101

Deng, X., Zhang, F., Rui, W., Long, F., Wang, L., Feng, Z.,…Ding, W. (2013). PM2.5-induced oxidative stress triggers autophagy in human lung epithelial A549 cells. *Toxicology in vitro.*, *27*(6), 1762-1770. https://doi.org/10.1016/j.tiv.2013.05.004

Development, I. B. f. R. a., & Bank, T. W. (2020). The global health cost of ambient PM2.5 air pollution. In.

Dexter, D. T., Carter, C. J., Wells, F. R., Javoy-Agid, F., Agid, Y., Lees, A.,…Marsden, C. D. (1989). Basal lipid peroxidation in substantia nigra is increased in Parkinson's disease. *Journal of neurochemistry.*, *52*(2), 381-389. https://doi.org/10.1111/j.1471-4159.1989.tb09133.x

Dexter, D. T., Wells, F. R., Agid, F., Agid, Y., Lees, A. J., Jenner, P., & Marsden, C. D. (1987). Increased nigral iron content in postmortem parkinsonian brain. *Lancet*, *2*(8569), 1219-1220. https://doi.org/10.1016/s0140-6736(87)91361-4

Dexter, D. T., Wells, F. R., Lees, A. J., Agid, F., Agid, Y., Jenner, P., & Marsden, C. D. (1989). Increased nigral iron content and alterations in other metal ions occurring in brain in Parkinson's disease. *Journal of neurochemistry.*, *52*(6), 1830-1836. https://doi.org/10.1111/j.1471-4159.1989.tb07264.x

Di Lazzaro, G., Picca, A., Boldrini, S., Bove, F., Marzetti, E., Petracca, M.,…Calabresi, P. (2024). Differential profiles of serum cytokines in Parkinson's disease according to disease duration. *Neurobiology of disease*, *190*, 106371. https://doi.org/10.1016/j.nbd.2023.106371

Dias, V., Junn, E., & Mouradian, M. M. (2013). The role of oxidative stress in Parkinson's disease. *J Parkinsons Dis*, *3*(4), 461-491. https://doi.org/10.3233/JPD-130230

Dimakakou, E., Johnston, H. J., Streftaris, G., & Cherrie, J. W. (2018). Exposure to Environmental and Occupational Particulate Air Pollution as a Potential Contributor to Neurodegeneration and Diabetes: A Systematic Review of Epidemiological Research. *International journal of environmental research and public health.*, *15*(8). https://doi.org/10.3390/ijerph15081704

Dixon, S. J., Lemberg, K. M., Lamprecht, M. R., Skouta, R., Zaitsev, E. M., Gleason, C. E.,…Stockwell, B. R. (2012). Ferroptosis: an iron-dependent form of nonapoptotic cell death. *Cell.*, *149*(5), 1060-1072. https://doi.org/10.1016/j.cell.2012.03.042

Djouina, M., Ollivier, A., Waxin, C., Kervoaze, G., Pichavant, M., Caboche, S.,…Body-Malapel, M. (2024). Chronic Exposure to Both Electronic and Conventional Cigarettes Alters Ileum and Colon Turnover, Immune Function, and Barrier Integrity in Mice. *Journal of xenobiotics.*, *14*(3), 950-969. https://doi.org/10.3390/jox14030053

Do Van, B., Gouel, F., Jonneaux, A., Timmerman, K., Gelé, P., Pétrault, M.,…Devedjian, J.-C. (2016). Ferroptosis, a newly characterized form of cell death in Parkinson's disease that is regulated by PKC. *Neurobiology of disease*, *94*, 169-178. https://doi.org/10.1016/j.nbd.2016.05.011

Donaldson, K., Tran, L., Jimenez, L. A., Duffin, R., Newby, D. E., Mills, N.,…Stone, V. (2005). Combustion-derived nanoparticles: a review of their toxicology following inhalation exposure. *Particle and fibre toxicology.*, *2*, 10. https://doi.org/10.1186/1743-8977-2-10

Donley, N. (2019). The USA lags behind other agricultural nations in banning harmful pesticides. *Environmental Health*, *18*(1), 44. https://doi.org/10.1186/s12940-019-0488-0

Dorsey, E. R., Constantinescu, R., Thompson, J. P., K M Biglan , Holloway, R. G., Kieburtz, K.,…r, C. M. T. (2007). Projected number of people with Parkinson disease in the most populous nations, 2005 through 2030. *Neurology*, *68*(5), 384-386. https://doi.org/10.1212/01.wnl.0000247740.47667.03

Dorsey, E. R., Elbaz, A., Nichols, E., & Collaborators, G. P. s. D. (2018). Global, regional, and national burden of Parkinson's disease, 1990-2016: a systematic analysis for the Global Burden of Disease Study 2016. *Lancet neurology*, *17*(11), 939-953. https://doi.org/10.1016/S1474-4422(18)30295-3

Dorsey, E. R., Sherer, T., Okun, M. S., & Bloem, B. R. (2018). The Emerging Evidence of the Parkinson Pandemic. *J Parkinsons Dis*, *8*(s1), S3-S8. https://doi.org/10.3233/JPD-181474

Dou, C., Zhang, J., & Qi, C. (2018). Cooking oil fume-derived PM2.5 induces apoptosis in A549 cells and MAPK/NF-κB/STAT1 pathway activation. *Environmental science and pollution research.*, *25*(10), 9940-9948. https://doi.org/10.1007/s11356-018-1262-5

Drayton, R. M., Dudziec, E., Peter, S., Bertz, S., Hartmann, A., Bryant, H. E., & Catto, J. W. (2014). Reduced expression of miRNA-27a modulates cisplatin resistance in bladder cancer by targeting the cystine/glutamate exchanger SLC7A11. *Clin Cancer Res*, *20*(7), 1990-2000. https://doi.org/10.1158/1078-0432.CCR-13-2805

Dringen, R., Gutterer, J. M., & Hirrlinger, J. (2000). Glutathione metabolism in brain: Metabolic interaction between astrocytes and neurons in the defense against reactive oxygen species. *Eur J Biochem*, *267*(16), 4912-4916. https://doi.org/10.1046/j.1432-1327.2000.01597.x

Du, Y., Zhang, H., Lu, J., & Holmgren, A. (2012). Glutathione and glutaredoxin act as a backup of human thioredoxin reductase 1 to reduce thioredoxin 1 preventing cell death by aurothioglucose. *J Biol Chem*, *287*(45), 38210-38219. https://doi.org/10.1074/jbc.M112.392225

Duh, E. J., Maury, W. J., Folks, T. M., Fauci, A. S., & Rabson, A. B. (1989). Tumor necrosis factor alpha activates human immunodeficiency virus type 1 through induction of nuclear factor binding to the NF-kappa B sites in the long terminal repeat. *Proceedings of the National Academy of Sciences of the United States of America*, *86*(15), 5974-5978. https://doi.org/10.1073/pnas.86.15.5974

Duman, R. S., Aghajanian, G. K., Sanacora, G., & Krystal, J. H. (2016). Synaptic plasticity and depression: new insights from stress and rapid-acting antidepressants. *Nature medicine.*, *22*(3), 238-249. https://doi.org/10.1038/nm.4050

Dyke, T. V., Knudson, C. M., Yin, C., & Korsmeyer, S. J. (1997). Bax suppresses tumorigenesis and stimulates apoptosis in vivo. *Nature*, *385*(6617), 637-640. https://doi.org/10.1038/385637a0

Dziewulska, D., Doi, H., Fasano, A., Erro, R., Fatehi, F., Fekete, R.,…McNeill, A. (2013). Olfactory impairment and pathology in neurodegenerative disorders with brain iron accumulation. *Acta neuropathologica.*, *126*(1), 151-153. https://doi.org/10.1007/s00401-013-1136-3

E. Ray Dorsey, & Collaborators, G. P. s. D. (2018). Global, regional, and national burden of Parkinson's disease, 1990-2016: a systematic analysis for the Global Burden of Disease Study 2016. *Lancet neurology*, *17*(11), 939-953. https://doi.org/10.1016/S1474-4422(18)30295-3

Edman, L. C., Mira, H., Erices, A., Malmersjö, S., Andersson, E., Uhlén, P., & Arenas, E. (2008). Alpha-chemokines regulate proliferation, neurogenesis, and dopaminergic differentiation of ventral midbrain precursors and neurospheres. *Stem cells.*, *26*(7), 1891-1900. https://doi.org/10.1634/stemcells.2007-0753

Ehsanifar, M., Montazeri, Z., Taheri, M. A., Rafati, M., Behjati, M., & Karimian, M. (2021). Hippocampal inflammation and oxidative stress following exposure to diesel exhaust nanoparticles in male and female mice. *Neurochemistry international.*, *145*, 104989. https://doi.org/10.1016/j.neuint.2021.104989

Enogieru, A. B., Omoruyi, S. I., Hiss, D. C., & Ekpo, O. E. (2019). GRP78/BIP/HSPA5 as a Therapeutic Target in Models of Parkinson's Disease: A Mini Review. *Advances in pharmacological sciences.*, *2019*, 2706783. https://doi.org/10.1155/2019/2706783

EPA, U. (1993). Health Effects Assessement Summary Tables; Office of Research and Development. In. Washington, DC, USA: US EPA.

EPA, U. (2010). Development of a Relative Potency Factor (RPF) Approach for Polycyclic Aromatic Hydrocarbon (PAH) Mixtures: EPA/635/R-08/012A. In. Washington, DC, USA: US EPA.

Evidence of Impending Parkinson's Disease Pandemic Identified. (2019). NeuroscienceNews.com. https://neurosciencenews.com/parkinsons-pandemic-10661/

Facciolà, A., Visalli, G., La Maestra, S., Ceccarelli, M., D'Aleo, F., Nunnari, G.,…Di Pietro, A. (2019). Carbon nanotubes and central nervous system: Environmental risks, toxicological aspects and future perspectives. *Environmental toxicology and pharmacology.*, *65*, 23-30. https://doi.org/10.1016/j.etap.2018.11.006

Fahey, J. W., Haristoy, X., Dolan, P. M., Kensler, T. W., Scholtus, I., Stephenson, K. K.,…Lozniewski, A. (2002). Sulforaphane inhibits extracellular, intracellular, and antibiotic-resistant strains of Helicobacter pylori and prevents benzo[a]pyrene-induced stomach tumors. *Proceedings of the National Academy of Sciences of the United States of America*, *99*(11), 7610-7615. https://doi.org/10.1073/pnas.112203099

Fearnley, J. M., & Lees, A. J. (1991). Ageing and Parkinson's disease: substantia nigra regional selectivity. *Brain*, *114 (Pt 5)*, 2283-2301. https://doi.org/10.1093/brain/114.5.2283

Fechter, L. D., Johnson, D. L., & Lynch, R. A. (2002). The relationship of particle size to olfactory nerve uptake of a non-soluble form of manganese into brain. *Neurotoxicology.*, *23*(2), 177-183. https://doi.org/10.1016/s0161-813x(02)00013-x

Ferreira, B. L., Ferreira, É. R., de Brito, M. V., Salu, B. R., Oliva, M. L. V., Mortara, R. A., & Orikaza, C. M. (2018). BALB/c and C57BL/6 Mice Cytokine Responses to Trypanosoma cruzi Infection Are Independent of Parasite Strain Infectivity. *Frontiers in microbiology.*, *9*, 553. https://doi.org/10.3389/fmicb.2018.00553

Finch, G. L., Hobbs, C. H., Blair, L. F., Barr, E. B., Hahn, F. F., Jaramillo, R. J.,…Howell, S. (2002). Effects of subchronic inhalation exposure of rats to emissions from a diesel engine burning soybean oil-derived biodiesel fuel. *Inhalation toxicology.*, *14*(10), 1017-1048. https://doi.org/10.1080/08958370290084764

Fine particulate matter (PM2.5) is the pollutant that causes the largest health impact globally, contributing to millions of deaths each year. (2024). State of Global Air https://www.stateofglobalair.org/pollution-sources/pm25

Flohe, L., Günzler, W. A., & Schock, H. H. (1973). Glutathione peroxidase: a selenoenzyme. *FEBS letters*, *32*(1), 132-134. https://doi.org/10.1016/0014-5793(73)80755-0

Fonken, L. K., Xu, X., Weil, Z. M., Chen, G., Sun, Q., Rajagopalan, S., & Nelson, R. J. (2011). Air pollution impairs cognition, provokes depressive-like behaviors and alters hippocampal cytokine expression and morphology. *Molecular psychiatry.*, *16*(10), 987-995, 973. https://doi.org/10.1038/mp.2011.76

Foot, N. J., Dalton, H. E., Shearwin-Whyatt, L. M., Dorstyn, L., Tan, S. S., Yang, B., & Kumar, S. (2008). Regulation of the divalent metal ion transporter DMT1 and iron homeostasis by a ubiquitin-dependent mechanism involving Ndfips and WWP2. *Blood*, *112*(10), 4268-4275. https://doi.org/10.1182/blood-2008-04-150953

Fox, S. H., & Brotchie, J. M. (2010). The MPTP-lesioned non-human primate models of Parkinson's disease. Past, present, and future. *Prog Brain Res*, *184*, 133-157. https://doi.org/10.1016/S0079-6123(10)84007-5

Frank, B., Manfred E Schuster , & Robert Schlögl , D. S. S. (2013). Emission of highly activated soot particulate--the other side of the coin with modern diesel engines. *Angewandte Chemie : International edition*, *52*(10), 2673-2677. https://doi.org/10.1002/anie.201206093

Freney, E. J., Heal, M. R., Donovan, R. J., Mills, N. L., Donaldson, K., Newby, D. E.,…Cassee, F. R. (2006). A single-particle characterization of a mobile Versatile Aerosol Concentration Enrichment System for exposure studies. *Particle and fibre toxicology.*, *3*, 8. https://doi.org/10.1186/1743-8977-3-8

Friedmann Angeli, J. P., Schneider, M., Proneth, B., Tyurina, Y. Y., Tyurin, V. A., Hammond, V. J.,…Conrad, M. (2014). Inactivation of the ferroptosis regulator Gpx4 triggers acute renal failure in mice. *Nat Cell Biol*, *16*(12), 1180-1191. https://doi.org/10.1038/ncb3064

Fu, Q., Lyu, D., Zhang, L., Qin, Z., Tang, Q., Yin, H.,…Yao, K. (2017). Airborne particulate matter (PM2.5) triggers autophagy in human corneal epithelial cell line. *Environmental pollution.*, *227*, 314-322. https://doi.org/10.1016/j.envpol.2017.04.078

Gandhi, S., & Abramov, A. Y. (2012). Mechanism of Oxidative Stress in Neurodegeneration. *Oxid Med Cell Longev*, *2012*, 428010-428011. https://doi.org/10.1155/2012/428010

Gao, M., Monian, P., Quadri, N., Ramasamy, R., & Jiang, X. (2015). Glutaminolysis and Transferrin Regulate Ferroptosis. *Molecular cell.*, *59*(2), 298-308. https://doi.org/10.1016/j.molcel.2015.06.011

Garcia, Y., & Esquivel, N. (2018). Comparison of the Response of Male BALB/c and C57BL/6 Mice in Behavioral Tasks to Evaluate Cognitive Function. *Behav Sci (Basel)*, *8*(1). https://doi.org/10.3390/bs8010014

Gardner, B., Dieriks, B. V., Cameron, S., Mendis, L. H. S., Turner, C., Faull, R. L. M., & Curtis, M. A. (2017). Metal concentrations and distributions in the human olfactory bulb in Parkinson's disease. *Scientific reports.*, *7*(1), 10454. https://doi.org/10.1038/s41598-017-10659-6

Gatto, N. M., Henderson, V. W., Hodis, H. N., St John, J. A., Lurmann, F., Chen, J.-C., & Mack, W. J. (2014). Components of air pollution and cognitive function in middle-aged and older adults in Los Angeles. *Neurotoxicology.*, *40*, 1-7. https://doi.org/10.1016/j.neuro.2013.09.004

Ghezzi, P. (2011). Role of glutathione in immunity and inflammation in the lung. *International journal of general medicine.*, *4*, 105-113. https://doi.org/10.2147/IJGM.S15618

Glowacki, S., Synowiec, E., & Blasiak, J. (2013). The Role of Mitochondrial DNA Damage and Repair in the Resistance of BCR/ABL-Expressing Cells to Tyrosine Kinase Inhibitors. *International Journal of Molecular Sciences*, *14*(8), 16348-16364. https://doi.org/10.3390/ijms140816348

Go, Y. M., Roede, J. R., Walker, D. I., Duong, D. M., Seyfried, N. T., Orr, M.,…Jones, D. P. (2013). Selective targeting of the cysteine proteome by thioredoxin and glutathione redox systems. *Mol Cell Proteomics*, *12*(11), 3285-3296. https://doi.org/10.1074/mcp.M113.030437

Gobba, F. (2006). Olfactory toxicity: long-term effects of occupational exposures. *International archives of occupational and environmental health.*, *79*(4), 322-331. https://doi.org/10.1007/s00420-005-0043-x

Goldman, S. M. (2014). Environmental toxins and Parkinson's disease. *Annual review of pharmacology and toxicology.*, *54*, 141-164. https://doi.org/10.1146/annurev-pharmtox-011613-135937

Golts, N., Snyder, H., Frasier, M., Theisler, C., Choi, P., & Wolozin, B. (2002). Magnesium inhibits spontaneous and iron-induced aggregation of alpha-synuclein. *J Biol Chem*, *277*(18), 16116-16123. https://doi.org/10.1074/jbc.M107866200

Gu, Y., Hao, S., Liu, K., Gao, M., Lu, B., Sheng, F.,…Fu, Q. (2022). Airborne fine particulate matter (PM2.5) damages the inner blood-retinal barrier by inducing inflammation and ferroptosis in retinal vascular endothelial cells. *The science of the total environment.*, *838*(Pt 4), 156563. https://doi.org/10.1016/j.scitotenv.2022.156563

Guascito, M. R., Lionetto, M. G., Mazzotta, F., Conte, M., Giordano, M. E., Caricato, R.,…Contini, D. (2023). Characterisation of the correlations between oxidative potential and in vitro biological effects of PM10 at three sites in the central Mediterranean. *Journal of hazardous materials.*, *448*, 130872. https://doi.org/10.1016/j.jhazmat.2023.130872

Guerra, R., Vera-Aguilar, E., Uribe-Ramirez, M., Gookin, G., Camacho, J., Osornio-Vargas, A. R.,…De Vizcaya-Ruiz, A. (2013). Exposure to inhaled particulate matter activates early markers of oxidative stress, inflammation and unfolded protein response in rat striatum. *Toxicology letters.*, *222*(2), 146-154. https://doi.org/10.1016/j.toxlet.2013.07.012

Gui, J., Liu, J., Han, Z., Yang, X., Ding, R., Yang, J.,…Jiang, L. (2023). The dysfunctionality of hippocampal synapses may be directly related to PM-induced impairments in spatial learning and memory in juvenile rats. *Ecotoxicology and environmental safety.*, *254*, 114729. https://doi.org/10.1016/j.ecoenv.2023.114729

Gui, J., Liu, J., Wang, L., Yang, X., Tian, B., Luo, H.,…Jiang, L. (2024). Autophagy alleviates hippocampal neuroinflammation by inhibiting the NLRP3 inflammasome in a juvenile rat model exposed particulate matter. *Toxicology*, *502*, 153730. https://doi.org/10.1016/j.tox.2024.153730

Guo, Z., Zhang, P., Chakraborty, S., Chetwynd, A. J., Abdolahpur Monikh, F., Stark, C.,…Valsami-Jones, E. (2021). Biotransformation modulates the penetration of metallic nanomaterials across an artificial blood-brain barrier model. *Proceedings of the National Academy of Sciences of the United States of America*, *118*(28). https://doi.org/10.1073/pnas.2105245118

Gupta, S. C., Kim, J. H., Prasad, S., & Aggarwal, B. B. (2010). Regulation of survival, proliferation, invasion, angiogenesis, and metastasis of tumor cells through modulation of inflammatory pathways by nutraceuticals. *Cancer and metastasis reviews.*, *29*(3), 405-434. https://doi.org/10.1007/s10555-010-9235-2

Gusdon, A. M., Zhu, J., Van Houten, B., & Chu, C. T. (2011). ATP13A2 regulates mitochondrial bioenergetics through macroautophagy. *Neurobiol Dis*, *45*(3), 962-972. https://doi.org/10.1016/j.nbd.2011.12.015

Guéraud, F., Atalay, M., Bresgen, N., Cipak, A., Eckl, P. M., Huc, L.,…Uchida, K. (2010). Chemistry and biochemistry of lipid peroxidation products. *Free radical research.*, *44*(10), 1098-1124. https://doi.org/10.3109/10715762.2010.498477

Hambright, W. S., Fonseca, R. S., Chen, L., Na, R., & Ran, Q. (2017). Ablation of ferroptosis regulator glutathione peroxidase 4 in forebrain neurons promotes cognitive impairment and neurodegeneration. *Redox Biol*, *12*, 8-17. https://doi.org/10.1016/j.redox.2017.01.021

Hankinson, O. (1995). The aryl hydrocarbon receptor complex. *Annu Rev Pharmacol Toxicol*, *35*, 307-340. https://doi.org/10.1146/annurev.pa.35.040195.001515

Hanson, L. R., & Frey, W. H. (2008). Intranasal delivery bypasses the blood-brain barrier to target therapeutic agents to the central nervous system and treat neurodegenerative disease. *BMC neuroscience.*, *9 Suppl 3*, S5. https://doi.org/10.1186/1471-2202-9-S3-S5

Hartmann, A., Hunot, S., Michel, P. P., Muriel, M.-P., Vyas, S., Faucheux, B. A.,…Hirsch, E. C. (2000). Caspase-3: A Vulnerability Factor and Final Effector in Apoptotic Death of Dopaminergic Neurons in Parkinson's Disease. *Proc Natl Acad Sci U S A*, *97*(6), 2875-2880. https://doi.org/10.1073/pnas.040556597

Hartz, A. M. S., Bauer, B., Block, M. L., Hong, J.-S., & Miller, D. S. (2008). Diesel exhaust particles induce oxidative stress, proinflammatory signaling, and P-glycoprotein up-regulation at the blood-brain barrier. *The FASEB journal.*, *22*(8), 2723-2733. https://doi.org/10.1096/fj.08-106997

Heber, D., Li, Z., Garcia-Lloret, M., Wong, A. M., Lee, T. Y., Thames, G.,…Nel, A. (2014). Sulforaphane-rich broccoli sprout extract attenuates nasal allergic response to diesel exhaust particles [10.1039/C3FO60277J]. *Food & Function*, *5*(1), 35-41. https://doi.org/10.1039/C3FO60277J

Hetz, C. (2012). The unfolded protein response: controlling cell fate decisions under ER stress and beyond. *Nature reviews.*, *13*(2), 89-102. https://doi.org/10.1038/nrm3270

Hirsch, E. C., Brandel, J. P., Galle, P., Javoy-Agid, F., & Agid, Y. (1991). Iron and aluminum increase in the substantia nigra of patients with Parkinson's disease: an X-ray microanalysis. *Journal of neurochemistry.*, *56*(2), 446-451. https://doi.org/10.1111/j.1471-4159.1991.tb08170.x

Hirtz, D., Thurman, D. J., Gwinn-Hardy, K., Mohamed, M., Chaudhuri, A. R., & Zalutsky, R. (2007). How common are the "common" neurologic disorders? *Neurology*, *68*(5), 326-337. https://doi.org/10.1212/01.wnl.0000252807.38124.a3

Hochstrasser, H., Bauer, P., Walter, U., Behnke, S., Spiegel, J., Csoti, I.,…Berg, D. (2004). Ceruloplasmin gene variations and substantia nigra hyperechogenicity in Parkinson disease. *Neurology*, *63*(10), 1912-1917. https://doi.org/10.1212/01.wnl.0000144276.29988.c3

Hu, R., Xie, X.-Y., Xu, S.-K., Wang, Y.-N., Jiang, M., Wen, L.-R.,…Guan, L. (2017). PM2.5 Exposure Elicits Oxidative Stress Responses and Mitochondrial

Apoptosis Pathway Activation in HaCaT Keratinocytes. *Chinese medical journal*, *130*(18), 2205-2214. https://doi.org/10.4103/0366-6999.212942

Hu, W., Zhang, C., Wu, R., Sun, Y., Levine, A., & Feng, Z. (2010). Glutaminase 2, a novel p53 target gene regulating energy metabolism and antioxidant function. *Proceedings of the National Academy of Sciences of the United States of America*, *107*(16), 7455-7460. https://doi.org/10.1073/pnas.1001006107

Huang, T., Guo, W., Wang, Y., Chang, L., Shang, N., Chen, J.,…Zhang, Q. (2021). Involvement of Mitophagy in Aluminum Oxide Nanoparticle-Induced Impairment of Learning and Memory in Mice. *Neurotoxicity research.*, *39*(2), 378-391. https://doi.org/10.1007/s12640-020-00283-0

Hulin, M., Caillaud, D., & Annesi-Maesano, I. (2010). Indoor air pollution and childhood asthma: variations between urban and rural areas. *Indoor air.*, *20*(6), 502-514. https://doi.org/10.1111/j.1600-0668.2010.00673.x

Ioannides, C., & Lewis, D. F. V. (2004). Cytochromes P450 in the bioactivation of chemicals. *Current topics in medicinal chemistry*, *4*(16), 1767-1788. https://doi.org/10.2174/1568026043387188

Izumi, Y., Clifford, D. B., & Zorumski, C. F. (1992). Inhibition of long-term potentiation by NMDA-mediated nitric oxide release. *Science.*, *257*(5074), 1273-1276. https://doi.org/10.1126/science.1519065

Jan, A. T., Azam, M., Siddiqui, K., Ali, A., Choi, I., & Haq, Q. M. R. (2015). Heavy Metals and Human Health: Mechanistic Insight into Toxicity and Counter Defense System of Antioxidants. *International journal of molecular sciences.*, *16*(12), 29592-29630. https://doi.org/10.3390/ijms161226183

Jan, N., Majeed, N., Ahmad, M., Ahmad Lone, W., & John, R. (2022). Nano-pollution: Why it should worry us. *Chemosphere.*, *302*, 134746. https://doi.org/10.1016/j.chemosphere.2022.134746

Jellinger, K., Paulus, W., Grundke-Iqbal, I., Riederer, P., & Youdim, M. B. (1990). Brain iron and ferritin in Parkinson's and Alzheimer's diseases. *Journal of neural transmission.*, *2*(4), 327-340. https://doi.org/10.1007/BF02252926

Jhurry, N. D., Chakrabarti, M., McCormick, S. P., Holmes-Hampton, G. P., & Lindahl, P. A. (2012). Biophysical investigation of the ironome of human jurkat cells and mitochondria. *Biochemistry.*, *51*(26), 5276-5284. https://doi.org/10.1021/bi300382d

Ji, X., Liu, R., Guo, J., Li, Y., Cheng, W., Pang, Y.,…Tang, J. (2022). Olfactory bulb microglia activation mediated neuronal death in real-ambient particulate matter exposure mice with depression-like behaviors. *The science of the total environment.*, *821*, 153456. https://doi.org/10.1016/j.scitotenv.2022.153456

Jiang, L., Hickman, J. H., Wang, S.-J., & Gu, W. (2015). Dynamic roles of p53-mediated metabolic activities in ROS-induced stress responses. *Cell Cycle*, *14*(18), 2881-2885. https://doi.org/10.1080/15384101.2015.1068479

Jiang, L., Kon, N., Li, T., Wang, S.-J., Su, T., Hibshoosh, H.,…Gu, W. (2015). Ferroptosis as a p53-mediated activity during tumour suppression. *Nature.*, *520*(7545), 57-62. https://doi.org/10.1038/nature14344

Jiang, S., Liang, J., Li, W., Wang, L., Song, M., Xu, S.,…Zhang, B. (2023). The role of CXCL1/CXCR2 axis in neurological diseases. *International immunopharmacology.*, *120*, 110330. https://doi.org/10.1016/j.intimp.2023.110330

Jiang, X., Stockwell, B. R., & Conrad, M. (2021). Ferroptosis: mechanisms, biology and role in disease. *Nature Reviews Molecular Cell Biology*, *22*(4), 266-282. https://doi.org/10.1038/s41580-020-00324-8

Jin, H., Kanthasamy, A., Ghosh, A., Anantharam, V., Kalyanaraman, B., & Kanthasamy, A. G. (2014). Mitochondria-targeted antioxidants for treatment of Parkinson's disease: preclinical and clinical outcomes. *Biochimica et biophysica acta*, *1842*(8), 1282-1294. https://doi.org/10.1016/j.bbadis.2013.09.007

Jin, L., Ni, J., Tao, Y., Weng, X., Zhu, Y., Yan, J., & Hu, B. (2019). N-acetylcysteine attenuates PM2.5-induced apoptosis by ROS-mediated Nrf2 pathway in human embryonic stem cells. *The science of the total environment.*, *666*, 713-720. https://doi.org/10.1016/j.scitotenv.2019.02.307

Jin, X., Xue, B., Zhou, Q., Su, R., & Li, Z. (2018). Mitochondrial damage mediated by ROS incurs bronchial epithelial cell apoptosis upon ambient PM2.5 exposure. *The Journal of toxicological sciences.*, *43*(2), 101-111. https://doi.org/10.2131/jts.43.101

Jo, S., Kim, Y.-J., Park, K. W., Hwang, Y. S., Lee, S. H., Kim, B. J., & Chung, S. J. (2021). Association of NO2 and Other Air Pollution Exposures With the Risk of Parkinson Disease. *JAMA neurology.*, *78*(7), 800-808. https://doi.org/10.1001/jamaneurol.2021.1335

Jones, D. P., & Go, Y. M. (2010). Redox compartmentalization and cellular stress. *Diabetes, obesity & metabolism.*, *12 Suppl 2*(Suppl 2), 116-125. https://doi.org/10.1111/j.1463-1326.2010.01266.x

Jovanović, M., Podolski-Renić, A., Krasavin, M., & Pešić, M. (2022). The Role of the Thioredoxin Detoxification System in Cancer Progression and Resistance. *Frontiers in molecular biosciences.*, *9*, 883297. https://doi.org/10.3389/fmolb.2022.883297

Juárez-Rebollar, D., Rios, C., Nava-Ruíz, C., & Méndez-Armenta, M. (2017). Metallothionein in Brain Disorders. *Oxidative medicine and cellular longevity.*, *2017*, 5828056. https://doi.org/10.1155/2017/5828056

Kaltschmidt, C., Kaltschmidt, B., & Baeuerle, P. A. (1993). Brain synapses contain inducible forms of the transcription factor NF-kappa B. *Mechanisms of development.*, *43*(2-3), 135-147. https://doi.org/10.1016/0925-4773(93)90031-r

Kao, Y.-Y., Cheng, T.-J., Yang, D.-M., Wang, C.-T., Chiung, Y.-M., & Liu, P.-S. (2012). Demonstration of an olfactory bulb-brain translocation pathway for ZnO nanoparticles in rodent cells in vitro and in vivo. *Journal of molecular neuroscience.*, *48*(2), 464-471. https://doi.org/10.1007/s12031-012-9756-y

Kao, Y. Y., Cheng, T. J., Yang, D. M., Wang, C. T., Chiung, Y. M., & Liu, P. S. (2012). Demonstration of an olfactory bulb-brain translocation pathway for ZnO nanoparticles in rodent cells in vitro and in vivo. *J Mol Neurosci*, *48*(2), 464-471. https://doi.org/10.1007/s12031-012-9756-y

Kempuraj, D., Thangavel, R., Selvakumar, G. P., Ahmed, M. E., Zaheer, S., Raikwar, S. P.,…Zaheer, A. (2019). Mast Cell Proteases Activate Astrocytes and Glia-Neurons and Release Interleukin-33 by Activating p38 and ERK1/2 MAPKs and NF-κB. *Molecular neurobiology.*, *56*(3), 1681-1693. https://doi.org/10.1007/s12035-018-1177-7

Kempuraj, D., Thangavel, R., Yang, E., Pattani, S., Zaheer, S., Santillan, D. A.,…Zaheer, A. (2015). Dopaminergic Toxin 1-Methyl-4-Phenylpyridinium, Proteins α-Synuclein and Glia Maturation Factor Activate Mast Cells and Release Inflammatory Mediators. *PloS one.*, *10*(8), e0135776. https://doi.org/10.1371/journal.pone.0135776

Kensler, T. W., Wakabayashi, N., & Biswal, S. (2007). Cell survival responses to environmental stresses via the Keap1-Nrf2-ARE pathway. *Annual review of pharmacology and toxicology.*, *47*, 89-116. https://doi.org/10.1146/annurev.pharmtox.46.120604.141046

Kim, H., Lee, D., & Kim, K. (2021). Combined Exposure to Metals in Drinking Water Alters the Dopamine System in Mouse Striatum. *International journal of environmental research and public health.*, *18*(12). https://doi.org/10.3390/ijerph18126558

Kim, J. Y., Hong, S., Bolormaa, O., Seo, J. H., Eom, S.-Y., Kim, Y.-D., & Kim, H. (2022). Effects of diesel exhaust particles and urban particles on brain endothelial cells. *Toxicol Res*, *38*(1), 91-98. https://doi.org/10.1007/s43188-021-00110-4

Kim, K.-H., Kabir, E., & Kabir, S. (2015). A review on the human health impact of airborne particulate matter. *Environment International*, *74*, 136-143. https://doi.org/10.1016/j.envint.2014.10.005

Kim, T. D., Paik, S. R., Yang, C. H., & Kim, J. (2000). Structural changes in alpha-synuclein affect its chaperone-like activity in vitro. *Protein science : a publication of the Protein Society.*, *9*(12), 2489-2496. https://doi.org/10.1110/ps.9.12.2489

Kioumourtzoglou, M.-A., Schwartz, J. D., Weisskopf, M. G., Melly, S. J., Wang, Y., Dominici, F., & Zanobetti, A. (2016). Long-term PM2.5 Exposure and Neurological Hospital Admissions in the Northeastern United States. *Environmental health perspectives : EHP.*, *124*(1), 23-29. https://doi.org/10.1289/ehp.1408973

Kitagishi, Y., & Matsuda, S. (2013). Redox regulation of tumor suppressor PTEN in cancer and aging (Review). *Int J Mol Med*, *31*(3), 511-515. https://doi.org/10.3892/ijmm.2013.1235

Kling, M. A. (2011). A review of respiratory system anatomy, physiology, and disease in the mouse, rat, hamster, and gerbil. *Vet Clin North Am Exot Anim Pract*, *14*(2), 287-337, vi. https://doi.org/10.1016/j.cvex.2011.03.007

Klocke, C., Allen, J. L., Sobolewski, M., Blum, J. L., Zelikoff, J. T., & Cory-Slechta, D. A. (2018). Exposure to fine and ultrafine particulate matter during gestation alters postnatal oligodendrocyte maturation, proliferation capacity, and myelination. *Neurotoxicology*, *65*, 196-206. https://doi.org/10.1016/j.neuro.2017.10.004

Kobayashi, A., Kang, M.-I., Okawa, H., Ohtsuji, M., Zenke, Y., Chiba, T.,…Yamamoto, M. (2004). Oxidative stress sensor Keap1 functions as an adaptor for Cul3-based

E3 ligase to regulate proteasomal degradation of Nrf2. *Mol Cell Biol*, *24*(16), 7130-7139. https://doi.org/10.1128/MCB.24.16.7130-7139.2004

Koike, E., Hirano, S., Shimojo, N., & Kobayashi, T. (2002). cDNA microarray analysis of gene expression in rat alveolar macrophages in response to organic extract of diesel exhaust particles. *Toxicol Sci*, *67*(2), 241-246. https://doi.org/10.1093/toxsci/67.2.241

Komatsu, M., Waguri, S., Koike, M., Sou, Y.-s., Ueno, T., Hara, T.,…Tanaka, K. (2007). Homeostatic Levels of p62 Control Cytoplasmic Inclusion Body Formation in Autophagy-Deficient Mice. *Cell*, *131*(6), 1149-1163. https://doi.org/10.1016/j.cell.2007.10.035

Kou, Z., Tran, F., Colon, T., Shteynfeld, Y., Noh, S., Chen, F.,…Dai, W. (2024). AhR signaling modulates Ferroptosis by regulating SLC7A11 expression. *Toxicology and applied pharmacology.*, *486*, 116936. https://doi.org/10.1016/j.taap.2024.116936

Krebiehl, G., Ruckerbauer, S., Burbulla, L. F., Kieper, N., Maurer, B., Waak, J.,…Krüger, R. (2010). Reduced basal autophagy and impaired mitochondrial dynamics due to loss of Parkinson's disease-associated protein DJ-1. *PLoS One*, *5*(2), e9367-e9367. https://doi.org/10.1371/journal.pone.0009367

Kreuter, J. (2001). Nanoparticulate systems for brain delivery of drugs. *Advanced drug delivery reviews.*, *47*(1), 65-81. https://doi.org/10.1016/s0169-409x(00)00122-8

Kristensen, K., Lunderberg, D. M., Liu, Y., Misztal, P. K., Tian, Y., Arata, C.,…Goldstein, A. H. (2023). Gas-Particle Partitioning of Semivolatile Organic Compounds in a Residence: Influence of Particles from Candles, Cooking, and Outdoors. *Environmental science & technology*, *57*(8), 3260-3269. https://doi.org/10.1021/acs.est.2c07172

Krug, A. K., Gutbier, S., Zhao, L., Pöltl, D., Kullmann, C., Ivanova, V.,…Leist, M. (2014). Transcriptional and metabolic adaptation of human neurons to the mitochondrial toxicant MPP(+). *Cell Death Dis*, *5*(5), e1222. https://doi.org/10.1038/cddis.2014.166

Krzyzanowski, B., Mullan, A. F., Turcano, P., Camerucci, E., Bower, J. H., & Savica, R. (2024). Air Pollution and Parkinson Disease in a Population-Based Study. *JAMA Netw Open*, *7*(9), e2433602. https://doi.org/10.1001/jamanetworkopen.2024.33602

Ku, T., Li, B., Gao, R., Zhang, Y., Yan, W., Ji, X.,…Sang, N. (2017). NF-κB-regulated microRNA-574-5p underlies synaptic and cognitive impairment in response to atmospheric PM2.5 aspiration. *Particle and fibre toxicology.*, *14*(1), 34. https://doi.org/10.1186/s12989-017-0215-3

Kuehn, B. M. (2014). WHO: More than 7 million air pollution deaths each year. *JAMA : the journal of the American Medical Association.*, *311*(15), 1486. https://doi.org/10.1001/jama.2014.4031

Kumagai, Y., Koide, S., Taguchi, K., Endo, A., Nakai, Y., Yoshikawa, T., & Shimojo, N. (2002). Oxidation of proximal protein sulfhydryls by phenanthraquinone, a component of diesel exhaust particles. *Chemical research in toxicology.*, *15*(4), 483-489. https://doi.org/10.1021/tx0100993

Kumar, S., Verma, M. K., & Srivastava, A. K. (2013). Ultrafine particles in urban ambient air and their health perspectives. *Reviews on environmental health.*, *28*(2-3), 117-128. https://doi.org/10.1515/reveh-2013-0008

Kösel, S., Egensperger, R., von Eitzen, U., Mehraein, P., & Graeber, M. B. (1997). On the question of apoptosis in the parkinsonian substantia nigra. *Acta Neuropathol*, *93*(2), 105-108. https://doi.org/10.1007/s004010050590

Künzli, N., Jerrett, M., Mack, W. J., Beckerman, B., LaBree, L., Gilliland, F.,…Hodis, H. N. (2005). Ambient air pollution and atherosclerosis in Los Angeles. *Environmental health perspectives : EHP.*, *113*(2), 201-206. https://doi.org/10.1289/ehp.7523

Langston, J. W., Ballard, P., Tetrud, J. W., & Irwin, I. (1983). Chronic Parkinsonism in humans due to a product of meperidine-analog synthesis. *Science Online.*, *219*(4587), 979-980. https://doi.org/10.1126/science.6823561

Lau, A., Zheng, Y., Tao, S., Wang, H., Whitman, S. A., White, E., & Zhang, D. D. (2013). Arsenic inhibits autophagic flux, activating the Nrf2-Keap1 pathway in a p62-dependent manner. *Mol Cell Biol*, *33*(12), 2436-2446. https://doi.org/10.1128/MCB.01748-12

Lee, S., Hwang, N., Seok, B. G., Lee, S. J., & Chung, S. W. (2023). Autophagy mediates an amplification loop during ferroptosis. *Cell Death Dis*, *14*(7), 464. https://doi.org/10.1038/s41419-023-05978-8

Lee, Y.-H., Lin, C.-H., Hsu, P.-C., Sun, Y.-Y., Huang, Y.-J., Zhuo, J.-H.,…Shie, F.-S. (2015). Aryl hydrocarbon receptor mediates both proinflammatory and anti-inflammatory effects in lipopolysaccharide-activated microglia. *GLIA.*, *63*(7), 1138-1154. https://doi.org/10.1002/glia.22805

Levenson, J. M., Choi, S., Lee, S.-Y., Cao, Y. A., Ahn, H. J., Worley, K. C.,…Sweatt, J. D. (2004). A bioinformatics analysis of memory consolidation reveals involvement of the transcription factor c-rel. *The Journal of neuroscience*, *24*(16), 3933-3943. https://doi.org/10.1523/JNEUROSCI.5646-03.2004

Lewerenz, J., Ates, G., Methner, A., Conrad, M., & Maher, P. (2018). Oxytosis/Ferroptosis-(Re-) Emerging Roles for Oxidative Stress-Dependent Non-apoptotic Cell Death in Diseases of the Central Nervous System. *Frontiers in neuroscience.*, *12*, 214. https://doi.org/10.3389/fnins.2018.00214

Lhermitte, J., Kraus, W. M., & McAlpine, D. (1924). Original Papers: ON THE OCCURRENCE OF ABNORMAL DEPOSITS OF IRON IN THE BRAIN IN PARKINSONISM WITH SPECIAL REFERENCE TO ITS LOCALISATION. *The journal of neurology and psychopathology.*, *5*(19), 195-208. https://doi.org/10.1136/jnnp.s1-5.19.195

Li, J., Zhou, Q., Yang, T., Li, Y., Zhang, Y., Wang, J., & Jiao, Z. (2018). SGK1 inhibits PM2.5-induced apoptosis and oxidative stress in human lung alveolar epithelial A549 cells. *Biochemical and biophysical research communications*, *496*(4), 1291-1295. https://doi.org/10.1016/j.bbrc.2018.02.002

Li, N., Alam, J., Venkatesan, M. I., Eiguren-Fernandez, A., Schmitz, D., Di Stefano, E.,…Nel, A. E. (2004). Nrf2 is a key transcription factor that regulates antioxidant defense in macrophages and epithelial cells: protecting against the

proinflammatory and oxidizing effects of diesel exhaust chemicals. *The journal of immunology.*, *173*(5), 3467-3481. https://doi.org/10.4049/jimmunol.173.5.3467

Li, N., Georas, S., Alexis, N., Fritz, P., Xia, T., Williams, M. A.,…Nel, A. (2016). A work group report on ultrafine particles (American Academy of Allergy, Asthma & Immunology): Why ambient ultrafine and engineered nanoparticles should receive special attention for possible adverse health outcomes in human subjects. *The journal of allergy and clinical immunology.*, *138*(2), 386-396. https://doi.org/10.1016/j.jaci.2016.02.023

Li, R., Mittelstein, D., Kam, W., Pakbin, P., Du, Y., Tintut, Y.,…Hsiai, T. (2013). Atmospheric ultrafine particles promote vascular calcification via the NF-κB signaling pathway. *American journal of physiology.*, *304*(4), C362-C369. https://doi.org/10.1152/ajpcell.00322.2012

Lingappan, K. (2018). NF-κB in Oxidative Stress. *Curr Opin Toxicol*, *7*, 81-86. https://doi.org/10.1016/j.cotox.2017.11.002

Liu, J., Liang, S., Du, Z., Zhang, J., Sun, B., Zhao, T.,…Sun, Z. (2019). PM2.5 aggravates the lipid accumulation, mitochondrial damage and apoptosis in macrophage foam cells. *Environmental pollution.*, *249*, 482-490. https://doi.org/10.1016/j.envpol.2019.03.045

Liu, J., Zhang, Z., Yang, Y., Di, T., Wu, Y., & Bian, T. (2022). NCOA4-Mediated Ferroptosis in Bronchial Epithelial Cells Promotes Macrophage M2 Polarization in COPD Emphysema. *International journal of chronic obstructive pulmonary disease.*, *17*, 667-681. https://doi.org/10.2147/COPD.S354896

Liu, M., Shin, E.-J., Dang, D.-K., Jin, C.-H., Lee, P. H., Jeong, J. H.,…Kim, H.-C. (2018). Trichloroethylene and Parkinson's Disease: Risk Assessment. *Molecular neurobiology.*, *55*(7), 6201-6214. https://doi.org/10.1007/s12035-017-0830-x

Liu, N., Liang, Y., Wei, T., Zou, L., Huang, X., Kong, L.,…Zhang, T. (2022). The role of ferroptosis mediated by NRF2/ERK-regulated ferritinophagy in CdTe QDs-induced inflammation in macrophage. *Journal of hazardous materials.*, *436*, 129043. https://doi.org/10.1016/j.jhazmat.2022.129043

Liu, R., Young, M. T., Chen, J.-C., Kaufman, J. D., & Chen, H. (2016). Ambient Air Pollution Exposures and Risk of Parkinson Disease. *Environmental health perspectives : EHP.*, *124*(11), 1759-1765. https://doi.org/10.1289/EHP135

Liu, T., Jiang, L., Tavana, O., & Gu, W. (2019). The Deubiquitylase OTUB1 Mediates Ferroptosis via Stabilization of SLC7A11. *Cancer research*, *79*(8), 1913-1924. https://doi.org/10.1158/0008-5472.CAN-18-3037

Liu, W., Kato, M.,, Akhand, A. A., Hayakawa, A., Suzuki, H., Miyata, T., Kurokawa, K., Hotta, Y.,, & Ishikawa, N., & Nakashima, I. (2000). 4-hydroxynonenal induces a cellular redox status-related activation of the caspase cascade for apoptotic cell death. *Journal of Cell Science*, *113 (Pt 4)*, 635-641. https://doi.org/10.1242/jcs.113.4.635

Liu, X., Yamada, N., Maruyama, W., & Osawa, T. (2008). Formation of dopamine adducts derived from brain polyunsaturated fatty acids: mechanism for Parkinson disease. *Journal of biological chemistry.*, *283*(50), 34887-34895. https://doi.org/10.1074/jbc.M805682200

Liu, X.-X., Li, X.-J., Zhang, B., Liang, Y.-J., Zhou, C.-X., Cao, D.-X.,…Jian-Rong He , Q. Z. (2011). MicroRNA-26b is underexpressed in human breast cancer and induces cell apoptosis by targeting SLC7A11. *FEBS letters*, *585*(9), 1363-1367. https://doi.org/10.1016/j.febslet.2011.04.018

Liu, Y., Gao, Y., Zhang, L., Wang, T., Wang, J., Jiao, F.,…Chen, C. (2009). Potential health impact on mice after nasal instillation of nano-sized copper particles and their translocation in mice. *J Nanosci Nanotechnol*, *9*(11), 6335-6343. https://doi.org/10.1166/jnn.2009.1320

Loeffler, D. A., LeWitt, P. A., Juneau, P. L., Sima, A. A., Nguyen, H. U., DeMaggio, A. J.,…Kanaley, L. (1996). Increased regional brain concentrations of ceruloplasmin in neurodegenerative disorders. *Brain research.*, *738*(2), 265-274. https://doi.org/10.1016/s0006-8993(96)00782-2

Long, C. M., Nascarella, M. A., & Valberg, P. A. (2013). Carbon black vs. black carbon and other airborne materials containing elemental carbon: physical and chemical distinctions. *Environmental pollution.*, *181*, 271-286. https://doi.org/10.1016/j.envpol.2013.06.009

Loop, M. S., Kent, S. T., Al-Hamdan, M. Z., Crosson, W. L., Estes, S. M., Estes, M. G.,…McClure, L. A. (2013). Fine particulate matter and incident cognitive impairment in the REasons for Geographic and Racial Differences in Stroke (REGARDS) cohort. *PloS one.*, *8*(9), e75001. https://doi.org/10.1371/journal.pone.0075001

Lopez, B., Wang, X., Chen, L.-W. A., Ma, T., Mendez-Jimenez, D., Cobb, L. C.,…Jung, H. (2023). Metal contents and size distributions of brake and tire wear particles dispersed in the near-road environment. *The science of the total environment.*, *883*, 163561. https://doi.org/10.1016/j.scitotenv.2023.163561

Lu, J., & Holmgren, A. (2009). Selenoproteins. *J Biol Chem*, *284*(2), 723-727. https://doi.org/10.1074/jbc.R800045200

Lu, J., & Holmgren, A. (2014). The thioredoxin antioxidant system. *Free radical biology & medicine.*, *66*, 75-87. https://doi.org/10.1016/j.freeradbiomed.2013.07.036

Luo, C.-W., Kuan, Y.-H., Chen, W.-Y., Chen, C.-J., Lin, F. C.-F., & Tsai, S. C.-S. (2023). Association between PM2.5 exposure and risk of Parkinson's disease in individuals with chronic obstructive pulmonary disease in Taiwan: a nested case-control study. *Epidemiology and health.*, *45*, e2023094. https://doi.org/10.4178/epih.e2023094

Luo, Y., Jiang, C., Yu, L., & Yang, A. (2020). Chemical Biology of Autophagy-Related Proteins With Posttranslational Modifications: From Chemical Synthesis to Biological Applications. *Front Chem*, *8*, 233. https://doi.org/10.3389/fchem.2020.00233

Lyons, J., Rauh-Pfeiffer, A., Ming-Yu, Y., Lu, X. M., Zurakowski, D., Curley, M.,…Castillo, L. (2001). Cysteine metabolism and whole blood glutathione synthesis in septic pediatric patients. *Critical care medicine.*, *29*(4), 870-877. https://doi.org/10.1097/00003246-200104000-00036

Lücke, C., Gantz, D. L., Klimtchuk, E., & Hamilton, J. A. (2006). Interactions between fatty acids and alpha-synuclein. *Journal of lipid research.*, *47*(8), 1714-1724. https://doi.org/10.1194/jlr.M600003-JLR200

Ma, C.-l., Su, L., Xie, J.-j., Long, J.-x., Wu, P., & Gu, L. (2014). The prevalence and incidence of Parkinson's disease in China: a systematic review and meta-analysis. *Journal of neural transmission.*, *121*(2), 123-134. https://doi.org/10.1007/s00702-013-1092-z

Maciejczyk, P., Chen, L.-C., & Thurston, G. (2021). The Role of Fossil Fuel Combustion Metals in PM2.5 Air Pollution Health Associations. *Atmosphere*, *12*(9), 1086.

Maher, P. (2018). Potentiation of glutathione loss and nerve cell death by the transition metals iron and copper: Implications for age-related neurodegenerative diseases. *Free radical biology & medicine.*, *115*, 92-104. https://doi.org/10.1016/j.freeradbiomed.2017.11.015

Mahoney-Sanchez, L., Bouchaoui, H., Boussaad, I., Jonneaux, A., Timmerman, K., Berdeaux, O.,…Devedjian, J.-C. (2022). Alpha synuclein determines ferroptosis sensitivity in dopaminergic neurons via modulation of ether-phospholipid membrane composition. *Cell Rep*, *40*(8), 111231. https://doi.org/10.1016/j.celrep.2022.111231

Mahoney-Sánchez, L., Bouchaoui, H., Ayton, S., Devos, D., Duce, J. A., & Devedjian, J.-C. (2021). Ferroptosis and its potential role in the physiopathology of Parkinson's Disease. *Progress in neurobiology.*, *196*, 101890. https://doi.org/10.1016/j.pneurobio.2020.101890

Maiorino, M., Gregolin, C., & Ursini, F. (1990). Phospholipid hydroperoxide glutathione peroxidase. *Methods Enzymol*, *186*, 448-457. https://doi.org/10.1016/0076-6879(90)86139-m

Malik, S., Muhammad, K., & Waheed, Y. (2023). Nanotechnology: A Revolution in Modern Industry. *Molecules : a journal of synthetic chemistry and natural product chemistry.*, *28*(2). https://doi.org/10.3390/molecules28020661

Mancias, J. D., Pontano Vaites, L., Nissim, S., Biancur, D. E., Kim, A. J., Wang, X.,…Harper, J. W. (2015). Ferritinophagy via NCOA4 is required for erythropoiesis and is regulated by iron dependent HERC2-mediated proteolysis. *ELife.*, *4*. https://doi.org/10.7554/eLife.10308

Marcos, L. S. O. a. M. I. a. X. Q. a. R. N. L. a. B. K. S. a. L. F. O. S. (2019). Nanoparticles from construction wastes: A problem to health and the environment. *Journal of Cleaner Production*, *219*, 236-243. https://doi.org/https://doi.org/10.1016/j.jclepro.2019.02.096

Marianthi-Anna, K., elinda, C. P. M., E, H. J., I, O. O., A, C. B., Francine, L., & G, W. M. (2017). The Association Between Air Pollution and Onset of Depression Among Middle-Aged and Older Women. *American journal of epidemiology*, *185*(9), 801-809. https://doi.org/10.1093/aje/kww163

Martins, A. C., Morcillo, P., Ijomone, O. M., Venkataramani, V., Harrison, F. E., Lee, E.,…Aschner, M. (2019). New Insights on the Role of Manganese in Alzheimer's Disease and Parkinson's Disease. *International journal of environmental research and public health.*, *16*(19). https://doi.org/10.3390/ijerph16193546

Mathiassen, S. G., De Zio, D., & Cecconi, F. (2017). Autophagy and the Cell Cycle: A Complex Landscape. *Front. Oncol.*, *7*. https://doi.org/10.3389/fonc.2017.00051

Matz, C. J., Stieb, D. M., & Brion, O. (2015). Urban-rural differences in daily time-activity patterns, occupational activity and housing characteristics. *Environmental health : a global access science source.*, *14*, 88. https://doi.org/10.1186/s12940-015-0075-y

Meng, L., Jiang, A., Chen, R., Li, C.-z., Wang, L., Qu, Y.,…Chen, C. (2013). Inhibitory effects of multiwall carbon nanotubes with high iron impurity on viability and neuronal differentiation in cultured PC12 cells. *Toxicology*, *313*(1), 49-58. https://doi.org/10.1016/j.tox.2012.11.011

Mescher, M., & Haarmann-Stemmann, T. (2018). Modulation of CYP1A1 metabolism: From adverse health effects to chemoprevention and therapeutic options. *Pharmacology & therapeutics.*, *187*, 71-87. https://doi.org/10.1016/j.pharmthera.2018.02.012

Mesci, P., Zaïdi, S., Lobsiger, C. S., Millecamps, S., Escartin, C., Seilhean, D.,…Boillée, S. (2015). System xC- is a mediator of microglial function and its deletion slows symptoms in amyotrophic lateral sclerosis mice. *Brain.*, *138*(Pt 1), 53-68. https://doi.org/10.1093/brain/awu312

Mhyre, T. R., Boyd, J. T., Hamill, R. W., & Maguire-Zeiss, K. A. (2012). Parkinson's disease. *Subcell Biochem*, *65*, 389-455. https://doi.org/10.1007/978-94-007-5416-4_16

Michael, G. J., Esmailzadeh, S., Moran, L. B., Christian, L., Pearce, R. K. B., & Graeber, M. B. (2011). Up-regulation of metallothionein gene expression in parkinsonian astrocytes. *Neurogenetics.*, *12*(4), 295-305. https://doi.org/10.1007/s10048-011-0294-5

Migliore, L., Uboldi, C., Di Bucchianico, S., & Coppedè, F. (2015). Nanomaterials and neurodegeneration. *Environmental and molecular mutagenesis.*, *56*(2), 149-170. https://doi.org/10.1002/em.21931

Miki, Y., Tanji, K., Mori, F., Utsumi, J., Sasaki, H., Kakita, A.,…Wakabayashi, K. (2016). Alteration of Upstream Autophagy-Related Proteins (ULK1, ULK2, Beclin1, VPS34 and AMBRA1) in Lewy Body Disease. *Brain pathology.*, *26*(3), 359-370. https://doi.org/10.1111/bpa.12297

Milkovic, L., Siems, W., Siems, R., & Zarkovic, N. (2014). Oxidative stress and antioxidants in carcinogenesis and integrative therapy of cancer. *Current pharmaceutical design.*, *20*(42), 6529-6542. https://doi.org/10.2174/13816128206661408261528 22

Miller, K. M., Mercado, N. M., & Sortwell, C. E. (2021). Synucleinopathy-associated pathogenesis in Parkinson's disease and the potential for brain-derived neurotrophic factor. *NPJ Parkinson's disease.*, *7*(1), 35. https://doi.org/10.1038/s41531-021-00179-6

Mirończuk-Chodakowska, I., Witkowska, A. M., & Zujko, M. E. (2018). Endogenous non-enzymatic antioxidants in the human body. *Advances in medical sciences.*, *63*(1), 68-78. https://doi.org/10.1016/j.advms.2017.05.005

Miyazaki, I., Asanuma, M., Hozumi, H., Miyoshi, K., & Sogawa, N. (2007). Protective effects of metallothionein against dopamine quinone-induced dopaminergic neurotoxicity. *FEBS letters*, *581*(25), 5003-5008. https://doi.org/10.1016/j.febslet.2007.09.046

Miyazaki, I., Sogawa, C. A., Asanuma, M., Higashi, Y., Tanaka, K. I., Nakanishi, T., & Ogawa, N. (2000). Expression of metallothionein-III mRNA and its regulation by levodopa in the basal ganglia of hemi-parkinsonian rats. *Neuroscience letters*, *293*(1), 65-68. https://doi.org/10.1016/s0304-3940(00)01488-9

Mohajerani, A., Burnett, L., Smith, J. V., Kurmus, H., Milas, J., Arulrajah, A.,…Abdul Kadir, A. (2019). Nanoparticles in Construction Materials and Other Applications, and Implications of Nanoparticle Use. *Materials.*, *12*(19). https://doi.org/10.3390/ma12193052

Morawska, L., Ristovski, Z., Jayaratne, R., Keogh, D., & Ling, X. (2008). Ambient nano and ultrafine particles from motor vehicle emissions: characteristics, ambient processing and implications on human exposure. *Atmospheric Environment*, *42*(35), 8113-8138. https://doi.org/10.1016/j.atmosenv.2008.07.050

Morens, D. M., Folkers, G. K., & Fauci, A. S. (2009). What is a pandemic? *The journal of infectious diseases.*, *200*(7), 1018-1021. https://doi.org/10.1086/644537

Morgan, M. J., & Liu, Z.-g. (2011). Crosstalk of reactive oxygen species and NF-κB signaling. *Cell Res*, *21*(1), 103-115. https://doi.org/10.1038/cr.2010.178

Muralikrishnan, D., & Mohanakumar, K. P. (1998). Neuroprotection by bromocriptine against 1-methyl-4-phenyl-1,2,3,6-tetrahydropyridine-induced neurotoxicity in mice. *The FASEB journal.*, *12*(10), 905-912. https://doi.org/10.1096/fasebj.12.10.905

Mussalo, L., Lampinen, R., Avesani, S., Závodná, T., Krejčík, Z., Kalapudas, J.,…Kanninen, K. M. (2024). Traffic-related ultrafine particles impair mitochondrial functions in human olfactory mucosa cells - Implications for Alzheimer's disease. *Redox Biol*, *75*, 103272. https://doi.org/10.1016/j.redox.2024.103272

Mühlfeld, C., Rothen-Rutishauser, B., Blank, F., Vanhecke, D., Ochs, M., & Gehr, P. (2008). Interactions of nanoparticles with pulmonary structures and cellular responses. *American journal of physiology.*, *294*(5), L817-L829. https://doi.org/10.1152/ajplung.00442.2007

Naujokas, M. F., Anderson, B., Ahsan, H., Aposhian, H. V., Graziano, J. H., Thompson, C., & Suk, W. A. (2013). The broad scope of health effects from chronic arsenic exposure: update on a worldwide public health problem. *Environmental health perspectives : EHP.*, *121*(3), 295-302. https://doi.org/10.1289/ehp.1205875

Noorimotlagh, Z., Azizi, M., Pan, H. F., Mami, S., & Mirzaee, S. A. (2021). Association between air pollution and Multiple Sclerosis: A systematic review. *Environ Res*, *196*, 110386. https://doi.org/10.1016/j.envres.2020.110386

Nordic Pharmacological, S. (1996). Uptake of manganese and cadmium from the nasal mucosa into the central nervous system via olfactory pathways in rats. *Pharmacology & toxicology*, *79*(6), 347-356. https://doi.org/10.1111/j.1600-0773.1996.tb00021.x

Nowack, B., David, R. M., Fissan, H., Morris, H., Shatkin, J. A., Stintz, M.,…Brouwer, D. (2013). Potential release scenarios for carbon nanotubes used in composites. *Environment international*, *59*, 1-11. https://doi.org/10.1016/j.envint.2013.04.003

Nunez, Y., Boehme, A. K., Weisskopf, M. G., Re, D. B., Navas-Acien, A., van Donkelaar, A.,…Kioumourtzoglou, M.-A. (2021). Fine Particle Exposure and Clinical Aggravation in Neurodegenerative Diseases in New York State. *Environmental health perspectives : EHP.*, *129*(2), 27003. https://doi.org/10.1289/EHP7425

O'Riordan, K. J., Huang, I. C., Pizzi, M., Spano, P., Boroni, F., Egli, R.,…Levenson, J. M. (2006). Regulation of nuclear factor kappaB in the hippocampus by group I metabotropic glutamate receptors. *The Journal of neuroscience*, *26*(18), 4870-4879. https://doi.org/10.1523/JNEUROSCI.4527-05.2006

Obata, T., & Chiueh, C. C. (1992). In vivo trapping of hydroxyl free radicals in the striatum utilizing intracranial microdialysis perfusion of salicylate: effects of MPTP, MPDP+, and MPP+. *Journal of neural transmission.*, *89*(1-2), 139-145. https://doi.org/10.1007/BF01245361

Oberdörster, G., Sharp, Z., Atudorei, V., Elder, A., Gelein, R., Kreyling, W., & Cox, C. (2004). Translocation of inhaled ultrafine particles to the brain. *Inhalation toxicology.*, *16*(6-7), 437-445. https://doi.org/10.1080/08958370490439597

Oberdörster, G., & Utell, M. J. (2002). Ultrafine particles in the urban air: to the respiratory tract--and beyond? *Environmental health perspectives : EHP.*, *110*(8), A440-A441. https://doi.org/10.1289/ehp.110-1240959

Ohi, N., Nishikawa, Y., Tokairin, T., Yamamoto, Y., Doi, Y., Omori, Y., & Enomoto, K. (2006). Maintenance of Bad phosphorylation prevents apoptosis of rat hepatic sinusoidal endothelial cells in vitro and in vivo. *Am J Pathol*, *168*(4), 1097-1106. https://doi.org/10.2353/ajpath.2006.050462

Oppenheim, H. A., Lucero, J., Guyot, A.-C., Herbert, L. M., McDonald, J. D., Mabondzo, A., & Lund, A. K. (2013). Exposure to vehicle emissions results in altered blood brain barrier permeability and expression of matrix metalloproteinases and tight junction proteins in mice. *Particle and fibre toxicology.*, *10*, 62. https://doi.org/10.1186/1743-8977-10-62

Ou, Y., Wang, S.-J., Li, D., Chu, B., & Gu, W. (2016). Activation of SAT1 engages polyamine metabolism with p53-mediated ferroptotic responses. *Proceedings of the National Academy of Sciences of the United States of America*, *113*(44), E6806-E6812. https://doi.org/10.1073/pnas.1607152113

Ou, Z., Pan, J., Tang, S., Duan, D., Yu, D., Nong, H., & Wang, Z. (2021). Global Trends in the Incidence, Prevalence, and Years Lived With Disability of Parkinson's Disease in 204 Countries/Territories From 1990 to 2019. *Front Public Health*, *9*, 776847. https://doi.org/10.3389/fpubh.2021.776847

Oudin, A., Forsberg, B., Adolfsson, A. N., Lind, N., Modig, L., Nordin, M.,…Nilsson, L.-G. (2016). Traffic-Related Air Pollution and Dementia Incidence in Northern Sweden: A Longitudinal Study. *Environmental health perspectives : EHP.*, *124*(3), 306-312. https://doi.org/10.1289/ehp.1408322

Pannala, V. R., & Dash, R. K. (2015). Mechanistic characterization of the thioredoxin system in the removal of hydrogen peroxide. *Free radical biology & medicine.*, *78*, 42-55. https://doi.org/10.1016/j.freeradbiomed.2014.10.508

Park, B., Donaldson, K., Duffin, R., Tran, L., Kelly, F., Mudway, I.,…Martin, P. (2008). Hazard and risk assessment of a nanoparticulate cerium oxide-based diesel fuel

additive - a case study. *Inhalation toxicology.*, *20*(6), 547-566. https://doi.org/10.1080/08958370801915309

Park, J.-H., Gopishetty, S., Szewczuk, L. M., Troxel, A. B., Harvey, R. G., & Penning, T. M. (2005). Formation of 8-oxo-7,8-dihydro-2'-deoxyguanosine (8-oxo-dGuo) by PAH o-quinones: involvement of reactive oxygen species and copper(II)/copper(I) redox cycling. *Chemical research in toxicology.*, *18*(6), 1026-1037. https://doi.org/10.1021/tx050001a

Patra, R. C., Swarup, D., & Dwivedi, S. K. (2001). Antioxidant effects of alpha tocopherol, ascorbic acid and L-methionine on lead induced oxidative stress to the liver, kidney and brain in rats. *Toxicology*, *162*(2), 81-88. https://doi.org/10.1016/s0300-483x(01)00345-6

Pearce, R. K. B., Owen, A., Daniel, S., Jenner, P., & Marsden, C. D. (1997). Alterations in the distribution of glutathione in the substantia nigra in Parkinson's disease. *J Neural Transm (Vienna)*, *104*(6), 661-677. https://doi.org/10.1007/BF01291884

Pei, J., Pan, X., Wei, G., & Hua, Y. (2023). Research progress of glutathione peroxidase family (GPX) in redoxidation. *Frontiers in pharmacology.*, *14*, 1147414. https://doi.org/10.3389/fphar.2023.1147414

Peters, R., Ee, N., Peters, J., Booth, A., Mudway, I., & Anstey, K. J. (2019). Air Pollution and Dementia: A Systematic Review. *J Alzheimers Dis*, *70*(s1), S145-S163. https://doi.org/10.3233/JAD-180631

Petersen, S. L., Curran, M. A., Marconi, S. A., Carpenter, C. D., Lubbers, L. S., & McAbee, M. D. (2000). Distribution of mRNAs encoding the arylhydrocarbon receptor, arylhydrocarbon receptor nuclear translocator, and arylhydrocarbon receptor nuclear translocator-2 in the rat brain and brainstem. *The Journal of comparative neurology.*, *427*(3), 428-439. https://doi.org/10.1002/1096-9861(20001120)427:3<428::aid-cne9>3.0.co;2-p

Piper, C. J. M., Rosser, E. C., Oleinika, K., Nistala, K., Krausgruber, T., Rendeiro, A. F.,…Mauri, C. (2019). Aryl Hydrocarbon Receptor Contributes to the Transcriptional Program of IL-10-Producing Regulatory B Cells. *Cell Rep*, *29*(7), 1878-1892.e1877. https://doi.org/10.1016/j.celrep.2019.10.018

Pizzimenti, S., Ciamporcero, E., Daga, M., Pettazzoni, P., Arcaro, A., Cetrangolo, G.,…Barrera, G. (2013). Interaction of aldehydes derived from lipid peroxidation and membrane proteins. *Front Physiol*, *4*, 242. https://doi.org/10.3389/fphys.2013.00242

Platel, A., Privat, K., Talahari, S., Delobel, A., Dourdin, G., Gateau, E.,…Nesslany, F. (2020). Study of in vitro and in vivo genotoxic effects of air pollution fine (PM2.5-0.18) and quasi-ultrafine (PM0.18) particles on lung models. *The science of the total environment.*, *711*, 134666. https://doi.org/10.1016/j.scitotenv.2019.134666

Power, J. H. T., & Blumbergs, P. C. (2009). Cellular glutathione peroxidase in human brain: cellular distribution, and its potential role in the degradation of Lewy bodies in Parkinson's disease and dementia with Lewy bodies. *Acta neuropathologica.*, *117*(1), 63-73. https://doi.org/10.1007/s00401-008-0438-3

Power, M. C., Kioumourtzoglou, M.-A., Hart, J. E., Okereke, O. I., Laden, F., & Weisskopf, M. G. (2015). The relation between past exposure to fine particulate

air pollution and prevalent anxiety: observational cohort study. *BMJ : British medical journal.*, *350*, h1111. https://doi.org/10.1136/bmj.h1111

Pringsheim, T., Jette, N., Frolkis, A., & Steeves, T. D. L. (2014). The prevalence of Parkinson's disease: a systematic review and meta-analysis. *Movement disorders.*, *29*(13), 1583-1590. https://doi.org/10.1002/mds.25945

Przedborski, S., Jackson-Lewis, V., Naini, A. B., Jakowec, M., Petzinger, G., Miller, R., & Akram, M. (2001). The parkinsonian toxin 1-methyl-4-phenyl-1,2,3,6-tetrahydropyridine (MPTP): a technical review of its utility and safety. *Journal of neurochemistry.*, *76*(5), 1265-1274. https://doi.org/10.1046/j.1471-4159.2001.00183.x

Pyatigorskaya, N., Sharman, M., Corvol, J.-C., Valabregue, R., Yahia-Cherif, L., Poupon, F.,…Lehéricy, S. (2015). High nigral iron deposition in LRRK2 and Parkin mutation carriers using R2 relaxometry. *Mov Disord*, *30*(8), 1077-1084. https://doi.org/10.1002/mds.26218

Qi, Y., Wei, S., Xin, T., Huang, C., Pu, Y., Ma, J.,…Liu, S. (2022). Passage of exogeneous fine particles from the lung into the brain in humans and animals. *Proc Natl Acad Sci U S A*, *119*(26), e2117083119. https://doi.org/10.1073/pnas.2117083119

Qin, S., Zeng, H., Wu, Q., Li, Q., Zeeshan, M., Ye, L.,…Zeng, X.-W. (2023). An integrative analysis of lipidomics and transcriptomics in various mouse brain regions in response to real-ambient PM2.5 exposure. *The science of the total environment.*, *895*, 165112. https://doi.org/10.1016/j.scitotenv.2023.165112

Qiu, Y., Zheng, Z., Kim, H., Yang, Z., Zhang, G., Shi, X.,…Zhang, K. (2017). Inhalation Exposure to PM2.5 Counteracts Hepatic Steatosis in Mice Fed High-fat Diet by Stimulating Hepatic Autophagy. *Scientific reports.*, *7*(1), 16286. https://doi.org/10.1038/s41598-017-16490-3

Que, E. L., Domaille, D. W., & Chang, C. J. (2008). Metals in neurobiology: probing their chemistry and biology with molecular imaging. *Chemical reviews.*, *108*(5), 1517-1549. https://doi.org/10.1021/cr078203u

Rabinovich, D., Yaniv, S. P., Alyagor, I., & Schuldiner, O. (2016). Nitric Oxide as a Switching Mechanism between Axon Degeneration and Regrowth during Developmental Remodeling. *Cell.*, *164*(1-2), 170-182. https://doi.org/10.1016/j.cell.2015.11.047

Rakowska, J., Rachwał, M., & Walczak, A. (2022). Health Exposure Assessment of Firefighters Caused by PAHs in PM4 and TSP after Firefighting Operations. *Atmosphere*, *13*(8), 1263.

Ramesh, G., MacLean, A. G., & Philipp, M. T. (2013). Cytokines and chemokines at the crossroads of neuroinflammation, neurodegeneration, and neuropathic pain. *Mediators of inflammation.*, *2013*, 480739. https://doi.org/10.1155/2013/480739

Ramos-Gomez, M., Dolan, P. M., Itoh, K., Yamamoto, M., & Kensler, T. W. (2003). Interactive effects of nrf2 genotype and oltipraz on benzo[a]pyrene–DNA adducts and tumor yield in mice. *Carcinogenesis*, *24*(3), 461-467. https://doi.org/10.1093/carcin/24.3.461

Ramos-Gomez, M., Kwak, M. K., Dolan, P. M., Itoh, K., Yamamoto, M., Talalay, P., & Kensler, T. W. (2001). Sensitivity to carcinogenesis is increased and chemoprotective efficacy of enzyme inducers is lost in nrf2 transcription factor-deficient mice. *Proceedings of the National Academy of Sciences of the United States of America*, *98*(6), 3410-3415. https://doi.org/10.1073/pnas.051618798

Ranft, U., Schikowski, T., Sugiri, D., Krutmann, J., & Krämer, U. (2009). Long-term exposure to traffic-related particulate matter impairs cognitive function in the elderly. *Environmental research.*, *109*(8), 1004-1011. https://doi.org/10.1016/j.envres.2009.08.003

Rauen, U., Springer, A., Weisheit, D., Petrat, F., Korth, H.-G., de Groot, H., & Sustmann, R. (2007). Assessment of chelatable mitochondrial iron by using mitochondrion-selective fluorescent iron indicators with different iron-binding affinities. *Chembiochem.*, *8*(3), 341-352. https://doi.org/10.1002/cbic.200600311

Ravanan, P., Srikumar, I. F., & Talwar, P. (2017). Autophagy: The spotlight for cellular stress responses. *Life Sciences*, *188*, 53-67. https://doi.org/10.1016/j.lfs.2017.08.029

Ren, X., Zou, L., Zhang, X., Branco, V., Wang, J., Carvalho, C.,…Lu, J. (2017). Redox Signaling Mediated by Thioredoxin and Glutathione Systems in the Central Nervous System. *Antioxid Redox Signal*, *27*(13), 989-1010. https://doi.org/10.1089/ars.2016.6925

Rhew, S. H., Kravchenko, J., & Lyerly, H. K. (2021). Exposure to low-dose ambient fine particulate matter PM2.5 and Alzheimer's disease, non-Alzheimer's dementia, and Parkinson's disease in North Carolina. *PloS one.*, *16*(7), e0253253. https://doi.org/10.1371/journal.pone.0253253

Riccò, M., Vezzosi, L., Balzarini, F., Gualerzi, G., Ranzieri, S., Signorelli, C.,…Bragazzi, N. L. (2020). Prevalence of Parkinson Disease in Italy: a systematic review and meta-analysis. *Acta Biomed*, *91*(3), e2020088. https://doi.org/10.23750/abm.v91i3.9443

Riederer, P., Sofic, E., Rausch, W. D., Schmidt, B., Reynolds, G. P., Jellinger, K., & Youdim, M. B. (1989). Transition metals, ferritin, glutathione, and ascorbic acid in parkinsonian brains. *Journal of neurochemistry.*, *52*(2), 515-520. https://doi.org/10.1111/j.1471-4159.1989.tb09150.x

Rolls, A., Shechter, R., London, A., Ziv, Y., Ronen, A., Levy, R., & Schwartz, M. (2007). Toll-like receptors modulate adult hippocampal neurogenesis. *Nature cell biology.*, *9*(9), 1081-1088. https://doi.org/10.1038/ncb1629

Roqué, P. J., Dao, K., & Costa, L. G. (2016). Microglia mediate diesel exhaust particle-induced cerebellar neuronal toxicity through neuroinflammatory mechanisms. *Neurotoxicology.*, *56*, 204-214. https://doi.org/10.1016/j.neuro.2016.08.006

Rossi, A., Berger, K., Chen, H., Leslie, D., Mailman, R. B., & Huang, X. (2018). Projection of the prevalence of Parkinson's disease in the coming decades: Revisited. *Movement disorders.*, *33*(1), 156-159. https://doi.org/10.1002/mds.27063

Rothhammer, V., Mascanfroni, I. D., Bunse, L., Takenaka, M. C., Kenison, J. E., Mayo, L.,…Antel, J. (2016). Type I interferons and microbial metabolites of tryptophan modulate astrocyte activity and central nervous system inflammation via the aryl

hydrocarbon receptor. *Nature medicine.*, *22*(6), 586-597. https://doi.org/10.1038/nm.4106

Rotruck, J. T., Pope, A. L., Ganther, H. E., Swanson, A. B., Hafeman, D. G., & Hoekstra, W. G. (1973). Selenium: biochemical role as a component of glutathione peroxidase. *Science.*, *179*(4073), 588-590. https://doi.org/10.1126/science.179.4073.588

Ruef, J., Moser, M., Bode, C., Kübler, W., & Runge, M. S. (2001). 4-hydroxynonenal induces apoptosis, NF-kappaB-activation and formation of 8-isoprostane in vascular smooth muscle cells. *Basic research in cardiology.*, *96*(2), 143-150. https://doi.org/10.1007/s003950170064

Rui, W., Guan, L., Zhang, F., Zhang, W., & Ding, W. (2016). PM2.5-induced oxidative stress increases adhesion molecules expression in human endothelial cells through the ERK/AKT/NF-κB-dependent pathway. *J Appl Toxicol*, *36*(1), 48-59. https://doi.org/10.1002/jat.3143

Ryou, H. G., Heo, J., & Kim, S.-Y. (2018). Source apportionment of PM10 and PM2.5 air pollution, and possible impacts of study characteristics in South Korea. *Environmental pollution.*, *240*, 963-972. https://doi.org/10.1016/j.envpol.2018.03.066

Saleh, W. M., Ahmad, M. I., Yahya, E. B., & H P S, A. K. (2023). Nanostructured Bioaerogels as a Potential Solution for Particulate Matter Pollution. *Gels.*, *9*(7). https://doi.org/10.3390/gels9070575

Saleh, Y., Antherieu, S., Dusautoir, R., Y Alleman, L., Sotty, J., De Sousa, C.,…Lo-Guidice, J.-M. (2019). Exposure to Atmospheric Ultrafine Particles Induces Severe Lung Inflammatory Response and Tissue Remodeling in Mice. *International journal of environmental research and public health.*, *16*(7). https://doi.org/10.3390/ijerph16071210

Santaella, A., Kuiperij, H. B., van Rumund, A., Esselink, R. A. J., van Gool, A. J., Bloem, B. R., & Verbeek, M. M. (2020). Cerebrospinal fluid monocyte chemoattractant protein 1 correlates with progression of Parkinson's disease. *NPJ Parkinson's disease.*, *6*, 21. https://doi.org/10.1038/s41531-020-00124-z

Sasaki, H., Sato, H., Kuriyama-Matsumura, K., Sato, K., Maebara, K., Wang, H.,…Bannai, S. (2002). Electrophile response element-mediated induction of the cystine/glutamate exchange transporter gene expression. *J Biol Chem*, *277*(47), 44765-44771. https://doi.org/10.1074/jbc.M208704200

Savica, R., Grossardt, B. R., Bower, J. H., Ahlskog, J. E., & Rocca, W. A. (2016). Time Trends in the Incidence of Parkinson Disease. *JAMA neurology.*, *73*(8), 981-989. https://doi.org/10.1001/jamaneurol.2016.0947

Scheperjans, F., Pekkonen, E., Kaakkola, S., & Auvinen, P. (2015). Linking Smoking, Coffee, Urate, and Parkinson's Disease - A Role for Gut Microbiota? *J Parkinsons Dis*, *5*(2), 255-262. https://doi.org/10.3233/JPD-150557

Scholz, D., Pöltl, D., Genewsky, A., Weng, M., Waldmann, T., Schildknecht, S., & Leist, M. (2011). Rapid, complete and large-scale generation of post-mitotic neurons from the human LUHMES cell line. *J Neurochem*, *119*(5), 957-971. https://doi.org/10.1111/j.1471-4159.2011.07255.x

Schraufnagel, D. E. (2020). The health effects of ultrafine particles. *Experimental and molecular medicine.*, *52*(3), 311-317. https://doi.org/10.1038/s12276-020-0403-3

Schuman, E. M., & Madison, D. V. (1991). A requirement for the intercellular messenger nitric oxide in long-term potentiation. *Science.*, *254*(5037), 1503-1506. https://doi.org/10.1126/science.1720572

Schwarz, J. M., Sholar, P. W., & Bilbo, S. D. (2012). Sex differences in microglial colonization of the developing rat brain. *Journal of neurochemistry.*, *120*(6), 948-963. https://doi.org/10.1111/j.1471-4159.2011.07630.x

Selvaraj, V., Armistead, M. Y., Cohenford, M., & Murray, E. (2013). Arsenic trioxide (As(2)O(3)) induces apoptosis and necrosis mediated cell death through mitochondrial membrane potential damage and elevated production of reactive oxygen species in PLHC-1 fish cell line. *Chemosphere.*, *90*(3), 1201-1209. https://doi.org/10.1016/j.chemosphere.2012.09.039

Shah, S. A., Yoon, G. H., Ahmad, A., Ullah, F., Ul Amin, F., & Kim, M. O. (2015). Nanoscale-alumina induces oxidative stress and accelerates amyloid beta (Aβ) production in ICR female mice. *Nanoscale*, *7*(37), 15225-15237. https://doi.org/10.1039/c5nr03598h

Sharma, S., & Ebadi, M. (2014). Significance of metallothioneins in aging brain. *Neurochemistry international.*, *65*, 40-48. https://doi.org/10.1016/j.neuint.2013.12.009

Sharma, S., Moon, C. S., Khogali, A., Haidous, A., Chabenne, A., Ojo, C.,…Ebadi, M. (2013). Biomarkers in Parkinson's disease (recent update). *Neurochemistry international.*, *63*(3), 201-229. https://doi.org/10.1016/j.neuint.2013.06.005

Sharon, R., Goldberg, M. S., Bar-Josef, I., Betensky, R. A., Shen, J., & Selkoe, D. J. (2001). alpha-Synuclein occurs in lipid-rich high molecular weight complexes, binds fatty acids, and shows homology to the fatty acid-binding proteins. *Proceedings of the National Academy of Sciences of the United States of America*, *98*(16), 9110-9115. https://doi.org/10.1073/pnas.171300598

Shen, G., Wang, W., Yang, Y., Zhu, C., Min, Y., Xue, M.,…Tao, S. (2010). Emission factors and particulate matter size distribution of polycyclic aromatic hydrocarbons from residential coal combustions in rural Northern China. *Atmospheric environment*, *44*(39), 5737-5743. https://doi.org/10.1016/j.atmosenv.2010.08.042

Shi, W., Zhang, H., Zhang, Y., Lu, L., Zhou, Q., Wang, Y.,…Yin, L. (2023). Co-exposure to Fe, Zn, and Cu induced neuronal ferroptosis with associated lipid metabolism disorder via the ERK/cPLA2/AA pathway. *Environmental pollution.*, *336*, 122438. https://doi.org/10.1016/j.envpol.2023.122438

Shih, R.-H., Wang, C.-Y., & Yang, C.-M. (2015). NF-kappaB Signaling Pathways in Neurological Inflammation: A Mini Review. *Frontiers in molecular neuroscience.*, *8*, 77. https://doi.org/10.3389/fnmol.2015.00077

Shimada, T., & Fujii-Kuriyama, Y. (2004). Metabolic activation of polycyclic aromatic hydrocarbons to carcinogens by cytochromes P450 1A1 and 1B1. *Cancer science.*, *95*(1), 1-6. https://doi.org/10.1111/j.1349-7006.2004.tb03162.x

Shimada, T., Martin, M. V., Pruess-Schwartz, D., Marnett, L. J., & Guengerich, F. P. (1989). Roles of individual human cytochrome P-450 enzymes in the bioactivation of benzo(a)pyrene, 7,8-dihydroxy-7,8-dihydrobenzo(a)pyrene, and other dihydrodiol derivatives of polycyclic aromatic hydrocarbons. *Cancer research*, *49*(22), 6304-6312.

Shin, S., Burnett, R. T., Kwong, J. C., Hystad, P., van Donkelaar, A., Brook, J. R.,…Chen, H. (2018). Effects of ambient air pollution on incident Parkinson's disease in Ontario, 2001 to 2013: a population-based cohort study. *International journal of epidemiology.*, *47*(6), 2038-2048. https://doi.org/10.1093/ije/dyy172

Sian, J., D T Dexter , Lees, A. J., Daniel, S., Agid, Y., Javoy-Agid, F.,…Marsden, C. D. (1994). Alterations in glutathione levels in Parkinson's disease and other neurodegenerative disorders affecting basal ganglia. *Ann Neurol*. https://doi.org/10.1002/ana.410360305

Sofic, E., Lange, K. W., Jellinger, K., & Riederer, P. (1992). Reduced and oxidized glutathione in the substantia nigra of patients with Parkinson's disease. *Neurosci Lett*, *142*(2), 128-130. https://doi.org/10.1016/0304-3940(92)90355-B

Sofic, E., Paulus, W., Jellinger, K., Riederer, P., & Youdim, M. B. (1991). Selective increase of iron in substantia nigra zona compacta of parkinsonian brains. *Journal of neurochemistry.*, *56*(3), 978-982. https://doi.org/10.1111/j.1471-4159.1991.tb02017.x

Sofic, E., Riederer, P., Heinsen, H., Beckmann, H., Reynolds, G. P., Hebenstreit, G., & Youdim, M. B. (1988). Increased iron (III) and total iron content in post mortem substantia nigra of parkinsonian brain. *Journal of neural transmission.*, *74*(3), 199-205. https://doi.org/10.1007/BF01244786

Son, E. S., Park, J.-W., Kim, Y. J., Jeong, S. H., Hong, J. H., Kim, S.-H., & Kyung, S. Y. (2020). Effects of antioxidants on oxidative stress and inflammatory responses of human bronchial epithelial cells exposed to particulate matter and cigarette smoke extract. *Toxicology in vitro.*, *67*, 104883. https://doi.org/10.1016/j.tiv.2020.104883

Song, J., Zhao, Y., Shan, X., Luo, Y., Hao, N., & Zhao, L. (2024). Active ingredients of Chinese medicine with immunomodulatory properties: NF-κB pathway and Parkinson's disease. *Brain research.*, *1822*, 148603. https://doi.org/10.1016/j.brainres.2023.148603

Song, X., & Long, D. (2020). Nrf2 and Ferroptosis: A New Research Direction for Neurodegenerative Diseases. *Frontiers in neuroscience.*, *14*, 267. https://doi.org/10.3389/fnins.2020.00267

Sotty, J., Garçon, G., Denayer, F. O., Alleman, L. Y., Saleh, Y., Perdrix, E.,…Canivet, L. (2019). Toxicological effects of ambient fine (PM2.5-0.18) and ultrafine (PM0.18) particles in healthy and diseased 3D organo-typic mucocilary-phenotype models. *Environmental research.*, *176*, 108538. https://doi.org/10.1016/j.envres.2019.108538

Sotty, J., Kluza, J., De Sousa, C., Tardivel, M., Anthérieu, S., Alleman, L. Y.,…Garçon, G. (2020). Mitochondrial alterations triggered by repeated exposure to fine (PM2.5-0.18) and quasi-ultrafine (PM0.18) fractions of ambient particulate

matter. *Environment international*, *142*, 105830. https://doi.org/10.1016/j.envint.2020.105830

Starkov, A. A., Andreyev, A. Y., Zhang, S. F., Starkova, N. N., Korneeva, M., Syromyatnikov, M., & Popov, V. N. (2014). Scavenging of H2O2 by mouse brain mitochondria. *Journal of bioenergetics and biomembranes.*, *46*(6), 471-477. https://doi.org/10.1007/s10863-014-9581-9

Stone, K. P., Kastin, A. J., & Pan, W. (2011). NFκB is an unexpected major mediator of interleukin-15 signaling in cerebral endothelia. *Cell Physiol Biochem*, *28*(1), 115-124. https://doi.org/10.1159/000331720

Sun, Y., Chen, P., Zhai, B., Zhang, M., Xiang, Y., Fang, J.,…Li, G. (2020). The emerging role of ferroptosis in inflammation. *Biomedicine & pharmacotherapy.*, *127*, 110108. https://doi.org/10.1016/j.biopha.2020.110108

Sun, Y., Sukumaran, P., Selvaraj, S., Cilz, N. I., Schaar, A., Lei, S., & Singh, B. B. (2018). TRPM2 Promotes Neurotoxin MPP. *Mol Neurobiol*, *55*(1), 409-420. https://doi.org/10.1007/s12035-016-0338-9

Swanson, H. I., Chan, W. K., & Bradfield, C. A. (1995). DNA binding specificities and pairing rules of the Ah receptor, ARNT, and SIM proteins. *J Biol Chem*, *270*(44), 26292-26302. https://doi.org/10.1074/jbc.270.44.26292

Sánchez-Rodríguez, M. A., Santiago, E., Arronte-Rosales, A., Vargas-Guadarrama, L. A., & Mendoza-Núñez, V. M. (2006). Relationship between oxidative stress and cognitive impairment in the elderly of rural vs. urban communities. *Life Sci*, *78*(15), 1682-1687. https://doi.org/10.1016/j.lfs.2005.08.007

Tang, Q., Bai, L., Zou, Z., Meng, P., Xia, Y., Cheng, S.,…Chen, C. (2018). Ferroptosis is newly characterized form of neuronal cell death in response to arsenite exposure. *Neurotoxicology.*, *67*, 27-36. https://doi.org/10.1016/j.neuro.2018.04.012

Tanner, C. M., Kamel, F., Ross, G. W., Hoppin, J. A., Goldman, S. M., Korell, M.,…Langston, J. W. (2011). Rotenone, paraquat, and Parkinson's disease. *Environmental health perspectives : EHP.*, *119*(6), 866-872. https://doi.org/10.1289/ehp.1002839

Tarze, A., Deniaud, A., Le Bras, M., Maillier, E., Molle, D., Larochette, N.,…Brenner, C. (2007). GAPDH, a novel regulator of the pro-apoptotic mitochondrial membrane permeabilization. *Oncogene*, *26*(18), 2606-2620. https://doi.org/10.1038/sj.onc.1210074

Tatton, N. A. (2000). Increased Caspase 3 and Bax Immunoreactivity Accompany Nuclear GAPDH Translocation and Neuronal Apoptosis in Parkinson's Disease. *Exp Neurol*, *166*(1), 29-43. https://doi.org/10.1006/exnr.2000.7489

Tavares, W. M., Araujo de França, S., Paiva, W. S., & Teixeira, M. J. (2023). Early tracheostomy versus late tracheostomy in severe traumatic brain injury or stroke: A systematic review and meta-analysis. *Australian critical care : official journal of the Confederation of Australian Critical Care Nurses.*, *36*(6), 1110-1116. https://doi.org/10.1016/j.aucc.2022.12.012

Thangavel, P., Park, D., & Lee, Y.-C. (2022). Recent Insights into Particulate Matter (PM2.5)-Mediated Toxicity in Humans: An Overview. *International journal of*

environmental research and public health., *19*(12). https://doi.org/10.3390/ijerph19127511

Thomas, B., & Beal, M. F. (2007). Parkinson's disease. *Hum Mol Genet*, *16 Spec No. 2*, R183-194. https://doi.org/10.1093/hmg/ddm159

Tjälve, H., & Henriksson, J. Uptake of metals in the brain via olfactory pathways. *Neurotoxicology.*, *20*(2-3), 181-195.

Trépanier, G., Furling, D., Puymirat, J., & Mirault, M. E. (1996). Immunocytochemical localization of seleno-glutathione peroxidase in the adult mouse brain. *Neuroscience.*, *75*(1), 231-243. https://doi.org/10.1016/0306-4522(96)00222-9

Tzivian, L., Dlugaj, M., Winkler, A., Weinmayr, G., Hennig, F., Fuks, K. B.,…Hoffmann, B. (2016). Long-Term Air Pollution and Traffic Noise Exposures and Mild Cognitive Impairment in Older Adults: A Cross-Sectional Analysis of the Heinz Nixdorf Recall Study. *Environmental health perspectives : EHP.*, *124*(9), 1361-1368. https://doi.org/10.1289/ehp.1509824

Uitti, R. J., Rajput, A. H., Rozdilsky, B., Bickis, M., Wollin, T., & Yuen, W. K. (1989). Regional metal concentrations in Parkinson's disease, other chronic neurological diseases, and control brains. *Canadian journal of neurological sciences*, *16*(3), 310-314. https://doi.org/10.1017/s0317167100029140

Umek, N., Geršak, B., Vintar, N., Šoštarič, M., & Mavri, J. (2018). Dopamine Autoxidation Is Controlled by Acidic pH. *Frontiers in molecular neuroscience.*, *11*, 467. https://doi.org/10.3389/fnmol.2018.00467

United.States.Environmental.Protection.Agency. (2022). *Particulate Matter (PM) Basics*.

Uversky, V. N., Li, J., & Fink, A. L. (2001). Metal-triggered structural transformations, aggregation, and fibrillation of human alpha-synuclein. A possible molecular NK between Parkinson's disease and heavy metal exposure. *J Biol Chem*, *276*(47), 44284-44296. https://doi.org/10.1074/jbc.M105343200

Vallerga, C. L., Zhang, F., Fowdar, J., McRae, A. F., Qi, T., Nabais, M. F.,…Gratten, J. (2020). Analysis of DNA methylation associates the cystine-glutamate antiporter SLC7A11 with risk of Parkinson's disease. *Nat Commun*, *11*(1), 1238-1238. https://doi.org/10.1038/s41467-020-15065-7

Vallerga, C. L., Zhang, F., Fowdar, J., McRae, A. F., Qi, T., Nabais, M. F.,…Gratten, J. (2020). Analysis of DNA methylation associates the cystine-glutamate antiporter SLC7A11 with risk of Parkinson's disease. *Nat Commun*, *11*(1), 1238. https://doi.org/10.1038/s41467-020-15065-7

Van den Berg, M., Birnbaum, L. S., Denison, M., De Vito, M., Farland, W., Feeley, M.,…Peterson, R. E. (2006). The 2005 World Health Organization Reevaluation of Human and Mammalian Toxic Equivalency Factors for Dioxins and Dioxin-Like Compounds. *Toxicological Sciences*, *93*(2), 223-241. https://doi.org/10.1093/toxsci/kfl055

Vanbrabant, K., Rasking, L., Vangeneugden, M., Bové, H., Ameloot, M., Vanmierlo, T.,…Plusquin, M. (2024). Impact on murine neurodevelopment of early-life exposure to airborne ultrafine carbon nanoparticles. *Particle and fibre toxicology.*, *21*(1), 51. https://doi.org/10.1186/s12989-024-00612-7

Vanbrabant, K., Van Dam, D., Bongaerts, E., Vermeiren, Y., Bové, H., Hellings, N.,…Nawrot, T. S. (2024). Accumulation of Ambient Black Carbon Particles Within Key Memory-Related Brain Regions. *JAMA Netw Open*, *7*(4), e245678. https://doi.org/10.1001/jamanetworkopen.2024.5678

Vergne, I., & Deretic, V. (2010). The role of PI3P phosphatases in the regulation of autophagy. *FEBS Lett*, *584*(7), 1313-1318. https://doi.org/10.1016/j.febslet.2010.02.054

Viana, M., Salmatonidis, A., Bezantakos, S., Ribalta, C., Moreno, N., Córdoba, P.,…Monfort, E. (2021). Characterizing the Chemical Profile of Incidental Ultrafine Particles for Toxicity Assessment Using an Aerosol Concentrator. *Ann Work Expo Health*, *65*(8), 966-978. https://doi.org/10.1093/annweh/wxab011

Visanji, N. P., Collingwood, J. F., Finnegan, M. E., Tandon, A., House, E., & Hazrati, L.-N. (2013). Iron deficiency in parkinsonism: region-specific iron dysregulation in Parkinson's disease and multiple system atrophy. *J Parkinsons Dis*, *3*(4), 523-537. https://doi.org/10.3233/JPD-130197

Viswanath, V., Wu, Y., Boonplueang, R., Chen, S., Stevenson, F. F., Yantiri, F.,…Andersen, J. K. (2001). Caspase-9 Activation Results in Downstream Caspase-8 Activation and Bid Cleavage in 1-Methyl-4-Phenyl-1,2,3,6-Tetrahydropyridine-Induced Parkinson's Disease. *J Neurosci*, *21*(24), 9519-9528. https://doi.org/10.1523/JNEUROSCI.21-24-09519.2001

Vogel, C. F. A., Van Winkle, L. S., Esser, C., & Haarmann-Stemmann, T. (2020). The aryl hydrocarbon receptor as a target of environmental stressors - Implications for pollution mediated stress and inflammatory responses. *Redox Biol*, *34*, 101530. https://doi.org/10.1016/j.redox.2020.101530

Vouk, V. B., & Piver, W. T. (1983). Metallic elements in fossil fuel combustion products: amounts and form of emissions and evaluation of carcinogenicity and mutagenicity. *Environmental health perspectives : EHP.*, *47*, 201-225. https://doi.org/10.1289/ehp.8347201

Wang, B., Feng, W. Y., Wang, M., Shi, J. W., Zhang, F., Ouyang, H.,…Wang, J. (2007). Transport of intranasally instilled fine Fe2O3 particles into the brain: micro-distribution, chemical states, and histopathological observation. *Biological trace element research.*, *118*(3), 233-243. https://doi.org/10.1007/s12011-007-0028-6

Wang, J., Sun, P., Bao, Y., Dou, B., Song, D., & Li, Y. (2012). Vitamin E renders protection to PC12 cells against oxidative damage and apoptosis induced by single-walled carbon nanotubes. *Toxicology in vitro.*, *26*(1), 32-41. https://doi.org/10.1016/j.tiv.2011.10.004

Wang, J., Sun, P., Bao, Y., Liu, J., & An, L. (2011). Cytotoxicity of single-walled carbon nanotubes on PC12 cells. *Toxicology in vitro.*, *25*(1), 242-250. https://doi.org/10.1016/j.tiv.2010.11.010

Wang, J., Sun, P., Bao, Y., Liu, J., & An, L. (2011). Cytotoxicity of single-walled carbon nanotubes on PC12 cells. *Toxicol In Vitro*, *25*(1), 242-250. https://doi.org/10.1016/j.tiv.2010.11.010

Wang, J., Wu, N., Peng, M., Oyang, L., Jiang, X., Peng, Q.,…Liao, Q. (2023). Ferritinophagy: research advance and clinical significance in cancers. *Cell death discovery.*, *9*(1), 463. https://doi.org/10.1038/s41420-023-01753-y

Wang, Q., Gan, X., Li, F., Chen, Y., Fu, W., Zhu, X.,…Xu, D. (2019). PM2.5 Exposure Induces More Serious Apoptosis of Cardiomyocytes Mediated by Caspase3 through JNK/ P53 Pathway in Hyperlipidemic Rats. *International journal of biological sciences.*, *15*(1), 24-33. https://doi.org/10.7150/ijbs.28633

Wang, Q., Yang, K., Han, B., Sheng, B., Yin, J., Pu, A.,…Yang, H. (2018). Aryl hydrocarbon receptor inhibits inflammation in DSS-induced colitis via the MK2/p-MK2/TTP pathway. *Int J Mol Med*, *41*(2), 868-876. https://doi.org/10.3892/ijmm.2017.3262

Wang, T., Xie, Z., & Lu, B. (1995). Nitric oxide mediates activity-dependent synaptic suppression at developing neuromuscular synapses. *Nature.*, *374*(6519), 262-266. https://doi.org/10.1038/374262a0

Wang, W., Deng, Z., Feng, Y., Liao, F., Zhou, F., Feng, S., & Wang, X. (2017). PM2.5 induced apoptosis in endothelial cell through the activation of the p53-bax-caspase pathway. *Chemosphere.*, *177*, 135-143. https://doi.org/10.1016/j.chemosphere.2017.02.144

Wang, Y., Arellanes, C., Curtis, D. B., & Paulson, S. E. (2010). Probing the source of hydrogen peroxide associated with coarse mode aerosol particles in southern California. *Environmental science & technology*, *44*(11), 4070-4075. https://doi.org/10.1021/es100593k

Wang, Y., Lin, Z., Huang, H., He, H., Yang, L., Chen, T.,…Liu, G. (2015). AMPK is required for PM2.5-induced autophagy in human lung epithelial A549 cells. *Int J Clin Exp Med*, *8*(1), 58-72.

Wang, Y., Liu, Y., & Yan, H. (2020). Effect of long-term particulate matter exposure on Parkinson's risk. *Environmental geochemistry and health.*, *42*(7), 2265-2275. https://doi.org/10.1007/s10653-019-00484-3

Wang, Y., & Tang, M. (2019). PM2.5 induces ferroptosis in human endothelial cells through iron overload and redox imbalance. *Environmental Pollution*, *254*(Pt A). https://doi.org/10.1016/j.envpol.2019.07.105

Wanneveich, M., Moisan, F., Jacqmin-Gadda, H., Elbaz, A., & Joly, P. (2018). Projections of prevalence, lifetime risk, and life expectancy of Parkinson's disease (2010-2030) in France. *Movement disorders.*, *33*(9), 1449-1455. https://doi.org/10.1002/mds.27447

Wei, H., Chen, C., Di, F., Sun, C., Wang, X., Sun, M.,…Liang, X. (2024). PM2.5-induced ferroptosis by Nrf2/Hmox1 signaling pathway led to inflammation in microglia. *Environmental pollution.*, *352*, 124130. https://doi.org/10.1016/j.envpol.2024.124130

Wei, Y., Cao, X.-N., Tang, X.-L., Shen, L.-J., Lin, T., He, D.-W.,…Wei, G.-H. (2018). Urban fine particulate matter (PM2.5) exposure destroys blood-testis barrier (BTB) integrity through excessive ROS-mediated autophagy. *Toxicology mechanisms and methods.*, *28*(4), 302-319. https://doi.org/10.1080/15376516.2017.1410743

Weuve, J., Puett, R. C., Schwartz, J., Yanosky, J. D., Laden, F., & Grodstein, F. (2012). Exposure to particulate air pollution and cognitive decline in older women. *Archives of internal medicine.*, *172*(3), 219-227. https://doi.org/10.1001/archinternmed.2011.683

Whitby, K. T., Kittelson, D. B., Cantrell, B. K., Barsic, N. J., & Bolan, D. F. (1976). Aerosol size distributions and concentrations measured during the General Motors proving grounds sulfate study. In (2 ed., Vol. 16). Washington D.C., U.S.A., American Chem. Soc: American Chemical Society.

Wilker, E. H., Mittleman, M. A., Coull, B. A., Gryparis, A., Bots, M. L., Schwartz, J., & Sparrow, D. (2013). Long-term exposure to black carbon and carotid intima-media thickness: the normative aging study. *Environmental health perspectives : EHP.*, *121*(9), 1061-1067. https://doi.org/10.1289/ehp.1104845

Wilkinson, N., & Pantopoulos, K. (2014). The IRP/IRE system in vivo: insights from mouse models. *Frontiers in pharmacology.*, *5*, 176. https://doi.org/10.3389/fphar.2014.00176

Winslow, A. R., & Rubinsztein, D. C. (2011). The Parkinson disease protein α-synuclein inhibits autophagy. *Autophagy*, *7*(4), 429-431. https://doi.org/10.4161/auto.7.4.14393

Woodward, N. C., Crow, A. L., Zhang, Y., Epstein, S., Hartiala, J., Johnson, R.,…Allayee, H. (2019). Exposure to Nanoscale Particulate Matter from Gestation to Adulthood Impairs Metabolic Homeostasis in Mice. *Scientific reports.*, *9*(1), 1816. https://doi.org/10.1038/s41598-018-37704-2

Wu, T., Liang, X., Liu, X., Li, Y., Wang, Y., Kong, L., & Tang, M. (2020). Induction of ferroptosis in response to graphene quantum dots through mitochondrial oxidative stress in microglia. *Particle and fibre toxicology.*, *17*(1), 30. https://doi.org/10.1186/s12989-020-00363-1

Wu, T., Wang, X., Cheng, J., Liang, X., Li, Y., Chen, M.,…Tang, M. (2022). Nitrogen-doped graphene quantum dots induce ferroptosis through disrupting calcium homeostasis in microglia. *Particle and fibre toxicology.*, *19*(1), 22. https://doi.org/10.1186/s12989-022-00464-z

Wu, X., Cobbina, S. J., Mao, G., Xu, H., Zhang, Z., & Yang, L. (2016). A review of toxicity and mechanisms of individual and mixtures of heavy metals in the environment. *Environmental science and pollution research.*, *23*(9), 8244-8259. https://doi.org/10.1007/s11356-016-6333-x

Wu, Y., Sun, X., Song, B., Qiu, X., & Zhao, J. (2017). MiR-375/SLC7A11 axis regulates oral squamous cell carcinoma proliferation and invasion. *Cancer medicine.*, *6*(7), 1686-1697. https://doi.org/10.1002/cam4.1110

Xia, W.-R., Fu, W., Wang, Q., Zhu, X., Xing, W.-W., Wang, M.,…Xu, D.-G. (2017). Autophagy Induced FHL2 Upregulation Promotes IL-6 Production by Activating the NF-κB Pathway in Mouse Aortic Endothelial Cells after Exposure to PM2.5. *International journal of molecular sciences.*, *18*(7). https://doi.org/10.3390/ijms18071484

Xie, Y., Hou, W., Song, X., Yu, Y., Huang, J., Sun, X.,…Tang, D. (2016). Ferroptosis: process and function. *Cell death and differentiation.*, *23*(3), 369-379. https://doi.org/10.1038/cdd.2015.158

Xiong, Q., Tian, X., Xu, C., Ma, B., Liu, W., Sun, B.,…Shu, X. (2022). PM2 .5 exposure-induced ferroptosis in neuronal cells via inhibiting ERK/CREB pathway. *Environmental toxicology.*, *37*(9), 2201-2213. https://doi.org/10.1002/tox.23586

Xu, X., Wang, H., Liu, S., Xing, C., Liu, Y., Zhou, W.,…Song, L. (2016). TP53-dependent autophagy links the ATR-CHEK1 axis activation to proinflammatory VEGFA production in human bronchial epithelial cells exposed to fine particulate matter (PM2.5). *Autophagy*, *12*(10), 1832-1848. https://doi.org/10.1080/15548627.2016.1204496

Xu, Y., Zhao, Y., Liu, S., Lv, S., Chen, L., Wang, W.,…Xu, H. (2022). Zinc Oxide Particles Can Cause Ovarian Toxicity by Oxidative Stress in Female Mice Model. *International journal of nanomedicine.*, *17*, 4947-4960. https://doi.org/10.2147/IJN.S373147

Yamamoto, S., Ahmed, S., Kakeyama, M., Kobayashi, T., & Fujimaki, H. (2006). Brain cytokine and chemokine mRNA expression in mice induced by intranasal instillation with ultrafine carbon black. *Toxicology letters.*, *163*(2), 153-160. https://doi.org/10.1016/j.toxlet.2005.10.006

Yang, S., & Lian, G. (2020). Correction to: ROS and diseases: role in metabolism and energy supply. *Molecular and cellular biochemistry.*, *467*(1-2), 13. https://doi.org/10.1007/s11010-020-03697-8

Yang, W. S., SriRamaratnam, R., Welsch, M. E., Shimada, K., Skouta, R., Viswanathan, V. S.,…Stockwell, B. R. (2014). Regulation of ferroptotic cancer cell death by GPX4. *Cell.*, *156*(1-2), 317-331. https://doi.org/10.1016/j.cell.2013.12.010

Yang, X., Zhao, T., Feng, L., Shi, Y., Jiang, J., Liang, S.,…Sun, Z. (2019). PM2.5-induced ADRB2 hypermethylation contributed to cardiac dysfunction through cardiomyocytes apoptosis via PI3K/Akt pathway. *Environment international*, *127*, 601-614. https://doi.org/10.1016/j.envint.2019.03.057

Yao, Y., & Tsirka, S. E. (2014). Monocyte chemoattractant protein-1 and the blood-brain barrier. *Cellular and molecular life sciences : CMLS.*, *71*(4), 683-697. https://doi.org/10.1007/s00018-013-1459-1

Yen, Y.-P., Tsai, K.-S., Chen, Y.-W., Huang, C.-F., Yang, R.-S., & Liu, S.-H. (2012). Arsenic induces apoptosis in myoblasts through a reactive oxygen species-induced endoplasmic reticulum stress and mitochondrial dysfunction pathway. *Archives of toxicology*, *86*(6), 923-933. https://doi.org/10.1007/s00204-012-0864-9

Yin, J., Xia, W., Li, Y., Guo, C., Zhang, Y., Huang, S.,…Zhang, A. (2017). COX-2 mediates PM2.5-induced apoptosis and inflammation in vascular endothelial cells. *Am J Transl Res*, *9*(9), 3967-3976.

You, R., Ho, Y.-S., & Chang, R. C.-C. (2022). The pathogenic effects of particulate matter on neurodegeneration: a review. *Journal of biomedical science.*, *29*(1), 15. https://doi.org/10.1186/s12929-022-00799-x

Yuan, J., Mo, L., Mo, Y., Zhang, Y., Zhang, Y., & Zhang, Q. (2022). A protective role of autophagy in fine airborne particulate matter-induced apoptosis in LN-229 cells. *Toxicology*, *477*, 153271. https://doi.org/10.1016/j.tox.2022.153271

Yuan, X., Wang, Y., Li, L., Zhou, W., Tian, D., Lu, C.,…Peng, S. (2016). PM2.5 induces embryonic growth retardation: Potential involvement of ROS-MAPKs-apoptosis and G0/G1 arrest pathways. *Environmental toxicology.*, *31*(12), 2028-2044. https://doi.org/10.1002/tox.22203

Zanobetti, A., Dominici, F., Wang, Y., & Schwartz, J. D. (2014). A national case-crossover analysis of the short-term effect of PM2.5 on hospitalizations and mortality in subjects with diabetes and neurological disorders. *Environmental health : a global access science source.*, *13*(1), 38. https://doi.org/10.1186/1476-069X-13-38

Zatloukal, K., Stumptner, C., Fuchsbichler, A., Heid, H., Schnoelzer, M., Kenner, L.,…Denk, H. (2002). p62 Is a common component of cytoplasmic inclusions in protein aggregation diseases. *The American journal of pathology.*, *160*(1), 255-263. https://doi.org/10.1016/S0002-9440(10)64369-6

Zhang, C., Liu, Z., Zhang, Y., Ma, L., Song, E., & Song, Y. (2020). "Iron free" zinc oxide nanoparticles with ion-leaking properties disrupt intracellular ROS and iron homeostasis to induce ferroptosis. *Cell Death Dis*, *11*(3), 183. https://doi.org/10.1038/s41419-020-2384-5

Zhang, G., Ding, C., Jiang, X., Pan, G., Wei, X., & Sun, Y. (2020). Chemical Compositions and Sources Contribution of Atmospheric Particles at a Typical Steel Industrial Urban Site. *Scientific reports.*, *10*(1), 7654. https://doi.org/10.1038/s41598-020-64519-x

Zhang, H., Jiao, W., Cui, H., Sun, Q., & Fan, H. (2021). Combined exposure of alumina nanoparticles and chronic stress exacerbates hippocampal neuronal ferroptosis via activating IFN-γ/ASK1/JNK signaling pathway in rats. *Journal of hazardous materials.*, *411*, 125179. https://doi.org/10.1016/j.jhazmat.2021.125179

Zhang, J., Wang, X., Vikash, V., Ye, Q., Wu, D., Liu, Y., & Dong, W. (2016). ROS and ROS-Mediated Cellular Signaling. *Oxidative medicine and cellular longevity.*, *2016*, 4350965. https://doi.org/10.1155/2016/4350965

Zhang, L. P., Maiorino, M., Roveri, A., & Ursini, F. (1989). Phospholipid hydroperoxide glutathione peroxidase: specific activity in tissues of rats of different age and comparison with other glutathione peroxidases. *Biochimica et biophysica acta*, *1006*(1), 140-143. https://doi.org/10.1016/0005-2760(89)90336-6

Zhang, X., Chen, X., & Zhang, X. (2018). The impact of exposure to air pollution on cognitive performance. *Proceedings of the National Academy of Sciences of the United States of America*, *115*(37), 9193-9197. https://doi.org/10.1073/pnas.1809474115

Zhang, X. M., Yin, M., & Zhang, M. H. (2014). Cell-based assays for Parkinson's disease using differentiated human LUHMES cells. *Acta Pharmacol Sin*, *35*(7), 945-956. https://doi.org/10.1038/aps.2014.36

Zhang, Y., Li, S., Li, J., Han, L., He, Q., Wang, R.,…Liu, K. (2018). Developmental toxicity induced by PM2.5 through endoplasmic reticulum stress and autophagy pathway in zebrafish embryos. *Chemosphere.*, *197*, 611-621. https://doi.org/10.1016/j.chemosphere.2018.01.092

Zhongyin, Z., Wei, W., Juan, X., & Guohua, F. (2022). Epigallocatechin Gallate Relieved PM2.5-Induced Lung Fibrosis by Inhibiting Oxidative Damage and Epithelial-Mesenchymal Transition through AKT/mTOR Pathway. *Oxidative medicine and cellular longevity.*, *2022*, 7291774. https://doi.org/10.1155/2022/7291774

Zhou, D., Shao, L., & Spitz, D. R. (2014). Reactive oxygen species in normal and tumor stem cells. *Advances in cancer research*, *122*, 1-67. https://doi.org/10.1016/B978-0-12-420117-0.00001-3

Zhou, T., Hu, Y., Wang, Y., Sun, C., Zhong, Y., Liao, J., & Wang, G. (2019). Fine particulate matter (PM2.5) aggravates apoptosis of cigarette-inflamed bronchial epithelium in vivo and vitro. *Environmental pollution.*, *248*, 1-9. https://doi.org/10.1016/j.envpol.2018.11.054

Zhou, T., Zhong, Y., Hu, Y., Sun, C., Wang, Y., & Wang, G. (2018). PM2.5 downregulates miR-194-3p and accelerates apoptosis in cigarette-inflamed bronchial epithelium by targeting death-associated protein kinase 1. *International journal of chronic obstructive pulmonary disease.*, *13*, 2339-2349. https://doi.org/10.2147/COPD.S168629

Zhou, Y., Zhao, W.-J., Quan, W., Qiao, C.-M., Cui, C., Hong, H.,…Shen, Y.-Q. (2021). Dynamic changes of activated AHR in microglia and astrocytes in the substantia nigra-striatum system in an MPTP-induced Parkinson's disease mouse model. *Brain research bulletin.*, *176*, 174-183. https://doi.org/10.1016/j.brainresbull.2021.08.013

Zhu, J., Luo, L., Tian, L., Yin, S., Ma, X., Cheng, S.,…Liang, H. (2018). Aryl Hydrocarbon Receptor Promotes IL-10 Expression in Inflammatory Macrophages Through Src-STAT3 Signaling Pathway. *Frontiers in immunology.*, *9*, 2033. https://doi.org/10.3389/fimmu.2018.02033

Zhu, L., Zhu, D., Ran, J., Li, M., Lai, Z., Zhou, Y.,…Tian, K. (2024). Autophagy aggravates multi-walled carbon nanotube-induced ferroptosis by suppressing PGC-1 dependent-mitochondrial biogenesis in lung epithelial cells. *Chemico-biological interactions.*, *400*, 111158. https://doi.org/10.1016/j.cbi.2024.111158

Zhu, X.-M., Wang, Q., Xing, W.-W., Long, M.-H., Fu, W.-L., Xia, W.-R.,…Xu, D.-G. (2018). PM2.5 induces autophagy-mediated cell death via NOS2 signaling in human bronchial epithelium cells. *International journal of biological sciences.*, *14*(5), 557-564. https://doi.org/10.7150/ijbs.24546

SUPPLEMENTAL DATA

Table S1: PAH composition of Lille recuperated UFP quantified by HPLC-Fluorimetry. Values are the mean of measurements carried out on three sub-samples representative of the initial sample.

PAH	Concentration (ng/mg)	TEF[c]
AN	0.93	0.001
ANL	2.10	0.001
AA	0.30 [b]	0.3
BaA	5.80	0.1
BaP	7.40[b]	1
BbF	12.74 [b]	0.62
BeP	11.90	0.002
BghiP	10.73	0.02
BkF	5.70	0.1
CH	11.30 [b]	0.17
DBahA	1.73 [b]	1.1
FA	5.51	0.05
FE	2.10	0.001
IP	7.90 [b]	0.1
Nap	4.30 [b]	0.001[d]
PH	4.94 [b]	0.0005
Pyr	4.10 [b]	0.001
Σ PAH[a]	**99.48**	
TEQ[e]		**21.6827**

Abbreviations: PAH: Polycyclic Aromatic Hydrocarbons; AN: Acenaphthene; ANL: Acenaphthylene; AA: Anthracene; BaA: Benzo[a]antracene; BaP: Benzo[a]pyrene; BbF: Benzo[b]fluoranthene; BeP: Benzo[e]pyrene; BghiP: Benzo[g,h,i]perylene; BkF: Benzo[k]fluoranthene; CH: Chrysene; DBahA: Dibenzo[a,h]anthracene; FA: Fluoranthene; FE: Fluorene; IP: Indeno[1,2,3-c,d]pyrene; Nap: Naphthalene; PH: Phenanthrene; Pyr: Pyrene.

[a]: Σ PAH was calculated as the sums of PAH.
[b]: PAH undergo oxidation to form quinones.
[c]: Toxicity Equivalency Factor (TEF) from the most recent publication reported by (EPA, 2010).
[d]: TEF from (EPA, 1993).
[e]: Toxicity Equivalent (TEQ) calculated by $\Sigma C_{PAH} \times TEF_{PAH}$ (Rakowska *et al.*, 2022)

Table S2: PAH composition of Dunkirk recuperated UFP quantified by HPLC-Fluorimetry. Values are the mean of measurements carried out on three sub-samples representative of the initial sample.

PAH	Concentration (ng/mg)
FLA	4.3
PYR	3.7
BcPHE	0.2
BaA	4.2
CHR	2.8 [b]
5MCHR	3.4 [b]
BeP	0.8
BbF	8.0 [b]
BjF	9.9
BkF	4.6 [b]
BaP	5.3 [b]
DalP	0.4
DahA	1.5 [b]
BghiP	12.5
IP	12.1 [b]
DaeP	2.7
ANTH	3.3
COR	4.5
Σ PAH[a]	**84.2**

Abbreviations: PAH: Polycyclic Aromatic Hydrocarbons; FLA: Fluoranthene; PYR: Pyrene; BcPHE: Benzo(c)phenanthrene; BaA: Benzo(a)anthracene; CHR: Chrysene; 5MHCHR: 5-Methylchrysene; BeP: Benzo(e)pyrene; BbF: Benzo(b)fluoranthene; BjF: Benzo(j)fluoranthene; BkF: Benzo(k)fluoranthene; BaP: Benzo(a)pyrene; DalP: Dibenzo(a,l)pyrene; DahA: Dibenzo(a,h)anthracene; BghiP: Benzo(g,h,i)perylene; IP: Indeno(1,2,3-c,d)pyrene; DaeP: Dibenzo(a,e)pyrene; ANTH: Anthanthrene; COR: Coronene.

[a]: Σ PAH was calculated as the sums of PAH.
[b]: PAH undergo oxidation to form quinones.

	Partenaire 1 : Equipe EA4483-IMPECS Université de Lille	Partenaire 2 : Equipe SAGE-IMT Lille Douai	Partenaire 3 : Equipe INSERM UMR-S1172 CRJPA	Partenaire 4 : Equipe INSERM U1171
Personnel éligible non permanent	3 600	0	0	0
Personnel éligible permanent	0	0	0	0
Personne éligible autre	0	0	0	0
Gros équipements	28 000	0	0	0
Déplacements	3 000	3 000	0	0
Valorisation	3 000	1 000	0	0
Sous-traitants	0	0	0	0
Consommables	97 848	12 700	17 170	22 990
Petits équipements	0	0	0	0
Frais généraux	5 418	668	687	920
Aide demandée(€)	**140 866**	**17 368**	**17 857**	**23 910**
Total Général(€)	**200 000**			

Figure S1: Financial distribution of the PUF-EXPOmiR project.

The total some obtained by ANSES funding was 200,000 €. This PhD project could count on the financial support of the main laboratories: IMPECS (140,866 €) and LilNCog (23,910 €), and also experiments are performed by SAGE-IMT Lille Douai (17,368 €) which are included in this PhD research.

Table S3: Elemental composition of Lille recuperated UFP quantified by ICP-MS. Values are the mean of measurements carried out on three sub-samples representative of the initial sample.

Element	Concentration (µg/g)
Al	3,510
As	9.4
Ba	83[b]
Be	0.06
Ca	12,258
Cd	2.9[b]
Ce	6.4
Co	2.9
Cr	145[b]
Cs	1.3
Cu	812 [b]
Fe	4,108 [b]
K	3,317*
La	3.1
Li	4.1
Mg	916*
Mn	329 [b]
Mo	13
Na	3,946*
Ni	73[b]
Pb	114 [b]
Pd	0.71
Pt	0.29
Rb	11
Sb	84
Sc	0.99
Se	15
Si	9,723
Sn	38
Sr	48
Th	0.45
Ti	249
Tl	0.85
U	0.23
V	22
Zn	775 [b]
Σ elements[a]	**40,622.68**

*: Values not considered in the analysis due to their high amount in HBSS.
[a]: Σ elements was calculated as the sums of metals.
[b]: Anthropogenic elements linked to industrial air pollution.

Table S4: Elemental composition of Dunkirk recuperated UFP quantified by ICP-MS. Values are the mean of measurements carried out on three sub-samples representative of the initial sample.

Element	Concentration (µg/g)
As	64.8
Ba	64.4[b]
Be	0.3
Cd	19.3[b]
Ce	6.3
Co	9.3
Cs	8.9
Cu	425.2 [b]
La	3.1
Mn	582.2 [b]
Mo	36.7
Ni	199.7 [b]
Pb	541.9 [b]
Rb	44.1
Sb	49.3
Sn	111.1
Sr	49.3
Ti	5.7
Zn	2460.7 [b]
Cr	120.7[b]
V	196.3
Al	3621.1
Ca	11,857.4
Fe	10,267.0 [b]
K	30,368*
Mg	6344.8*
Na	283,147*
Si	7568.1
Σ elements[a]	**358,172.7**

*: Values not considered in the analysis due to their high amount in HBSS.
[a]: Σ elements was calculated as the sums of metals.
[b]: anthropogenic elements linked to industrial air pollution.

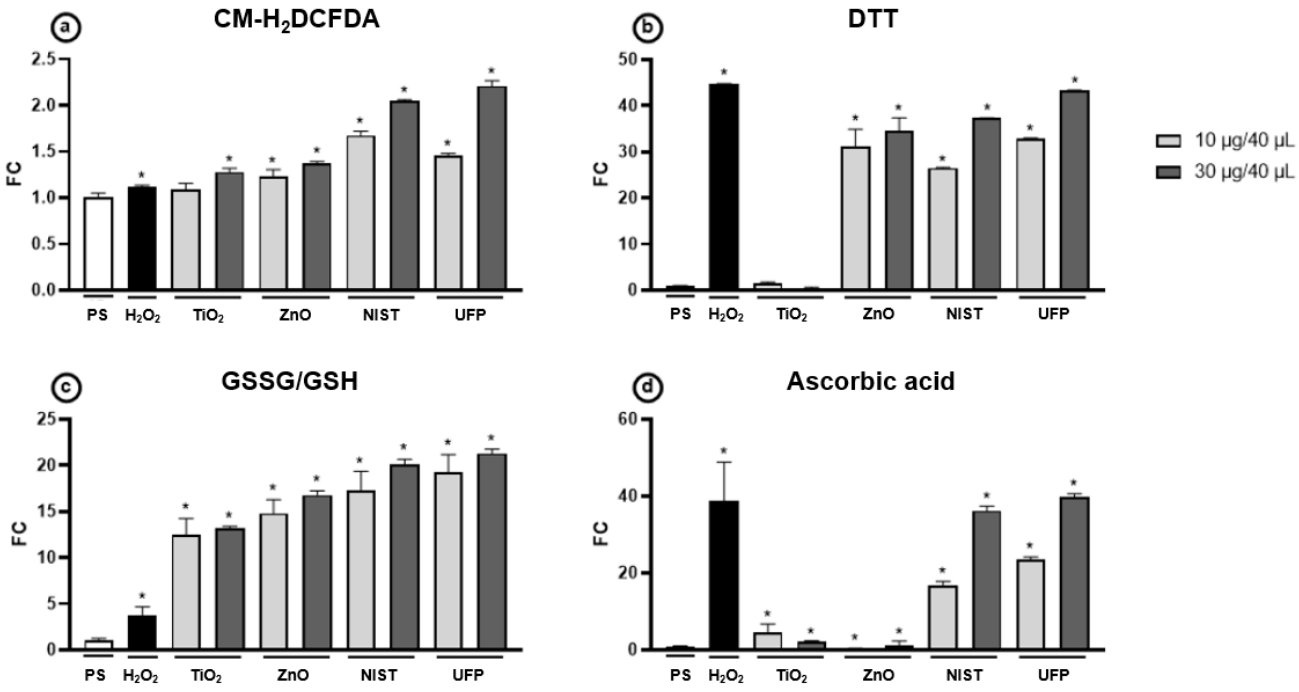

Figure S2: Oxidative potential of UFP recuperated in Lille.

However, each particle type gave a significant results in all tests (except TiO_2 for CM-H2DCFDA and DTT), the oxidative potential of UFP particles was comparable to NIST and, depending on which measurement higher than metallic nanoparticles (TiO_2 and ZnO).

1) Prefrontal cortex (olfactive / cortex)

B 3.08 mm

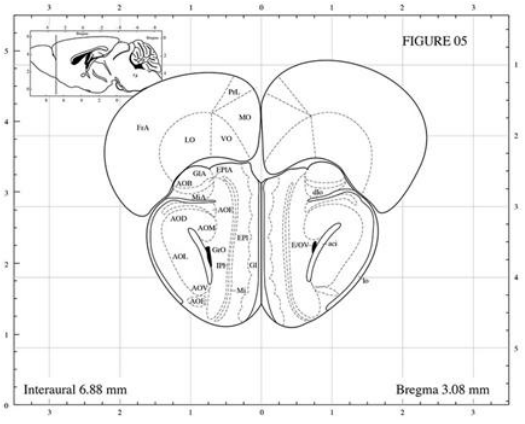

B 1.70mm

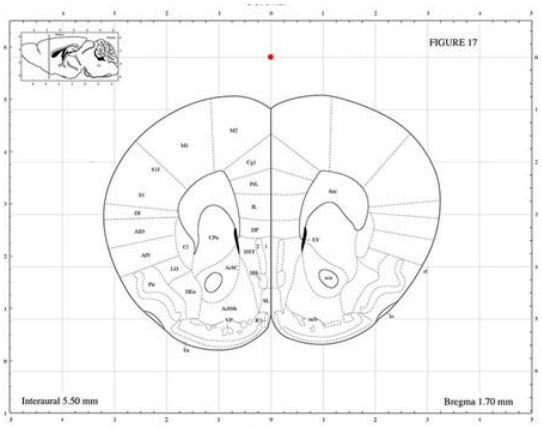

2) Striatum

B 1.7 mm

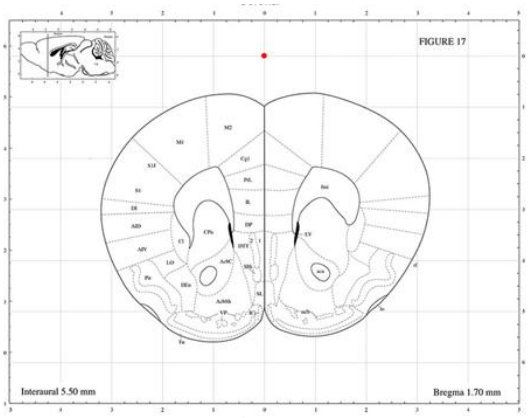

B -0.22 mm

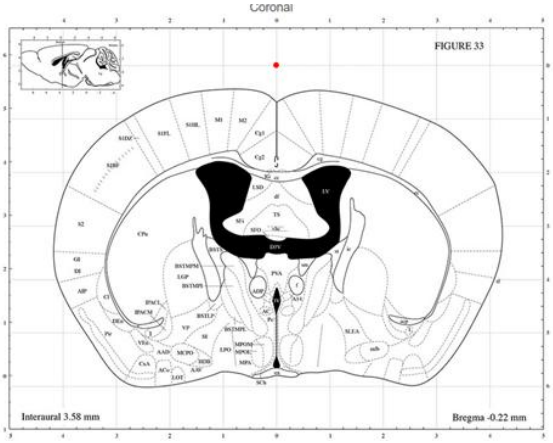

3) Hippocampus

B -1.06 mm

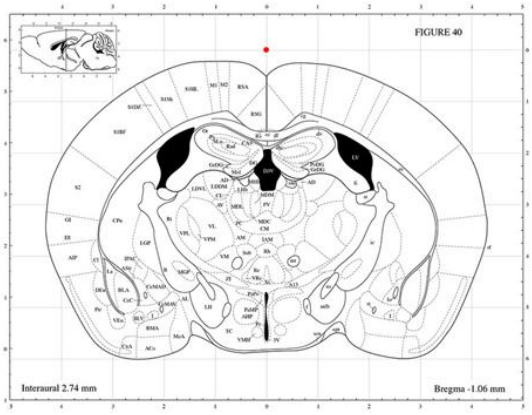

B – 2.70 mm

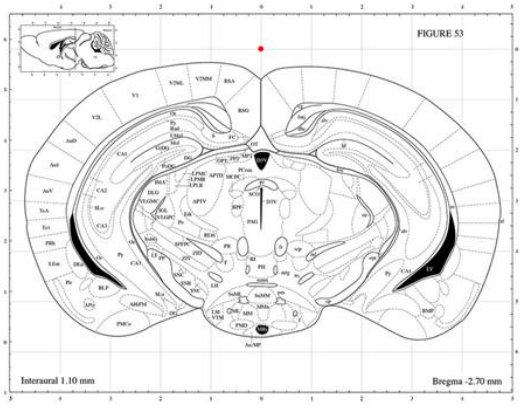

4) Substantia Nigra (SN)

B -2.92 mm

B – 3.80 mm

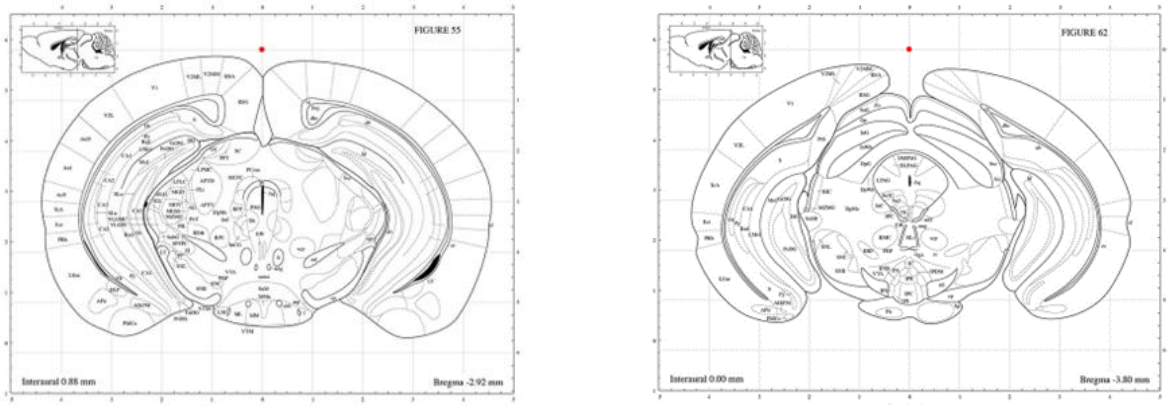

Figure S3: Methodological overview of the four brain regions: Prefrontal cortex, Striatum, Hippocampus, Substantia Nigra.

This figure provides an anatomical overview of the four selected brain regions analyzed for UFP detection using femtosecond pulsed laser microscopy (Cf. p. 84) and immunohistochemistry for TH and NeuN (Cf. p. 93). “B” indicates the bregma reference point, followed by the distance anterior or posterior to this stereotactic brain mapping landmark.

Control (physiological serum)

Mouse 351

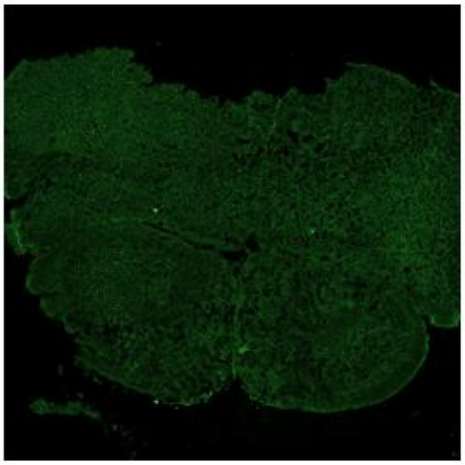

Region 1: Prefrontal Cortex

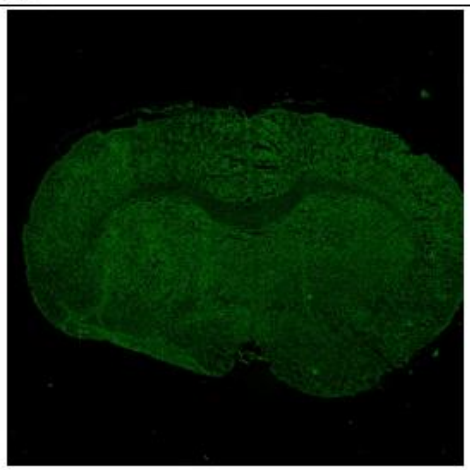

Region 2: Striatum

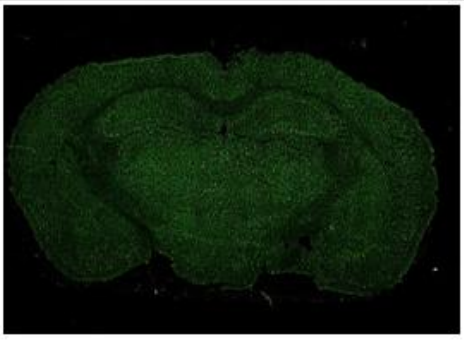

Region 3: Hippocampus

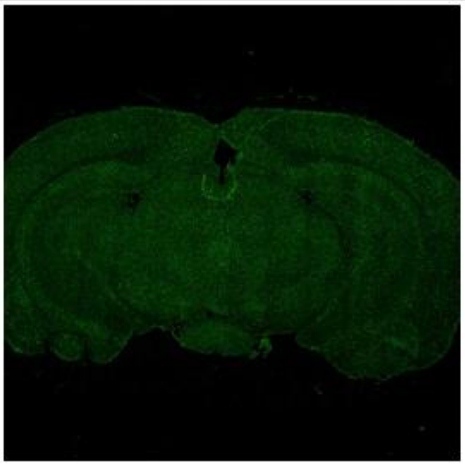

Region 4: SN

Dose 2 UFP (30 µg/adm)

Mouse 492

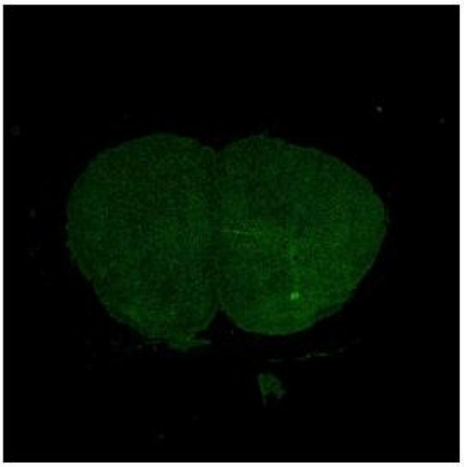

Region 1: Prefrontal Cortex

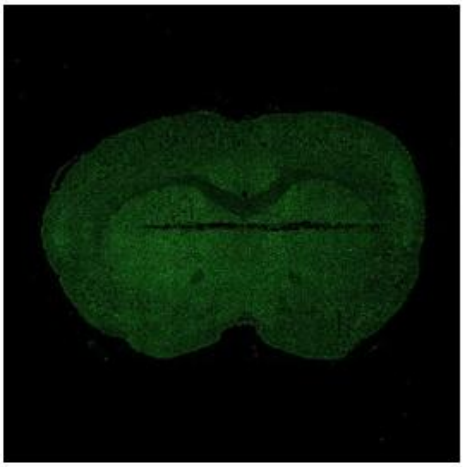

Region 2: Striatum

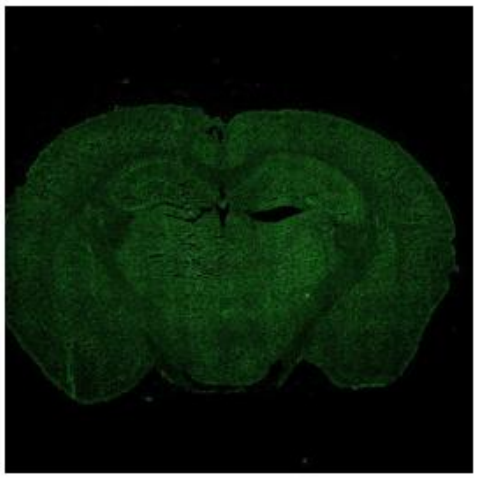

Region 3: Hippocampus

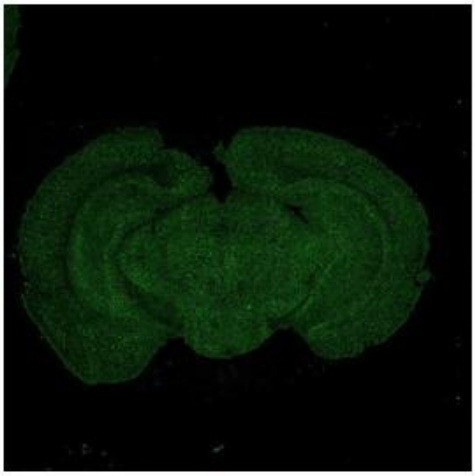

Region 4: SN

Control (physiological serum) + recovery

Mouse 333

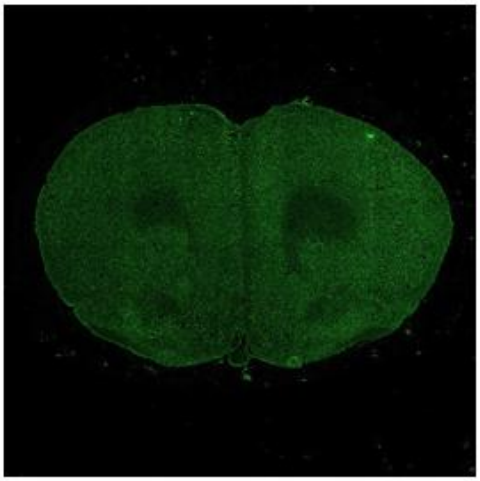

Region 1: Prefrontal Cortex

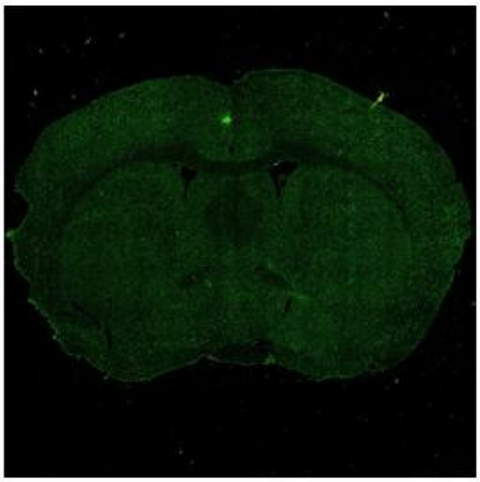

Region 2: Striatum

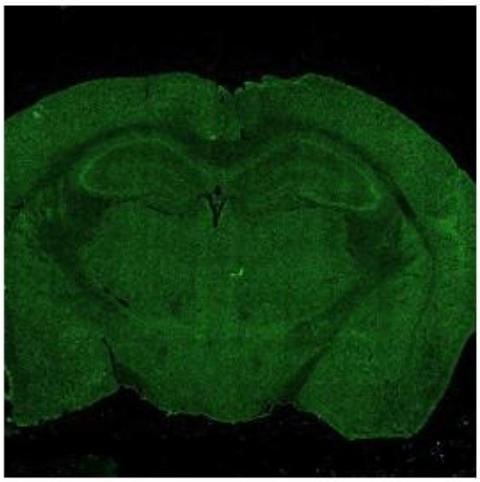

Region 3: Hippocampus

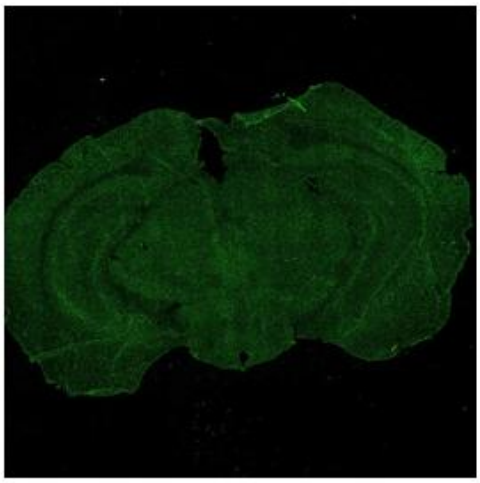

Region 4: SN

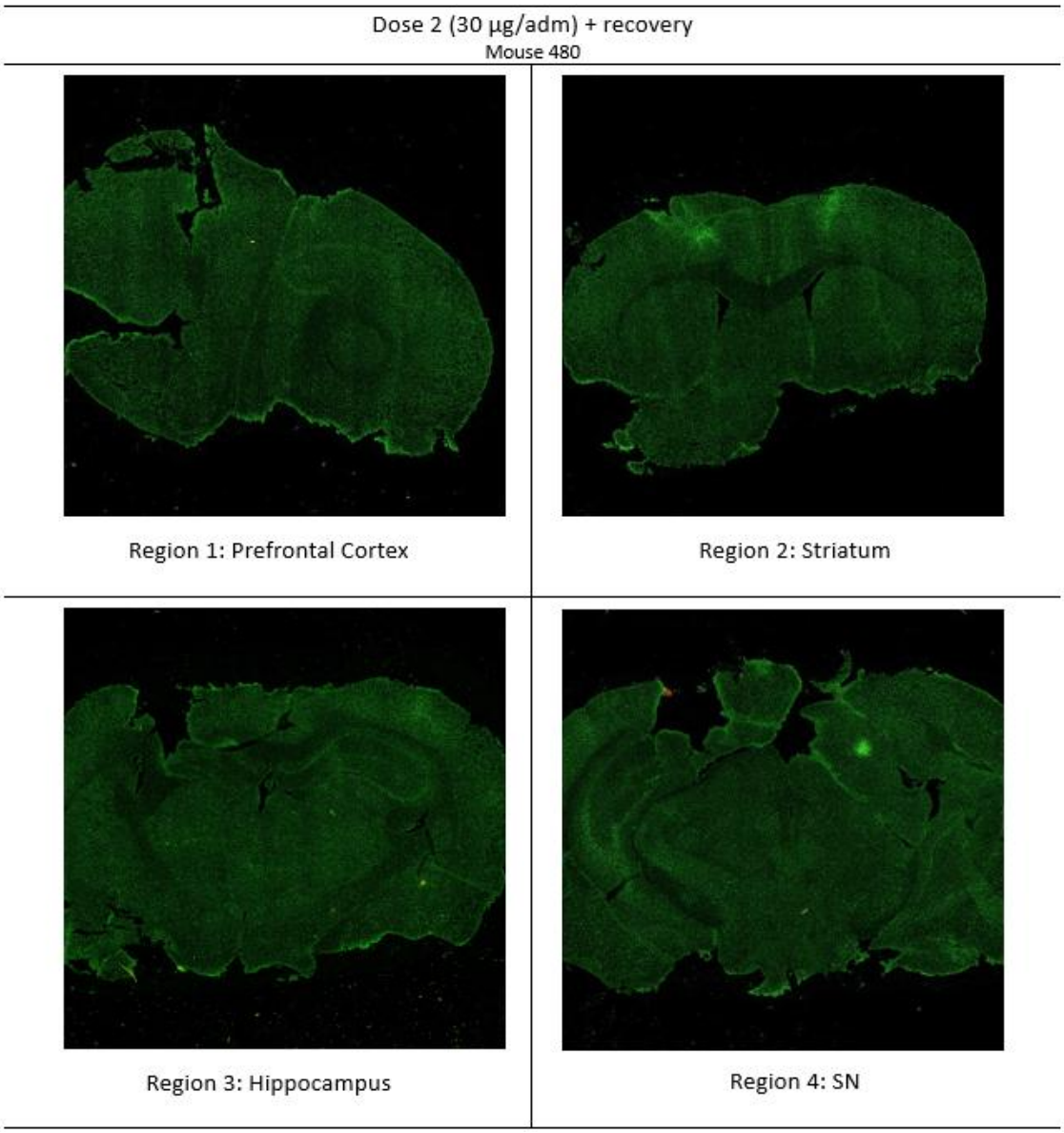

Figure S4: Visual overview of the two-photon excited autofluorescence signal of brain slices.

For label-free detection of carbon particles by femtosecond pulsed laser microscopy, the two-photon excited autofluorescence (TPAF) signal which gives the green background signal (emission filter 450-650 nm). To illustrate, from each conditions (Control, D2 (30 µg/adm) exposed, Control with recovery, D2 (30 µg/adm) exposed with recovery) this figure give the TPAF pictures of the four brain regions, namely Prefrontal Cortex, Striatum, Hippocampus, and SN.

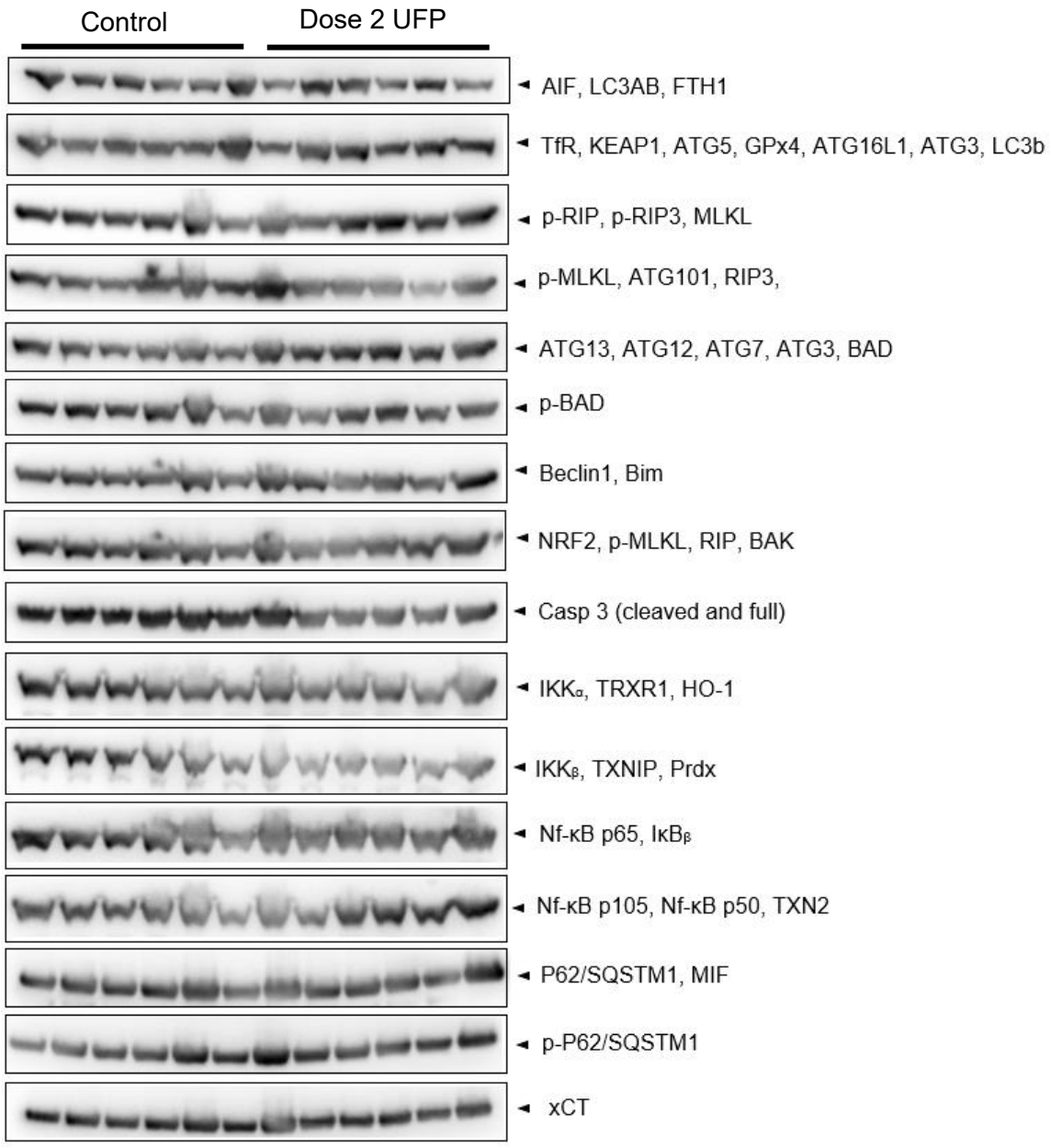

Figure S5: β-Actin WB images of oxidative stress, neuroinflammation and regulated cell death markers in whole brain tissue of control (vehicle-exposed) and UFP-exposed mice.

The first six samples are proteins originating from vehicle-exposed mice, and the last six from Dose 2 (30 µg/adm). The images are from the Actin protein in whole brain tissue.

Table S5: Overview of the neurological markers analyzed by immunohistochemistry, including their associated brain regions, functional indications, references, primary and secondary antibody conditions, and detection methodologies.

Marker	Brain Region	Indication	Ref	Primary AB Dilution	Secondary AB Dilution	Detection method
Tyrosine hydroxylase (TH)	- Striatum (Reg. 2) - Substantia Nigra (Reg.4)	Enzyme dopamine cascade : conversion of tyrosine to L-DOPA → Dopaminergic neurons (Parkinson's disease)	Tyrosine Hydroxylase (E2L6M) Rabbit mAb #58844	1/1000 (24h at 4°C) in PBS-Tween 0.2% + 5% goat serum solution	Goat anti-rabbit (1/500)	Str = fibers → OD SN*pc* = neuronal bodies → spots VTA = neuronal bodies → spots
Neuronal-Nuclei (NeuN)	- Hippocampus (Reg. 3)	Nuclear and cytoplasmic protein marks mature neurons → less signal = less neurons (general cell death)	NeuN (D4G4O) XP® Rabbit mAb #24307	1/400 (24h at 4°C) in PBS-Tween 0.2% + 5% goat serum solution	Goat anti-rabbit (1/500)	% loss of signal → cell damage / cell death

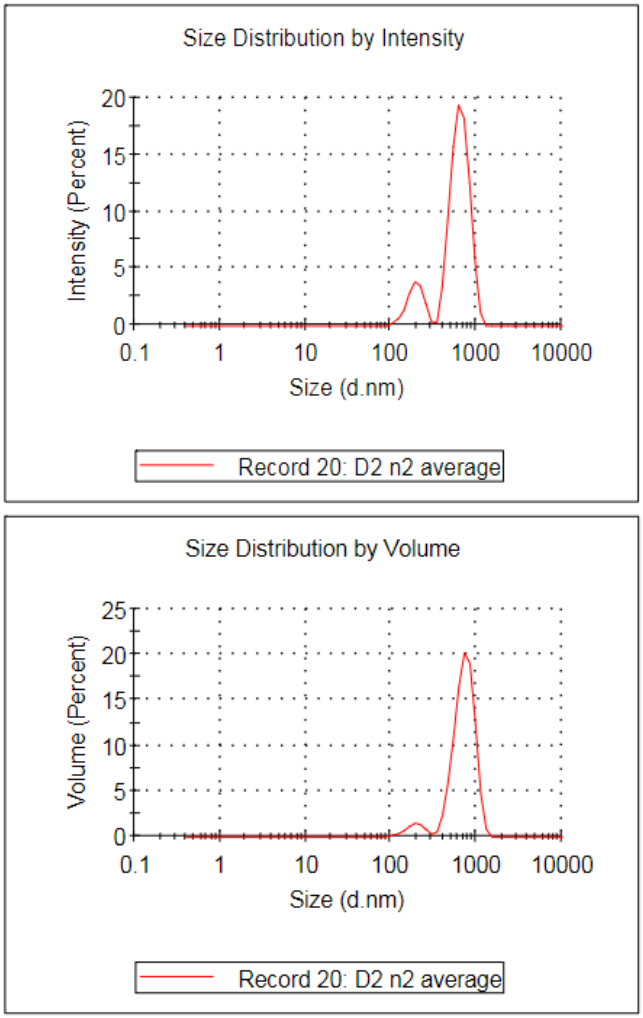

Z-Average (d.nm): 1113
Count Rate (kcps): 162,1
PdI Width (d.nm): 925,9
PdI: 0,692

INTENSITY

	Mean (nm)	Percent
Peak 1 :	653,3	84,9
Peak 2 :	197,4	15,1
Peak 3 :	0,000	0,0

VOLUME

	Mean (nm)	Percent
Peak 1 :	726,5	93,4
Peak 2 :	191,7	6,6
Peak 3 :	0,000	0,0

Figure S6: Granulometry results presented as intensity/size and volume/size.

The granulometry of UFP recovered in Lille is also described in terms of intensity value on size and volume value on size, although these metrics are less commonly used. Two peaks are observed: the smaller peak represents the UFP, while the larger peak corresponds to particle aggregation.

Table S6: Dioxins and Furans composition of UFP quantified by HRGC/HRMS. Values are the mean of measurements carried out on three sub-samples representative of the initial sample.

Chlorinated dibenzo-*p*-dioxin	Concentration (ng/g)	TEF[c]
2,3,7,8-TCDD	0.0225	1
1,2,3,7,8-PeCDD	0.0580	1
1,2,3,4,7,8-HxCDD	0.0847	0.1
1,2,3,6,7,8-HxCDD	0.2666	0.1
1,2,3,7,8,9-HxCDD	0.2862	0.1
1,2,3,4,6,7,8-HpCDD	2.3362	0.01
OCDD	5.0146	0.0003
Σ Dioxins[a]	**8.0688**	
TEQ[d]		**0.169**
Chlorinated dibenzofurans	Concentration (ng/g)	
2,3,7,8-TCDF	0.0991	0.1
1,2,3,7,8-PeCDF	0.2229	0.03
2,3,4,7,8-PeCDF	0.3997	0.3
1,2,3,4,7,8-HxCDF	0.4122	0.1
1,2,3,6,7,8-HxCDF	0.3758	0.1
2,3,4,6,7,8-HxCDF	0.5009	0.1
1,2,3,7,8,9-HxCDF	0.2157	0.1
1,2,3,4,6,7,8-HpCDF	1.3001	0.01
1,2,3,4,7,8,9-HpCDF	0.2997	0.01
OCDF	4.9694	0.0003
Σ Furans[b]	**8.7955**	
TEQ[d]		**0.304**

Abbreviations: Dioxins: TCDD: Tetrachlorodibenzo-p-dioxin; PeCDD: Pentachlorodibenzo-p-dioxin ; HxCDD: Hexachlorodibenzo-p-dioxin; HpCDD: Heptachlorodibenzo-p-dioxin; Furans: TCDF: Tetrachlorodibenzofuran; PeCDF: Pentachlorodibenzofuran; HxCDF: Hexachlorodibenzofuran; HpCDF: Heptachlorodibenzofuran; OCDD: Octachlorodibenzodioxin; OCDF: Octachlorodibenzofuran

[a]: Σ Dioxins was calculated as the sums of each Dioxin.
[b]: Σ Furans was calculated as the sums of each Furan.
[c]: TEF for Dioxins and Furans from the WHO reevaluated in 2005 (Van den Berg *et al.*, 2006).
[d]: Toxicity Equivalent (TEQ) calculated by $\Sigma C_{PCB} \times TEF_{PCB}$ (Rakowska *et al.*, 2022).

Table S7: PCB composition of UFP quantified by HRGC/HRMS. Values are the mean of measurements carried out on three sub-samples representative of the initial sample.

PCB Dioxin-like	Concentration (ng/g)	TEF[d]
PCB 81	0.8286	0.0003
PCB 77	0.8836	0.0001
PCB 123	0.9094	0.00003
PCB 118	22.2155	0.00003
PCB 114	0.8821	0.00003
PCB 105	10.4657	0.00003
PCB 126	1.1551	0.01
PCB 167	0.8443	0.00003
PCB 156	0.8728	0.00003
PCB 157	0.9070	0.00003
PCB 169	1.0394	0.03
PCB 189	0.5376	0.00003
Σ PCB $_{\text{Dioxin-like}}$[a]	**41.54**	
TEQ[e]		**0.04**
PCB Indicators	Concentration (ng/g)	
PCB 28	15.534	
PCB 52	16.520	
PCB 101	25.907	
PCB 138	44.516	
PCB 153	39.062	
PCB 180	20.071	
Σ PCB $_{\text{Indicators}}$[b]	**161.61**	
Σ PCB[c]	**203.15**	

Abbreviations: PCB: Polychlorinated biphenyls: 3,4,4',5-tetraCB (PCB 81), 3,3',4,4'-tetraCB (PCB 77), 3,3',4,4',5-pentaCB (PCB 126), 3,3',4,4',5,5'-hexaCB (PCB 169), 2,3,3',4,4'-pentaCB (PCB 105), 2,3,4,4',5-pentaCB (PCB 114), 2,3',4,4',5-pentaCB (PCB 118), 2',3,4,4',5-penta (PCB 123), 2,3,3',4,4',5-hexaCB (PCB 156), 2,3,3',4,4',5'-hexa (PCB 157), 2,3',4,4',5,5'-hexaCB (PCB 167), 2,3,3',4,4',5,5'-heptaCB (PCB 189), PCB 28, PCB 52, PCB 101, PCB 138, PCB 153, PCB 180.

[a]: Σ PCB $_{\text{Dioxin-like}}$ was calculated as the sums of PCB $_{\text{Dioxin-like}}$.
[b]: Σ PCB $_{\text{Indicators}}$ was calculated as the sums of PCB $_{\text{Indicators}}$
[c]: Σ PCB was calculated as the sums of PCB $_{\text{Dioxin-like}}$ and PCB $_{\text{Indicators}}$
[d]: TEF only for PCB $_{\text{Dioxin-like}}$ from the WHO reevaluated in 2005 (Van den Berg *et al.*, 2006).
[e]: Toxicity Equivalent (TEQ) calculated by $\Sigma C_{PCB} \times TEF_{PCB}$ (Rakowska *et al.*, 2022).

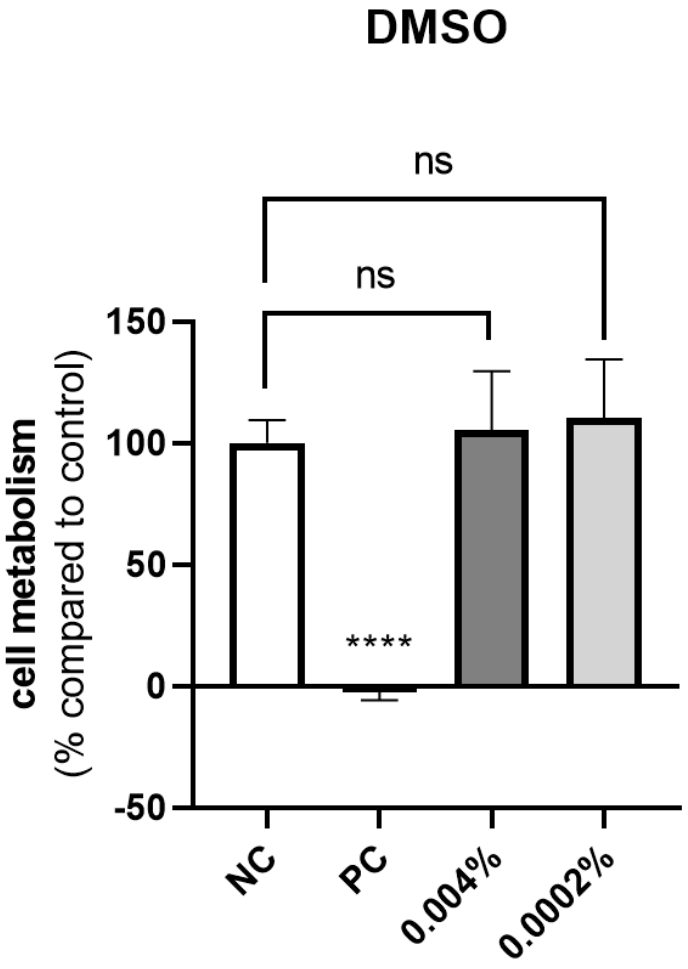

Figure S7: Comparison cell metabolism of Triton (0.1%), 0.004% DMSO and 0.0002% DMSO treated LUHMES cells to negative control (non-treated cells).

The resazurin assay demonstrated that there is no difference in cell metabolism on LUHMES cells treated with 0.004% and 0.0002% DMSO compared to negative control cells.

(n=6; mean ± SD; ANOVA, ****p<0.0001)

Abbreviations: DSMO: dimethylsufoxide; LUHMES: Lund Human Mesencephalic; NC: Negative Control; PC: Positive Control (Triton)

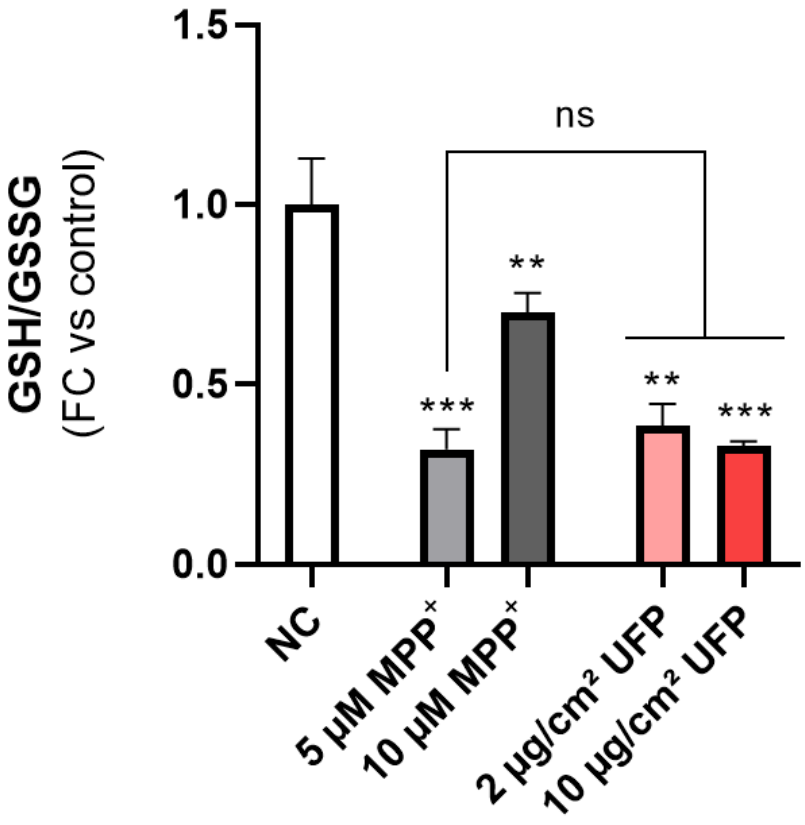

Figure S8: Comparison glutathione ratios in response to MPP^+ and UFP acute exposure.

The glutathione ratio (GSH/GSSG) was assessed after 24-hour treatment with 5 µM MPP^+, 10 µM MPP^+, 2 µg/cm² UFP, and 10 µg/cm² UFP in differentiated LUHMES cells. All treatments resulted in a significant decrease compared to control conditions. However, exposure to 5 µM MPP^+ (mean 0.43) showed no statistical difference in GSH/GSSG ratio compared to 2 µg/cm² and 10 µg/cm² UFP (mean 0.52 and 0.51, respectively).

(FC: Fold Changes; n=3; mean ± SD; unpaired t-test, **p<0.01, ***p<0.001)

Abbreviations: GSH: glutathione; GSSG: Glutathione; UFP: Ultrafine Particles; MPP^+: 1-methyl-4-phenylpyridinium; LUHMES: Lund Human Mesencephalic; NC: Negative Control

VALORISATION

ARTICLES IN INTERNATIONAL PEER-REVIEWED JOURNALS

ORCiD: 0009-0002-6806-0985

- **Air pollution iron-containing ultrafine particles induce ferroptotic features and lipid peroxidation in dopaminergic neurons via the P53/x_c^-/GSH/GPx4 axis**

  (Emma Theerens, Aurélie Jonneaux, Ophélie Simonin, Jean-Christophe Devedjian, Espéranza Perdrix, Véronique Riffault, Laurent Alleman, Anne-Sophie Rolland, Lydia Nikasinovic, Guillaume Garçon, David Devos)

  Toxicology and Applied Pharmacology 2025, Manuscript Number: TAAP-D-25-00312

  Impact Factor: 3.3

- **Persistence of air pollution-derived $PM_{2.5}$-related genetic and epigenetic alterations in mouse lungs after cessation of sub-chronic exposure**

  (Emeline Barbier, Ophélie Simonin, Jessica Carpentier, Emma Theerens, Mélanie Happillon, Laurent Y. Alleman, Esperanza Perdrix, Véronique Riffault, Fabrice Nesslany, Jean-Marc Lo Guidice, Sébastien Antherieu, Anne Platel, Guillaume Garçon)

  Environmental Pollution, Manuscript Number: ENVPOL-D-23-063142024

  Impact Factor: 8.07

In preparation

- **Does subchronic inhalation to ultrafine particles induce Parkinson's disease-like neurotoxicity in mice?** (temporary title)

  (Emma Theerens, Kenneth Vanbrabant, Ophélie Simonin, Emeline Barbier, Jessica Carpentier, Kelly Timmerman, Charlotte Laloux, Laurent Y. Alleman, Esperanza Perdrix, Véronique Riffault, Michelle Plusquin, Guillaume Garçon, David Devos, Lydia Nikasinovic)

  Particle and Fibre Toxicology

  Impact Factor: 7.2

PROCEEDINGS

- **Air pollution-derived ultrafine particles induce ferroptosis in differentiated human dopaminergic neuronal LUHMES cells**

  (E. Theerens, O. Simonin, H. Bouchaoui, A. Jonneaux, F. Gouel, J.-C. Devedjian, J.-M. Lo Guidice, D. Devos, A.-S. Rolland, G. Garçon)

  16th International Congress of Toxicology (ICT)
  - Uniting in Toxicology

  2022, Toxicology Letters, Volume 368, pp.S129-S130

- **Emerging role of epigenetic alterations in the lung inflammation and tissue remodeling induced by air pollution-derived $PM_{2.5}$ in mice**

  (E. Barbier, S. Antherieu, C. Grare, E. Theerens, LY. Alleman, J-M, Lo Guidice, G. Garçon)

  56th Congress of the European-Societies-of-Toxicology (EUROTOX)
  - Toxicology of the Next Generation

  2021 Toxicology Letters, Volume 350, pp.S66-S67

INTERNATIONAL AND NATIONAL COMMUNICATIONS

(🏆 AWARDED)

2024 🏆 2th Congress of FHU Respire (Cabourg)
Oral presentation: Air pollution-derived ultrafine particles induce neurological disorders in BALB/c mice and differentiated human dopaminergic neuronal LUHMES cells

2024 9th Symposium Ultrafine Particles – Air Quality and Climate (Brussels)
Oral presentation: Air pollution-derived ultrafine particles induce neurological disorders in BALB/c mice and differentiated human dopaminergic neuronal LUHMES cells

2023 🏆 PhD Day André Verbert (Lille)
Oral presentation: Air pollution-derived ultrafine particles induce neurological disorders in BALB/c mice and differentiated human dopaminergic neuronal LUHMES cells

2023 🏆 1st Summer School Precision Health (Lille)
3 min Flash talk & Poster presentation: Air pollution-derived ultrafine particles induce ferroptosis in differentiated human dopaminergic neuronal LUHMES cells

2023 🏆 LilNDoc Day (Lille)
3 min Flash talk: Air pollution-derived ultrafine particles induce ferroptosis in differentiated human dopaminergic neuronal LUHMES cells

2023 EURON PhD Days 2023 (Maastricht)
Poster presentation: Air pollution-derived ultrafine particles induce ferroptosis in differentiated human dopaminergic neuronal LUHMES cells

2022 XVIth International Congress of Toxicology (ICT + Eurotox) (Maastricht)
Poster presentation: Air pollution-derived ultrafine particles induce ferroptosis in differentiated human dopaminergic neuronal LUHMES cells

2022 Congrès annuel: Société de Toxicologie Cellulaire et Moléculaire (online)
Oral presentation: Environmental factors involved in Parkinson's Disease : How do ultrafine particles induce neuronal cell death?

2022 EURON PhD Days 2022 (Hasselt)
Oral presentation: Air pollution-derived ultrafine particles induce ferroptosis in an in vitro model of human dopaminergic neurons

2021 🏆 Summer School: From Genes to Cells : A Basic course of molecular cellular and ultrastructural biology (Universita Di Pisa/online)
Oral presentation: Environmental factors involved in Parkinson's Disease : How do ultrafine particles induce neuronal cell death?

POSTER

XVIth International Congress of Toxicology (ICT + EUROTOX) (Maastricht)

AIR POLLUTION-DERIVED ULTRAFINE PARTICLES INDUCE FERROPTOSIS IN DIFFERENTIATED HUMAN DOPAMINERGIC NEURONAL LUHMES CELLS

Emma THEERENS[1,2], Ophélie SIMONIN[1], Hind BOUCHAOUI[1,2], Aurélie JONNEAUX[2], Flore GOUEL[2], Jean-Marc LO GUIDICE[1], David DEVOS[2], Anne-Sophie ROLLAND[2], Guillaume GARÇON[1]

[1] Univ. Lille, CHU Lille, Institut Pasteur de Lille, ULR4483-IMPECS, Lille, France
[2] Univ. Lille, Inserm, CHU Lille, U1172 LilNCog, Lille, France

INTRODUCTION

Parkinson's disease (PD), the second most prevalent age-related neurodegenerative disorder, is characterized by a predominance of regulated cell death (RCD) of dopaminergic neurons of the Substantia Nigra *pars compacta*. Only 5% of the disease risk can be attributed to genetic variations, implying that the environment plays a crucial role. Air pollution-derived particulate matter (PM) and, more specifically, the smallest fraction of ultrafine particles (UFP), can translocate into the circulation to cross the blood-brain-barrier or penetrate directly the olfactory mucosa to reach the brain, where it can lead to molecular and biochemical neuronal alterations. If cells are unable to overcome those negative effects, it can exacerbate in progressive cell death.

To better understand which RCD form occurs after dopaminergic neuronal intoxication with UFP, this *in vitro* study measured specific biomarkers of autophagy, apoptosis and ferroptosis after 24h UFP-exposure on dopaminergic neurons. Whereafter results were compared to PD-phenotype by the use of MPP$^+$.

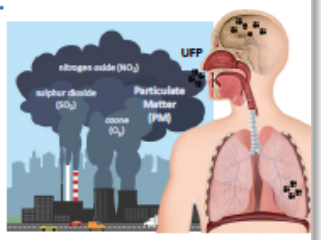

MATERIALS AND METHODS

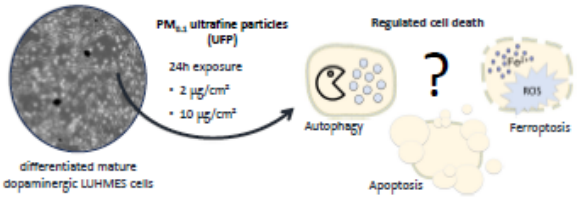

- **Autophagy:** Protein expression LC3b Western Blotting
- **Apoptosis:** Caspase-3/7, -8, -9 activity (fluorescence)
- **Ferroptosis:**

1) Protection by anti-ferroptotic drugs: liproxstatin-1 (LPX) and deferiprone (DFP): G6PD fluorometric cell viability assay
2) Intracellular iron storage: ferritin (ELISA-MSD)
3) Lipid peroxidation: 4-hydroxynonenal: 4-HNE adducts (ELISA-MSD), glutathione status: GSSH/GSH (bioluminescence), glutathione peroxidase activity: GPx (fluorescence)

RESULTS

Autophagy

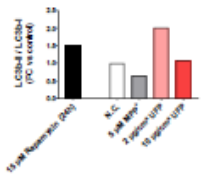

Apoptosis

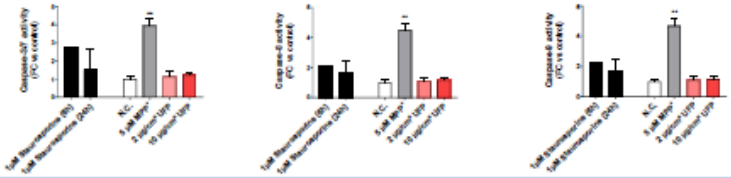

Ferroptosis

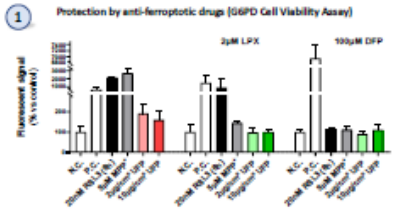

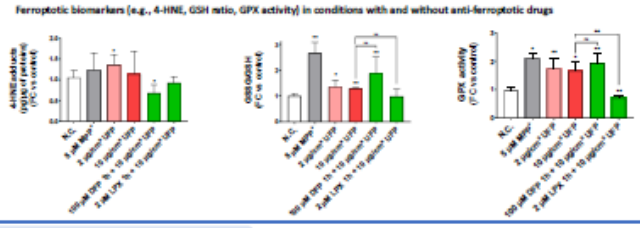

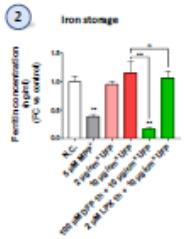

CONCLUSION

Our investigation showed that differentiated dopaminergic LUHMES cells exposed to UFP died by ferroptosis and that the main regulated cell death form after UFP exposure of 2 and 10 µg/cm² for 24h is ferroptosis, compared to autophagy and apoptosis. Interestingly MPP$^+$-induced PD condition and the exposure of UFP both led to the same results, leading to the conclusion that UFP could contribute to the development of a PD phenotype. Further *in vitro* and *in vivo* experiments are now required to support this statement.

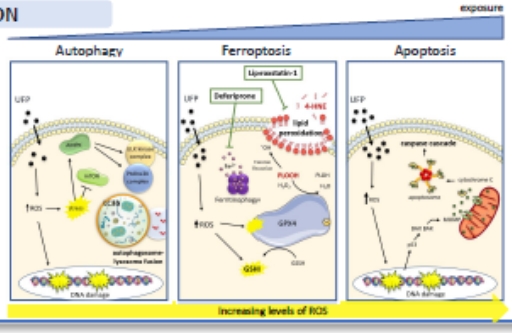

FORMATIONS ORGANIZED BY THE DOCTORAL SCHOOL

Free to choose

- Conducting your doctoral project
  Credits: 10

- Revealing the entrepreneurial potential of PhD students
  Credits : 10

- Boost your digital identity and use of social media
  Credits: 7

- PhD's and International career
  Credits: 4

- Current concepts in Precision Health - Ethics, health and society
  Credits: 4

- Current concepts in Precision Health - Imaging and precision health
  Credits: 4

- Current concepts in Precision Health - Pathophysiology and molecular basis of diseases and treatments applied to precision health
  Credits: 7

- Current concepts in Precision Health - From cohorts to cutting-edge researches
  Credits: 4

- Current concepts in Precision Health - Medical devices and precision health
  Credits: 7

- Current concepts in Precision Health - Novel Mode of actions for personalized drugs
  Credits: 10

Obligatory

- Formation éthique pour une conduite responsable en recherche - choix atelier 3. pratique éthique du métier de chercheur (06 mai 2022)
  Credits: 5

Finished 93 credits* / 60 required credits

* sum of credits with scientific communications and extracurricular formations

EXTRACURRICULAR CERTIFICATES

2021 – present Certificate of Excellence
European Graduate School of Neuroscience (EURON), Maastricht University

2021 – present Graduate programme: Precision Health
Université de Lille, Lille

2024 The course: “Human neuroanatomy and its clinical application”
Université de Lille, Lille Mental Health & Neuroscience Research Institute (MHeNs) / European Graduate School of Neuroscience (EURON), Maastricht University

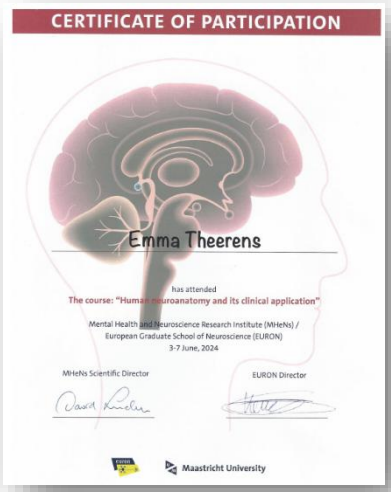
CERTIFICATE OF PARTICIPATION

Emma Theerens

has attended

The course: "Human neuroanatomy and its clinical application"

Mental Health and Neuroscience Research Institute (MHeNs) / European Graduate School of Neuroscience (EURON)
3-7 June, 2024

MHeNs Scientific Director

EURON Director

Maastricht University

2024 Certificate B2 English
Université de Lille, Lille


RÉPUBLIQUE FRANÇAISE
Liberté
Égalité
Fraternité

Université de Lille

Attestation de réussite au diplôme

Le Président atteste que le diplôme de

CERTIFICAT DE COMPÉTENCES EN LANGUES DE L'ENSEIGNEMENT SUPÉRIEUR EN ANGLAIS
Mention B2

a été décerné à

EMMA THEERENS
Date de naissance : 10 juin 1994
Lieu de naissance : KNOKKEHEIST (BELGIQUE)
INE : 0CSPSV04WT1

au titre de l'année universitaire 2023-2024

Fait à LILLE, le 11 juin 2024

Régis BORDET
Président de l'Université de Lille

2021 – 2022 Diplôme Universitaire (DU) Health Entrepreneurship
Université de Lille (faculté de pharmacie), Lille


RÉPUBLIQUE FRANÇAISE

UNIVERSITE DE LILLE

DIPLÔME UNIVERSITAIRE

Vu le code de l'éducation, notamment son article L. 613-2

Vu la décision du Conseil de la Formation et de la Vie Universitaire

Vu les pièces justificatives produites par Mme EMMA THEERENS, née le 10 juin 1994 à KNOKKEHEIST (BELGIQUE), en vue de son inscription au DIPLÔME UNIVERSITAIRE Health entrepreneurship program

Vu les procès-verbaux du jury attestant que l'intéressée a satisfait au contrôle des connaissances et des aptitudes prévu par les textes réglementaires

LE DIPLÔME UNIVERSITAIRE HEALTH ENTREPRENEURSHIP PROGRAM, *mention bien*

est décerné à Mme EMMA THEERENS

au titre de l'année universitaire 2021–2022.

Fait à LILLE, le 29 mars 2023

Le Président

Régis BORDET

Le titulaire

0CSPS2021 1602

VOLUNTARY WORK

EUROPEAN GRADUATE SCHOOL OF NEUROSCIENCE

- *Organization committee member of the EURON PhD days 2023 in Lille*
- *Current PhD representative for the University of Lille*

SCAN ME

UC Leuven Limburg
MOVING MINDS

- *Jury member 3th bachelor's dissertation Pharmaceutical and Biological Laboratory Technology (Leuven - June 2024)*
- *Erasmus representative for Lille (last presentation given 6/12/2024)*

Lille Neuroscience & Cognition

Assisting Master 2 students in preparing their presentation for securing a PhD scholarship (2023)

FUNDING

This work was supported by the French Ministère de l'Enseignement Supérieur et de la Recherche, the Hauts de France Region and the European Funds of Regional Economic Development (CPER ECRIN), and the French National Research Program for Environmental and Occupational Health Anses with the support of the Cancer TMOI of the French National Alliance for Life and Health Sciences (AVIESAN) (2018/1/073). IMT Nord Europe acknowledges financial support from the Labex CaPPA project, which is funded by the French National Research Agency (ANR) through the PIA (Programme d'Investissement d'Avenir) under contract ANR-11-LABX-0005-01.

Me, Emma Theerens, received a PhD fellowship funded by Lille University and the Regional Council of Hauts-de-France (convention n° 2021-2024, contract n° 21003026).

For the three-months stay as **guest-researcher** at the Centre for Environmental Science (CMK), University of Hasselt, Belgium, two mobility grants were achieved:

1) Mobility grand Graduate School Precision Health
2) Mobility grand EURON

PHD CERTIFICATES

This manuscript is submitted in pursuit of a PhD degree. To recognize interdisciplinary and international collaboration, both the European Label awarded by European Universities and the International Label from the University of Lille are being requested.

European Label

- ➔ A minimum three-month stay in another European country.
- ➔ Three reviewers, with at least two from a European country other than France.
- ➔ The PhD defense must be conducted in English.

International Label

- ➔ Completion of training in Intercultural Communication.
- ➔ A minimum stay of two consecutive months abroad during the PhD program.
- ➔ Proficiency in a foreign language, demonstrated by at least a B2-level certificate.